RESEARCH

MINNESOTA DEPARTMENT OF TRANSPORTATION

2009-27A

Appendices to

Use of Fly Ash for Reconstruction of Bituminous Roads

LRRB
LOCAL
ROAD RESEARCH
BOARD

Take the steps...

Research...Knowledge...Innovative Solutions!

Transportation Research

Technical Report Documentation Page

1. Report No. MN/RC 2009-27A	2.	3. Recipients Accession No.	
4. Title and Subtitle Appendices to Use of Fly Ash for Reconstruction of Bituminous Roads		5. Report Date August 2009	
		6.	
7. Author(s) C. Benson, T. Edil, A. Ebrahimi, B. Kootstra, L. Li, and P. Bloom		8. Performing Organization Report No.	
9. Performing Organization Name and Address Dept. of Civil and Environmental Engineering University of Wisconsin Madison, WI 53706 Dept. of Soil, Water, and Climate University of Minnesota St. Paul, MN 55108		10. Project/Task/Work Unit No.	
		11. Contract (C) or Grant (G) No. (c) 89261 (wo) 5	
12. Sponsoring Organization Name and Address Minnesota Department of Transportation 395 John Ireland Boulevard Mail Stop 330 St. Paul, Minnesota 55155		13. Type of Report and Period Covered Final Report	
		14. Sponsoring Agency Code	
15. Supplementary Notes http://www.lrrb.org/pdf/200927A.pdf This report contains the appendices to report number 2009-27: http://www.lrrb.org/pdf/200927.pdf			

16. Abstract (Limit: 250 words)

Recycling part or all of the pavement materials in an existing road during reconstruction is an attractive construction alternative. When reconstructing roads surfaced with hot mix asphalt (HMA), the HMA, underlying base, and a portion of the existing subgrade often are pulverized to form a new base material referred to as recycled pavement material (RPM). Compacted RPM is overlain with a new HMA layer to create a reconstructed or rehabilitated pavement. This process is often referred to as full-depth reclamation. Similarly, when an unpaved road with a gravel surface is upgraded to a paved road, the existing road surface gravel (RSG) is blended and compacted to form a new base layer that is overlain with an HMA surface. Recycling pavement and road materials in this manner is both cost effective and environmentally friendly. However, recycled base materials may contain asphalt binder, fines, and/or other deleterious materials that can adversely affect strength and stiffness. To address this issue, chemical stabilizing agents can be blended with RPM or RSG. Use of industrial material resources for stabilization (e.g., cementitious coal fly ash) is particularly attractive in the context of sustainability. The purpose of this study was to develop a practical method to design local roadways using stabilized RPM or SRSG as the base layer and Class C fly ash as the stabilizing agent. The design method was developed in the context of the "gravel equivalency" (GE) design methodology employed for local roads in Minnesota.

17. Document Analysis/Descriptors Recycled materials, sustainability, gravel, full-depth reclamation, modulus of resilience, design methods, field tests, environmental impact analysis, environmental modeling, fly ash, pavement maintenance, environmental risk assessment		18. Availability Statement No restrictions. Document available from: National Technical Information Services, Springfield, Virginia 22161	
19. Security Class (this report) Unclassified	20. Security Class (this page) Unclassified	21. No. of Pages 301	22. Price

Appendices to
Use of Fly Ash for Reconstruction of Bituminous Roads

Final Report

Prepared by

Craig H. Benson
Tuncer B. Edil
Ali Ebrahimi
Brian Kootstra
Lin Li

Department of Civil and Environmental Engineering
University of Wisconsin

Paul Bloom

Department of Soil, Water, and Climate
University of Minnesota

August 2009

ACKNOWLEDGMENTS

TABLE OF CONTENTS: APPENDICES TO 2009-27

EXECUTIVE SUMMARY

Recycling part or all of the pavement materials in an existing road during rehabilitation and reconstruction is attractive. For roads surfaced with hot mix asphalt (HMA), the HMA, underlying base, and a portion of the existing subgrade often are pulverized to form a new base material referred to as recycled pavement material (RPM). Compacted RPM is overlain with a new HMA layer to create a reconstructed or rehabilitated pavement. This process is often referred to as full-depth reclamation (FDR). Similarly, when an unpaved road with a gravel surface is upgraded to a paved road, the existing road surface gravel (RSG) is blended and compacted to form a new base layer that is overlain with a surface of HMA. Recycling pavement and road materials in this manner is cost effective, environmentally friendly, and more sustainable.

Recycled base materials may contain asphalt binder, fines, and/or other deleterious materials that can adversely affect strength and stiffness. To address this issue, chemical stabilizing agents such as cement, asphalt emulsions, lime, cement kiln dust (CKD), or cementitious fly ash can be blended with RPM or RSG to increase the strength and stiffness. This "stabilized" material is referred to as SRPM or SRSG. Use of industrial material resources for stabilization, such as cementitious coal fly ash, is particularly attractive in the context of sustainability.

The purpose of this study was to develop a practical method to design local roadways using SRPM or SRSG as the base layer and Class C fly ash as the stabilizing agent in the context of the "gravel equivalency" (GE) design methodology employed for local roads in Minnesota. The project consisted of four major elements: (i) laboratory testing, (ii) prototype pavement evaluation, (iii) field assessment of two existing roadways constructed with SRPM and SRSG, and (iv) assessment of potential impacts to ground water. Findings from the study are described in a summary report and a set of detailed appendices focused on individual elements of the study. The summary report contains a step-by-step design procedure along with practical implications relevant to implementation.

The design procedure was developed using a three-pronged approach that used analysis to couple findings from (i) laboratory bench-scale testing, (ii) prototype-scale testing, and (iii) field monitoring. Laboratory tests were conducted on conventional test specimens to evaluate how fly ash content, curing time, and freeze-thaw cycling affect the strength and stiffness of RPM, RSG, SRPM, and SRSG. Prototype-scale tests were conducted to understand the stiffness of RPM, RSG, SRPM, and SRSG operative in full-scale pavement profiles under cyclic loading representative of field conditions. Results of these prototype-scale tests were used to develop the design procedure. Pavement monitoring was conducted at two field sites employing SRPM and SRSG to confirm that the pavements were performing satisfactorily when subjected to full-scale loading under realistic conditions, including exposure to severe weather conditions imposed by winter in Minnesota.

The bench-scale and field-scale testing program was conducted with three different base course materials: (i) a granular base comparable to Class 5 base used in Minnesota, (ii) RPM from a FDR project in Madison, WI, and (iii) a simulated RSG. SRPM and SRSG were created by blending the RPM and RSG with Class C fly ash from Columbia Power Station in Portage, Wisconsin. The fly ash content was maintained at 10% in the prototype evaluation due to the high level of effort associated with prototype-scale testing. However, 10% is the common fly ash content used in practice.

The design procedure is used to select the thickness of SRPM or SRSG base that has equivalent structural capacity as conventional Class 5 base course. The steps are as follows:

1. Create a conventional pavement design with Class 5 base material (or comparable aggregate base) using methods published by MnDOT or using local experience.

2. Determine the gravel equivalency factor for the recycled base material using the thickness of Class 5 base material from the conventional design (D_c) and design equations in the report.

3. Compute the thickness of the alternative base course (D_a) as $D_a = D_c(a_a^{-1})$, where a_a is the gravel equivalency factor for the stabilized base material (SRPM or SRSG)

Methods to account for fly ash contents other than 10% are also described as are the implications of freeze-thaw cycling and long-term curing. Field data from two sites in Minnesota are used to illustrate the efficacy of using SRPM and SRSG on actual projects.

Environmental monitoring was conducted at the two field sites, environmental testing was conducted in the laboratory, and environmental modeling was conducted to assess how ground water might be affected by trace elements leaching from the fly ash. This effort showed that trace elements in water percolating from the base of a roadway with SRPM or SRSG can have concentrations exceeding drinking water standards. However, these concentrations diminish over time, and the effects of dilution and attenuation prevent concentrations above drinking water standards at the limits of the right of way during the service life of a roadway.

APPENDIX A

SUMMARY OF CSAH 8 EXPERIENCE

FLY ASH SOIL STABILIZATION ON WASECA CSAH 8
LRRB INVESTIGATION 736
EXECUTIVE SUMMARY

17 October 2000

John Siekmeier, MnDOT Office of Materials and Road Research
Jeff Blue, Waseca County Highway Department

INTRODUCTION

The project is located on Waseca CSAH 8 south of Waseca, MN. The anticipated benefits of mixing coal fly ash into the silty-clay-loam subgrade were to dry and stabilize the subgrade and to increase subgrade stiffness and uniformity. Grading and ash stabilization occurred in the Fall 1999. Paving was conducted in Fall 2000. The ADT is estimated at about 750 vehicles per day and the soil type is a silty-clay-loam with a soil factor of 130. There are five one-half mile test sections that contain the following ash blends:

1. 100% Class C fly ash
2. 65% Sherco #3 ash, 35% Riverside #8 ash
3. 100% Sherco #3 ash
4. 65% Sherco #3 ash, 35% Class C fly ash
5. Control section without ash

Fly ash is produced by burning pulverized coal in coal-fired boilers. The powdery ash is collected by electrostatic precipitators, baghouses, or mechanical devices such as cyclones. The various ash types were produced by NSP in Minnesota and supplied to the project by Mineral Solutions. The ash types and sources are Class C fly ash from NSP's Blackdog and High Bridge power plants, dry scrubber ash from the NSP's Sherco Unit 3 in Becker, MN, and cyclone ash from NSP's Riverside Unit 8 in Minneapolis, MN.

CONSTRUCTION

Construction was performed jointly by Midstate Reclamation and Trucking (Lakeville, MN) and the Waseca County Highway Department. The ash was blended into the soil at a rate of 14% by weight of dry soil to a depth of 8 inches. The total width was 40 feet (two 12-foot lanes plus 8-foot shoulders). The construction process included the following steps:

1. Embankment construction
2. Salvaged aggregate wind-rowed to sides
3. Ash end-dumped on subgrade
4. Ash spread with motor grader
5. Dry-mixed with rotary mixer
6. Wet-mixed as water was added at mixer
7. Pad-foot vibratory compaction
8. Pneumatic-tire compaction
9. Smooth-drum compaction
10. All compaction completed in two hours
11. Subgrade shaped with motor grader
12. Salvaged aggregate replaced
13. 4 inches of new Mn/DOT Class 5
14. Hot mix asphalt in 2000

The production rate at start up was about 0.33 mile per day and by completion had reached about 0.75 mile per day. A realistic estimate for future projects would be about one mile per day with an experienced construction team and few problems. The factors affecting production included delivery of ash and water, ability to measure mixing rates, weather, and equipment breakdowns.

TESTING

An extensive testing program was implemented to measure and document the results of this project. The tests included laboratory tests to develop target water content and density for maximum strength, field tests before, during, and after construction including long term tests, laboratory tests before and after ash addition for classification and mechanical properties, and environmental tests both field and laboratory. The results will be used to quantify both moisture and stiffness before and after ash addition and to assess environmental impacts. Preliminary results show an increase in stiffness and uniformity, but raise questions about environmental issues.

PAVEMENT DESIGN

The potential benefit of using ash for soil stabilization can be summarized by comparing a pre-ash pavement design, which is based the soil properties prior to ash addition, with a post-ash pavement design, based on modified soil-ash properties. To quantify the structural benefit of ash stabilization, the increase in the subgrade modulus must be measured. Also, an empirical relationship between the modulus and the R-value must be determined to use the existing design procedure recommended in the Mn/DOT State Aid Manual. Therefore the following mechanical properties were measured using both in situ and laboratory tests and related to one another using an empirical correlation.

The pre-ash properties were a soil factor of about 130 with an assumed R-value of 10. The actual mean R-value was 18.6 (standard deviation of 1.9). This results in a design R-value (mean minus one standard deviation) of 16.7, which was rounded to 15. Given this soil type (R-value 10 to 15) and the estimated traffic, the HMA thickness is 8 to 8.75 inches based on the design procedure recommended in the Mn/DOT State Aid Manual.

The pre-ash subgrade modulus was estimated using the empirical relationship to be 30.4 MPa (4400 psi) based on an R-value of 18.6. The actual measured modulus, based on falling weight deflectometer (FWD) measurements, was 31 MPa (4500 psi). The design modulus used for the pre-ash design (8 to 8 3/4 inches HMA) was 25.2 MPa (3700 psi) based on the design R-value of 15. An additional note of interest is that the mean measured moisture content at the time of in situ testing was 17.8% for the silty-clay-loam soil, which has a standard Proctor optimum moisture content of 18.0%.

The post-ash design used a design modulus of 42.8 MPa (6200 psi) based on the mechanical properties measured about one month after ash stabilization. The FWD modulus increased by a factor of about 1.7 for the composite soil-ash over soil structure and the dynamic cone penetrometer (DCP) modulus increased by a factor of about 3.7 for the soil-ash layer. In order to use the same design procedure recommended in the State Aid Manual, this post-ash composite modulus was converted to an estimated R-value of 27.5, which was rounded to 25 for

design. The resulting pavement design has a HMA thickness of 7 inches. Again an interesting note is that the mean measured moisture content post-ash averaged 17.7% compared to the 17.8% pre-ash.

In summary, the possible affect on design would be a HMA thickness reduction of 1 to 1.75 inches. The equivalent structural sections would be a no ash section (subgrade R-value of 10 to 15) with 8 to 8-3/4 inches of HMA or an ash modified section (subgrade R-value of 25) with 7 inches of HMA. The reduction in HMA thickness would be based on the assumption that the subgrade modulus has been permanently modified by the ash addition. Retrieving additional undisturbed samples for laboratory testing or conducting additional in situ testing has not been purposed at this time. Only pavement surface quality testing is anticipated.

COSTS

The additional costs related to the ash modification portion of the project were $50,000 for ash material and delivery, $25,000 for the rotary mixer and operator, and an additional estimated amount for grading and compaction by county staff. Therefore the additional cost for ash modification was estimated to be about $1.60 per square yard given the 14% addition rate and 8-inch depth. This can be compared to the estimated cost of HMA. Given a 1 to 1.75 inch reduction in thickness and a cost of $1.25 per square yard per inch of HMA, it is estimated that $1.25 to $2.20 per square yard would be saved in HMA costs.

CONCLUSIONS AND RECOMMENDATIONS

For this Waseca CSAH 8 project, it was decided not to use a thin HMA layer, but rather to expect a longer design life and lower maintenance. Additional factors in this decision were that the paving and grading were part of a single contract, which complicated thinning the HMA after the contract had begun. Also, the construction transitions between ash-stabilized and non-stabilized sections were a consideration.

In summary, the ash improved stability and uniformity and was able to be used with minimal contracted equipment at a reasonable cost. However, several modifications are needed that would improve the construction process. Some areas for improvement include: controlling dust while dumping, spreading the ash uniformly, controlling water at the rotary mixer, and monitoring the moisture content before and after ash addition.

For future projects it is recommended that the grading and stabilization be included in the first contract with the intent of using ash to improve the worst locations. A bid price per square yard of ash stabilization is recommended. Following the grading and stabilization work, in situ testing and final pavement design would occur. The resulting pavement design would require less HMA since the design would be based on a more uniform subgrade where the worst-case locations had been improved. The final paving contract would then be less costly.

In conclusion, ash stabilization has been proven to be beneficial in providing a durable construction platform that can carry construction equipment and local traffic prior to and during HMA paving. Ash stabilization appears to be capable of providing relatively long-term pavement support, however additional observation and testing of pavement condition is required. Performance, in terms of ride (PSR) and pavement distress, should be monitored for five to ten years. Yet to be determined is resolution of several environmental issues concerning the possible toxicity of the ash. It is likely that future specifications will place strict limits on metal and chemical concentrations in the ash.

APPENDIX B

REPORT FOR TASK 1

**STRENGTH AND STIFFNESS OF RECYCLED BASE
MATERIALS BLENDED WITH FLY ASH**

STRENGTH AND STIFFNESS OF RECYCLED BASE
MATERIALS BLENDED WITH FLY ASH STRENGTH AND STIFFNESS OF RECYCLED BASE
MATERIALS BLENDED WITH FLY ASH

USE OF FLY ASH FOR RECONSTRUCTION
OF BITUMINOUS ROADS

REPORT FOR TASK 1

STRENGTH AND STIFFNESS OF RECYCLED BASE
MATERIALS BLENDED WITH FLY ASH

Prepared by:

Felipe F. Camargo
Craig H. Benson
Tuncer B. Edil
Department of Civil and Environmental Engineering
University of Wisconsin-Madison
Madison, WI 53706

February 2009

EXECUTIVE SUMMARY

The objectives of this study were to assess the engineering properties of two recycled materials. Laboratory experiments were conducted in which a recycled pavement material (RPM) and a road surface gravel (RSG) were tested to determine the California bearing ratio (CBR), resilient modulus (M_r), and unconfined compressive strength (UCS). Results of these tests were compared to the properties of a conventional base material (Class 5 base). The recycled materials were blended with two fly ash contents (10 and 15%) and three curing times (7, 28, and 56 d). Resilient modulus and unconfined compression strength tests were also conducted after 5 cycles of freezing and thawing to assess the impact of freeze-thaw cycling.

RSG and RPM had CBRs greater than that of Class 5 base, but all three materials had CBR less than typically desired for base course (CBR $\geq$ 50). After 7 d of curing, CBRs of RPM with fly ash (67 and 134) were 3 to 6 times the CBR of RPM alone (22), whereas CBRs of RSG with fly ash (183 and 334) were 6 to 11 times the CBR of RSG alone (31). The CBR for RPM and RSG increased with increasing fly ash content.

The UCS for RPM with fly ash ranged from 0.78 to 2.26 MPa, whereas the UCS for RSG with fly ash ranged from 1.41 to 3.61 MPa. The UCS of RPM and RSG mixed with fly ash increased with increasing fly ash content and curing time, with significant increases occurring even after 28 d. The UCS was maintained even when the RPM and RSG were exposed to freezing. After 5 freeze-thaw cycles, the UCS of RPM and RSG mixed with fly ash was higher (5 and 18%) than the UCS not subjected to freeze-thaw cycling.

RPM had a higher summary resilient modulus (SRM) than Class 5 base, whereas the SRM for RSG was slightly lower than that of Class 5 base. RPM also exhibited smaller plastic strains during resilient modulus testing than Class 5 base, whereas RSG showed similar plastic strains to Class 5 base. SRM for RPM and RSG mixed with fly ash were independent of bulk stress and were described by a single modulus. The SRM of RPM with fly ash ranged from 1800 to 6800 MPa, whereas SRM of RPM alone was 309 MPa. The SRM of RSG blended with fly ash ranged from 5800 to 12000 MPa, whereas the SRM of RSG alone was 212 MPa. The SRM of RPM and RSG blended with fly ash increased with fly ash content and curing time, with the rate of increase being largest between 7 and 28 d of curing. Addition of fly ash reduced plastic strains of RPM and RSG during resilient modulus testing. Freeze-thaw cycling had a small effect on the SRM of Class 5 base (7% change), RPM (15% change), or RSG (5% change) with or without fly ash, with no consistent effect for materials mixed with fly ash.

ACKNOWLEDGEMENT

TABLE OF CONTENTS

LIST OF FIGURES

LIST OF TABLES

1. INTRODUCTION

There is growing interest in reducing construction costs and increasing sustainability when reconstructing paved roads and upgrading unpaved roads to paved roads. One approach is to use recycled materials in place of conventional materials. For example, road surface gravel (RSG) from a gravel road undergoing rehabilitation may be reused as the base layer for newly paved roads (Hatipoglu et al. 2008). Alternatively, recycled pavement material (a mixture of pulverized asphalt, base, and subgrade from the existing road) may be used as base course for the new pavement (Wen et al. 2004). In some cases, the strength and stiffness of these recycled materials are enhanced by blending them with cementitious material, such as fly ash from coal-fired electric power plants (Hatipoglu et al. 2008, Li et al. 2007).

An impediment to more common use of recycled materials in roadway reconstruction is lack of information on their engineering properties. In addition, pavement engineers need to know how to design pavements using recycled materials that will yield equal or better performance than pavements constructed with virgin materials. This study was conducted to describe the engineering properties of a typical recycled pavement material (RPM) and recycled road surface gravel (RSG) blended with fly ash.

The particular objectives of this study were to assess the engineering properties of recycled materials with and without fly ash and to study how freezing and thawing may affect the engineering properties of recycled pavement materials blended with fly ashes. This report describes the findings of this study. Background information is provided in Section 2. Materials and methods are described in Sections 3 and 4. Results and analysis are provided in Section 5. A summary and conclusions are in Section 6.

2. BACKGROUND

2.1 IN SITU PAVEMENT RECYCLING

An alternative to common methods of pavement rehabilitation/reconstruction is to recycle the existing pavement materials. In-situ recycling is a pavement rehabilitation method in which some, if not all, of the materials from the existing pavement are used for constructing a new pavement structure. In situ recycling is attractive because of the potential reduction in costs and consumption of natural resources. For example, the Nevada Department of Transportation (NDOT) has reported a savings of $600 million over a span of 20 years by employing in situ recycling methods in lieu of common reconstruction methods (Bemanian et al. 2006). Additional benefits of in-situ recycling include conservation of energy, waste reduction, and reduction of greenhouse gas emissions (Kearney and Huffman 1999).

There are three different types of in situ recycling in pavement rehabilitation: hot in-place recycling (HIR), cold in-place recycling (CIR), and full-depth reclamation (FDR). The three in-situ recycling methods are typically classified according to the procedures used for recycling, and the materials to be recycled into the new pavement. Because of their similarity, however, the nomenclature for in situ recycling is often used interchangeably.

2.1.1 Hot In-Place Recycling

Hot in-place recycling (HIR) is an in situ pavement rehabilitation process where a fraction of the existing asphalt course is used in the new asphalt surface. The existing asphalt is softened by applying heat, mechanically removed, blended with a chemical additive and virgin aggregates or asphalt if needed, and then replaced onto the pavement structure (Button et al. 1999). Typical HIR pavement depths range from 25 to 50 mm.

HIR is typically used to correct for pavement distress, such as rutting, corrugations, thermal cracking, raveling, flushing and loss of surface friction (Kuennen 1988). HIR is an attractive alternative for pavement rehabilitation because it has been shown to reduce construction costs and energy consumption by as much as 25% and 30%, respectively, when compared with conventional methods (Button et al. 1994).

2.1.2 Cold In-Place Recycling

Cold in-place recycling (CIR) is similar to hot in-place recycling, but without heat. CIR can be performed either partially or to the full depth of the existing pavement structure. Recycled asphalt pavement (RAP), the material obtained by pulverizing the existing asphalt layer, is reused for the new pavement. Typical depths for CIR range from 50 to 100 mm (Salomon and Newcomb 2000).

CIR consists of pulverizing the existing asphalt layer to a specified depth, mixing the recycled asphalt pavement (RAP) aggregates with an emulsion, compacting the material to the desired density, and letting the material cure. The recycled layer is typically used as a base layer that is surfaced with a thin layer of wearing course. However, CIR has been used for surface course for roadways with low to medium traffic volume (Epps 1990). Typical chemical additives

used in CIR include soft asphalt cements, cutback asphalt, foamed asphalt cements, and emulsions combined with cement, fly ash, or lime (AASHTO-AGC-ARTBA 1998).

2.1.3 Full-Depth Reclamation

Full-depth reclamation (FDR) consists of pulverizing and mixing the existing asphalt layer with the underlying aggregate base, and sometimes subgrade, to form a recycled base layer for a new asphalt pavement. This method is also referred to as full-depth cold in-place recycling. A primary difference between FDR and CIR is the depth of pulverization of the existing pavement. FDR extends 100 to 300 mm deep, depending on the dimensions of the existing pavement structure (Salomon and Newcomb 2000). In contrast, CIR consists of depths only 50 to 100 mm. The material generated from FDR, comprised of existing RAP and underlying base and subgrade materials, is referred to as recycled pavement material (RPM) (Li et al. 2007).

RPM can be used as base course for a new pavement (Wilson et al. 1998). In practice, however, RPM is often mixed with a binder or admixture to enhance the strength and stiffness (Wen et al. 2004; Taha et al. 2002; Crovetti 2000; Misra et al. 2005; Li et al. 2007). RPM can be improved by adding good quality granular material, or by blending with Portland cement, hydrated lime, fly ash, or bituminous agents (slow or medium set asphalt emulsions) (Kearney and Huffman 1999).

FDR is also used to upgrade unpaved pavements to asphalt pavements (Hatipoglu et al. 2008). The existing road surface gravel is blended with fly ash and reused as the base course of a new pavement.

2.2 RECYCLED ROADWAY MATERIALS BLENDED WITH FLY ASH

The effect of RAP content on strength and stiffness may be an impediment for using recycled materials as base course for a new pavement (Taha et al. 1999; Cooley 2005; Kim et al. 2007). An alternative is to enhance the mechanical properties of recycled materials by adding cementitious fly ash. Cementitious fly ashes have been used to effectively improve the mechanical properties of soft subgrades (Edil et al. 2002; Senol et al. 2006). However, enhancing the mechanical properties of granular materials through fly ash addition is largely undocumented in the literature. Data on recycled materials blended with fly ash is even scarcer.

Li et al. (2007) evaluated the use of recycled asphalt pavement blended with fly ash as base course during the reconstruction of a 0.5-km section of asphalt pavement in Waseca, Minnesota. The recycled base layer was obtained by pulverizing the existing asphalt pavement and underlying materials to a depth of 300 mm, removing the uppermost 75 mm of RPM, uniformly spreading Class C fly ash (10% by dry weight) on the surface, and mixing the fly ash and RPM with water to a depth of 150 mm. Compaction was carried out within 1-2 hours of mixing and the final compacted layer was cured for 7 d prior to placing 75 mm of hot mix asphalt.

Strength and stiffness of field and laboratory specimens were measured to evaluate the effectiveness of enhancing the mechanical properties of RPM through fly ash addition. Strength was measured by CBR tests, whereas stiffness was measured by resilient modulus (M_r) tests. Field-mix specimens were prepared by collecting fly ash treated RPM and compacting the

mixture into CBR and M_r molds. The specimens were prepared at dry unit weights measured in the field, sealed with plastic, and cured (7 d for CBR, 14 d for M_r) at 100% relative humidity. Laboratory-mix specimens were prepared from fly ash and RPM samples obtained during construction. These specimens were prepared to mean field water contents and dry unit weights. RPM-only specimens were prepared in a similar manner.

CBR of RPM increased significantly with the addition of fly ash, ranging from 3 to 17 for RPM (laboratory) and from 70 to 94 for RPM with fly ash (laboratory). The RPM did not meet the CBR typically required for base course (CBR $\geq$ 50), whereas fly ash addition increased the CBR of RPM beyond 50. Field specimens exhibited CBRs approximately two thirds lower than laboratory specimens, but still had CBR significantly larger than RPM alone. Similar trends were observed for M_r of RPM. Addition of fly ash increased the M_r of laboratory RPM specimens appreciably (2.2 times, on average), whereas M_r of field specimens were 25% lower, on average, than the M_r of laboratory specimens.

A similar study was conducted by Hatipoglu et al. (2008) where cementitious fly ash was added to the existing road surface gravel (RSG) when upgrading a 3.5-km road section in Chisago, Minnesota from an unpaved road to a paved road. Cementitious off-specification fly ash was mixed (10% by dry weight) with the existing RSG and water to a depth of 250 mm and compacted within 1-2 hr. Following compaction, the RSG with fly ash was overlain by 90 mm of HMA within 3 to 7 d. Field and laboratory specimens of RSG and RSG with fly ash were prepared in the same manner as Li et al. (2007). However, the M_r specimens were cured for 7 d as opposed 14 d.

Results obtained by Hatipoglu et al. (2008) are very similar to those obtained by Li et al. (2007). The CBR of RSG was 24, thus not meeting the typical minimum CBR requirements for base course. However, RSG mixed with fly ash in the laboratory had a CBR of 154, whereas field-mix RSG had CBR ranging from 16 to 90. Field CBRs were as much as 60% lower than laboratory prepared specimens. Similar trends were observed for M_r of RSG. Addition of fly ash increased the M_r of laboratory prepared RSG by as much as 2 fold. In contrast to CBR, the M_r of the RSG field specimens was higher than the M_r of laboratory specimens.

Wen et al. (2007, 2008) evaluated using high carbon fly ash to increase the strength and stiffness of RPM. They found that CBR and M_r of RPM blended with fly ash were higher than CBR and M_r for RPM without fly ash. Moreover, the CBR of RPM was lower than the CBR of conventional crushed aggregate, whereas the CBR of RPM blended with fly ash was at least comparable to the CBR of conventional crushed aggregate. The M_r of RPM was higher than the M_r of conventional crushed aggregate, but RPM exhibited higher plastic deformations than those of conventional crushed aggregate during M_r testing. Addition of fly ash reduced plastic deformations for RPM, where RPM exhibited less plastic deformations than the conventional crushed aggregate.

Crovetti (2000) conducted falling weight deflectometer (FWD) tests on pavement test sections to evaluate the structural capacity of pavements containing recycled pavement material blended with fly ash (7% by dry weight) and asphalt emulsion (application rate of 7 L/m^2). Field structural capacity was computed from moduli defined from FWD tests. The test section containing recycled pavement materials blended with fly ash had the highest structural capacity, yielding increase in lifespan of 58% when compared to the control, and 28% when compared to the section with emulsified asphalt. No surface distresses were encountered in any of the test sections after one year of service. In a similar study, Wen et al. (2004) reported no surface distresses for test sections containing recycled pavement materials blended with fly ash after two

years of service. Moreover, backcalculated FWD data indicated that the structural capacity of the test section containing fly ash increased 49% after 1 year of service.

Addition of fly ash can also have detrimental effects on pavements. A series of cold in-place recycling (CIR) test sections using Class C fly ash were constructed by the Kansas Department of Transportation. Test sections with higher fly ash contents exhibited more initial cracking than those with lower fly ash contents. Cross and Young (1997) evaluated the durability, fatigue, and thermal cracking potential of laboratory-prepared samples of the CIR materials blended with Class C fly ash. Fatigue testing indicated an increase in brittleness with increasing fly ash content, which would yield a pavement structure with greater propensity for fatigue and thermal cracking. Thus, using more Class C fly ash than the necessary is not recommended.

2.3 EFFECT OF FREEZE-THAW CYCLING ON THE MECHANICAL PROPERTIES OF RECYCLED MATERIALS

Little data are available on the effects of freeze-thaw cycling on the engineering properties of granular materials. Furthermore, even less data are available on the effects of freeze-thaw cycling on the mechanical properties of recycled materials with and without fly ash.

Simonsen et al. (2002) investigated the effects of one freeze-thaw cycle on the resilient modulus of 5 soils: glacial till, silty fine sand, coarse gravelly sand, fine sand, and marine clay. Specimens were compacted at optimum water content using kneading compaction. No inflow or outflow (closed system) was allowed during omnidirectional (3D) freezing and thawing. Resilient modulus testing was carried out according to AASHTO TP46-94.

A reduction in resilient modulus was observed for all materials after 1 freeze-thaw cycle. The percent reduction in M_r for each material was as follows: glacial till (27%), silty fine sand (19%), coarse gravelly sand (23%), fine sand (50%), and marine clay (57%). Simonsen et al. (2002) indicate that freezing and thawing results in a looser soil structure, which causes a lower resilient modulus.

Rosa (2006) evaluated the effect of freeze-thaw on the engineering properties of one RSG and four RPMs mixed with fly ash. The materials were cured and then subjected to varying freeze-thaw cycles (0, 1, 3, 5, 10, and 12) using a closed system. Resilient modulus tests were performed after freeze-thaw cycling. The resilient modulus decreased with increasing freeze-thaw cycles, leveling off after 5 cycles. Reduction in resilient modulus for the coarse material-fly ash mixtures ranged from 7 to 42%, with an average of 24.5%. Furthermore, RPMs blended with fly ash showed higher reductions in resilient modulus as the fines content increased. Rosa (2006) also reports that the reduction in resilient modulus for materials blended with fly ash depends on the CaO content of the fly ash. For example, the M_r decrease of RPM blended with fly ash having 25.8% CaO ranged from 19-29%, whereas the RPM blended with fly ash having 24.0% CaO showed reductions in M_r ranging from 33-43%. No relationship was found between fly ash classification and reductions in M_r after freeze-thaw cycling.

Zaman and Naji (2003) evaluated the effect of freeze-thaw cycling on a typical Oklahoma base aggregate blended with Class C fly ash (10% by dry weight). Resilient modulus and unconfined compression strength tests were conducted on specimens after 0, 4, 12, and 30 freeze-thaw cycles (3 and 28 d cure). Resilient modulus increased up to 12 freeze-thaw cycles for specimens cured for 28 d, but exhibited a drop in resilient modulus for 30 freeze-thaw cycles. The specimens cured for 3 d, however, showed an increase in resilient modulus up to 30 cycles.

An increase in freeze-thaw cycles also resulted in an increase in UCS for all cases. The effect of freeze-thaw cycling on M_r and UCS was attributed to retardation or acceleration of cementitious reactions.

Baugh (2007) evaluated the effect of freeze-thaw cycling on the resilient modulus and unconfined compression strength of three recycled materials blended with cement kiln dust (5, 10, 15, and 20% by dry weight): recycled asphalt pavement (RAP), recycled pavement material (RPM), and road surface gravel (RSG). Specimens were prepared at 95% of maximum dry unit weight, cured for 7 d, soaked in water for 5 h, drained for 5 to 10 min, sealed in plastic, and subjected to freeze-thaw cycling (0, 5, and 10 cycles). Resilient modulus testing was carried out according to NCHRP 1-28A.

The summary resilient modulus (SRM) of RAP and RPM blended with cement kiln dust (CKD) decreased after 5 freeze-thaw cycles (33 and 37% reduction in SRM), whereas no further reductions in SRM occurred after 10 freeze-thaw cycles. In contrast, the SRM of RSG blended with CKD decreased up to 10 freeze-thaw cycles. The maximum reduction in SRM observed was approximately 50%. Increasing the CKD content resulted in a higher reduction in SRM for a given material.

The majority of the reduction in UCS for RAP and RPM also occurred within the first 5 freeze-thaw cycles (30% reduction in UCS). There was no observed trend in UCS of RSG blended with CKD as a function of freeze-thaw cycling, with a maximum change in UCS of 15%. The effect of freeze-thaw cycling on the SRM and UCS of the material-fly ash mixtures was attributed to ice expansion and formation of ice lenses, which break the bonds created between the fly ash and particles and result in a loss of strength and stiffness.

Li et al. (2007) conducted falling weight deflectometer (FWD) tests on a pavement structure, having a base layer of recycled pavement materials (RPM) blended with class C fly ash (10% by dry weight), to evaluate the changes in pavement modulus exposed to freeze-thaw cycling after the first winter after construction. FWD tests were conducted in 10 different stations along the pavement in November 2004 and August 2005 (3 months and 1 year after construction). Statistical analysis on the base moduli (RPM blended with fly ash) measured before and after 1 winter exposure showed the base moduli were statistically the same, suggesting no strength losses for the base layer after freeze-thaw cycling.

Hatipoglu et al. (2008) conducted a similar study on a pavement having a base layer of road surface gravel (RSG) blended with class C fly ash (10% by dry weight). FWD tests were conducted in different stations along the pavement in November 2005, May 2006, and October 2006 (2 months, 8 months, and 1 year after construction). Statistical analysis of the base moduli indicated strength losses after one winter exposure (from November 2005 to May 2006) followed by an increase in base modulus (from May 2006 to October 2006). The median base moduli in May 2006 for RSG blended with fly ash were comparable to those of RPM blended with fly ash (Li et al. 2007), even though a drop in modulus occurred for the RSG base layer.

3. MATERIALS

3.1 BASE AND RECYCLED MATERIALS

Two recycled materials and a conventional base material were selected for this study. The recycled materials consisted of a recycled pavement material (RPM) and a road surface gravel (RSG). The base material was a gravel meeting the Class 5 specifications for base course in Minnesota (MnDOT 2005). The Class 5 base was used as a control material. The Class 5 base and RSG were manufactured in the laboratory because the materials were not readily available for testing.

RPM was obtained from a roadway reconstruction project in southwestern Madison, Wisconsin, near the intersection of Muir Field Road and Carnwood Road. The RPM was a blend of pulverized asphalt and limestone base layers created by removing the existing pavement (approximately equal thickness of asphalt and base), having an asphalt content of 4.6% (ASTM D 6307). RPM used for testing was sieved through the 25 mm sieve.

Class 5 base meeting Minnesota Department of Transportation specifications (MnDOT) was created by blending pit run gravel obtained from Wimme Sand and Gravel (Plover, Wisconsin) with crushed pea gravel obtained from Midwest Decorative Stone and Landscape Supply (Madison, Wisconsin). The pit run gravel was sieved past the 25 mm sieve prior to blending with the pea gravel. The particle size distribution for the Class 5 base is shown in Fig. 1 (a) along with MnDOT specifications for Class 5 base used for base course applications.

A typical RSG was created by blending the manufactured Class 5 base with washed limestone fines obtained from Rosenbaum Crushing and Excavating (Stoughton, Wisconsin). The Class 5 base was sieved past the 19 mm sieve prior to blending with the washed limestone fines. The RSG meets the American Association of State Highway and Transportation Officials (AASHTO) gradation requirements for the surface course materials, as outlined in AASHTO M 147 (AASHTO 2001). The particle size distribution for RSG is shown in Fig. 1 (b) along with three AASHTO specifications for surface course gravel (Gradations D, E, and F).

A summary of the index properties and soil classifications for the three base materials is shown in Table 1. Particle size distribution (PSD) curves, which were determined using ASTM D 422, are shown in Fig. 2. Class 5 base classifies as SP according to the United States Soil Classification System (USCS), whereas RSG classifies as SM, and RPM as GW-GM. All three materials are nonplastic, even though RPM and RSG have more than 10% fines.

Compaction tests were performed at standard compactive effort for all three materials using the method in ASTM D 698. Optimum water contents and maximum dry unit weights are summarized in Table 3. Bell-shaped curves were obtained for RPM and RSG. Class 5 base, however, showed little variation in dry unit weight with water content (Fig. 3).

3.2 FLY ASH

The Columbia fly ash for this study was obtained from Columbia Power Plant Unit No. 2, in Portage, Wisconsin where sub-bituminous coal is burned in pulverized boilers. The fly ash is collected using electrostatic precipitators. Columbia fly ash has a powdery texture, light brown color, classifies as Class C according to ASTM C 618, has a specific gravity of 2.63, and has

cementitious properties. Physical properties and chemical composition of Columbia fly ash are summarized in Table 2.2 along with the typical chemical composition of Class C fly ash.

According to Janz and Johansson (2002), the ratio of CaO to SiO_2 is indicative of the potential for pozzolanic reactions, and binders containing larger ratios are likely to be more effective in enhancing the engineering properties of materials. Similarly, Tastan (2005) indicates that cementing is also related to the ratio of CaO to ($SiO_2 + Al_2O_3$). Tastan (2005) reported higher strengths for subgrade soils blended with fly ash at CaO/SiO2 ratios ranging from 0.5 to 1.0 and CaO/($SiO_2 + Al2O_3$) ratios ranging from 0.4 to 0.7. The ratio of CaO to SiO_2 for Columbia fly ash is 0.4, whereas the ratio of CaO to ($SiO_2 + Al_2O_3$) is 0.8. Rosa (2006) reports the pozzolanic activity of Columbia fly ash at 7 days is 95.8%.

4. METHODS

4.1 COMPACTION / CALIFORNIA BEARING RATIO

Specimens for compaction and California bearing ratio (CBR) tests were compacted in PVC molds following Method C in ASTM D 698. Particles larger than 25 mm were removed prior to compaction. Materials were compacted in three lifts of equal mass and thickness. CBR tests were performed on specimens without fly ash immediately after compaction, whereas specimens with fly ash were tested after 7 d of curing. All CBR tests were conducted following the methods in ASTM D 1883. To simulate condition shortly after construction, CBR specimens were not soaked prior to testing and 7 d curing was employed on specimens with fly ash (Bin-Shafique et al. 2004). An MTS Systems machine (model Sintec 10/GL) was used for loading the specimens. Data were collected with a PC equipped with TestWorks software.

4.2 RESILIENT MODULUS

The RPM and Class 5 base materials classify as Type I material in NCHRP 1-28A, which requires a specimen 152 mm in diameter and 305 mm in height for resilient modulus testing (NCHRP 2004). For consistency, all specimens were prepared to these dimensions even though smaller specimens could have been used for RSG. Specimens were compacted in six lifts of equal mass and thickness using a split mold 152 mm in diameter. All materials were compacted to 100% of maximum standard Proctor density at optimum water content. Specimens were compacted to within 1% of the target dry density and 0.5% of target moisture content (NCHRP 2004). Similar methods were employed for base materials prepared with and without fly ash.

Specimens of Class 5 base for resilient modulus (M_r) testing were prepared in a split mold placed directly on the bottom plate of the resilient modulus test cell. A latex membrane was placed inside the split mold. Vacuum was applied to attract the membrane to the inside surface of the mold.

Resilient modulus testing was performed in accordance with the NCHRP 1-28A protocol (NCHRP 2004). All materials were tested under Procedure Ia, which applies to base and subbase materials. All resilient modulus tests were conducted with both internal and external linear variable displacement transducers (LVDT). Clamps for the internal LVDTs (Fig. 4) were built in accordance with NCHRP 1-28A specifications. The external LVDTs had a measurement range of ± 5 mm for specimens without fly ash and ±1.5 mm for specimens with fly ash. Internal LVDTs used for specimens without fly ash had a measurement range of ±5 mm, whereas a range of ±1.5 mm was used for specimens with fly ash. The former had an accuracy of 0.005 mm, while the latter had an accuracy of 0.0015 mm. Calibration data for resilient modulus testing equipment is in Attachment E.

An MTS Systems Model 244.12 servo-hydraulic machine was used for loading the specimens. Loading sequences, confining pressure, and data acquisition were controlled by a PC equipped with Labview 8.5 software.

Resilient moduli (M_r) from the last 5 cycles of each test sequence were averaged to obtain the resilient modulus for each load sequence. The resilient modulus data were fit to the power function proposed by Moosazedh and Witczak (1981):

$$M_r = k_1 \theta^{k_2} \qquad\qquad (4.1)$$

where θ is bulk stress and k_1 and k_2 are fitting parameters. For a given material, k_2 was not expected to vary appreciably. Hence, k_2 obtained from replicate or triplicate tests were averaged and fixed for that material. A second fit was then performed using the average k_2 and fitting k_1 to all tests. A summary resilient modulus (SRM) was also computed, as suggested in Section 10.3.3.9 of NCHRP 1-28A. For base materials, the summary resilient modulus corresponds to the resilient modulus at a bulk stress of 208 kPa.

4.3 UNCONFINED COMPRESSION

Unconfined compression tests were conducted on the specimens with fly ash after resilient modulus testing. ASTM D 5102 was used for the unconfined compression tests. Stresses applied during resilient modulus testing are low enough that specimens with fly ash do not deform significantly. Therefore, resilient modulus specimens could be reused for unconfined compression tests. Strain rates ranging from 0.5% to 2.1% per minute are suggested in ASTM D 5102. However, slower rates are optional for stiffer materials. All specimens were loaded at a strain rate of 0.21% per minute (Acosta 2002), or 0.64 mm per minute for specimens that are 305 mm tall. A Satec Systems servo-hydraulic compression machine (Model MII 400 RD) was used for testing. Data were collected with a PC equipped with Partner software.

4.4 FREEZE-THAW DURABILITY

Tests were conducted to determine the effects of freeze-thaw cycling on the engineering properties of each of the materials. Rosa (2006) reports the effects of freeze and thawing on resilient modulus and unconfined compression generally occur within 5 cycles. Therefore, test specimens were subjected to 5 freeze-thaw cycles and then their resilient modulus was measured. Unconfined compression tests were also performed on the specimens with fly ash subjected to freeze-thaw after the resilient modulus tests were conducted.

Specimens for freeze-thaw testing were prepared in the same manner as other resilient modulus specimens. All specimens were compacted to 100% of maximum standard Proctor density at optimum water content. The saturation level for the Class 5 base was 49%, whereas the saturation level for RPM and RSG were 89% and 65%, respectively. Preliminary testing on a specimen instrumented with a thermocouple showed that complete freezing occurred within one day at -19°C. Thus, all specimens were retained in the freezer for at least 1 day. After freezing, the height and weight were measured and the specimen was allowed to thaw at room temperature. This process was repeated until 5 freeze-thaw cycles were completed. After the last cycle, specimens were extruded frozen and thawed inside the resilient modulus cell. Resilient modulus testing was then conducted as described previously. Unconfined compression tests were conducted on specimens with fly ash after the resilient modulus tests were completed.

5. RESULTS AND ANALYSIS

5.1 COMPACTION

Maximum dry unit weights and optimum water contents for RPM and RSG, with and without fly ash, are summarized in Table 3. The compaction characteristics of RPM and RSG blended with fly ash are similar to the compaction characteristics of RPM and RSG without fly ash (Fig. 5). However, increasing fly ash content resulted in an increase in optimum water content and a decrease in maximum dry unit weight. The shift in compaction curves with increasing fly ash content was more pronounced for RPM. The lower dry unit weights for material-fly ash mixtures is attributed to the loss of energy to breaking of the bonds, created as a result of cementation, during compaction.

Wen et al. (2008) and Senol et al. (2003) also report that adding fly ash to RPM or soil causes a shift in the compaction curve, and that the type of shift (up or down) can depend on the type of fly ash.

5.2 CALIFORNIA BEARING RATIO

5.2.1 Base and Recycled Materials without Fly Ash

CBR and dry unit weight are shown in Fig. 6 as a function of moisture content for Class 5 base, RPM, and RSG. There is little variation in CBR or dry unit weight with water content for Class 5 base because it is a granular material with low fines content. Bell-shaped curves were obtained for CBR and dry unit weight for both RPM and RSG. Optimum CBRs for all materials were at approximately the same water content as the maximum dry unit weight.

Both RPM and RSG had higher CBR than Class 5 base. The CBR for Class 5 base was 10, whereas RPM and RSG had CBRs of 22 and 31, respectively. The CBR for Class 5 base was significantly lower than expected (<50). However, a second CBR test confirmed the initial results (Fig. 6). The low CBR of the Class 5 base is attributed to its large sand fraction (59%), and the rounded to subrounded characteristics of the gravel fraction (Fig. 7). CBR decreases with increasing particle roundness because of the decrease in friction between particles.

CBRs obtained for RPM and RSG were higher than expected. Baugh (2008) reports an average CBR of 13 for RPM, whereas Li et al (2007) report CBRs ranging from 3 to 17. Similarly, Baugh (2008) reports an average CBR of 21 for RSG, whereas Hatipoglu et al. (2008) report a CBR of 24. These CBRs, however, were obtained for specimens prepared at optimum water content and 95% of standard Proctor dry unit weight, whereas optimum CBRs for this study were determined from the relationship between CBR and water content (Fig. 6).

5.2.2 Recycled Materials Blended with Fly Ash

CBRs for RPM and RSG blended with fly ash are summarized in Table 3. The variation of CBR and normalized CBR (defined as CBR of base material with fly ash over CBR of base material) with fly ash content for RPM and RSG are shown in Fig. 8. As expected, CBR increases significantly with increasing fly ash content for both recycled materials. The increase in CBR is attributed to cementation of the particles by the fly ash.

RSG with fly ash had CBRs greater than RPM with fly ash. RPM shows a threefold increase in CBR when mixed with 10% fly ash, whereas RSG shows a six fold increase. Addition of 15% fly ash yields further gains in CBR for both recycled materials. Hatipoglu et al. (2008) and Li et al. (2007) report similar increases in CBR for RPM and RSG mixed with 10% fly ash. Both RPM and RSG had CBR higher than the CBR typically desired for base materials (CBR ≥ 50) (Hunt 1986) when mixed with 10% fly ash (67 for RPM and 183 for RSG). RPM mixed with 15% fly ash had a CBR of 134, whereas RSG mixed with 15% fly ash had a CBR of 334. Thus, both recycled materials have very high bearing strength when mixed with 15% fly ash.

These results are similar to those reported by Wen et al. (2008) for RPM blended with high carbon fly ash. The CBR of RPM increased with increasing fly ash content up to 18% fly ash (from 38 to 212).

5.3 UNCONFINED COMPRESSION STRENGTH

5.3.1 Effect of Fly Ash Content and Curing Time

Unconfined compression strengths (UCS) for RPM and RSG blended with fly ash are summarized in Table 4 and are shown in Fig. 9. The UCS reported in Table 4 are the average of the UCS of duplicate specimens. The UCS for both RPM and RSG increase with increasing fly ash content and, under the same conditions, RSG exhibits higher UCS than RPM. The UCS of RPM and RSG mixed with fly ash also increased with curing time (Fig. 9), with significant increases occurring even after 28 d. The UCS in Table 4 are similar to those reported by Wen et al. (2008) (1.3 to 2.04 MPa for RPM mixed with up to 14% high carbon self-cementing fly ash and curing times up to 14 d).

Mechanistic Empirical Pavement Design Guide (MEPDG) suggests a minimum unconfined compressive strength (28 d cure) of 5.2 MPa for a chemically stabilized base layer and 1.7 MPa for a chemically stabilized subbase layer (ARA 2004). The highest unconfined compressive strength observed in this study was 3.61 MPa (RSG with 15% fly ash). Thus, the RPM and RSG blended with fly ash fall below the minimum suggested UCS for chemically stabilized base layers. The UCS requirement for a subbase layer were met for all but one mixture of RSG and fly ash, but for only one mixture prepared with RPM (15% fly ash and 28 d cure). Even though the UCS criteria are not satisfied for most cases of RPM, field experience (Hatipoglu et al. 2008, Wen et al. 2004, Crovetti 2000, Li et al 2007) has shown that RPM and RSG blended with 10-15% fly ash has more than adequate strength to support construction traffic and other loads commonly applied to base and subbase layers.

5.3.2 Effect of Freeze-Thaw

Summary resilient moduli (SRM) and UCS of base materials with and without fly ash, before and after 5 freeze-thaw cycles, are summarized in Table 5. UCS of RPM and RSG with 10% fly ash before and after 5 freeze-thaw cycles are shown in (Fig. 10). The UCS of RSG increased 18% after 5 freeze-thaw cycles and the UCS of RPM increased by 5%. Zaman and Naji (2003) report similar findings for the UCS of an aggregate base blended with 10% Class C

fly ash (28 d cure). They found that the UCS increased with increasing freeze-thaw cycles (up to 30 cycles). Zaman and Naji (2003) attribute the increase in UCS to accelerated cementitious reactions during thawing.

5.4 RESILIENT MODULUS

5.4.1 Base and Recycled Materials without Fly Ash

Analysis of resilient modulus data indicated deformations measured with internal LVDTs more accurately described deformation of the specimens (see Attachment I). Thus, the resilient moduli presented herein are based on deformations measured with internal LVDTs. The SRM for the Class 5 base, RPM, and RSG, computed in accordance with Procedure Ia of NCHRP 1-28A, are summarized in Table 6, along with the parameters k_1 and k_2 for the resilient modulus power function model (Eq. 4.1). These SRM and parameters correspond to compaction at optimum water content and at maximum dry unit weight.

SRM for Class 5 base, RPM, and RSG are shown in Fig. 11. RPM has the highest SRM (309 MPa) of the three base materials. Alternatively, RSG has the lowest SRM (212 MPa), whereas Class 5 base has a SRM of 236 MPa. The resilient moduli of the base materials do not follow the same hierarchy as observed for CBR (RSG has the highest CBR, followed by RPM and Class 5 base). However, other studies have reported similar differences between M_r and CBR. For example, Wen et al. (2007 and 2008) report CBRs for RPM that are lower than CBRs for Wisconsin Grade 2 gravel, whereas the resilient moduli had the opposite relationship. This difference, however, may be explained by the nature of the two tests. Resilient modulus testing induces small deformations to evaluate stiffness, whereas a CBR test induces larger deformations to assess bearing strength.

MEPDG reports typical ranges of resilient modulus for various materials based on their USCS classification (ARA 2004). The SRM for Class 5 base is higher than the suggested ranges (165 to 228 MPa) for materials having the same USCS classification (SP). Similarly, the SRM for RPM is higher than the suggested range (245 to 279 MPa) for materials classified as GW-GM. The SRM for RSG falls within the suggested range (193 to 259 MPa) for materials classified as SM. Even though Class 5 base has a low CBR, SRM of Class 5 base is typical of a base aggregate. For example, Kim and Labuz (2007) performed resilient modulus tests on CR 53, an aggregate base conforming to MnDOT's Class 5 specifications that was obtained from a full-depth reclamation (FDR) project in Wright County, MN. A SRM of 182 MPa was computed for the CR 53 aggregate base using data from Kim and Labuz (2007).

The high resilient modulus for RPM is attributed to its RAP content (50%). For example, Kim and Labuz (2007) performed resilient modulus tests on an aggregate base blended with varying RAP contents (0-75%), with the CR 53 material used as base aggregate. All blends of aggregate base and RAP had resilient moduli higher than the aggregate base alone, which explains the high SRM for RPM when compared to materials of similar USCS classification. Furthermore, increasing the RAP content for CR 53 aggregate resulted in increasing resilient modulus.

Average plastic strains were calculated for all base materials during resilient modulus testing (Table 6) using data from the internal LVDTs. Plastic strain for a resilient modulus test was calculated as the sum of the plastic strains for each loading sequence, excluding the plastic strains in the conditioning phase (Sequence 0). Class 5 base and RSG showed average plastic

strains of 3.35% and 3.33%, respectively, whereas RPM showed a plastic strain of only 1.94%. These results are different from those in Wen et al. (2008 and 2009) and Kim and Labuz (2007). They indicate that plastic strains for RPM are typically higher than plastic strains of typical aggregate base materials.

The plastic strains for RPM may be higher or lower than those of conventional base aggregates, depending on the type of aggregate. For example, the plastic strains ($\varepsilon_{plastic}$) for two RPMs and two conventional base aggregates, along with other material properties, are summarized in Table 7. The Class 5 base and WI RPM are the materials used in this study. The crushed granite aggregate and MnROAD RPM (Wen et al. 2009) were obtained from a research project at the MnROAD facility in Minnesota. The plastic strain of both RPMs (2.77% for MnROAD RPM and 1.94% for WI RPM) is lower than that of Class 5 base (3.35%), but is significantly higher than the plastic strain of crushed granite aggregate (0.71%). The high plastic strain for Class 5 base is attributed to its large sand fraction (59%) compared to crushed granite aggregate (30%).

5.4.2 Effect of Fly Ash Content and Curing Time

Summary resilient moduli for RPM and RSG blended with fly ash are summarized in Table 6, along with the parameters k_1 and k_2 for the resilient modulus power function model (Eq. 4.1). The resilient modulus of specimens blended with fly ash showed no apparent dependency on bulk stress (i.e. k_2 in Eq 4.1 was close to zero). An example of a resilient modulus test showing no trend is shown in Fig. 12. A linear regression analysis was performed on resilient modulus data for all specimens with fly ash to determine if a statistically significant relationship existed between resilient modulus and bulk stress. In this analysis, the probability of falsely rejecting the null hypothesis (slope is zero), referred to as the p-value, is determined and compared to the significance level, α. A p-value higher than α indicates the slope is statistically no different from zero and the resilient modulus is independent of bulk stress. Results of the regression analysis are summarized in Table 8. Two thirds of the tests showed no stress dependency for $\alpha = 0.05$, the significance level commonly used in hypothesis testing (Berthouex and Brown 2002). In those cases where k_2 was not found to be statistically insignificant, the p-value was only slightly smaller than α, suggesting only a slight dependency on bulk stress. Furthermore, the analysis was based on all bulk stresses employed in the resilient modulus test protocol, with some significantly higher than that would be encountered in a pavement structure. Thus, the resilient moduli of the materials blended with fly ash are described herein with a single modulus. This approach is consistent with MEPDG, which recommends a constant modulus for chemically stabilized materials (ARA 2004).

As in the CBR test, addition of fly ash resulted in a significant increase in SRM for both materials, with the RSG exhibiting higher SRM than RPM. Specimens cured for 28 days were used because MEPDG specifies properties at 28 d cure for other chemically stabilized materials. Summary resilient moduli for RPM and RSG blended with fly ash are shown in Fig. 13 as a function of fly ash content. SRM increases with increasing fly ash content. This finding is consistent with Wen et al. (2008). They report an increase in resilient modulus of RPM as the fly ash content was increased from 10 to 18%. Increasing the fly ash content causes more cementation of the particles, yielding specimens with higher stiffness. Diminishing returns are likely to be realized at fly ash contents higher than those described here. Additional testing is

needed to assess the fly ash content beyond which stiffness no longer increases. Moreover, higher fly ash contents may not necessarily be beneficial. For example, a series of cold in-place recycling (CIR) test sections mixed with varying Class C fly ash contents were constructed by the Kansas Department of Transportation. Test sections with higher fly ash contents exhibited more initial cracking than those with lower fly ash contents (Cross and Young 1997). A laboratory study confirmed an increase in brittleness (i.e. asphalt layer more prone to fatigue and thermal cracking) for CIR and fly ash mixtures as a result of increasing fly ash contents (Cross and Young 1997).

The effect of curing time on the SRM of RPM and RSG with fly ash is shown in Fig. 14. The data in Fig. 14 are from specimens blended with 10% fly ash that were cured for 7, 28, and 56 d. SRM increased with curing time for both RPM and RSG, with the increase rate being larger between 7 and 28 d. SRM for RPM increases an additional 250 MPa for 56 d of curing, whereas a more pronounced increase is observed for RSG (1000 MPa increase) for 56 d of curing. Wen et al (2008) also report an increase in resilient modulus with curing time for RPM mixed with fly ash.

Resilient moduli based on internal LVDT measurements for materials blended with fly ash were not found in the literature. However, a range of resilient moduli for chemically stabilized soils (Table 9) is reported by MEPDG (ARA 2004). The range of SRM for both materials blended with fly ash is similar to the ranges for materials stabilized with other chemicals. For example, resilient moduli for materials stabilized with lime-cement-fly ash range from 3500 to 13800 MPa, whereas resilient moduli of soil cement ranges from 350 to 6900 MPa.

The addition of fly ash not only increased resilient modulus, but also resulted in smaller plastic strains for both recycled materials (Table 6). Plastic strains ranged from 0.5 to 1.22% for RPM with fly ash, whereas plastic strains ranged from 0.62 to 2.18% for RSG with fly ash. Wen et al. (2008) also report a decrease in plastic strains for RPM specimens blended with fly ash.

5.4.3 Effect of Freeze-Thaw

The effect of freeze-thaw cycling on the SRM is shown in Fig. 15. Freeze-thaw cycling has a small effect on SRM of Class 5 base (7% change), RPM (15% change), or RSG (5% change) with or without fly ash. There is no consistent effect of freeze-thaw cycling on materials without fly ash; the SRM of Class 5 base decreased slightly (7%), whereas RPM and RSG increased slightly (14% and 1%). Rosa (2006) suggests a reduction of 20 to 66% for various coarse and fine grained materials. Freeze-thaw data on RPM alone were not found in the literature. RPM and RSG mixed with fly ash decreased modestly (15% and 5%). The decrease in SRM is smaller than the decreases reported by Rosa (2006) for RPM and RSG mixed with fly ash (7 to 42%).

The small effect of freeze-thaw cycling on the SRM is consistent with the small volume changes recorded during freezing and thawing, which cause little change in soil structure (Simosen et al. 2002). No net changes were observed for Class 5 base and RPM, whereas the volume change for RSG ranged from 0.4 to 0.6%. RSG and RPM with fly ash had no net increases in volume. Rosa (2006) also reports no net volume changes for RPM and RSG mixed with fly ash. The small decrease in SRM for RPM and RSG with fly ash is probably due to the breaking of cement bonds during freezing.

5.4.4 Relationship between SRM and UCS

The relationship between the SRM and UCS for RPM and RSG blended with fly ash is shown in Fig. 16. A strong relationship exists between SRM and UCS, which suggests that the SRM of RPM and RSG blended with fly ash could be estimated from a UC test. In particular, SRM can be estimated by:

$$SRM = 3280 \; UCS \tag{5.1}$$

A similar relationship with the initial tangent modulus (E_i) and the secant modulus at 50% of UCS (E_{50}), as obtained from the static UC test, are shown in Fig. 17. E_{50} was determined by dividing half of the UCS by the corresponding strain at that stress level, whereas the E_i was computed by modeling the stress-strain behavior using the hyperbolic equation (Krizek 1967):

$$\sigma = \frac{\varepsilon}{a + b\varepsilon} \tag{5.2}$$

where σ is axial stress, ε is axial strain, a and b are empirical coefficients, and $1/a$ is the initial tangent modulus (E_i). Eq. 5.2 was fit to the UCS data to determine E_i. The SRM of RSG and RPM blended with fly ash can also be estimated by:

$$SRM = 5.7 \; E_i \tag{5.3}$$

or by:

$$SRM = 5.7 \; E_{50} \tag{5.4}$$

The E_i and E_{50} have the same relationship with SRM (Eq. 3 and 4), which suggests that the stress-strain relationship of these materials are highly linear. The R^2 is 0.93 for Eq. 5.2, 0.65 for Eq. 5.3, and 0.58 for Eq. 5.4. Thus, UCS should provide a more reliable estimate of SRM rather than E_i or E_{50}.

6. SUMMARY AND CONCLUSIONS

This laboratory investigation dealt with the influence of fly ash addition and freeze-thaw cycling on the engineering properties of two recycled roadway materials, recycled pavement material (RPM) and recycled road surface gravel (RSG). The objectives were to assess the engineering properties of recycled materials with and without fly ash and to study how freezing and thawing may affect the engineering properties. California bearing ratio, resilient modulus, and unconfined compression tests were conducted on RPM and RSG with and without fly ash. Resilient modulus and unconfined compression tests were also performed on specimens with and without fly ash after 5 freeze-thaw cycles. Two fly ash contents (10 and 15%), corresponding to typical application ranges used in practice, were used and three curing times (7, 28, and 56 d) were evaluated. Class 5 base, with a conventional base material gradation employed in Minnesota, was used as a control.

RSG and RPM had CBRs greater than that of Class 5 base, but all three materials had CBR less than typically desired for base course material (CBR $\geq$ 50). Addition of fly ash to RSG or RPM significantly increased the CBR, and the CBR increased with increasing fly ash content for both materials. Adding fly ash increased the CBR of the RSG by at least 6 times and the CBR of RPM by at least 3 times. Moreover, addition of fly ash (10 and 15%) to RPM and RSG resulted in CBRs greater than the CBR typically desired for base course.

Unconfined compression tests were not conducted on Class 5 base, RPM, and RSG alone because they are granular materials with relatively low fines content (<15%) and therefore little cohesion. The UCS of RPM and RSG mixed with fly ash increased with increasing fly ash content. The UCS for both materials also increased with curing time, with significant increases occurring even after 28 d. RPM and RSG mixed with fly ash had UCS lower than the minimum suggested UCS for a chemically stabilized base layer (5.2 MPa), but field experience reported by others has shown RPM and RSG mixed with fly ash have more than adequate strength to support construction traffic and other loads commonly applied to base and subbase layers. In addition, the UCS is maintained even when the RPM and RSG are exposed to freezing. After 5 freeze-thaw cycles, the UCS of RPM and RSG mixed with fly ash was higher (5 and 18%) than the UCS not subjected to freeze-thaw cycling.

RPM had a higher summary resilient modulus (SRM) than Class 5 base, whereas the SRM for RSG was slightly lower than that of Class 5 base. RPM also exhibited smaller plastic strains during M_r testing than Class 5 base, whereas RSG showed similar plastic strains to Class 5 base. The SRM for RPM and RSG mixed with fly ash were independent of bulk stress and were described by a single modulus. Addition of fly ash significantly increased the SRM of RPM and RSG (at least a factor of 6 and 29, respectively), and the SRM increased as the fly ash content was increased for both materials. SRM also increased with curing time, with the rate of increase being largest between 7 and 28 d of curing. Plastic strains for RPM and RSG with fly ash were smaller than the plastic strains of the recycled materials alone.

Freeze-thaw cycling had a small effect on SRM of Class 5 base (7% change), RPM (15% change), or RSG (5% change) with or without fly ash, with no consistent effect for materials mixed with fly ash.

A strong relationship (R^2=0.93) was found for SRM and UCS of RPM and RSG mixed with fly ash, suggesting that the resilient moduli of these materials can be estimated from a UC test. SRM can be estimated by multiplying UCS by 3280. Recommended strengths and stiffness for the RPM and RSG are summarized in Table 10. The CBRs in Table 10 correspond to 7 d of

cure to simulate condition shortly after construction, whereas the SRM and UCS correspond to 28 d cure because the material-fly ash mixture will continue to gain strength and stiffness during that period of time. The SRM_{F-T} in Table 10 corresponds to the stiffness of the recycled materials subjected to freeze-thaw cycling due to seasonal changes (28 d cure).

REFERENCES

Acosta, H. A. (2002). "Stabilization of Soft Subgrade Soils Using Fly Ash," *MS Thesis,* University of Wisconsin-Madison, Madison, WI.

AASHTO (2001). *Standard Specifications for Transportation Materials and Methods of Sampling and Testing, 21ˢᵗ Ed.,* American Association of State Highway and Transportation Officials, Washington, D.C., *Part I, Specifications,* M 147-65.

AASHTO-AGC-ARTBA Joint Committee (1998). "Report of Cold Recycling of Asphalt Pavements," Task Force 38 Report. American Association of State Highway and Transportation Officials, Washington, D.C.

ARA (2004). "Guide for Mechanistic-Empirical Design on New and Rehabilitated Pavement Structures," NCHRP Project 1-37A. Prepared for National Cooperative Highway Research Program, Washington, D.C.

Baugh, J. (2008). "Suitability of Cement Kiln Dust for Reconstruction of Roads," *MS Thesis*, University of Wisconsin-Madison, Madison, WI.

Bemanian, S., Polish, P., and Maurer, G. (2006). Cold in-place recycling and full-depth reclamation projects by Nevada department of transportation, *Journal of the Transportation Research Board,* 1949, pp. 54-71.

Berthouex, P. and Brown, L. (2002). *Statistics for Environmental Engineers.* 2ⁿᵈ Ed., CRC Press, Boca Raton, Fla.

Bin-Shafique, S., Edil, T., Benson, C., and Senol, A. (2004). Incorporating a fly ash stabilized layer into pavement design, *Geotechnical Engineering*, 157(GE4), pp. 239-249.

Button, J., Little, D., and Estakhri, C. (1994). "Hot In-Place Recycling of Asphalt Concrete," NCHRP Synthesis of Highway Practice 193. National Cooperative Highway Research Program, Washington, D.C.

Button, J., Estakhri, C., and Little, D. (1999). Overview of hot in-place recycling of bituminous pavements, *Journal of the Transportation Research Board,* 1684, pp. 178-185.

Cooley, D. (2005). "Effects of Reclaimed Asphalt Pavement on Mechanical Properties of Base Materials," *MS Thesis*, Brigham Young University, Provo, UT.

Cross, S. A. and Young, D. A. (1997). Evaluation of type C fly ash in cold in-place recycling, *Journal of the Transportation Research Board,* 1583, pp. 82–90.

Crovetti, J. (2000). Construction and performance of fly ash-stabilized cold in-place recycled asphalt pavement in Wisconsin, *Journal of the Transportation Research Board,* 1730, pp. 161-166.

Edil, T. B., Benson, C., Bin-Shafique, M., Tanyu, B., Kim, W. and Senol, A. (2002). Field evaluation of construction alternatives for roadways over soft subgrade, *Journal of the Transportation Research Board,* 1786, pp. 36-48.

Epps, J. A. (1990). "Cold-Recycled Bituminous Concrete Using Bituminous Materials," NCHRP Synthesis of Highway Practice 160. National Cooperative Highway Research Program, Washington, D.C.

Hatipoglu, B., Edil, T., and Benson, C. (2008). Evaluation of base prepared from road surface gravel stabilized with fly ash, *ASCE Geotechnical Special Publication,* 177, pp. 288-295.

Hunt, R.E. (1986). *Geotechnical Engineering Techniques and Practices*. McGraw Hill Book Company, NY.

Janz, M. and Johansson, S.-E. (2002). "The Function of Different Binding Agents in Deep Stabilization," Report 9. Swedish Deep Stabilization Research Centre, Linkoping, Sweden.

Jong, D., Bosscher, P., and Benson, C. (1998). Field assessment of changes in pavement moduli caused by freezing and thawing, *Journal of the Transportation Research Board,* 1615, pp. 41-48.

Kearney, E.J. and Huffman, J.E. (1999). Full-depth reclamation process, *Journal of the Transportation Research Board,* 1684, pp.203-209.

Kim, W., Labuz, J., and Dai, S. (2007). Resilient modulus of base course containing recycled asphalt pavement, *Journal of the Transportation Research Board,* 2005, pp. 27-35.

Kuennen, T. (1988). Hot in-place recycling specs developed by ARRA, *Roads and Bridges*, 2(10), pp. 72.

Krizek, R. (1967). Stress-strain behavior of a marine clay, *Proceedings of 1st Southeast Asian Regional Conference on Soil Engineering*, Asian Institute of Technology, Bangkok, Thailand, pp. 95-102.

Li, L., Benson, C. H., Edil, T. B., Hatipoglu, B., and Tastan, E. (2007). Evaluation of recycled asphalt pavement material stabilized with fly ash, *ASCE Geotechnical Special Publication (CD-ROM)*, 169.

Mahoney, J.P., Lary, J.A., Sharma, J., and Jackson, N. (1985). Investigation of seasonal load restriction in Washington State, *Journal of the Transportation Research Board,* 1043, pp. 58-67.

Misra, A., Upadhyaya, S., Gustin, F., Roohanirad, A., and Stokes, J. (2005). Full-depth cold in-place recycling of asphalt pavements using self-cementing fly ash, *Proceedings of World of Coal Ash 2005,* University of Missouri-Kansas, Kansas.

Moosazedh, J., and Witczak, M. (1981). Prediction of subgrade moduli for soil that exhibits nonlinear behavior, *Journal of the Transportation Research Board*, 810, pp. 10-17.

MnDOT (2005). "Standard Specifications for Construction," Minnesota Department of Transportation, St. Paul, MN.

NCHRP (2004). Laboratory determination of resilient modulus for flexible pavement design, *National Cooperative Highway Research Program Research Results Digest*, 285, pp 1-48.

Ping, W. and Ge, L. (1996). Evaluation of resilient modulus of cemented limerock base materials in Florida, *Journal of the Transportation Research Board*, 1546, pp. 1-12.

Rosa, M. (2006). "Effect of Freeze and Thaw Cycling on Soils Stabilized using Fly Ash," *MS Thesis*, University of Wisconsin-Madison, Madison, WI.

Salomon, A. and Newcomb, D. (2000). "Cold In-Place Recycling Literature Review and Preliminary Mixture Design Procedure." Report MN-RC 2000-21. Minnesota Department of Transportation, St. Paul, MN.

Senol, A., Bin-Shafique, M. S., Edil, T.B., and Benson, C. (2003). Use of class C fly ash for stabilization of soft subgrade, *ARI Bulletin of the Istanbul Technical University*, 53(1), pp. 98-104.

Senol, A., Edil, T. B., Bin-Shafique, M. S., Acosta, H. A., and Benson, C. H. (2006). Soft subgrades' stabilization by using various fly ashes, *Resources Conservation and Recycling*, 46(4), pp. 365-376.

Simonsen, E., Janoo, V., and Isacsson, U. (2002). Resilient properties of unbound road material during seasonal frost conditions, *Journal of Cold Region Eng.*, 16(1), pp. 28-50.

Tastan, E. (2005). "Stabilization or Organic Soil using Fly Ash," *MS Thesis*, University of Wisconsin-Madison, Madison, WI.

Taha, R., Ali, G., Basma, A., and Al-Turk, O. (1999). Evaluation of reclaimed asphalt pavement aggregate in road bases and subbases, *Journal of the Transportation Research Board*, 1652, pp. 264-269.

Taha, R., Al-Harthy, A., Al-Shamsi, K., and Al-Zubeidi, M. (2002). Cement stabilization of reclaimed asphalt pavement aggregate for road bases and subbases, *Journal of Materials in Civil Engineering*, 14(3), pp. 239-245.

Tatsuoka, F., Teachavorasinskun, S., Dong, J., Kohata, Y., and Sato, T. (1994). Importance of measuring local strains in cyclic triaxial tests on granular materials, *ASTM Special Technical Publication*, 1213, pp. 288-302.

Wen, H., Tharaniyil, M., Ramme, B. and Krebs, U. (2004). Field performance evaluation of class C fly ash in full-depth reclamation: case history study, *Journal of the Transportation Research Board,* 1869, pp. 41-46.

Wen, H., Baugh, J., and Edil, T. (2007). Use of cementitious high carbon fly ash to stabilize recycled pavement materials as pavement base material, *Proceedings of 86th Annual Meeting (CD ROM)*, Transportation Research Board, Washington, D.C.

Wen, H., Warner, J., and Edil, T. (2008). Laboratory comparison of crushed aggregate and recycled pavement material with and without high-carbon fly ash, *Proceedings of 87th Annual Meeting (DVD)*, Transportation Research Board, Washington, D.C.

Wen, H., Camargo, F., and Edil, T. (2009). Field and laboratory evaluation of sustainable materials at MnROAD, Submitted to 88th Annual Meeting, Transportation Research Board, Washington, D.C.

Wilson, J., Fischer, D., and Martens, K. (1998). "Pulverize, Mill & Relay Asphaltic Pavement & Base Course," Construction Report WI-05-98. Wisconsin Department of Transportation, Madison, WI.

Zaman, M., and Naji, K. (2003). Effect of freeze-thaw cycles on class C fly ash stabilized aggregate base, *Proceedings of 82nd Annual Meeting (CD ROM)*, Transportation Research Board, Washington, D.C.

TABLES

Table 4. Index properties for Class 5 base, RPM, and RSG.

Sample	D_{50} (mm)	C_u	C_c	G_s	w_{opt} (%)	$\gamma_{d\,max}$ (kN/m³)	Asphalt Content (%)	LL (%)	PL (%)	Gravel Content (%)	Sand Content (%)	Fines Content (%)	USCS Symbol	AASHTO Symbol
Class 5 base	2.25	33.3	0.7	2.72	5.0	20.9	-	NP	NP	36.6	59.3	4.1	SP	A-1-a
RPM	3.89	89.5	2.5	2.64	7.5	21.2	4.6	NP	NP	46.0	43.0	10.6	GW-GM	A-1-a
RSG	0.62	27.6	0.5	2.73	6.0	21.4	-	NP	NP	20.9	64.9	14.2	SM	A-1-b

D_{50} = median particle size, C_u = coefficient of uniformity, C_c = coefficient of curvature, G_s = specific gravity, w_{opt} = optimum water content, $\gamma_{d\,max}$ = maximum dry density, LL = liquid limit, PL = plastic limit, NP = nonplastic.

Note: Particle size analysis conducted following ASTM D 422, G_s determined by ASTM D 854, $\gamma_{d\,max}$ and w_{opt} determined by ASTM D 698, USCS classification determined by ASTM D 2487, AASHTO classification determined by ASTM D 3282, asphalt content determined by ASTM D 6307, and Atterberg limits determined by ASTM D 4318.

Table 5. Columbia fly ash physical properties and chemical composition (from Tastan 2005).

Parameter	Columbia	Typical Class C
SiO_2 , %	31.1	40
Al_2O_3 , %	18.3	17
Fe_2O_3 , %	6.1	6
$SiO_2 + Al_2O_3 + Fe_2O_3$, %	55.5	63
CaO , %	23.3	24
MgO , %	3.7	2
SO_3 , %	-	3
CaO/SiO_2	0.8	-
$CaO/(SiO_2+Al_2O_3)$	0.4	-
Loss on Ignition, %	0.7	6
Fineness, amount retained on #325 sieve, %	12	-

Table 3. Maximum dry unit weights and optimum CBRs for Class 5 base, RPM, and RSG with and without fly ash.

Material	Fly Ash Content (%)	Optimum Water Content* (%)	Maximum Dry Unit Weight (kN/m^3)	CBR (%)
Class 5 base	0	5.0	20.9	10
RPM	0	7.5	21.2	22
	10	8.5	20.4	67
	15	9.5	20.1	134
RSG	0	6.0	21.4	31
	10	7.0	21.4	183
	15	7.5	21.2	334

* Optimum water content for dry unit weights.

Table 4. Summary of unconfined compressive strengths of RPM and RSG blended with fly ash.

Material	Fly Ash Content (%)	Curing Time (d)	Unconfined Compressive Strength (MPa)	Initial Tangent Modulus (MPa)
RPM	10	7	0.78	390
		28	1.02	526
		56	1.13	651
	15	7	1.50	590
		28	2.26	919
RSG	10	7	1.41	239
		28	1.79	1078
		56	2.45	1450
	15	7	3.30	1608
		28	3.61	2521

Table 5. SRM and UCS of base materials with and without fly ash before and after 5 freeze-thaw cycles (28 d cure).

Material	Fly Ash Content (%)	SRM (MPa)		SRM $_{after}$ / SRM $_{before}$	UCS (MPa)		UCS$_{after}$ / UCS$_{before}$
		Before	After		Before	After	
Class 5 base	0	236	220	0.93	-	-	-
RPM	0	309	353	1.14	-	-	-
	10	2702	2293	0.85	1.02	1.07	1.05
RSG	0	212	214	1.01	-	-	-
	10	7219	6872	0.95	1.79	2.11	1.18

Table 6. Summary resilient modulus and power model fitting parameters k_1 and k_2 (Eq. 4.1) for base materials with and without fly ash.

Material	Fly Ash Content (%)	Curing Time (d)	External			Internal			Plastic Strain (%)	SRM_{INT}/SRM_{EXT}
			k_1	k_2	SRM (MPa)	k_1	k_2	SRM (MPa)		
Class 5 base	0	-	18.3	0.422	174	13.6	0.534	236	3.35	1.4
RPM	0	-	33.5	0.352	220	49.2	0.344	309	1.94	1.4
	10	7	122.7	0.241	443	1753	0	1753	0.89	4.0
		28	194.7	0.190	537	2702	0	2702	0.80	5.0
		56	198.5	0.185	533	2947	0	2947	0.77	5.5
	15	7	239.5	0.180	625	4477	0	4477	0.50	7.2
		28	293.9	0.151	658	6816	0	6816	1.22	10.4
RSG	0	-	23.0	0.384	179	17.0	0.473	212	3.33	1.2
	10	7	158.1	0.218	507	5785	0	5785	2.18	11.4
		28	163.5	0.238	582	7219	0	7219	0.70	12.4
		56	206.0	0.204	614	8183	0	8183	0.71	13.3
	15	7	114.4	0.289	536	10118	0	10118	1.08	18.9
		28	197.9	0.228	667	12189	0	12189	0.62	18.3

Note: Bulk stress (θ) in terms of kPa in Eq. 4.1.

Table 7. Plastic strains, along with other material properties, for two RPMs and two conventional base aggregates.

Material	Gravel (%)	Sand (%)	Fines (%)	γ_d (kN/m^3)	Relative Density (%)	SRM (MPa)	$\varepsilon_{plastic}$ (%)
Class 5 base	37	59	4	20.9	100	236	3.35
Crushed granite aggregate	68	30	2	21.2	97.5*	238	0.71
MnROAD RPM	40	56	4	19.6	97.5*	287	2.77
WI RPM	46	43	11	21.2	100	309	1.94

* Modified Proctor

Table 8. Slopes and p statistics from linear regression analysis for SRM of RPM and RSG with fly ash.

Material	Fly Ash Content (%)	Curing Time (d)	Trial	k_2	p value
RPM	10	7	1	0.036	0.528
			2	0.083	0.316
	10	28	1	-0.058	**0.006***
			2	-0.103	0.380
	10	56	1	-0.062	0.051
			2	-0.084	0.301
	15	7	1	-0.043	0.179
			2	-0.041	0.305
	15	28	1	-0.027	0.131
			2	-0.026	**0.038***
			3	-0.029	**0.002***
RSG	10	7	1	0.035	0.314
			2	-0.032	**0.010***
	10	28	1	-0.026	**0.045***
			2	-0.026	**0.034***
	10	56	1	-0.023	0.293
			2	-0.024	0.849
	15	7	1	0.019	**0.027***
			2	0.007	0.072
	15	28	1	0.015	0.146
			2	-0.016	0.626

Table 9. Typical resilient moduli for chemically stabilized soils (ARA 2004).

Chemically Stabilized Material	Elastic or Resilient Modulus (MPa)		
	Min	Max	Typical
Lean concrete	10400	17300	13800
Cement stabilized aggregate	4800	10400	6900
Open graded cement stabilized aggregate	-	-	5200
Soil cement	350	6900	3500
Lime-cement-fly ash	3500	13800	10400
Lime stabilized soils*	207	414	311

*Reactive soils with at least 25% fines and a plasticity index of at least 10.

Table 10. Recommended strengths and stiffness for recycled materials with and without fly ash.

Material	Fly Ash Content (%)	CBR (%)	SRM (MPa)	SRM$_{F-T}$ (MPa)	UCS (kPa)
RPM	0	20	310	310	-
	10	70	2700	2300	1000
	15	130	6800	5800	2300
RSG	0	30	210	210	-
	10	180	7200	6900	1800
	15	330	12000	11000	3600

FIGURES
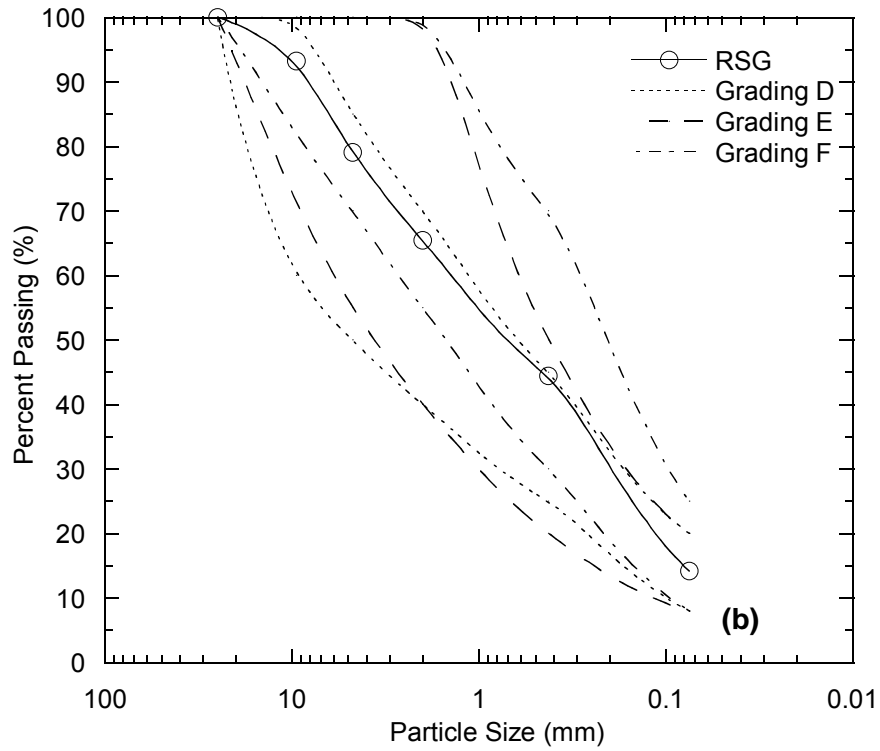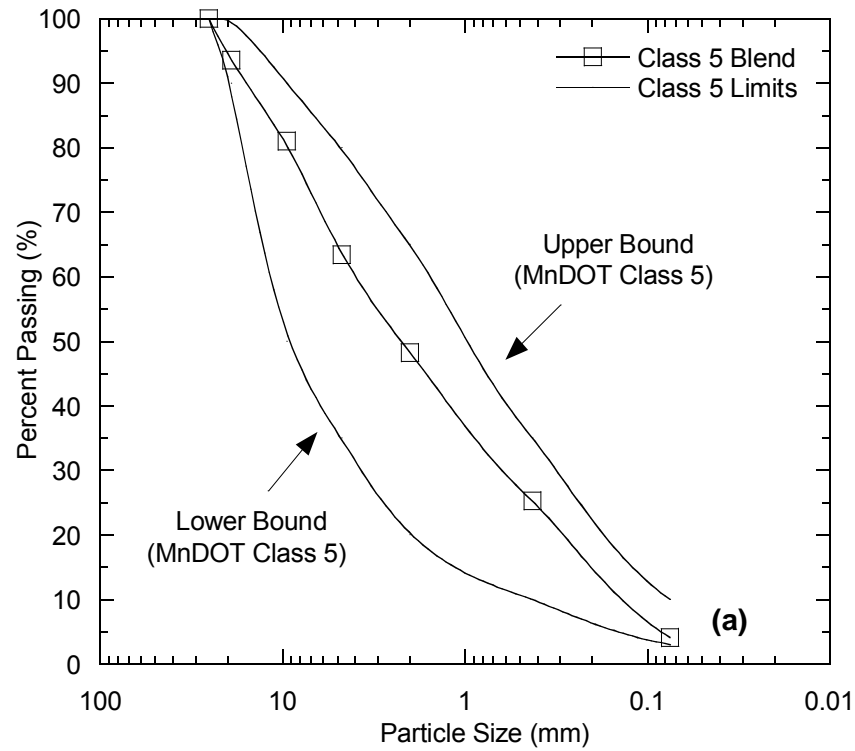
Fig. 1. Particle size distribution for Class 5 base used in this study with MnDOT Class 5 specifications (a) and RSG with AASHTO surface course specifications (b).
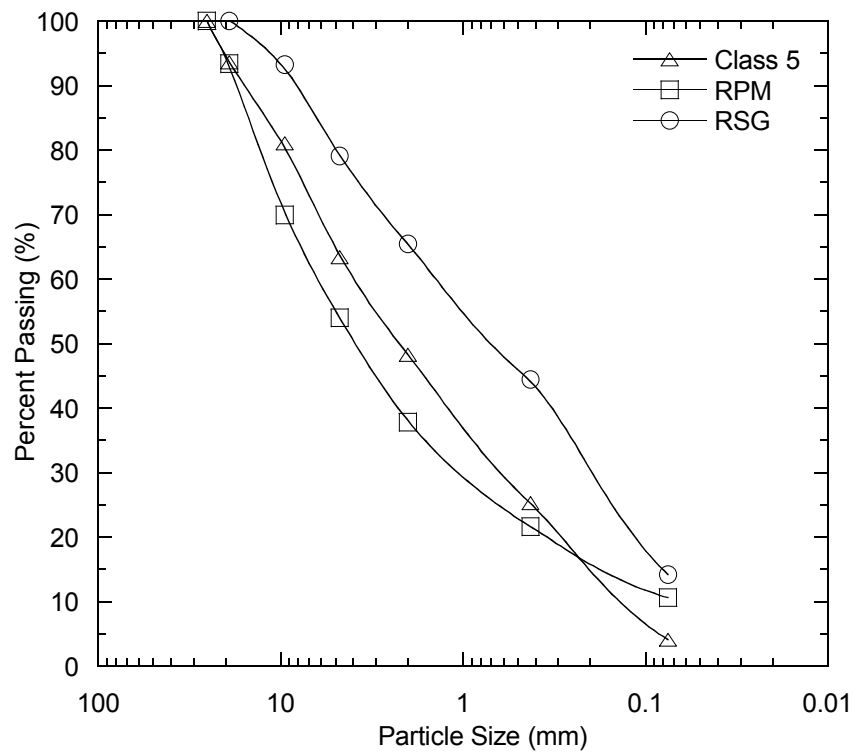
Fig. 2. Particle size distributions for Class 5 base, RPM, and RSG.
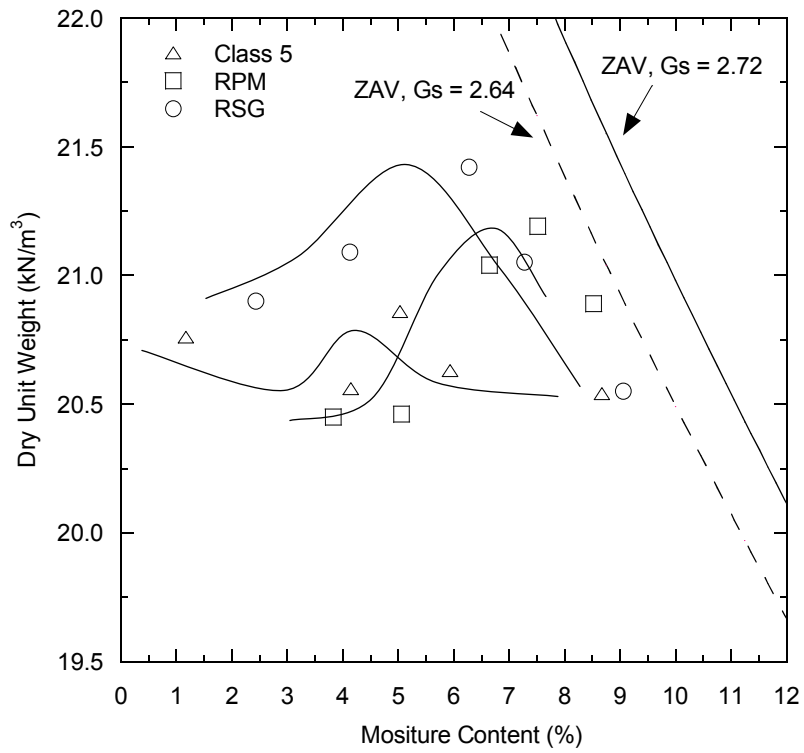
Fig. 3. Compaction curves for Class 5 base, RPM, and RSG for standard compactive effort.

Fig. 4. Internal LVDT clamps mounted on a resilient modulus specimen.
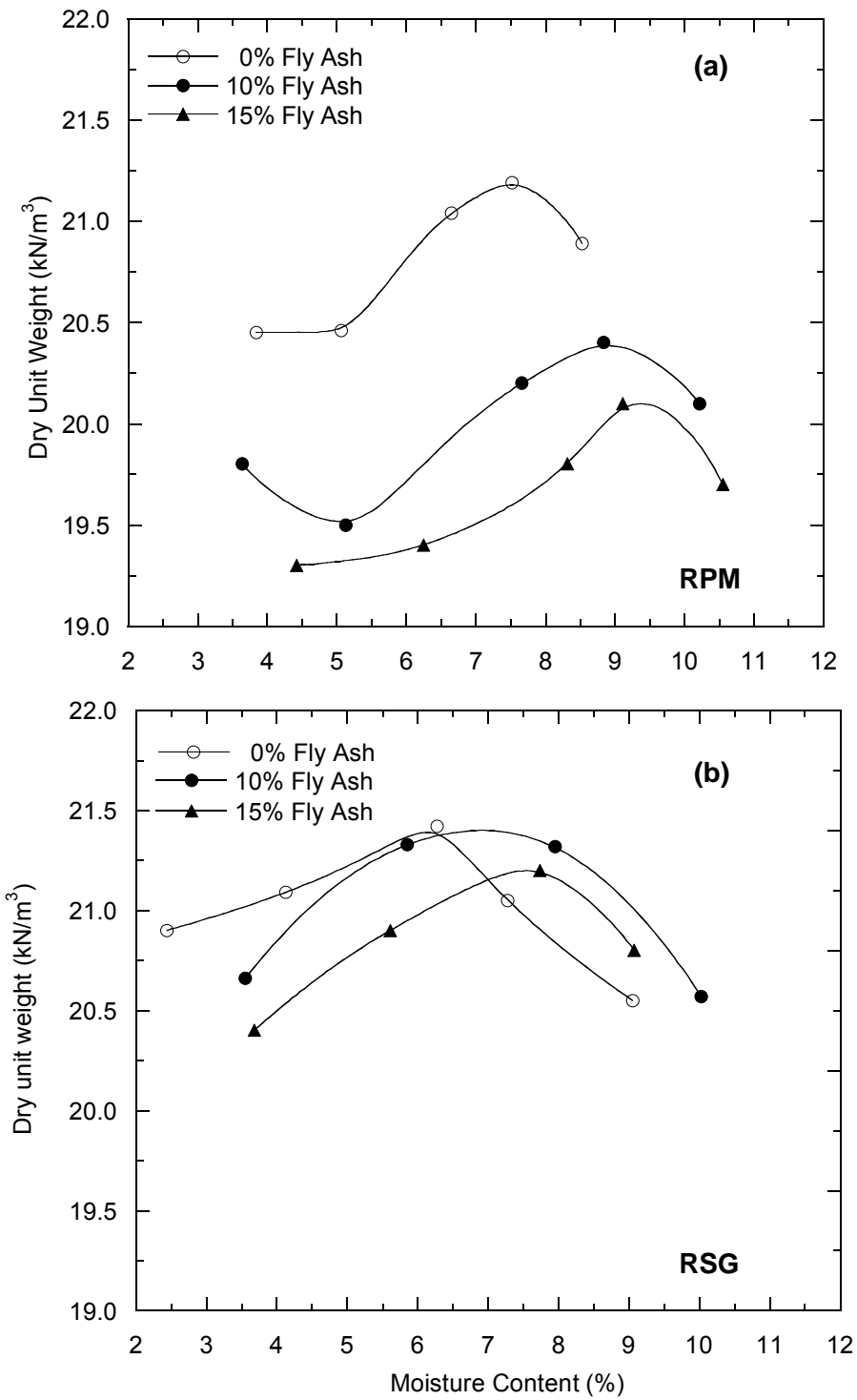
Fig. 5. Compaction curves for (a) RPM and (b) RSG blended with different fly ash contents.
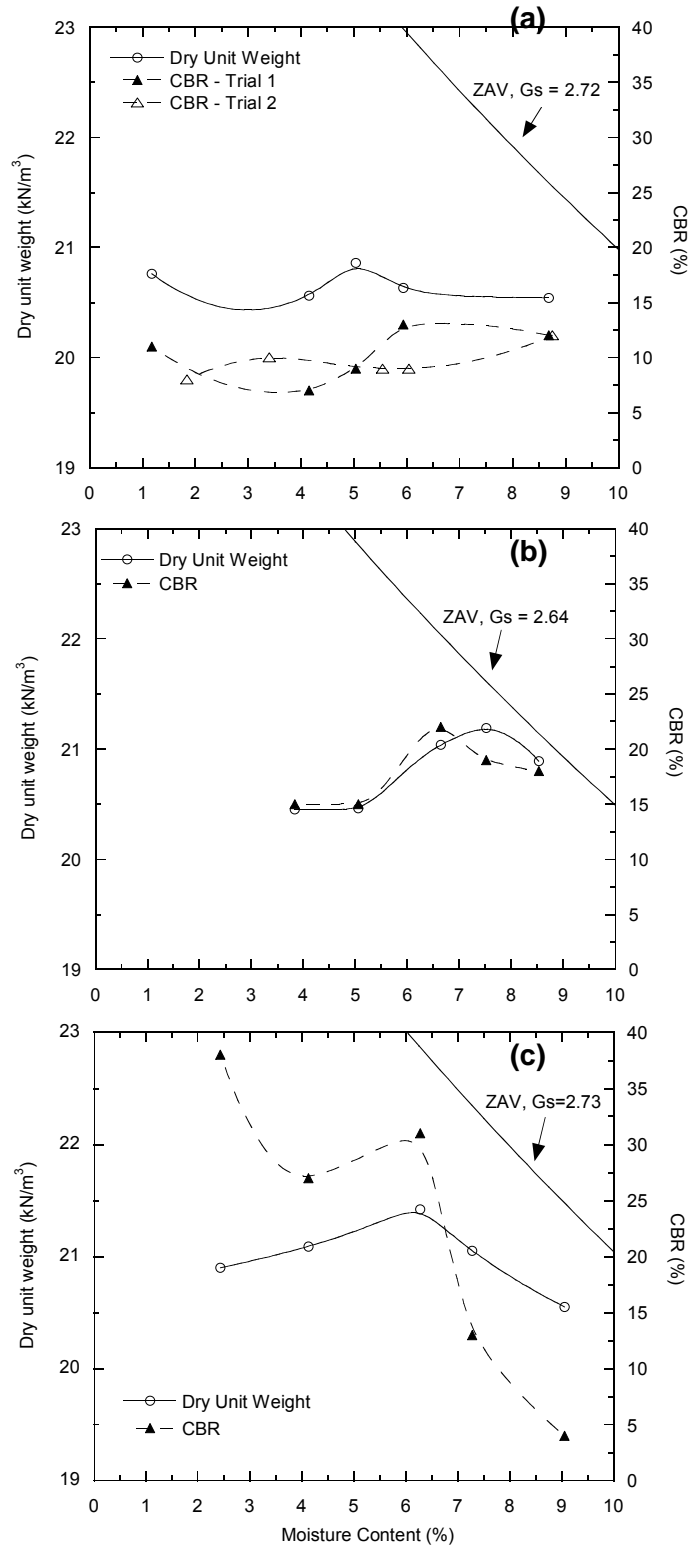
Fig. 6. CBR and dry unit weight with moisture content for (a) Class 5 base, (b) RPM, and (c) RSG.

Fig. 7. Photograph of gravel content from a sample of Class 5 base.
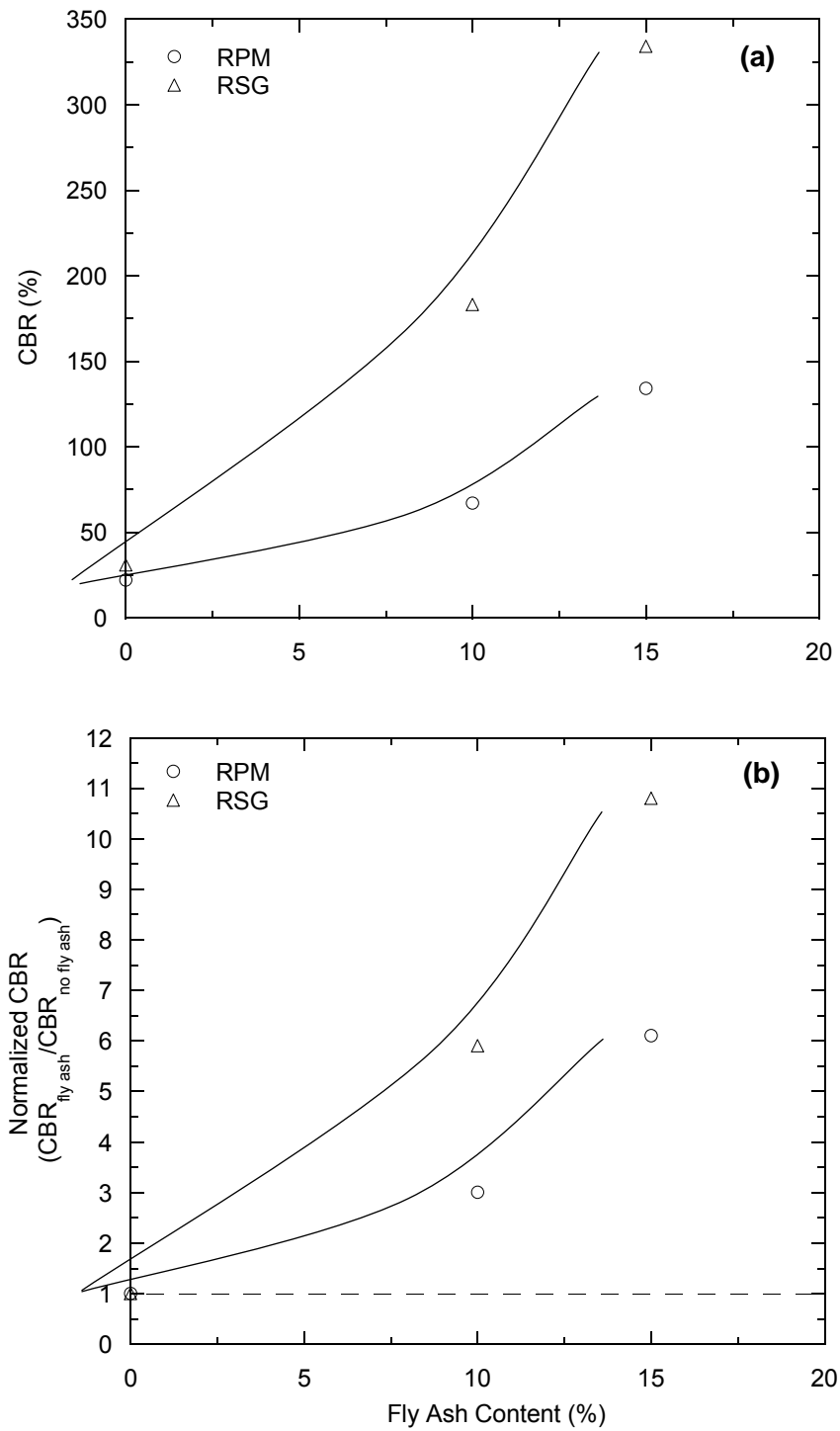
Fig. 8. CBR (a) and normalized CBR (b) with fly ash content for RSG and RPM.
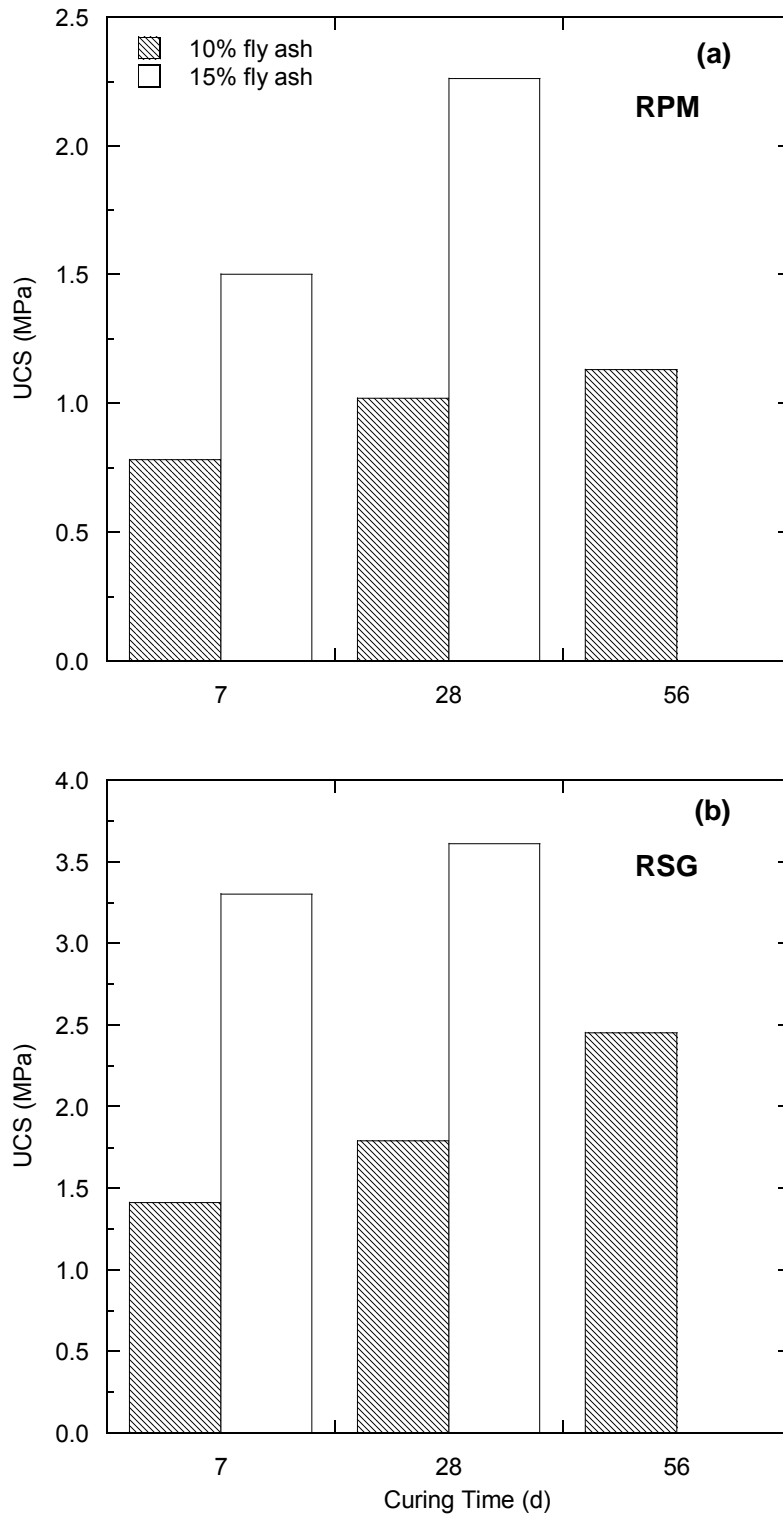
Fig. 9. Unconfined compression strength for RPM (a) and RSG (b) blended with fly ash.
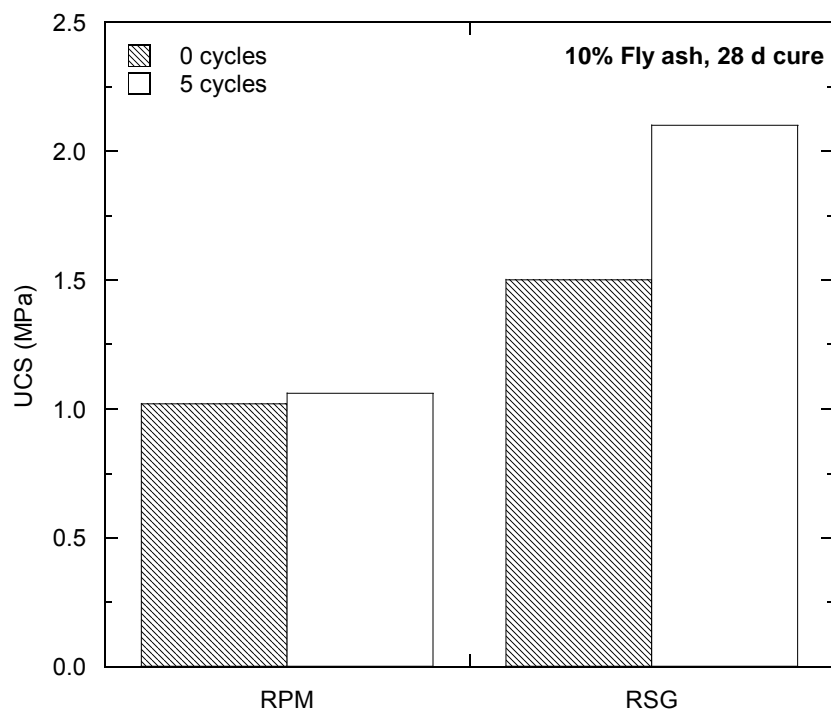
Fig. 10. Freeze-thaw effects on UCS of recycled materials with 10% fly ash (28 d cure).
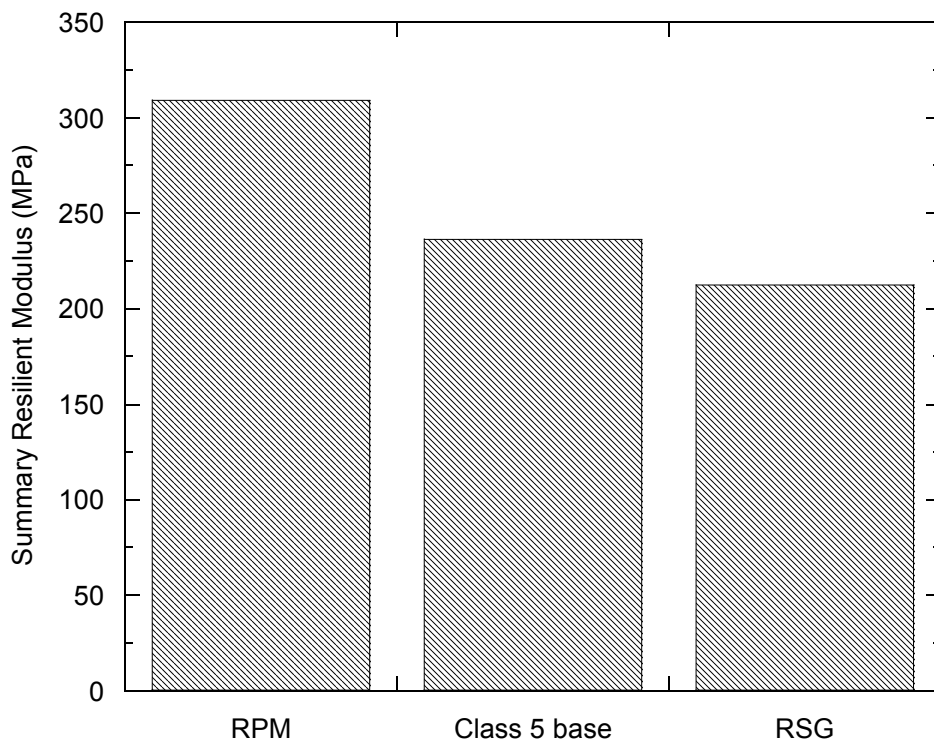
Fig. 11. Summary resilient modulus for Class 5 base, RPM, and RSG.
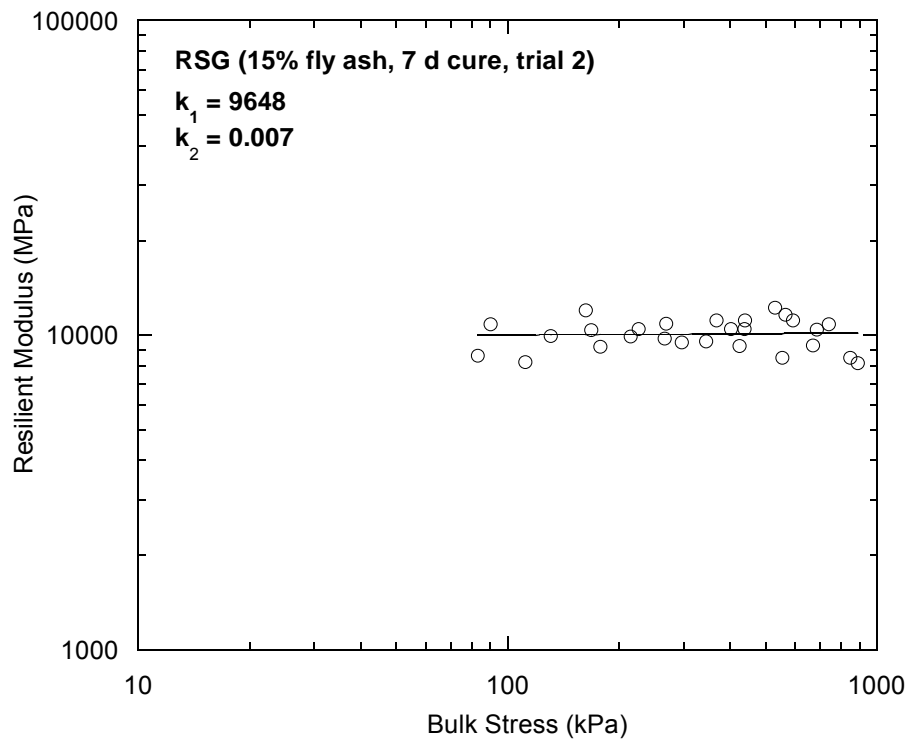
Fig. 12. Resilient modulus test showing no trend in resilient modulus with bulk stress (RSG with 15% fly ash, 7 d cure, trial 2).
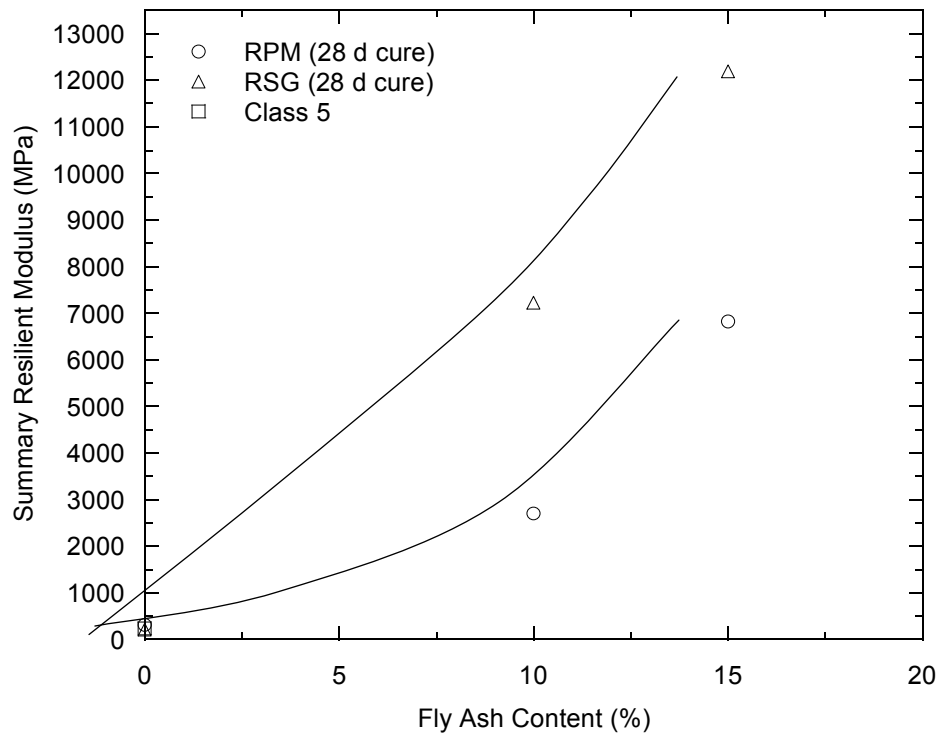
Fig. 13. Summary resilient modulus with fly ash content for recycled materials.
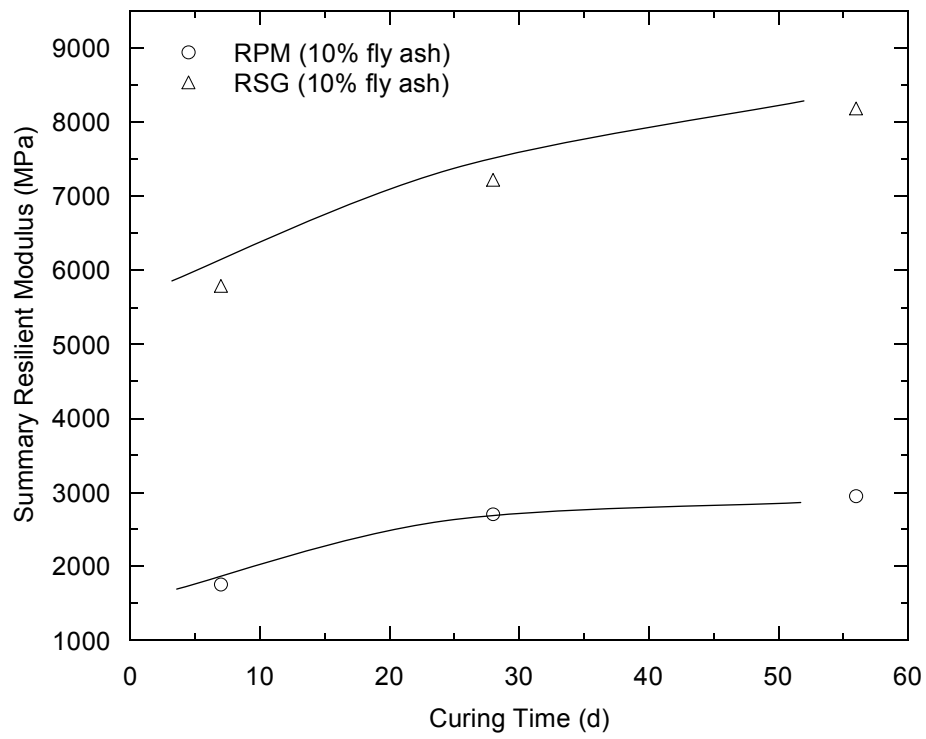
Fig. 14. Summary resilient modulus with curing time for recycled materials with 10% fly ash.
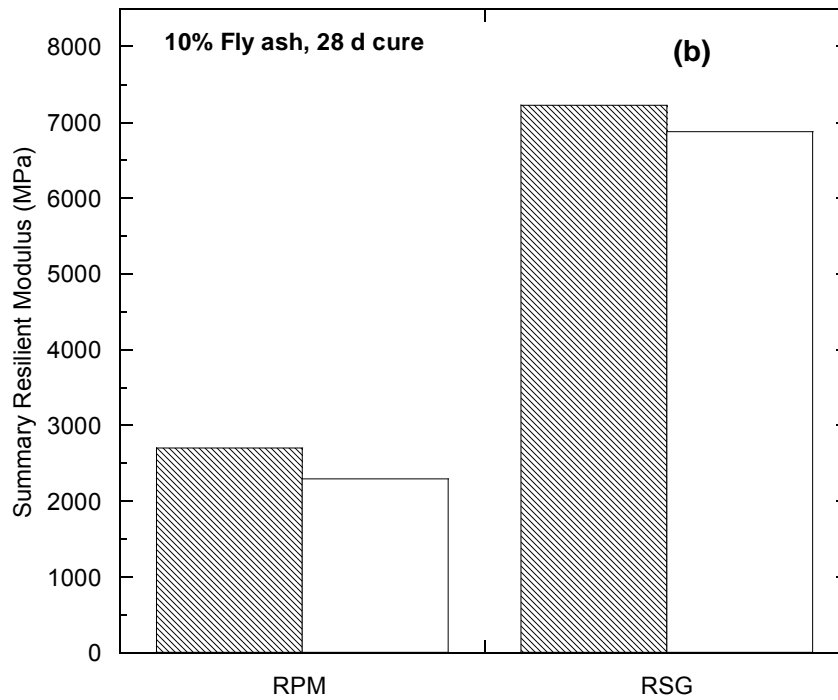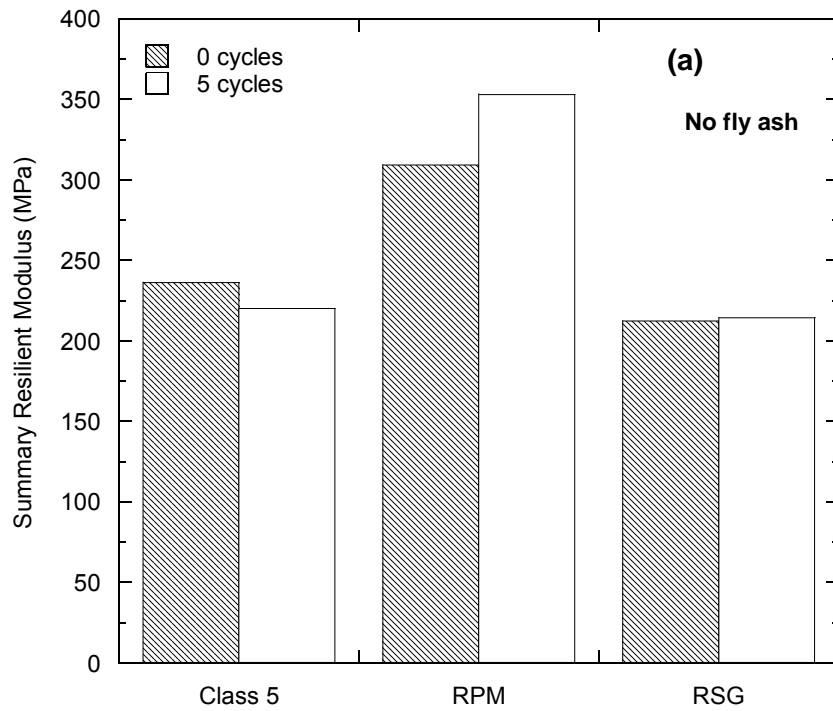
Fig. 15. Summary resilient modulus of base materials (a) and recycled materials with 10% fly ash (28 d cure) (b) before and after 5 freeze-thaw cycles.
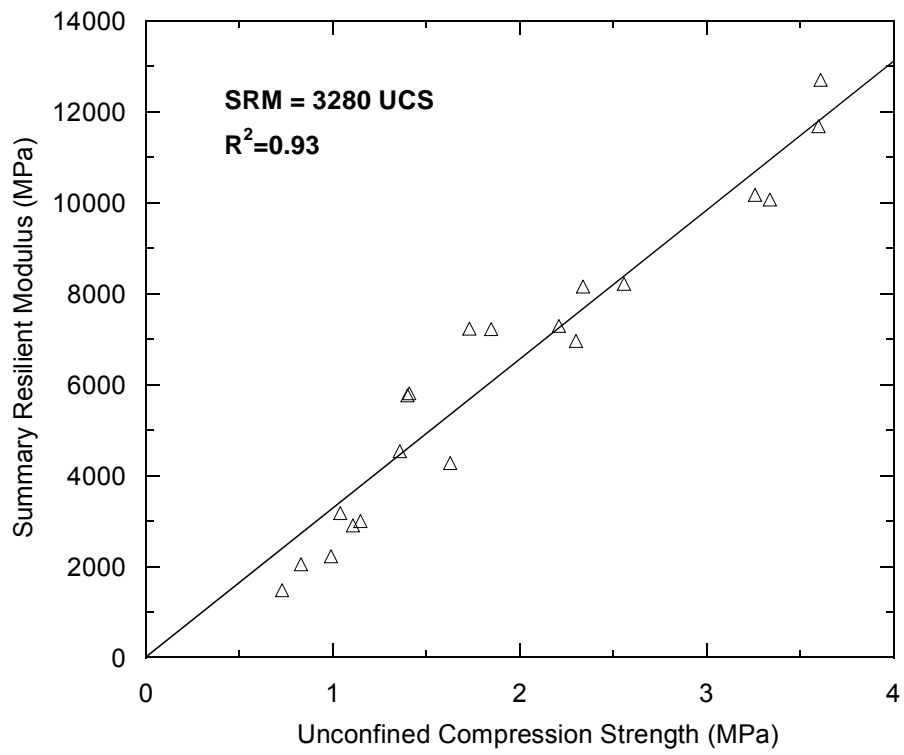
Fig. 16. SRM as a function of UCS for all recycled material specimens blended with fly ash.
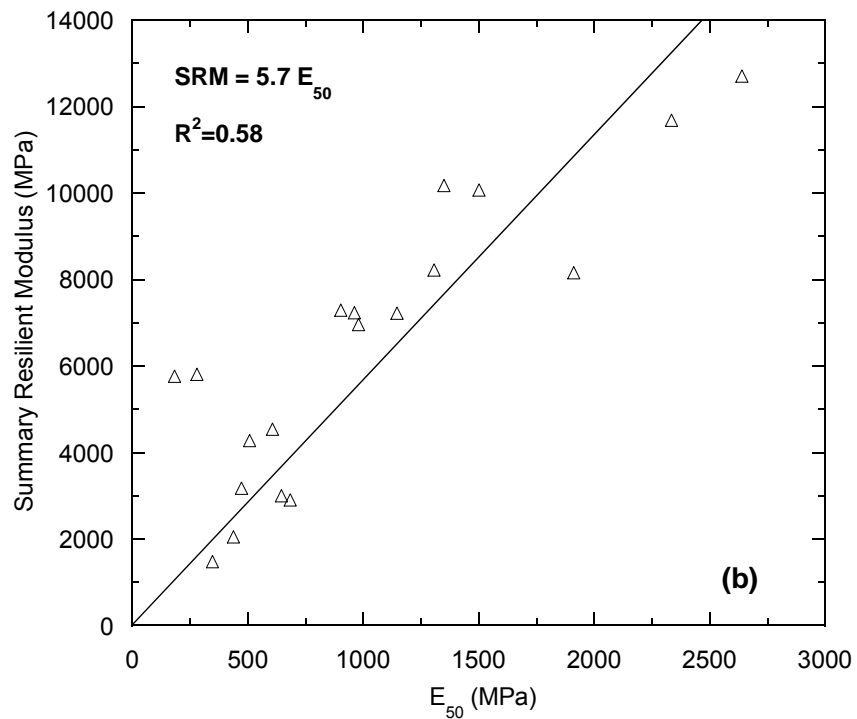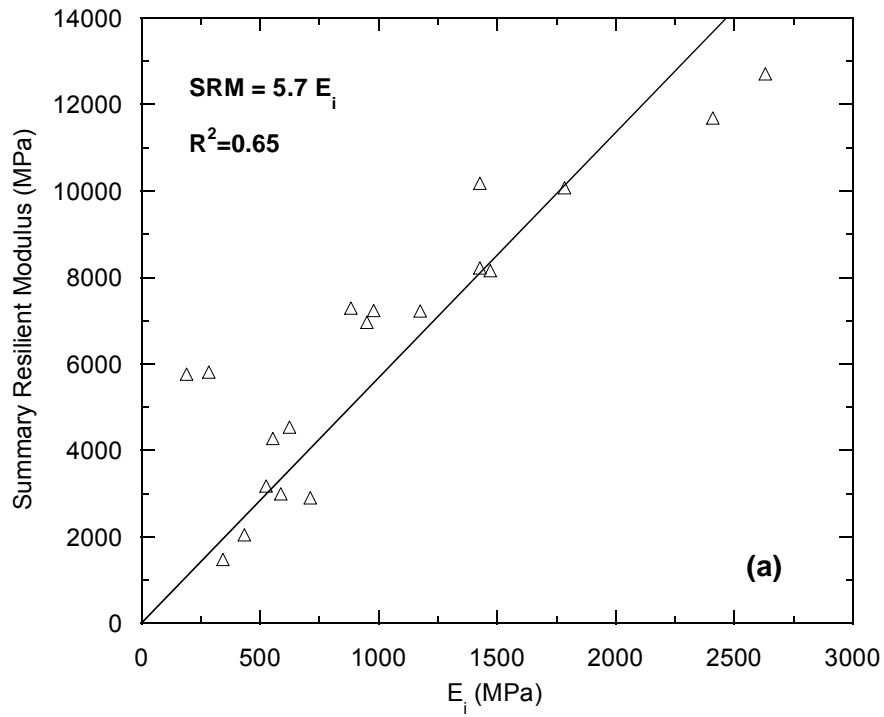
Fig. 17. SRM as a function of initial tangent modulus (E_i) (a) and modulus at 50% strain (E_{50}) (b) from UC test for all recycled material specimens blended with fly ash.

ATTACHMENT A: RESILIENT MODULI FOR EXTERNAL LVDT

MEASUREMENTS
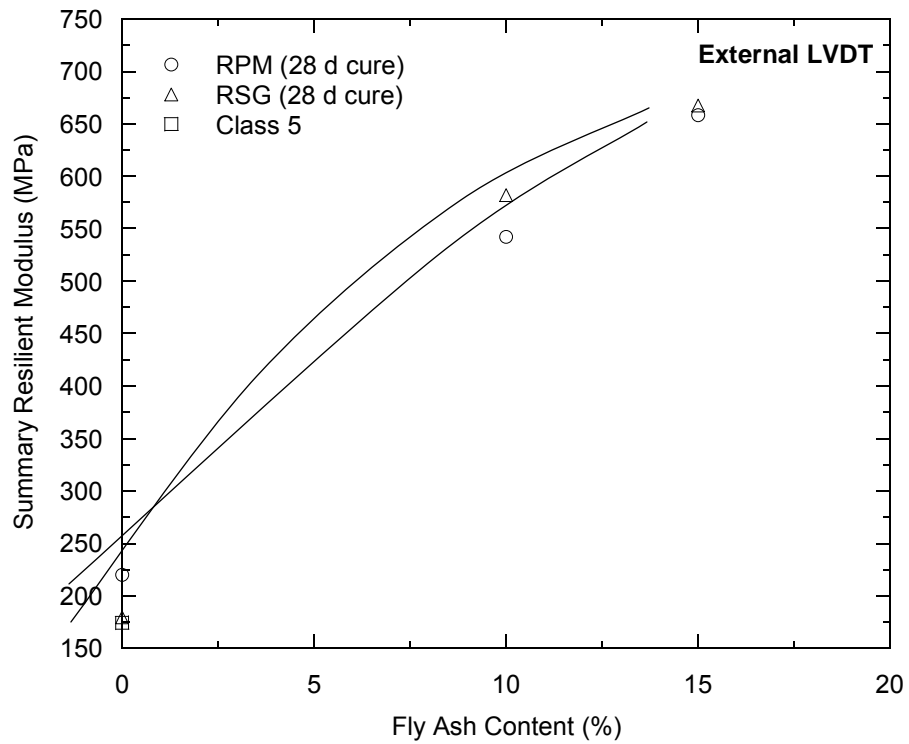
Fig. A.1. Summary resilient modulus based on external LVDT data as a function of fly ash content for base materials.
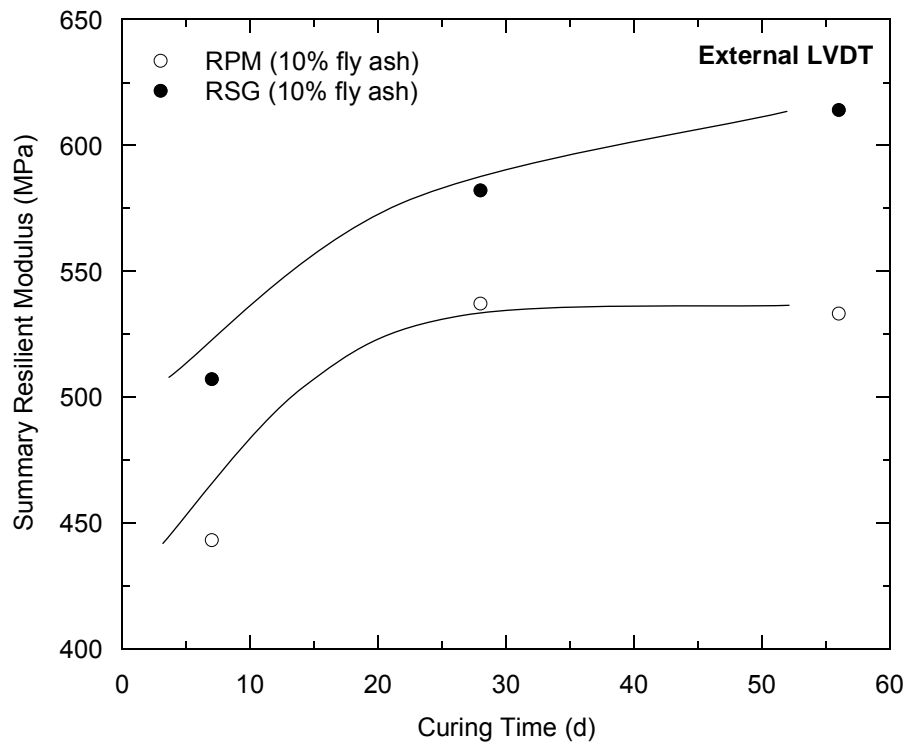
Fig. A.2. Summary resilient modulus based on external LVDT data as a function of curing time for recycled materials blended with 10% fly ash.
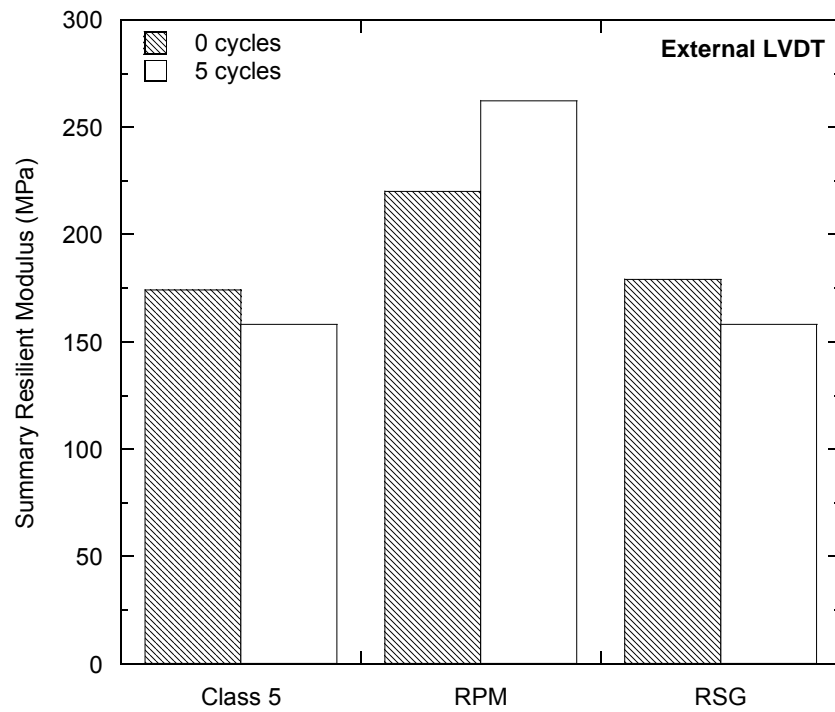
Fig. A.3. Summary resilient moduli of base materials based on external LVDT data before and after 5 freeze-thaw cycles.
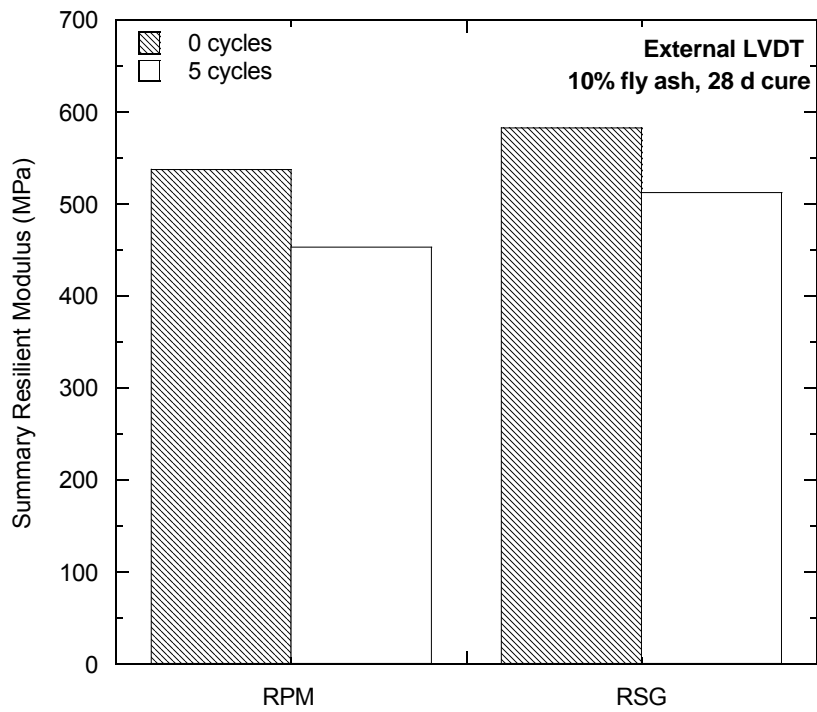
Fig. A.4. Summary resilient moduli of recycled materials blended with 10% fly ash (28 d cure) based on external LVDT data before and after 5 freeze-thaw cycles.

ATTACHMENT B: BASE COURSE TESTING PROTOCOL

This attachment summarizes testing procedures used at the University of Wisconsin – Madison for resilient modulus and California bearing ratio tests on granular materials used as base course.

B.1 CALIFORNIA BEARING RATIO (CBR)

The CBR test procedure has been combined with the compaction test procedure such that a CBR is calculated for each point on the compaction curve. This procedure yields the relationship between CBR and water content (e.g. Fig. B.1), from which the maximum CBR is obtained.

Material passing the 25 mm sieve is compacted into a 152-mm-diameter mold. Materials blended with fly ash are compacted 1 hour after fly ash and water have been added. A water content measurement is made on extra material immediately after compaction is completed. Compacted specimens are cured in a wet room for the desired curing time prior to testing.

A surcharge of 4.54 kg is applied to the specimen during testing. If a specimen is soaked, the surcharge of 4.54 kg is also applied during the soaking period. Soaking generally is not conducted because CBR is used to evaluate bearing resistance of the material immediately after construction.

B.2 RESILIENT MODULUS/UNCONFINED COMPRESSION

The resilient modulus test procedure is based on the NCHRP 1-28A protocol for base and subbase materials (NCHRP 2004). Material passing the 25 mm sieve is compacted at optimum water content using standard Proctor energy into a 152-mm-diameter mold PVC mold having a height of 305 mm. Material is compacted into the mold in 51 mm layers.

Two external and two internal LVDTs are used for collecting deformation data. Internal LVDTs are placed at quarter points of the specimen with a gauge length of 152 mm.

Base materials with and without fly ash are tested using Procedure Ia (NCHRP 2004) for base and subbase materials. In the past, base materials with fly ash were tested using Procedure II for fine-grained subgrades (cohesive soil). However, the stress conditions for each procedure were developed to cover the range of stress states likely to develop underneath flexible pavements subjected to moving loads (NCHRP 2004). Thus, the base and subbase procedure should be used for materials with fly ash to best represent field conditions. The base and subbase loading scheme is shown in Table B.1.

A summary resilient modulus is also computed, as suggested in Section 10.3.3.9 of NCHRP 1-28A. This summary resilient modulus corresponds to the resilient modulus at a bulk stress of 208 kPa for base materials (σ_{cyclic}=103 kPa, σ_3=35 kPa).

Specimens for freeze-thaw testing are prepared in PVC molds (152 mm diameter and 305 mm height) in the same manner as other resilient modulus specimens. Rosa (2006) reported that effects of freeze-thaw on resilient modulus and unconfined compression generally occur within 5 cycles. Therefore, test specimens are subjected to 5 freeze-thaw cycles, and then their resilient modulus are measured.

Preliminary testing is performed on a specimen instrumented with a thermocouple to evaluate the time necessary for complete freezing and thawing. Specimen height and weight are

monitored between freezing and thawing cycles. After the last cycle, specimens are extruded frozen and thawed inside the resilient modulus cell.

Unconfined compression tests are performed on specimens with fly ash after resilient modulus testing. Specimens are loaded with a strain rate of 0.21% per minute (Acosta et al. 2002), which is 0.64 mm per minute for specimens that are 305 mm tall.

Table B.1. NCHRP 1-28A Procedure Ia – resilient modulus test sequence for base and subbase materials.

Sequence	Confining Pressure, σ_3 (kPa)	Contact Stress, $\sigma_{contact}$ (kPa)	Cyclic Stress, σ_{cyclic} (kPa)	Maximum Stress, σ_{max} (kPa)	Cycles
0	103.5	20.7	207.0	227.7	1000
1	20.7	4.1	10.4	14.5	100
2	41.4	8.3	20.7	29.0	100
3	69.0	13.8	34.5	48.3	100
4	103.5	20.7	51.8	72.5	100
5	138.0	27.6	69.0	96.6	100
6	20.7	4.1	20.7	24.8	100
7	41.4	8.3	41.4	49.7	100
8	69.0	13.8	69.0	82.8	100
9	103.5	20.7	103.5	124.2	100
10	138.0	27.6	138.0	165.6	100
11	20.7	4.1	41.4	45.5	100
12	41.4	8.3	82.8	91.1	100
13	69.0	13.8	138.0	151.8	100
14	103.5	20.7	207.0	227.7	100
15	138.0	27.6	276.0	303.6	100
16	20.7	4.1	62.1	66.2	100
17	41.4	8.3	124.2	132.5	100
18	69.0	13.8	207.0	220.8	100
19	103.5	20.7	310.5	331.2	100
20	138.0	27.6	414.0	441.6	100
21	20.7	4.1	103.5	107.6	100
22	41.4	8.3	207.0	215.3	100
23	69.0	13.8	345.0	358.8	100
24	103.5	20.7	517.5	538.2	100
25	138.0	27.6	690.0	717.6	100
26	20.7	4.1	144.9	149.0	100
27	41.4	8.3	289.8	298.1	100
28	69.0	13.8	483.0	496.8	100
29	103.5	20.7	724.5	745.2	100
30	138.0	27.6	966.0	993.6	100
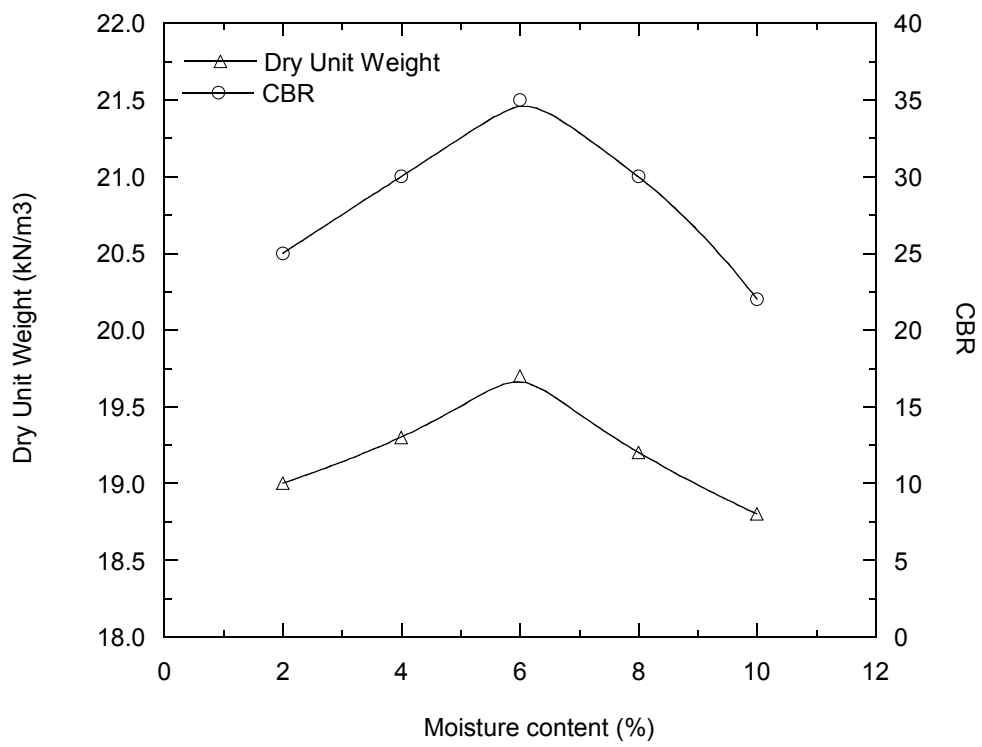
Fig. B.1. Sample CBR and compaction curves with water content.

B.3 RESILIENT MODULUS STEP-BY-STEP PROCEDURE

1) Turn on MTS 406 controller.

2) Turn hydrostatic pressure on low for 1-2 minutes.

3) Turn on LVDT power supply on Tektronix PS280, placed under computer desk.

4) If error light comes on, hit reset and turn hydrostatic pressure on low again.

5) Switch pressure to high.

6) Place filter paper on bottom plate. DO NOT USE GEOTEXTILES.

7) Measure specimen height and diameter at three spots and average them.

8) Place compacted specimen on bottom plate. If specimen is compacted on the bottom plate, skip to Step 12.

9) Place rubber membrane over specimen using a mold. Be careful not to disturb the sample. A vacuum pump for stretching the membrane should be used for wetter samples.

10) Place two o-rings on the bottom to hold the membrane in place.

11) Place filter paper and top plate over sample.

12) Place two more o-rings to secure membrane to top plate.

13) Apply vacuum to specimen. Fittings are placed on bottom cap.

14) Place lower clamps at 76 mm from the bottom of the specimen. Use spring stretcher for placing clamp over specimen. Place nuts on screw to secure spring during testing.

15) Place upper clamps at 228 mm from the bottom of the specimen. Measure distance between clamps at three points, making sure the distance corresponds to 152 mm.

16) Place LVDTs on pedestal (adjust pedestal height if needed). Fix LVDTs by using an L-wrench to tighten the screws, keeping LVDTs and pedestal vertically aligned. Make sure

there is enough stroke range for testing. Stroke range can be adjusted by monitoring voltage in the Measurement & Automation program.

17) Place chamber on bottom cap, making sure there is no soil on bottom cap.

18) Place cover plate, making sure it is not skewed.

19) Clean plunger and lubricate it with WD-40.

20) Place LVDT on top of specimen and make sure plunger is in the socket. Apply vacuum grease around plunger and cover plate to avoid air leaks.

21) Screw cover plate in uniformly.

22) Place ball bearing on top of plunger.

23) Plug air supply hose into cell (bottom cap).

24) Log into PC and start RM-MTS version 7 (Labview 8.5).

25) Chose base and subbase test protocol.

26) Input specimen diameter (152.4 mm).

27) Select file path to be saved (*.txt).

28) Hit run. Use mouse to control piston speed on program screen.

29) Apply contact pressure as specified on screen (<0.02 kN) and hit ok.

30) Apply seating load.

31) Turn vacuum pump off and remove hose from fitting.

32) Clamp both sides of bottom cap to lock it down.

33) Set external LVDTs with enough stroke range for testing.

34) Hit ok to start testing.

Some materials may require the LVDTs to be re-set during testing, depending on how much plastic strain occurs. If that is the case, re-set external LVDTs in between load sequences and monitor internal LVDTs so that stroke range is not exceeded.

ATTACHMENT C: MATERIAL CONSTRUCTION

Generating the Class 5 and RSG materials was a difficult task because of the large quantities that had to be sieved and uniformly mixed. In addition, the pit run material contained a considerable amount of cobbles and boulders. Therefore, a large sieve was constructed and the material was sieved by using a Bobcat 553 skid steer loader. The different stages of generating the Class 5 material are shown in Fig. C.1.

RSG required less effort to sieve because a smaller quantity was needed for laboratory testing. However, the addition of fines required a careful mixing procedure. The material was first sieved by hand, air dried at room temperature, and carefully mixed with a shovel until uniform. The samples were then placed in sealed buckets. Different stages of generating the RSG material are shown in Fig. C.2. Samples of the three base materials and Columbia fly ash are shown in Fig. C.3.
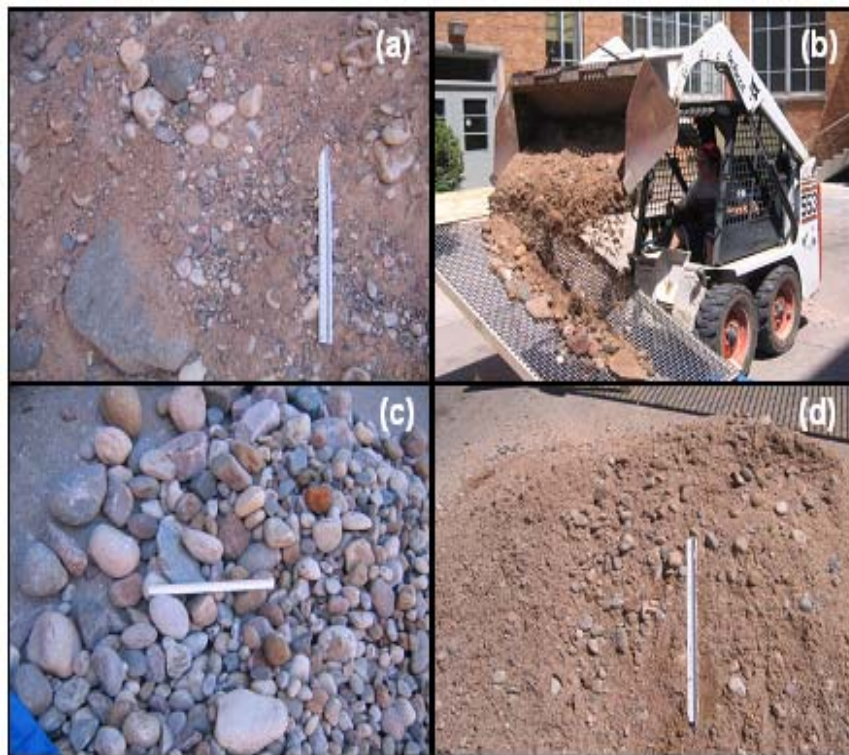
Fig. C.1. Different stages of Class 5 production: pit run (a), sieving material (b), material retained (c), and final Class 5 blend (d).

Fig. C.2. Different stages of RSG production: Class 5 base (a), material retained (b), mixing with fines (c), and final RSG blend (d).
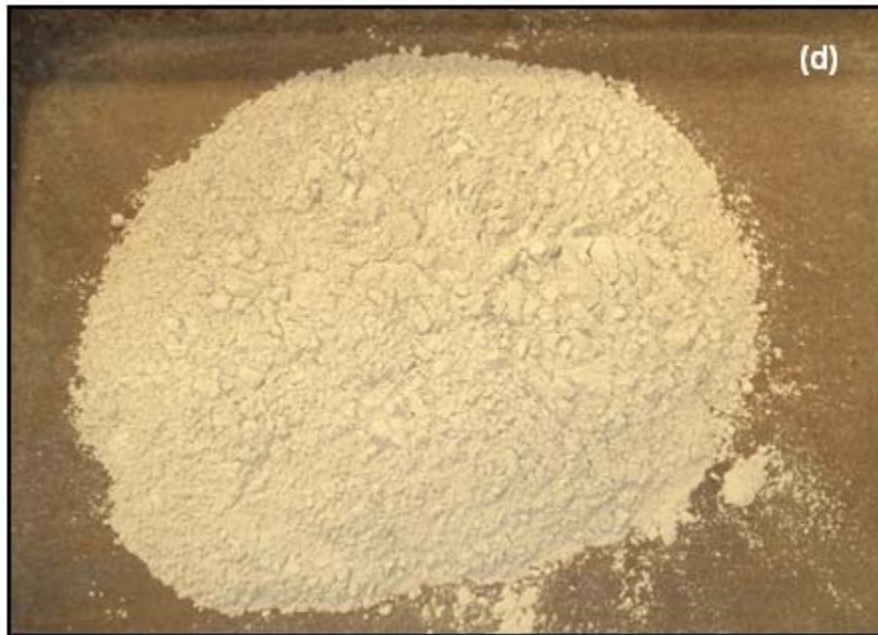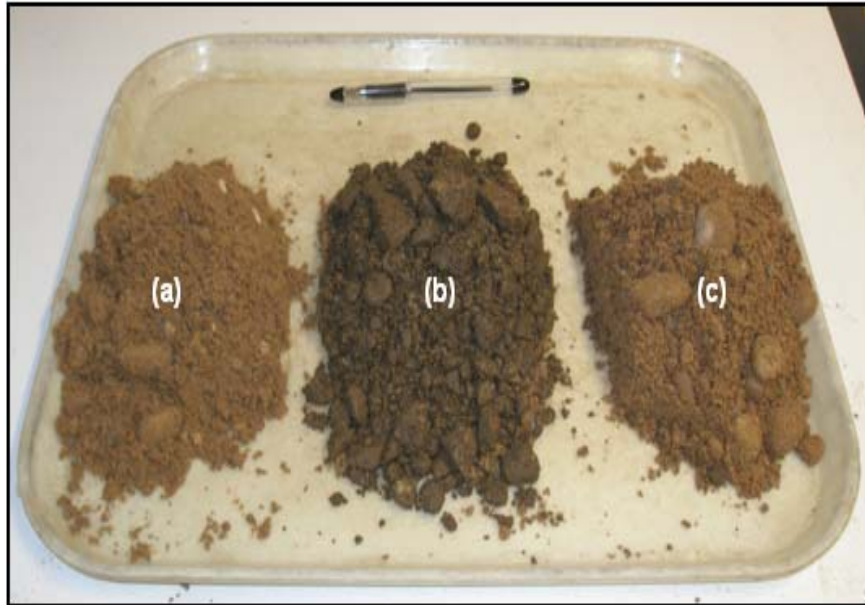
Fig. C.3. RSG (a), RPM (b), Class 5 (c); and Columbia fly ash (d).

ATTACHMENT D: TESTING EQUIPMENT

Table D.1. Volume for CBR and compaction (152-mm-diameter) PVC molds.

Mold	Mold + Plates + Grease	With Water	Water Temp	Density	Volume
	g	g	ºC	kg/m³	m³
A	3397.1	5534.2	18	998.6	0.002140
B	3399.1	5543.6	16	999.0	0.002147
C	3402.1	5541.7	17	998.8	0.002142
D	3389.5	5528.5	13	999.4	0.002140
E	3399.0	5540.4	13	999.4	0.002143
F	3396.2	5534.4	14	999.3	0.002140
G	3399.7	5539.8	15	999.1	0.002142
H	3394.2	5535.0	17	998.8	0.002143
I	3400.6	5541.1	16	999.0	0.002143
J	3398.6	5535.9	16	999.0	0.002140
K	3389.8	5527.2	20	998.2	0.002141
L	3392.2	5528.4	18	998.6	0.002139
M	3390.3	5528.2	17	998.8	0.002141
N	3392.3	5531.2	17	998.8	0.002142
O	3389.0	5533.0	16	999.0	0.002146
P	3394.5	5528.2	16	999.0	0.002136
Q	3397.0	5538.3	16	999.0	0.002144
R	3395.0	5535.9	16	999.0	0.002143
S	3419.1	5555.7	26	996.8	0.002143
T	3418.5	5562.2	24	997.3	0.002150
U	3506.2	5635.5	21	998.0	0.002134
V	3421.2	5567.1	21	998.0	0.002150

Fig. D.1. Compaction testing equipment.

Fig. D.2. CBR testing equipment.
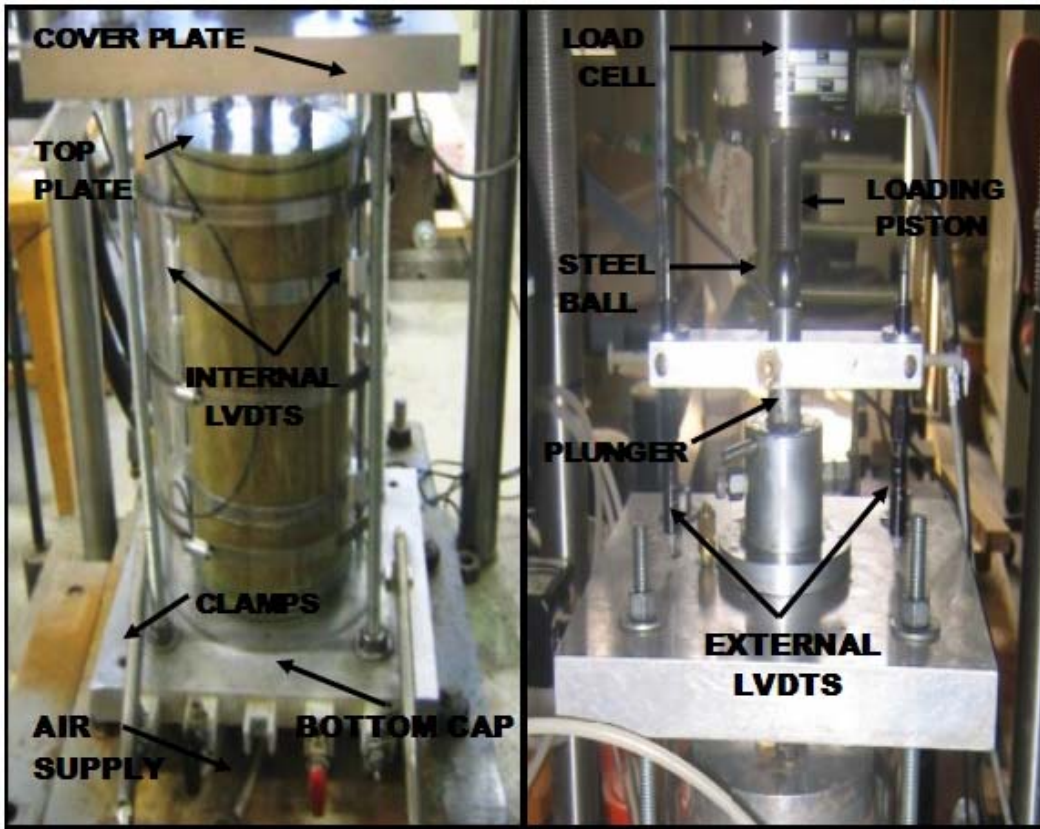
Fig. D.3. Resilient modulus testing equipment.

Fig. D.4. Unconfined compression testing equipment.
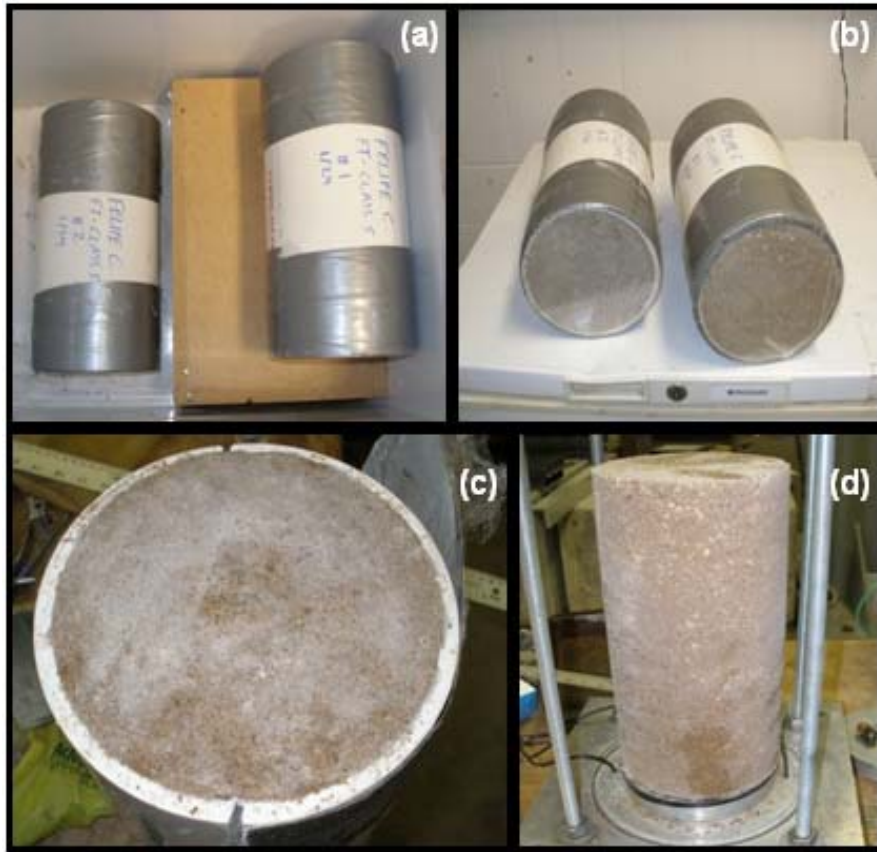
Fig. D.5. Different stages of freeze-thaw M_r testing: freezing specimens (a), thawing specimens (b), frozen end of a specimen (c), and frozen specimen in M_r cell (d).

ATTACHMENT E: CALIBRATION OF RESILIENT MODULUS TESTING

EQUIPMENT
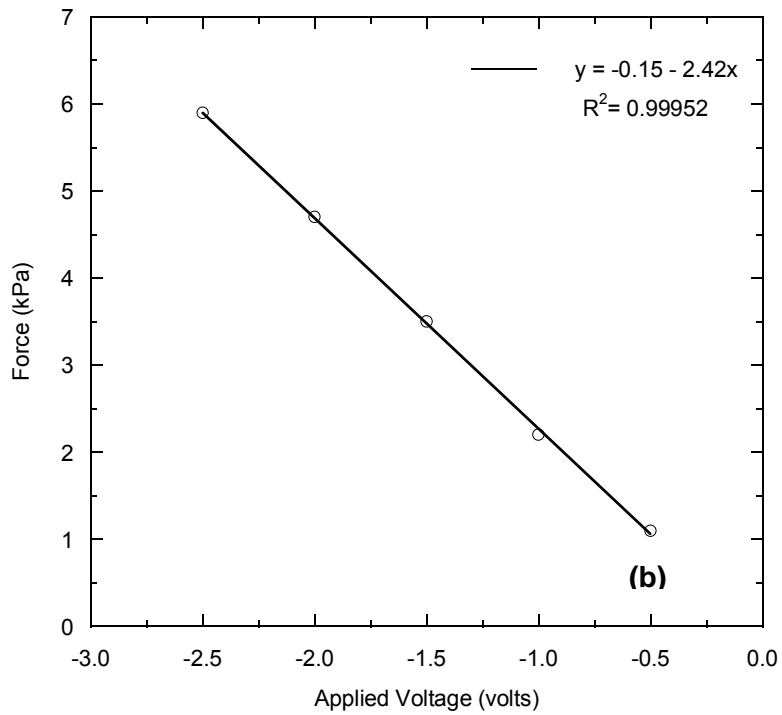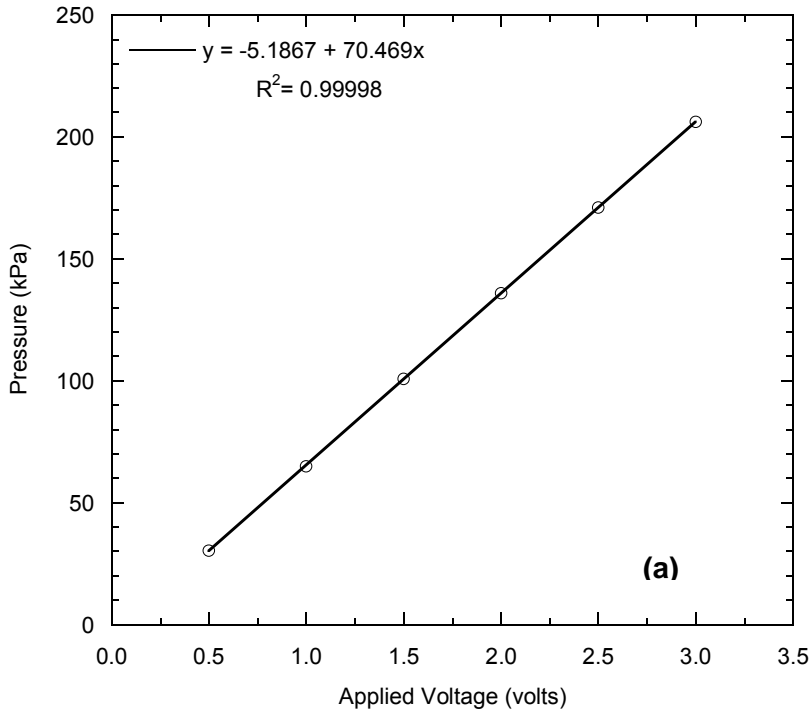
Fig. E.1. Calibration for pressure gauge (a) and load cell (b) for resilient modulus test.
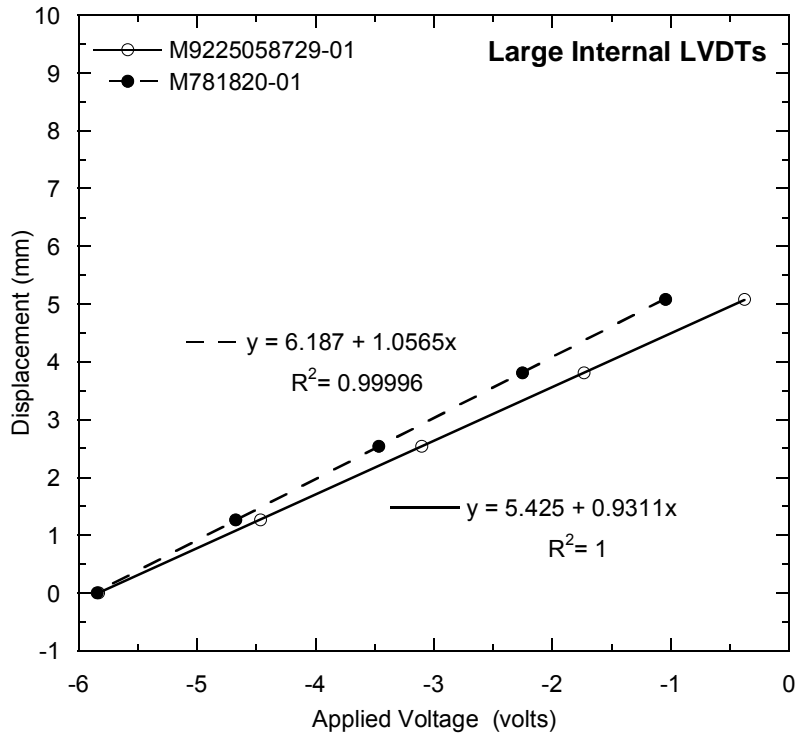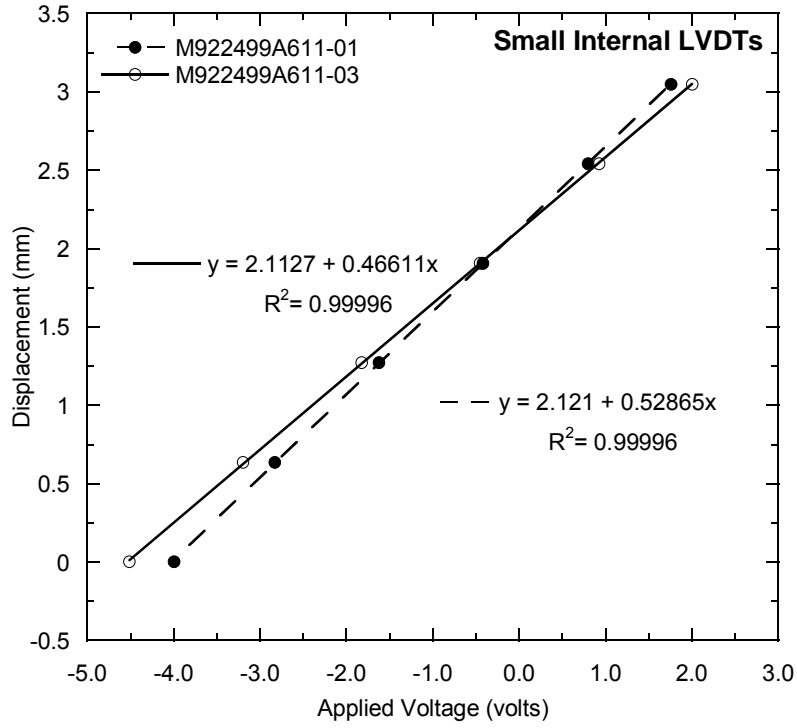
Fig. E.2. Calibration for small internal LVDTs (a) and large internal LVDTs (b) for resilient modulus test.
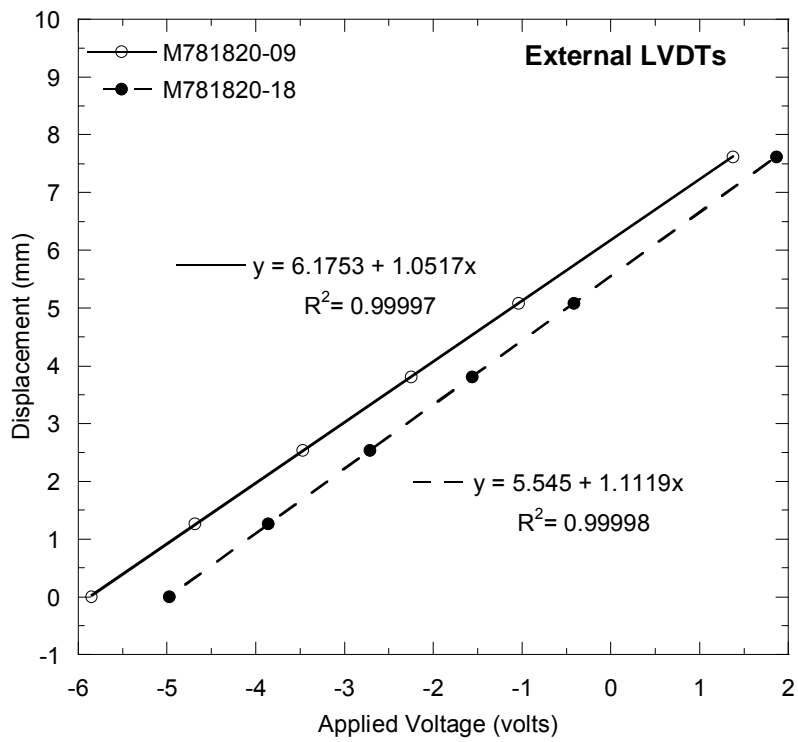
Fig. E.3. Calibration for external LVDTs for resilient modulus test.

ATTACHMENT F: RESILIENT MODULUS OF PORTAGE SAND

Two resilient modulus tests (PS-3, PS-4) were performed on Portage sand (PS) to check the resilient modulus testing equipment by comparison with data from a previous study (PS-1, PS-2). Specimens having 152-mm diameter and 305-mm height were prepared dry at 95% of maximum dry unit weight using the "rain-through-air" method (Sawangsuriya 2001). Resilient moduli were computed from external deformation readings and geotextiles were placed on either end of the test specimen to be consistent with previous tests (Fig. F.1 (a)). Resilient moduli computed from data from internal LVDTs for PS-3 and PS-4 are shown in Fig. F.1 (b).

Resilient moduli from external measurements were similar to those from the previous study. In addition, regression lines fitted with a power model were comparable for all tests. Resilient moduli from internal measurements were consistent for both tests (PS-3, PS-4) and their regression lines were practically the same.
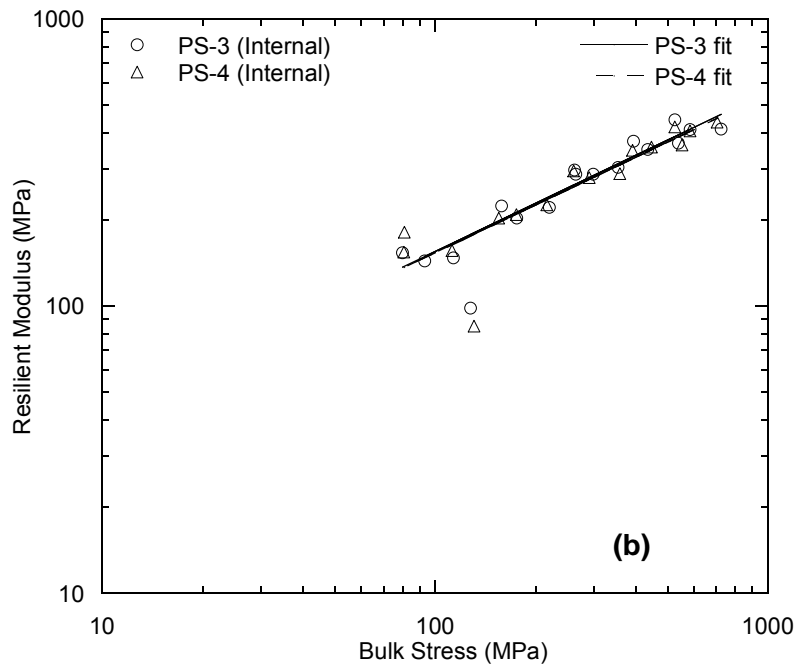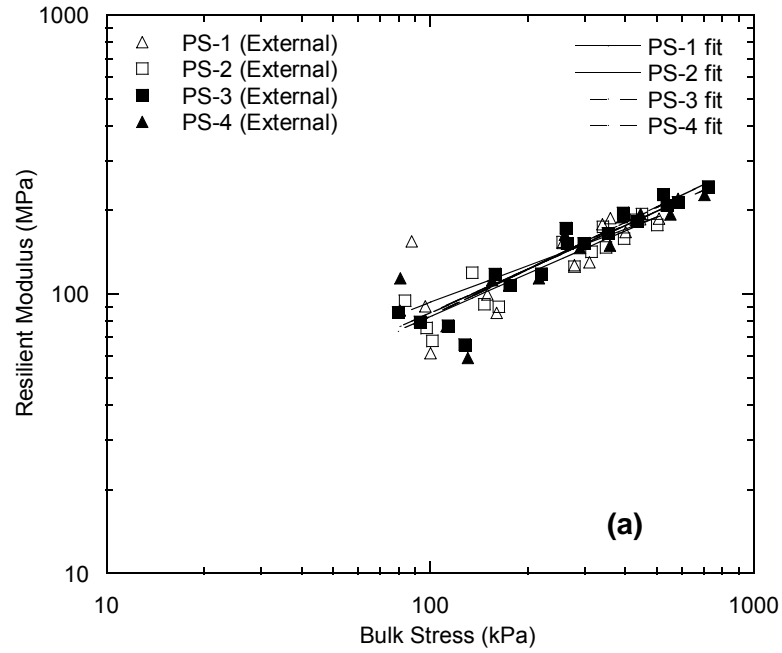
Fig. F.1. Resilient moduli from external LVDT measurements (a) and internal LVDT measurements (b) for Portage Sand.

ATTACHMENT G: INFLUENCE OF GEOTEXTILE ON RESILIENT

MODULUS

A specimen of RPM mixed with 10% fly ash was used to evaluate how geotextiles (GT) placed between the specimen and end platens affect the resilient modulus. A protocol consisting of 13 loading sequences was used, where the loads increase incrementally by 0.2 kN. Confining pressure was not applied. This protocol was used because it is simple and fast.

Resilient moduli from these tests are shown in Fig. G.1. The geotextiles significantly affected the resilient modulus computed from external LVDT measurements. For example, the M_r computed from external LVDT data more than doubled when geotextiles were not used, whereas the M_r computed using data from the internal LVDTs was not influenced by the GTs. Based on this test, filter paper was used between the specimen and end platens for all remaining tests in the study.
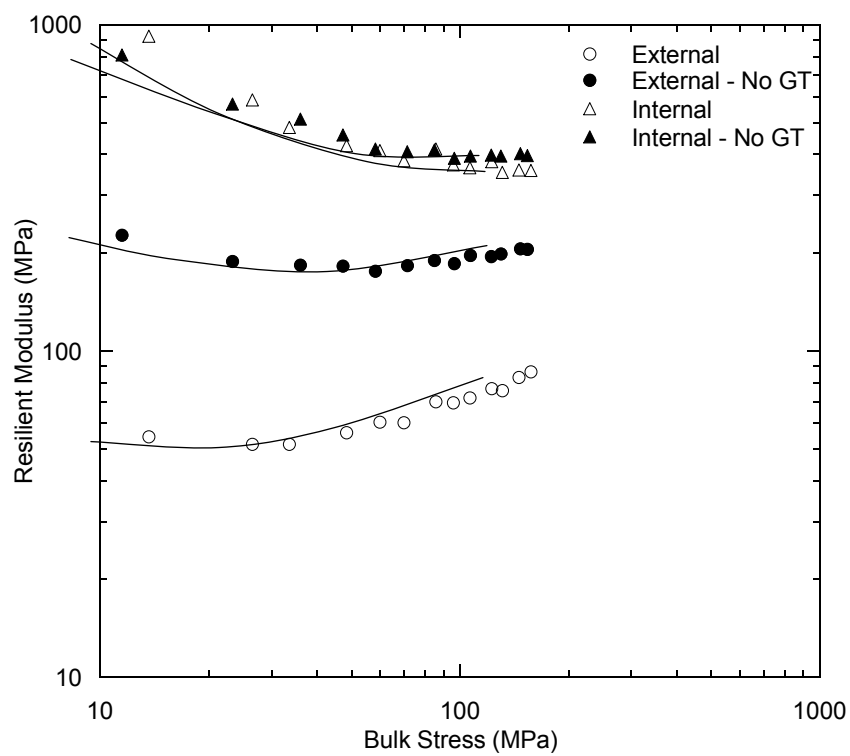
Fig. G.1. Resilient modulus tests on specimen of RPM with 10% fly ash with and without geotextiles.

ATTACHMENT H: TEMPERATURE RECORDS OBSERVED DURING

FREEZE-THAW TESTS
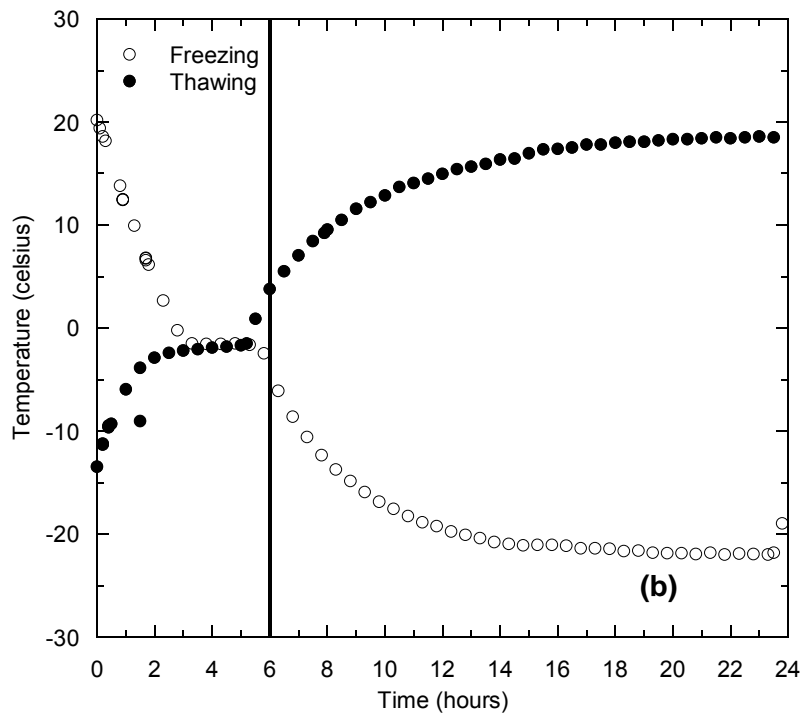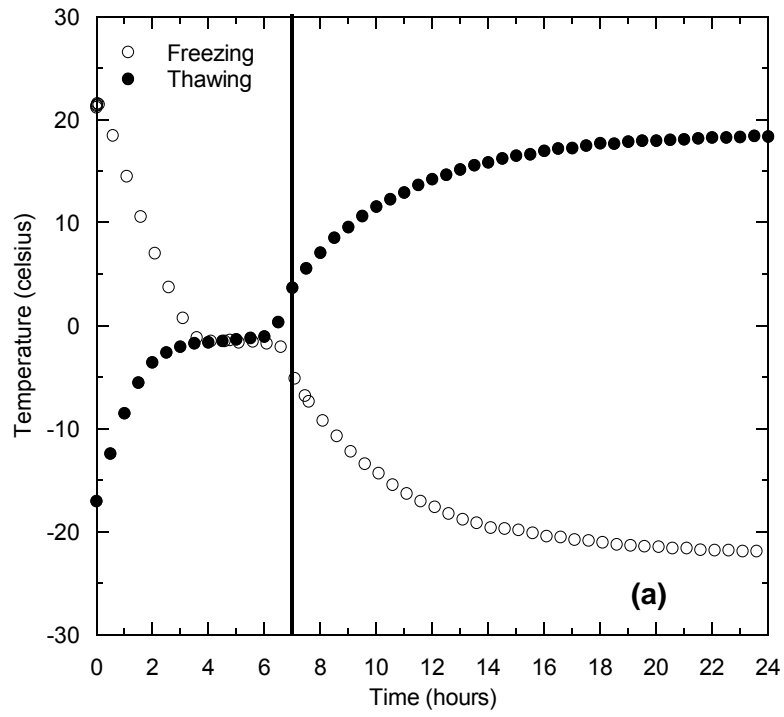
Fig. H.1. Temperature records for RPM (a) and RSG (b) with 10% fly ash (28 d cure).

ATTACHMENT I: RESILIENT MODULUS FROM INTERNAL AND

EXTERNAL LVDT MEASUREMENTS

I.1 DATA SUMMARY

Resilient modulus test specimens were instrumented with both internal and external LVDTs. Internal LVDTs were mounted on clamps around the specimen and membrane, whereas external LVDTs were mounted on the plunger outside the chamber and rested on the cover plate (Fig. D.3). Internal LVDTs were placed at quarter points of the specimen to measure deformations over half the length of the specimen, whereas external LVDTs measured deformations of the entire specimen length.

The summary resilient moduli (SRM) computed from internal LVDT measurements is higher than those for external LVDT measurements for all resilient modulus tests (Table 6). The ratio of internal to external SRM ranged from 1.2 to 1.4 for the base and recycled materials without fly ash and from 4.0 to 18.3 for the recycled materials blended with fly ash. The internal SRM are higher because displacement measurements for external LVDT readings are affected by bedding errors, sample end effects, and machine compliance (Tatsuoka et al. 1994, Ping et al. 2003, Bejarano et al. 2002).

The resilient modulus results for base and recycled materials without fly ash are similar to those found by Ping et al. (1996, 2003). Ping et al. (1996) conducted resilient modulus tests on lime rock, a weathered limestone base material commonly used in Florida, instrumented with internal and external LVDTs. The ratio of internal to external resilient moduli calculated from the data reported ranges from 0.85 to 1.48. Ping et al. (2003) conducted resilient modulus tests on granular soils (A-3 and A-2-4) instrumented with internal and external LVDTs. The ratio of internal to external resilient moduli ranged from 1.19 to 1.35 for A-3 soils, whereas the ratio ranged from 1.14 to 1.30 for A-2-4 soils.

The ratio of internal to external SRM for the recycled materials blended with fly ash was significantly higher than ratios for materials without fly ash (ranging from 4.0 to 18.3) (Table 6). The ratio of internal to external SRM also increases with increasing stiffness (Fig. I.1). The increase in ratio is attributed to an increase in overestimation of the displacement as the material becomes stiffer (i.e. lower displacements), increasing the difference between external and internal displacement measurements. Bejarano et al. (2002) also report higher M_r from internal readings, with an increase in the difference in M_r for increasing stiffness due to greater influence of machine compliance.

I.2 BASE MATERIALS

Additional resilient moduli computed from internal and external LVDT measurements were obtained from the Minnesota Department of Transportation (MnDOT) database for comparison with the data collected in this study. The ratio of internal to external M_r was computed for all cycles during resilient modulus testing, except those from the loading phase (Sequence 0). The ratio of internal to external M_r as a function of internal M_r for base and recycled materials without fly ash is shown in Fig. I.2, along with the corresponding bloxplot.

The Class 5 base, RPM, RSG, MnROAD Class 6, and MnROAD RPM in Fig. 1.2 are materials tested at the University of Wisconsin-Madison (UW). The MnROAD Class 6 base and RPM in Fig. I.2 were obtained from a research project at the MnROAD facility in Minnesota. The Class 6 material is a crushed aggregate conforming to Minnesota's Class 6 specifications (MnDOT 2005), and the RPM is a recycled material containing 50% RAP. The remaining tests

were conducted at MnDOT (MnDOT base, RPM, and reclaimed concrete). MnDOT base materials include gravels, granite, and taconite tailings. The MnDOT RPMs consist of base materials (Class 5, Class 6, and taconite tailings) having RAP contents of 30, 50, and 70%.

There is no apparent trend in the data (Fig. I.2 (a)). The boxplot shows that the majority of the ratios ranging are between 1.0 and 2.2, with a median ratio of 1.5 for all base and recycled materials (Fig. I.2 (b)).

The relationship between internal ($M_{r\,INT}$) and external resilient moduli ($M_{r\,EXT}$) for base and recycled materials is shown in Fig. I.3. This relationship can be described by:

$$M_{r\,INT} = 1.5\,M_{r\,EXT} \qquad (I.1)$$

Eq. I.1 has $R^2 = 0.85$. This slope of Eq. I.1 equals the median M_r ratio shown in the boxplot in Fig. I.2 (b).

I.3 SUBGRADE MATERIALS

Resilient modulus data for subgrade materials instrumented with both internal and external LVDTs were also obtained from the MnDOT database and from a previous UW study. The ratio of internal to external resilient moduli as a function of internal M_r for subgrade materials is shown in Fig. I.4. The ratio of internal to external resilient moduli for subgrade materials increases approximately linearly with increasing internal M_r, ranging from 1 to 10. This relationship can be described by:

$$\frac{M_{r\,INT}}{M_{r\,EXT}} = 0.007\,M_{r\,INT} + 1.05 \qquad (I.2)$$

which has $R^2 = 0.87$.

The relationship between internal and external M_r for subgrade materials is shown in Fig. I.5. The relationship between internal and external can be described by the power function:

$$M_{r\,INT} = 0.172\,(M_{r\,EXT})^{1.627} \qquad (I.3)$$

which has $R^2 = 0.86$.

I.4 RECYCLED MATERIALS WITH FLY ASH

The ratio of internal to external resilient moduli as a function of internal M_r for subgrade materials is shown in Fig. I.6. The ratio of internal to external M_r for recycled materials blended with fly ash increases with increasing internal M_r, ranging from 2 to 25. An approximate linear relationship exists between the ratio of internal to external M_r and internal M_r for the recycled materials with fly ash:

$$\frac{M_{r\,INT}}{M_{r\,EXT}} = 0.0014\,M_{r\,INT} + 1.195 \tag{I.4}$$

which has $R^2 = 0.76$.

The relationship between internal and external M_r for recycled materials blended with fly ash is shown in Fig. I.7. There is no apparent trend in internal to external M_r for these materials. The recycled materials blended with fly ash have significantly higher stiffness than those without fly ash, which results in less accurate external deformation measurements due to a higher machine compliance effect. This behavior is also observed in Fig. I.6, where larger scatter exists when the internal M_r exceeds 6000 MPa.

The ratio of external to internal M_r for a range of materials (fine-grained soils, crushed aggregates, recycled materials, recycled materials with fly ash, and concrete) is shown in Fig. I.8. To be consistent with the other data in Fig. I8, the data for fine-grained materials were limited to measurements on 150-mm diameter. The ratio of external to internal M_r decreases with increasing internal M_r. This trend is attributed to the increasing effect of machine compliance as the specimen becomes stiffer, which increases the difference between internal and external M_r and therefore decreases ratio of external to internal M_r.
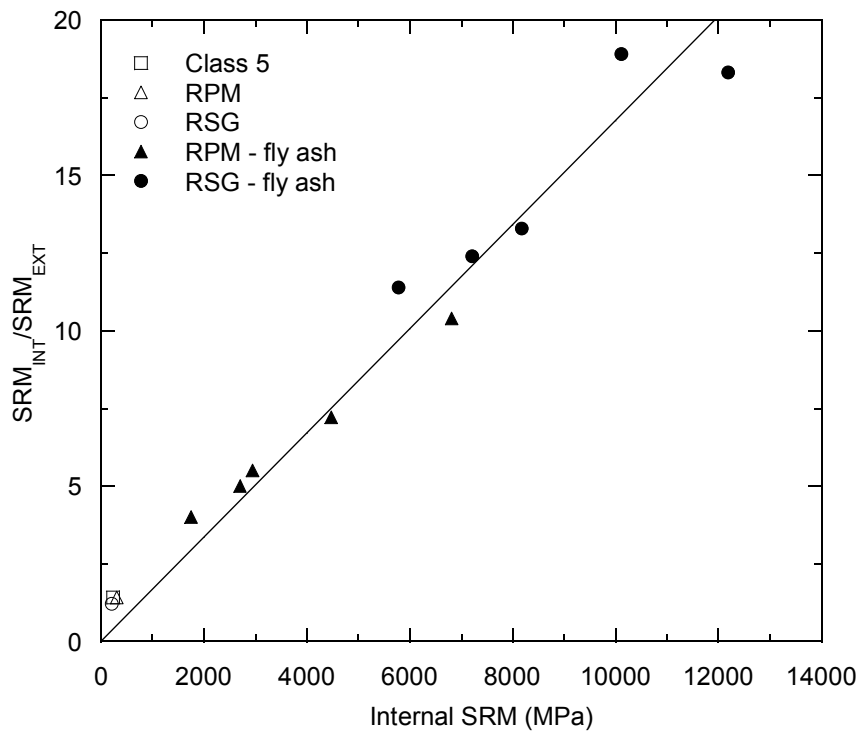
Fig. I.1. Ratio of internal to external SRM versus internal SRM for RPM and RSG with and without fly ash and Class 5 base.
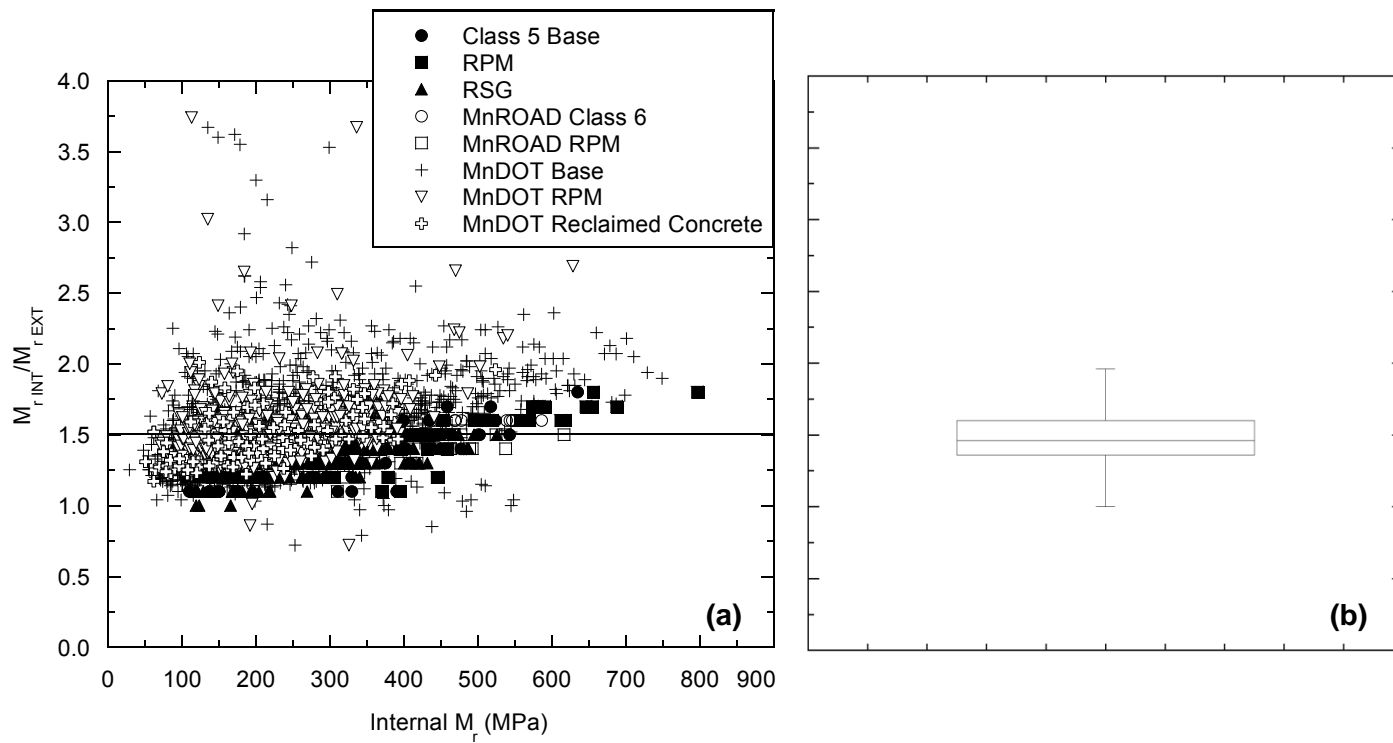
Fig. I.2. Ratio of internal to external M_r versus internal M_r for base materials (a) and boxplot of ratio of internal to external M_r versus internal M_r for base materials (b).
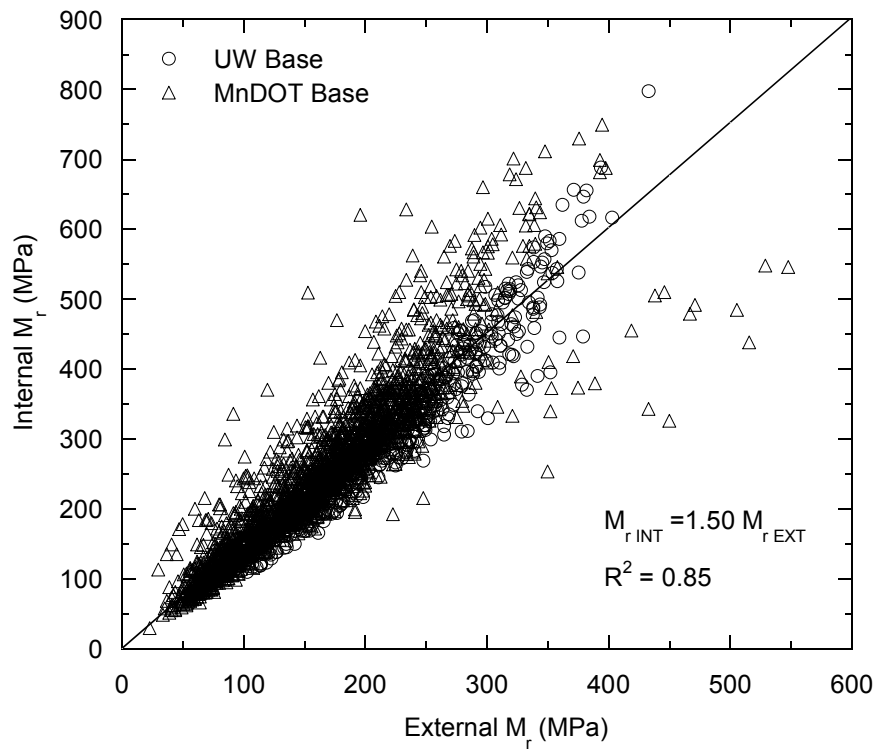
Fig. I.3. Internal versus external M_r for base materials.
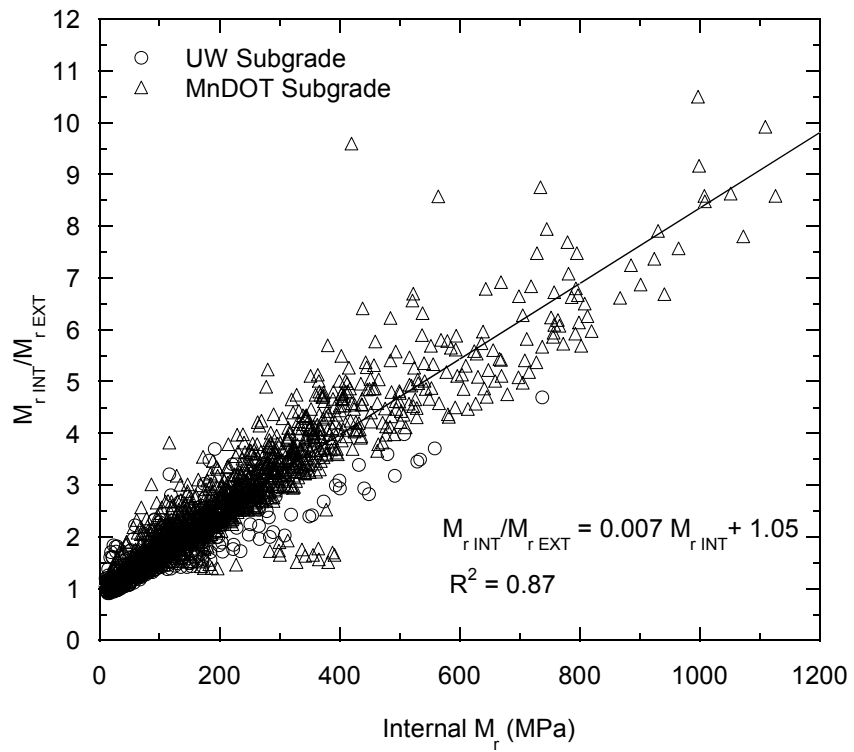
Fig. I.4. Ratio of internal to external M_r versus internal M_r for subgrade materials.
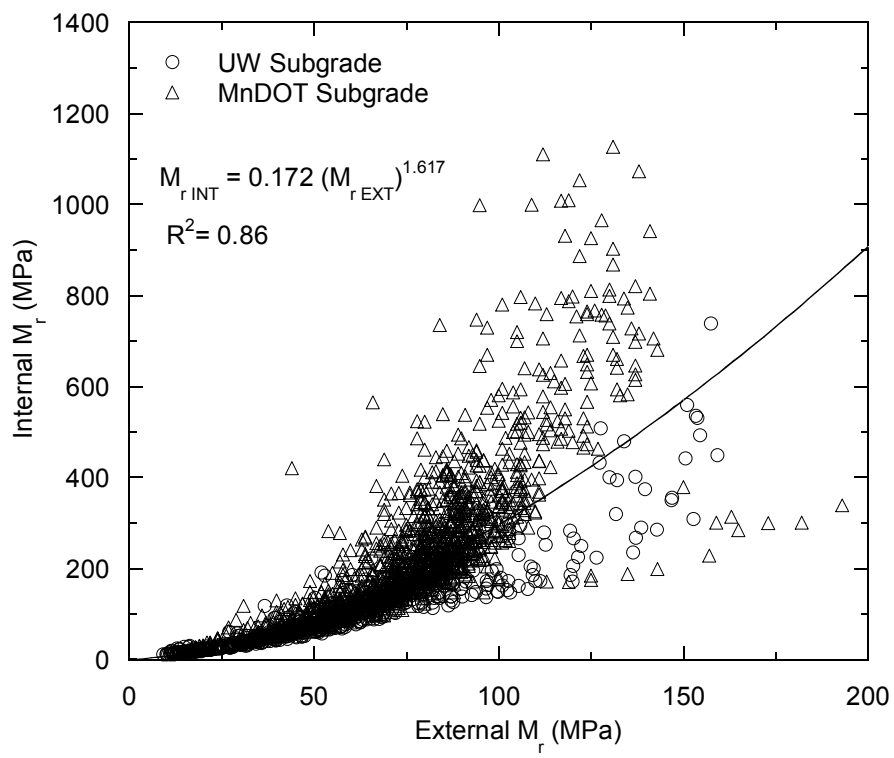
Fig. I.5. Internal versus external M$_r$ for subgrade materials.
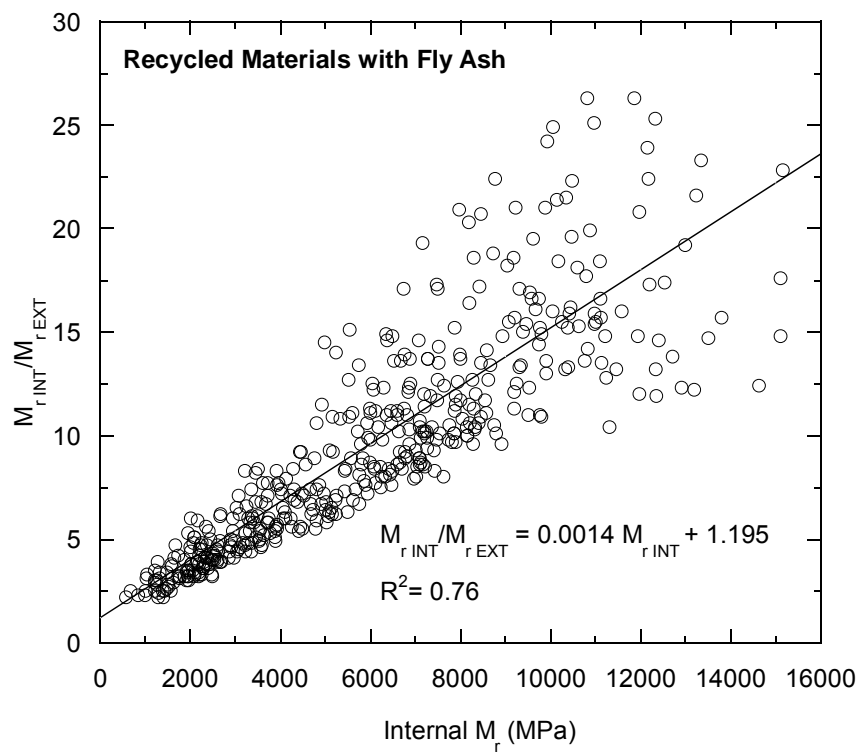
Fig. I.6. Ratio of internal to external M_r versus internal M_r for recycled materials blended with fly ash.
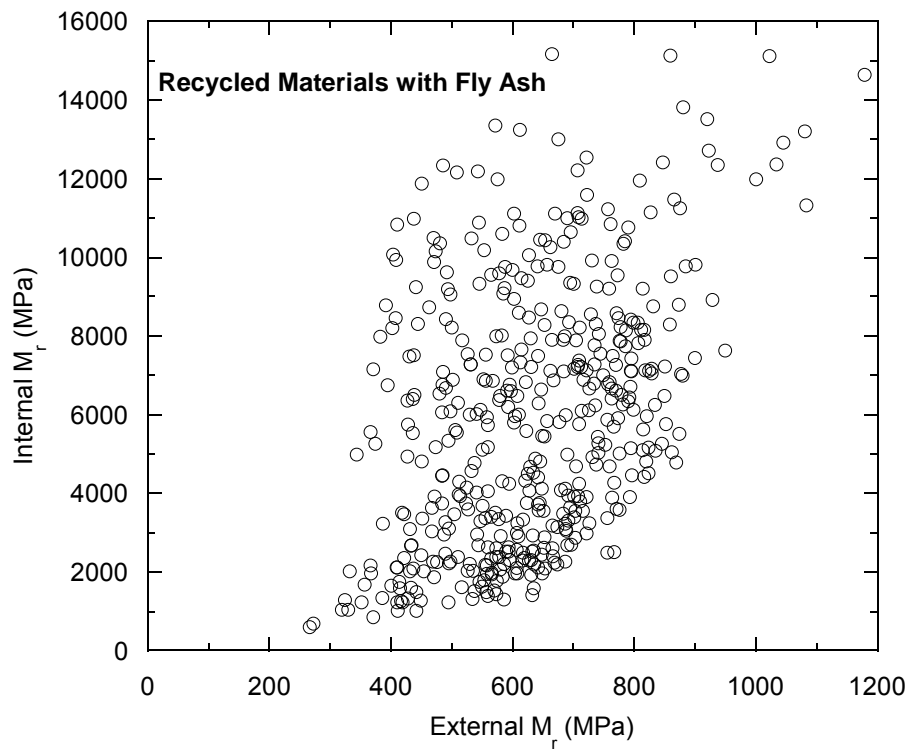
Fig. I.7. Internal versus external M_r for recycled materials blended with fly ash.

1.50

1.35

1.20

1.05

0.90

0.75

0.60

0.45

0.30

0.15

0.00

$M_{r\,EXT}/M_{r\,INT}$

Internal M_r (MPa)

0   2000   4000   6000   8000   10000 12000 14000 16000 18000

△ UW Base

○ MnDOT Base

✚ MnDOT Subgrade

□ Recycled Materials-Fly ash

◆ Concrete
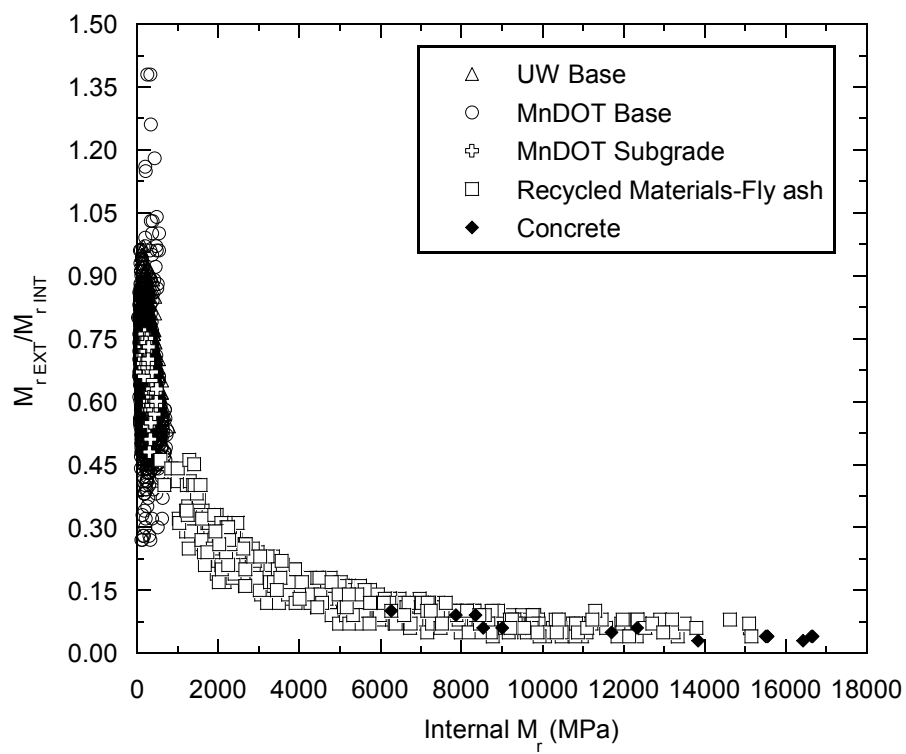
Fig. I.8. Ratio of external to internal M_r versus internal M_r for a range of materials.

APPENDIX C

REPORT FOR TASKS 2 AND 3

LARGE SCALE MODEL EXPERIMENTS

USE OF FLY ASH FOR RECONSTRUCTION OF BITUMINOUS ROADS

REPORT FOR TASKS 2 AND 3

LARGE SCALE MODEL EXPERIMENTS

Prepared by:

Brian R. Kootstra
Ali Ebrahimi
Tuncer B. Edil
Craig H. Benson

Department of Civil and Environmental Engineering
University of Wisconsin-Madison
Madison, WI 53706

February 2009

EXECUTIVE SUMMARY

The main objective was to develop the Gravel Equivalency (GE) of two recycled materials with and without fly ash stabilization. To meet this objective, the modulus of recycled materials with and without fly ash was determined from a Large Scale Model Experiment (LSME) and compared with the resilient modulus determined from the laboratory test method described by NCHRP 1-28A. The elastic modulus was also determined by other means, i.e., with a Soil Stiffness Gage (SSG), two types of Light Weight Deflectometer (LWD), and a Dynamic Cone Penetrometer (DCP), and compared to the modulus from the LSME. A Class C fly ash with a content of 10% by weight, which is typical of such applications, was used in stabilization of RPM and RSG and curing times of 7 and 28 days were evaluated. Class 5 gravel, with a conventional base material gradation employed in Minnesota, was used as a reference material.

The gravel equivalency (GE) factor for RPM was determined to be equal to 1.07 and did not vary with base layer thickness, indicating that this material is similar to that of Class 5 gravel having a GE factor of 1.00. The GE factor of RSG varied with thickness and was less than 1.00 indicating that RSG has less desirable structural properties than Class 5 gravel. The GE factor of RPM and RSG blended with fly ash varies with thickness of the base layer in a nearly identical manner, and is greater than 1.00 for base layer thicknesses less than 0.55 m. The GE factor of the fly ash stabilized materials decreases with increasing base layer thickness because the modulus of the materials blended with fly ash is assumed to be constant with layer thickness, while the modulus of Class 5 gravel is increasing with layer thickness.

Both the plastic deformations and the elastic deflections of the materials were significantly reduced with the addition of the fly ash. The greatest plastic deformations and elastic deflections measured in the LSME were for RSG without fly ash; however, with the addition of fly ash RSG had the least plastic deformations and elastic deflections. Both RPM and RSG had plastic deformations greater than Class 5 base. RSG without fly ash had the lowest modulus resulting from the largest elastic deflections (116 MPa for 200 mm thickness and 216 MPa for 300 mm thickness) while RSG blended with fly ash at 28 days of curing had the highest modulus (918 MPa) resulting in an increase of 325% for the 300 mm thickness. The increase in modulus of RPM with fly ash was 67% for the 300 mm thickness. For all three materials tested without fly ash, the resilient modulus increased with an increase in base layer thickness. The modulus determined from the LSME tests was less than half of that measured in the laboratory resilient modulus test due to the differences in mixing of the materials with fly ash and the curing conditions. The LSME modulus is expected to be closer to actual field conditions than the laboratory test.

The resilient modulus was found to increase with the bulk stress for the granular base course materials without fly ash indicating the nonlinearity of these soils. However with the addition of fly ash, the resilient modulus did not show stress dependency for a range of stresses typically resulting from wheel loads and was considered to be a linear elastic material.

The LSME modulus was found to be greater than the elastic modulus obtained with the SSG, LWDs and the DCP, but each test method gave a higher modulus for materials blended with fly ash than those without fly ash.

TABLE OF CONTENTS

LIST OF FIGURES

LIST OF TABLES

1. INTRODUCTION

There are approximately 4.0 million miles of public roads in the United States requiring billions of dollars and significant amounts of natural resources to maintain each year. The ability to reuse the materials comprising these existing roads, such as the deteriorated pavement and underlying base course which generally consists of coarse aggregate, spread and compacted to provide a stable base for the asphalt pavement, would provide an attractive alternative to using additional natural resources by providing both economic and environmental benefits.

During the process of reconstructing a road, a large supply of potentially useful material would be conveniently located along the existing roadway resulting in significant savings relative to conventional total reconstruction costs. These cost savings would result from less time and expense spent in the transportation and procurement of new materials and the disposal of the old material. Instead of disposing deteriorated roadway materials in a landfill, the material could be recycled and placed directly into the road as base course in a process known as full depth reclamation, relieving pressure on natural aggregate resources. The technology should be particularly useful to smaller communities and rural counties without large construction budgets.

Recycled pavement material (RPM) and road surface gravel (RSG) are two materials that can be reused as a new base course in the rehabilitation of roads (Wen et al. 2004; Li et al. 2008; Hatipoglu et al. 2008). RPM is a mixture of crushed deteriorated asphalt pavement and the underlying base course material. This material can be created in situ and then a new layer of hot mix asphalt is placed over the RPM. The riding surface of most unpaved roads consists of RSG. As pressure to convert these unpaved roads to paved surfaces increases annually in the United States, the RSG in these roads can also be recycled by forming a base for asphalt pavement.

Since RPM and RSG may not perform as well as natural high quality aggregates relative to strength and stiffness, the addition of a stabilizing material such as fly ash can improve these properties due to cementation. Fly ash is a byproduct resulting from the burning of coal in power plants. If fly ash or other less expensive binders such as cement kiln dust (CKD) are added, a use will be created for a material that is generally a waste product and disposed of in a landfill (Li et al. 2008, Hatipoglu et al. 2008).

The particular objectives of this study were to assess the engineering properties of recycled materials with and without fly ash in a Large Scale Model Experiment (LSME) and to develop the Gravel Equivalency (GE) for the tested materials. This report describes the findings of this study. Materials and methods are described in Sections 2 and 3. Results and analysis are provided in Section 4. A summary and conclusions are in Section 5.

2. MATERIALS

2.1 BASE MATERIALS

The three base materials selected for this study consisted of a conventional base material, recycled pavement material (RPM), and road surface gravel (RSG). RPM and RSG are recycled materials. The conventional base was used as a control material.

The conventional base material is referred to as Class 5 gravel, because it meets the Minnesota Department of Transportation (MnDOT) gradation specifications for Class 5 base course (MnDOT 2005). The particle size distribution for the Class 5 used in this study is shown in Fig. 2.1(a) along with the upper and lower boundaries of the MnDOT specification. The Class 5 gravel was created by combining a pit run sand obtained from Wimme Sand and Gravel (Plover, Wisconsin) with crushed pea gravel from Midwest Decorative Stone and Landscape Supply (Madison, WI). The pit run was screened using a 25 mm sieve before adding the pea gravel (Camargo 2008).

The RPM was obtained from a road reconstruction project near the intersection of Muir Field Road and Carnwood Road in southwestern Madison, WI. The RPM consisted of approximately equal fractions of pulverized hot mix asphalt and limestone base course from the roadway that was being reconstructed (Camargo 2008).

The RSG material was created by combining the previously made Class 5 gravel with fine-grained soil obtained from Rosenbaum Crushing and Excavating (Stoughton, Wisconsin) so that the combined material met the gradation and plasticity requirements for surface course materials that are described in AASHTO M 147 (AASHTO 2001). The particle size distribution of the RSG is shown if Fig. 2.1(b) along with the AASHTO limits for three types of surface course gravel stipulated as D, E, and F.   The RSG used for this study contained plastic fines resulting in the soil displaying some plasticity with 3% of the particle diameters less than the 2 micron clay fraction, whereas the RSG used by Camargo (2008) had non-plastic fines from limestone processing.

A summary of index properties and soil classifications for the three base materials is shown in Table 2.1. The Class 5 gravel classifies as SP, RPM as GW-GM, and RSG as SC-SM in the Unified Soil Classification System described in ASTM D 2487. In the AASHTO Soil Classification System (ASTM D 3282) Class 5 gravel and RPM classify as A-1-a and RSG as A-2-4. Class 5 and RPM are both non-plastic, while the RSG had a liquid limit (LL) of 21 and a plasticity index (PI) of 7. The particle size distribution curves of the materials, determined using ASTM D 422, are shown together in Fig. 2.2.

Compaction tests on each material were performed at standard compactive effort (ASTM D 698).   The compaction curves are shown in Fig 2.3. Optimum water contents and maximum dry unit weights for the materials are summarized in Table 2.3. The compaction curve for Class 5 gravel shows that the dry unit weight of this material is insensitive to water content, whereas the bell shaped curves obtained for the RPM and RSG show that the maximum dry unit weight is sensitive to the water content (Fig. 2.3).

2.2 FLY ASH

Fly ash for this study was obtained from Unit No. 2 of Columbia Power Plant operated by Alliant Energy (Portage, Wisconsin) where sub-bituminous coal is burned in pulverized boilers and fly ash is collected using electrostatic precipitators. Columbia fly ash has cementitous properties and classifies as Class C according to ASTM C 618. Columbia fly ash has a powdery texture, is light-brown in color, and has a specific gravity of 2.63. Physical properties and chemical composition of Columbia fly ash are summarized in Table 2.2, along with the typical chemical composition of Class C fly ash.

According to Janz and Johansson (2002), the ratio of CaO to SiO_2 is indicative of the potential for pozzolanic reactions, and binders containing larger ratios are likely to be more effective in enhancing the engineering properties of materials. Similarly, Tastan (2005) indicates that cementing is also related to the ratio of CaO to $(SiO_2 + Al_2O_3)$. Tastan (2005) reports higher strengths for subgrade soils blended with fly ash at CaO/SiO_2 ratios ranging from 0.5 to 1.0 and $CaO/(SiO_2 + Al2O_3)$ ratios ranging from 0.4 to 0.7. The ratio of CaO to SiO_2 for Columbia fly ash is 0.4, whereas the ratio of CaO to $(SiO_2 + Al_2O_3)$ is 0.8. Rosa (2006) reports the pozzolanic activity of Columbia fly ash at 7 days is 95.8%.

3. METHODS

3.1 LARGE SCALE MODEL EXPERIMENT

3.1.1 Apparatus and Loading Methodology

The large scale model experiment (LSME) is a test apparatus for evaluating deflections during cyclic loading of a prototype-scale pavement structure (or parts of it) in a manner that replicates field conditions as closely as practical (Tanyu et al 2003). A schematic of the LSME is shown in Fig. 3.1. The LSME consists of a pavement profile constructed in a 3 m x 3 m x 3 m test pit. A loading frame, actuator (280 L/m MTS hydraulic actuator with 100 kN capacity and 168 mm stroke), and steel loading plate (125 mm radius, 25 mm thickness) are used to apply loads simulating those applied by vehicles. Loads are applied with a load pulse consisting of a 0.1 s loading period followed by a 0.9 s rest period. The load (L) varies temporally as a haversine function: with t=0 at the peak, the load function is expressed as:

$$L(t) = q \sin^2(\frac{\pi}{2} + \frac{\pi t}{d}) \tag{3.1}$$

where q is the maximum load, d is the duration of load, and t is time. All pavement profiles in the LSME were subjected to 10,000 cycles of traffic wheel loads simulating 4-axle trucks (70 kN per axle and 35 kN per wheel set) with a tire pressure of 700 kPa and a circular contact area with radius of 125 mm.

The pavement profile consisted of a 2.5-m-thick bottom layer of uniform sand simulating a deep and stiff subgrade overlain by a base course layer comprised of the materials being evaluated (Class 5 gravel, RPM, RSG, and mixtures with fly ash). An asphalt surface layer was not included. The stress to be applied at the surface of the base course was estimated by conducting nonlinear finite-element analyses of the pavement profile with the program MICH-PAVE (Harichandran et al. 1989). The asphalt surface was assumed to have an elastic modulus of 3540 MPa, a Poisson's ratio (ν) of 0.35 (Huang, 1993), and a thickness of 0.13 m. The base course was assumed to be 0.20 m thick and to have ν = 0.35. Modulus (M_r) of the base layer was assumed to follow the non-linear elastic power function model:

$$M_r = k_1 \sigma_b^{k_2} \tag{3.2}$$

where k_1 and k_2 are empirical parameters and σ_b is the bulk stress. For the base course, the parameter k_1 was assumed to be 27.8 MPa and k_2 was 0.5 (Huang 1993). The subgrade was assumed to be linearly elastic with a modulus (E) of 48 MPa and ν = 0.45. The stress distribution predicted by MICH-PAVE is shown in Fig. 3.2, where vertical stress on the surface of the base layer and the subgrade layer is graphed as a function of the radial distance from the center of the applied load. Fig. 3.2 shows that the stress at the surface of the base course decreases from a maximum of 144 kPa with increasing distance from the load center. This stress was applied in the LSME by applying a force of 7.3 kN to the loading plate.

3.1.2 Deflections

Vertical deflections of the pavement profile were measured on the base course surface directly beneath the loading plate and at distances of 200 and 300 mm from the centerline of the actuator. Vertical deflections of the subgrade surface were measured directly beneath the loading plate and at 200 mm from the centerline of the actuator. Linear variable differential transducers (LVDT) were used to measure deflections during each loading cycle. The LVDTs were capable of measuring deflections to 0.005 mm. Deflection measurements taken at the subgrade surface were accomplished by mounting small plates on each end of a thin rod running through a tube that extended though the overlying layer of base course. One plate rested on the subgrade surface while the LVDT rested on the plate above the base course surface, with the tube eliminating friction between the base course and the rod and allowing the rod and plate assembly to move freely with the subgrade. The load and deflection data were collected with a desktop personal computer running a LABVIEW 7.1 software program developed specifically for this application.

3.1.3 Data Inversion

Resilient modulus of the base layer was obtained by inversion with MICH-PAVE using the applied loads and the measured deflections. Accumulated plastic (non-recoverable) deflections were subtracted from the total deflections measured by the LSME to obtain the elastic deflections for analysis. The underlying sand layer was assumed to be linearly elastic and the modulus of the base course was assumed to follow the elastic power function in Eq. 3.2. The parameter k_2 was fixed at the value obtained from a resilient modulus laboratory test conducted per NCHRP 1-28A and the parameter k_1 was varied until the predicted deflections from MICH-PAVE were within 0.005 mm of the measured deflections in the LSME. This approach assumes k_2 varies within a narrow range for a particular material type (Huang 2003) and follows the approach described by Tanyu et al. (2003).

3.1.4 Placement of Base Course

Base course materials were placed in lifts approximately 0.1 m thick so that each material could be compacted uniformly. A vibratory plate compactor was used to compact and a nuclear density gage was employed to measure the dry unit weight and water content. Each lift was compacted at the optimum water content (w_o) until the dry unit weight was 100% of the maximum dry unit weight ($\gamma_{d\ max}$) corresponding to standard Proctor effort. Soil specimens created for the NCHRP 1-28A resilient modulus tests were also compacted to $\gamma_{d\ max}$ and w_o allowing a more direct comparison of the M_r resulting from the two test methods.

For base course materials blended with fly ash, mixing of the soil and fly ash was accomplished using a skid loader. The amount of material required for one lift was spread out on a concrete surface, and 10% fly ash by weight was blended with the base material having water content dry of optimum. Once the fly ash was blended thoroughly and the material had a uniform color, additional water was added to bring the water content of the mixture to optimum. Water was sprinkled evenly over the material while mixing continued with the skid loader. After

mixing for approximately 20 minutes, the mixture was placed in the test pit and compacted immediately. The entire mixing and compacting procedure took about 45 min. Three separate lifts were mixed and placed in the test pit, with about 1 hour passing between compaction of subsequent lifts.

3.2 SUPPLEMENTAL TESTS

Modulus of the base course materials in the LSME test pit was measured with a soil stiffness gauge (SSG) and two types of light-weight deflectometers (LWD). Penetration testing of the base course was also conducted using a dynamic cone penetrometer (DCP).

3.2.1 SSG

The SSG measures the in-situ stiffness of soil (K_{SSG}) by transferring a small dynamic force to the soil through a ring-shaped foot at 25 steady-state frequencies between 100 and 196 Hz. The modulus (E_{SSG}) of the material is then computed from K_{SSG} and both properties are reported by the equipment. The modulus (E_{SSG}) of materials near the surface is calculated from:

$$K_{SSG} = \frac{1.77 E_{SSG} R}{(1 - v^2)} \qquad (3.3)$$

where R is the outside radius of the ring foot (110 mm) on the SSG (Sawangsuriya et. al 2005). The Poisson's ratio (v) used was 0.35 for materials without fly ash, and 0.20 for RSG and RPM blended with fly ash. The SSG device measures elastic modulus with v equal to 0.40, so the SSG measurements are corrected using the v of the material being measured. SSG tests were conducted with Model H-4140 manufactured by Humboldt Manufacturing Co. (Schiller Park, IL).

SSG tests were conducted by seating the device on a smooth level surface sprinkled with sand to allow complete contact with the ring shaped foot. The gauge was twisted back and forth by 90 degrees two to three times for good contact, and then the measurement was taken and the displayed K_{SSG} and E_{SSG} were recorded. The signal to noise ratio was limited to be greater than 15 and standard deviation less than 1.5 to prevent any erroneous measurement. Typically three measurements were taken for a single seating, and the results averaged. Measurements were taken in at least two different locations in the LSME test pit. A photo of the SSG displaying the results of a measurement is shown in Fig 3.3.

3.2.2 LWD

Two LWDs were used to determine elastic modulus of the base course material: a Keros 100 (Dynatest, Denmark) and a ZFG 2000 (Zorn, Germany). For the Keros 100, a 10-kg weight is dropped to produce a dynamic load on a plate. A load sensor measures the load pulse, and a geophone at the center of the plate measures the corresponding soil deflection. For the ZFG 2000, a plate stress is assumed based on a pre-defined calibration for a falling weight, and the

plate deflection is measured using an accelerometer. For both devices, the modulus for a specific drop height (DH) for either device can be calculated as (White et. al 2007):

$$E = \frac{f(1-v^2)\sigma r}{d} \tag{3.4}$$

where σ is the peak stress applied at the surface, r is the radius of the loading plate, f is a factor that depends on the stress distribution, and d is the deflection corresponding to the peak stress. The variables used for each material tested are described in Table 3.1, where values used for f were adopted from Terzaghi and Peck (1967). The Keros 100 allows the input of a specific f and v for a given testing scenario while measuring σ and d for calculating E. However, the ZFG 2000 uses fixed constants for f, v and σ, so the internally calculated E is reported by the ZFG 2000. The reported E was not used; instead, E was calculated with Eqn. 3.4 using the measured d.

LWD tests were conducted by first dropping three seating blows, followed by three additional blows where the measured deflections and moduli were recorded and averaged. Measurements were taken in at least two different locations in the LSME test pit. A photo of a measurement being taken with the Keros 100 is shown in Fig 3.4.

3.2.3 DCP

The DCP is used to measure the penetration resistance of soil by driving a cone tip (60° apex, 20 mm base diameter) vertically into the soil by dropping an 8 kg hammer a distance of 575 mm (Sawangsuriya and Edil 2005). Penetration of the cone (in mm) is measured for each blow that is applied. In this study, a Dual Mass DCP manufactured by Kessler Soils Engineering Products, Inc. (Springfield, Virginia) was used to apply two initial seating drops, followed by three additional measurement drops. The dynamic penetration index (DPI) was then computed using the MnDOT Modified Penetration Index Method:

$$DPI = \frac{P_5 - P_2}{3} \tag{3.5}$$

where P is the penetration reading (in mm) at the second and fifth blows. Modulus of the base course (E) in MPa was estimated with:

$$E = 10^{3.05 - (1.06\log(DPI))} \tag{3.5}$$

which has been used in studies conducted by MnDOT (Davich et al. 2006).

Measurements were taken in at least two different locations in the LSME test pit, and the results were averaged. A photo of a measurement being taken with the DCP is shown in Fig 3.5.

4. RESULTS AND ANALYSIS

4.1 LSME DEFLECTIONS

A graph showing total deflection and plastic deformation at the surfaces of the base and subgrade under the loading plate of the LSME as a function of the number of load cycles is displayed in Fig. 4.1 for a 0.30 m thick layer of Class 5 gravel. The total deflection is the maximum deflection measured during each 0.1 s loading cycle, and plastic deformation corresponds to the position of the layer surface measured during the 0.9 s rest period where only the plate seating load was applied. Plastic deformation of the base and subgrade accumulates monotonically during the test, with the highest rate of accumulation occurring in the first 50 cycles. The difference between the total deflection and plastic deformation is the elastic deflection. Elastic deflections graphed as a function of the number of load cycles is shown in Fig 4.2 for both 0.20 and 0.30 m thick layers of Class 5 gravel. Elastic deflections were directly measured at the surface of the base course and subgrade layer, and net base course elastic deflection was calculated as the difference between the surface and the subgrade deflections. Fig. 4.2 shows that surface elastic deflection, and therefore net base elastic deflection decrease slightly throughout the course of the test due to the material becoming densely compacted under the loading plate, while the subgrade elastic deflection remains relatively constant. Elastic deflections for the 0.30 m thick layer are slightly less than the 0.20 m thick layer. This decrease in elastic deflection indicates a more extensive stress distribution within the thicker base layer associated with the low strain in the bottom of the layer. A similar decrease was seen for RPM and RSG.

10,000 cycles were applied to RPM and RSG blended with fly ash at curing times of 7, 14, 21 and 28 days for a total of 40,000 loading cycles on the same profile. Fig. 4.3a and b compare total deflections and plastic deformations of RPM and RSG blended with fly ash, and Fig. 4.4a and b compare the elastic deflections. Fig. 4.4a shows a sharp drop in elastic deflection of the surface between the 7 and 14 day test due to cementation of the soil and fly ash. The net base elastic deflection of both RPM and RSG remains nearly constant throughout the 28 day curing test. In Fig. 4.3b, increasing plastic deformation at the subgrade is seen only with the RSG.

A comparison of the elastic and plastic deflections at the base and subgrade for all LSME tests conducted are shown in Fig. 4.5 and summarized in Table 4.1, where the sum of the plastic and elastic deflections is equal to the total deflection. RSG has both the largest plastic and elastic deflections of the materials tested, and RSG blended with fly ash has the smallest deflections. The elastic deflections decrease with increasing layer thickness for Class 5 gravel, RPM, and RSG, but only the RSG has a smaller plastic deformation with increasing thickness. Materials blended with fly ash were tested at one thickness of 0.30 m. Deflections of the material blended with fly ash were much lower than for those without fly ash due to the cementation characteristics of fly ash. The elastic deflection of the subgrade was consistent between tests for materials with and without fly ash.

4.2 COMPARISON OF BACK-CALCULATED RESILIENT MODULI FROM LSME WITH LABORATORY RESILIENT MODULUS

The resilient modulus of the base course materials measured in the LSME and the laboratory test (NCHRP 1-28A) are shown in Fig 4.6 as a function of bulk stress. This relationship was obtained from the MICH-PAVE backcalculation based on measured deflections in the LSME, and the laboratory resilient modulus test results were those reported by Camargo (2008). Table 4.2 lists the parameters k_1 and k_2 from Eqn. 3.2. For materials without fly ash, the elastic modulus increases with the bulk stress; however, the elastic modulus is not sensitive to bulk stress for materials blended with fly ash resulting in a horizontal line. For base materials without fly ash, the elastic modulus measured in the LSME is sensitive to the thickness of the base layer, where thicker layers have a higher modulus at a given bulk stress. This sensitivity can be explained by the level of strain being different in layers of varying thickness, which is known to affect the elastic modulus of granular materials (Seed and Idriss 1970, Hardin and Drnevich 1972). Under the same applied surface load, a lower vertical strain will exist in thicker layers due to greater stress distribution in a thicker layer compared to a thinner layer. Due to the variation of resilient modulus with bulk stress, a summary resilient modulus (SRM) of each test was computed as suggested in Section 10.3.3.9 of NCHRP 1-28A, where for base materials the SRM corresponds to a bulk stress of 208 kPa. This comparison is shown in Fig 4.7, with the SRM listed in Table 4.2. For tests conducted without fly ash, resilient modulus of 0.30 m thick layers are higher than the laboratory test results, but no clear trend is seen between the laboratory tests and the 0.20 m thick layer tests. For both the laboratory and LSME results, RSG has the lowest SRM, and RPM has the highest with Class 5 gravel in between. The SRM increases significantly when fly ash is added to the base materials. The SRM of laboratory test results with fly ash are more than double the LSME test results with fly ash, explained by more thorough mixing and controlled curing in 100% humidity, which was not feasible to replicate in the LSME. For both the laboratory and the LSME tests, the SRM increases over a 28 day curing period, as demonstrated in Fig 4.8 where the resilient modulus is normalized to the resilient modulus obtained at 7 days of curing. The LSME RPM shows the largest percent increase between 7 and 28 days, with the lowest increase corresponding to LSME RSG.

4.3 COMPARISON OF BACK-CALCULATED RESILIENT MODULI FROM LSME WITH ELASTIC MODULUS OF SUPPLEMENTARY TESTS.

The elastic moduli obtained from the SSG, LWDs, and DCP are compared to the SRM determined from the LSME tests in Fig. 4.9. All moduli obtained from these supplementary test methods are less than the LSME SRM, as they are located below the 1:1 line. All tests conducted on a specific base course material appear as a vertical column of data points on the graph, because each test method is being compared to the single LSME SRM at a thickness of 0.30 m. The ZFG 2000 LWD consistently gives the lowest elastic modulus for all materials, while the Keros 100 LWD gives the highest elastic modulus for materials blended with fly ash, which are also the closest to the LSME SRM. Class 5 gravel has the lowest measurements of modulus for all supplementary tests except the Keros 100, which indicated RSG to have the lowest modulus, consistent with the LSME SRM and the laboratory tests. Therefore, the Keros 100 LWD appears to most closely measure the modulus of the base course materials as tested in the lab and LSME of the various supplementary tests conducted.

A source of inconsistency between the LWD and LSME elastic modulus measurements is the effect of the subgrade material. The LWD calculates the modulus assuming an elastic-homogeneous half space and neglects the effect of the subgrade. Moreover, the level of stress and strain is different in the LSME and LWD. The elastic modulus measured by the Keros Pima 100 for materials with fly ash is relatively close to LSME SRM due to strain and stress independency of this material in the range of applied stress. The ZFG 2000 consistently gives a lower modulus than the Keros 100 at a similar stress level as Keros 100, which may result from the difference in measurement accuracy of these two devices.

4.4 DETERMINATION OF GRAVEL EQUIVALENCY OF THE BASE COURSE MATERIALS.

Determining the appropriate thickness of the pavement layers based on engineering properties is a critical task in the design of pavement structures, and MnDOT uses the concept of Gravel Equivalency (GE) (Kersten et. al 1968; Lukanen 1980) to determine layer thicknesses. GE factors provide a means of equating the structural performance of all bituminous and aggregate courses constituting a pavement structure with respect to the structural performance of a select, high-quality, aggregate base. MnDOT's Class 5 and 6 aggregate bases are used as the selected standards (MnDOT Specification 3138). The GE concept is convenient for rating pavement structures in similar "units" for the purposes of comparison. For example, a hot mix asphalt (HMA) surface layer would have a lower GE thickness than its actual thickness due to the superior performance of the material as compared to the Class 5 or 6 base material.

The GE was determined for the RPM and RSG with and without fly ash based on the results of the LSME tests. The method used for obtaining the GE incorporates existing procedures used by MnDOT and AASHTO (Skok et. al 2003; AASHTO 1993). The MnDOT Soil Factor Design Procedure defines a soil using a soil factor (SF) based on the AASHTO soil classification of the material. A chart is used that relates the SF to minimum bituminous GE and the total GE for specific traffic loading categories. The MnDOT R-Value design method uses a chart that determines the required GE based on the embankment R-Value and traffic evaluated in terms of 80 kN equivalent single axle loads (ESALs) estimated for a design lane in one direction. The embankment R-Value can be measured by the standard laboratory test described in ASTM D-2844 or estimated from soil type or classification.

The following equation is used to calculate the GE:

$$GE = a_1D_1 + a_2D_2 + a_3D_3 \tag{4.1}$$

where D_1, D_2, and D_3 are the thicknesses of the asphalt mix surface, the granular base course and granular subbase course (mm) respectively, and a_1, a_2, and a_3 are GE factors listed in Table 4.3. The GE factors are assigned to materials based on the MnDOT specification that they fall under and have been determined from decades of experience (Skok et. al 2003).

A similar method of determining layer thickness is described by AASHTO, where the quality of the HMA, base and subbase is each characterized by a structural layer coefficient depending on the mechanical properties of the material. The structural layer coefficient is used to calculate a layer structural number (SN) representing the required structural capacity of the pavement layer. Total SN is the summation of the structural number of each pavement layer:

$$SN = SN_1 + SN_2 m_2 + SN_3 m_3 = b_1 D_1 + b_2 D_2 m_2 + b_3 D_3 m_3 \tag{4.2}$$

where SN_i is the structural number, m_i is the drainage modification factor, b_i is the layer coefficient, and D_i is the thickness of the layer i.

The layer coefficient has been shown to be a function of resilient modulus of a granular base layer (Rada and Witczak 1981):

$$b_2 = 0.249 \log M_r - 0.977 \tag{4.3}$$

where M_r is the resilient modulus of the granular base material. Assuming the same subgrade resilient modulus and the same thickness and resilient modulus of the asphalt layer, the layer coefficient of an alternative base material can be determined. Both the GE and SN methods were based on the results of the AASHO Road Test used to determine the structural performance of pavement systems (Kersten and Skok 1968), and are therefore combined in determining the GE of the alternative materials used in this study (RPM or RSG with or without fly ash).

Thickness ratios of an alternative and conventional base material are determined from Eqn. 4.1. The GE using a conventional base material is:

$$GE = a_1 D_1 + a_c D_c \tag{4.4}$$

where the subscript c denotes a conventional base course material, which for this study is Class 5 gravel having a_c equal to 1.00. Similarly for an alternative base material:

$$GE = a_1 D_1 + a_a D_a \tag{4.5}$$

where the subscript a denotes an alternative base course material. Setting the GE of Eqn. 4.4 equal to that of Eqn. 4.5 and assuming a_1 and D_1 remain constant for the HMA surface layer, the relationship between the thicknesses and GE factors for the two base materials can be obtained as:

$$\frac{a_a}{a_c} = \frac{D_c}{D_a} \tag{4.6}$$

A similar procedure can be carried out with Eqn. 4.2 for the conventional and alternative base course materials to obtain the same relationship as in Eqn. 4.6, only with layer coefficients instead of GE factors. Substituting Eqn. 4.3 for the layer coefficients in Eqn. 4.6 results in:

$$\frac{D_c}{D_a} = \frac{0.249 \log M_{r_a} - 0.977}{0.249 \log M_{r_c} - 0.977} \tag{4.7}$$

Finally by substituting Eqn. 4.7 into 4.6 and setting a_c equal to 1.00, the GE factor of an alternative base material can be determined as:

$$a_a = \frac{0.249 \log M_{r_a} - 0.977}{0.249 \log M_{r_c} - 0.977}$$

(4.8)

The SRM of base materials blended with fly ash measured in the LSME can be input directly into Eqn. 4.8, since it has been shown that the resilient modulus is not dependent on bulk stress, and therefore assumed not to vary with thicknesses typically used in road construction. The resilient modulus varies with bulk stress and layer thickness for the granular materials without fly ash. Fig. 4.10 shows the relationship between base layer thickness and the SRM for Class 5 gravel, RPM and RSG. Only thicknesses of 0.20 and 0.30 m were tested in the LSME. The SRM corresponding to other typical base course thicknesses were predicted by using a backbone curve and a numerical analysis with MICH-PAVE described in Attachment A. Calculating the resilient modulus and substituting into Eq. 4.8 results in a relationship between the GE factor and the thickness of the base layer shown in Fig. 4.11. The GE factor for RPM of 1.07 is slightly higher than the GE factor of 1.00, and RPM is the only alternative material that has a constant GE factor because the resilient modulus of RPM and Class 5 gravel vary with layer thickness in a similar manner. The GE factors of RSG are less than 1.00, indicating that the material has less desirable structural properties than Class 5 gravel. The GE factors for RPM and RSG blended with fly ash are nearly identical, and described by a single function in Fig. 4.11. The materials blended with fly ash have a GE factor greater than 1.00, indicating a lesser thickness would be needed than that of Class 5 gravel. Fig. 4.12 shows the thickness of an alternative material compared to the required thickness of Class 5 gravel, and was developed by determining the GE factor for an alternative base material at a specific layer thickness of Class 5 gravel, and then inputting into Eq. 4.6. Fig. 4.12 is a tool that could be used to aid in the design of roads incorporating alternative materials.

5. SUMMARY AND CONCLUSIONS

This phase of laboratory investigation dealt with the influence of fly ash addition on the resilient modulus of two recycled roadway materials: recycled pavement material (RPM) and recycled road surface gravel (RSG). The main objective was to develop the Gravel Equivalency (GE) of these recycled materials with and without fly ash stabilization. To meet this objective, the modulus of recycled materials with and without fly ash was determined from a Large Scale Model Experiment (LSME) and compared with the resilient modulus determined from the laboratory test method described by NCHRP 1-28A. The elastic modulus was also determined by other means, i.e., with a Soil Stiffness Gage (SSG), two types of Light Weight Deflectometer (LWD), and a Dynamic Cone Penetrometer (DCP), and compared to the resilient modulus from the LSME. A Class C fly ash with a content of 10% by weight, which is typical of such applications, was used in stabilization of RPM and RSG and curing times of 7 and 28 days were evaluated. Class 5 gravel, with a conventional base material gradation employed in Minnesota, was used as a reference material.

The gravel equivalency (GE) factor for RPM was determined to be equal to 1.07 and did not vary with base layer thickness, indicating that this material is similar to that of Class 5 gravel having a GE factor of 1.00. The GE factor of RSG varied with thickness and was less than 1.00 indicating that RSG has less desirable structural properties than Class 5 gravel. The GE factor of RPM and RSG blended with fly ash varies with thickness of the base layer in a nearly identical manner so one relationship is used for both materials. The GE factor of the fly ash stabilized materials decreases with increasing base layer thickness with the constant modulus assumed for these materials, becoming approximately equal to 1.00 at a thickness of 0.55 m.

The following behavioral trends were observed for the materials tested in this program:
1. Both RPM and RSG had plastic deformations greater than Class 5 base. The greatest plastic deformation measured in the LSME was for RSG. The plastic deformation decreases significantly with the addition of fly ash, where RSG with fly ash had the least plastic deformation overall.
2. RSG had the largest elastic deformations, resulting in the lowest modulus (116 MPa for 200 mm thickness and 216 MPa for 300 mm thickness) and RSG blended with fly ash at 28 days of curing had the highest resilient modulus (918 MPa). RPM had a modulus slightly greater than Class 5 base for each thickness. For all three materials tested without fly ash, the modulus increased with an increase in base layer thickness. The modulus of RPM and RSG increased significantly with the addition of fly ash, and continued to increase in stiffness over a curing time of 28 days. For 300 mm thick layers, the modulus of RPM with fly ash after 28 days of curing was 67% higher than RPM without fly ash, while the modulus of RSG with fly ash increased by 325%. RPM with fly ash displayed the greatest rate of increase of modulus between 7 and 28 days. The modulus determined from the LSME tests was less than half of the summary modulus measured in the laboratory resilient modulus test due to the differences in mixing of the materials with fly ash and the curing conditions. The LSME modulus is expected to be closer to actual field conditions than the laboratory test.
3. The resilient modulus was found to increase with the bulk stress for the all three granular base course materials (i.e., without fly ash) indicating the nonlinearity or stress-dependency of these materials. However with the addition of fly ash, the resilient modulus did not show stress dependency for a range of stresses typically resulting from

wheel loads and was considered to be a linear elastic material as confirmed by laboratory resilient modulus tests and varying stress applied to the LSME specimen.

4. The LSME modulus was found to be greater than the elastic modulus obtained with the SSG, LWDs or the DCP performed on the same layer in the LSME. These test methods showed Class 5 base having the lowest modulus instead of RSG as determined to be the lowest with the LSME. All test methods gave a higher modulus for materials blended with fly ash than those without fly ash. The ZFG 2000 LWD consistently gave the lowest modulus for all materials, and the Keros 100 LWD gave the highest modulus for base materials blended with fly ash, which are relatively close to the LSME modulus. When the LWD deflections are corrected and compared to the LSME modulus based on the same stress level, the differences are significantly reduced as described in Attachment B.

REFERENCES

AASHTO (1993). *Guide for Design of Pavement Structures*, American Association of State Highway and Transportation Officials, Washington, D.C.

AASHTO (2001). *Standard Specifications for Transportation Materials and Methods of Sampling and Testing, 21st Ed*., American Association of State Highway and Transportation Officials, Washington, D.C., *Part 1, Specifications*, M 147-65

Analog Devices (2007). Analog Devices, Inc. Web Site. http://www.analog.com.

Brandl, H., Adam, D., Kopf, F., and Niederbrucker, R. (2003). "Der dynamische lastplattenversuch mit dem leichten fallgewischtesgerät," Bundesministerium für Verkehr: Innovation und Technologie, Straßenforschung, Heft 528, Wien.

Camargo, F. (2008). "Strength and Stiffness of Recycled Base Materials Blended with Fly Ash," *MS Thesis*, University of Wisconsin-Madison, Madison, WI.

Das, B. M. (1998). *Principles of geotechnical engineering,* 4th Ed., PWS Publishing Company, Boston, MA.

Davich, P. (2005). "Analysis of LWD load estimation from measurements of deflection, Final Report," Minnesota Department of Transportation, St. Paul, MN.

Davich, P., Camargo, F., Larsen, B., Roberson, R., and Siekmeier, J. (2006). "Validation of DCP and LWD Moisture Specifications for Granular Materials," Minnesota Department of Transportation Report No. MN/RC-2006-20

Deng-Fong, L., Chi-Chau, L., and Jyh-Dong, L (2006). "Factors affecting portable falling weight deflectometer measurements," *J. Geotech. and Geoenvir. Engrg*., ASCE, 132(6), 804-808.

Dynatest (2004). *Keros portable FWD – Instruction manual for use and maintenance*, Issue No. 010704, Denmark.

Edil, T. B. and Luh, G. F. (1978), "Dynamic Modulus and Damping Relationships for Sands," Proceedings of the Specialty Conference on Earthquake Engineering and Soil Dynamics, ASCE, Reston, VA, pp. 394-409.

Fleming, P. R., Rogers, C. D. F., and Frost, W. (1998). "Performance parameters and target values for construction of UK road foundations," Proc., 5th Intl. Conf. on Bearing Capacity of Roads and Airfields, Vol. 3, Trondheim, Norway, 1491-1502.

Fleming, P. R. (1998). "Recycled bituminous planings as unbound granular materials for road foundations in the UK," Proc., 5th Intl. Conf. on Bearing Capacity of Roads and Airfields, Vol. 3, Trondheim, Norway, 1581-1590.

Fleming, P. R. (2000). "Small-scale dynamic devices for the measurement of elastic stiffness modulus on pavement foundations," Nondestructive Testing of Pavements and Backcalculation of Moduli: Third Volume, ASTM STP 1375, Tayabji and Lukanen, eds., American Society of Testing and Materials, West Conshohocken, Pa., 41-58.

Fleming, P. R., Frost, M.W., and Rogers, C. (2000). "A comparison of devices for measuring stiffness in-situ." Proc., Unbound Aggregates in Road Construction – UNBAR 5, Dawson, A. R., ed., Balkema, Rotterdam, 193-200.

Fleming, P. R. (2001). "Field measurement of stiffness modulus for pavement foundations," Proc., 80th Annual Transportation Research Board Meeting, Washington D.C., Paper No. 01-2145.

Fleming, P. R., Lambert J. P., Frost M. W., and Rogers, C. (2002). "In-situ assessment of stiffness modulus for highway foundations during construction," Proc., 9th Intl. Conf. on Asphalt Pavements, Copenhagen, Denmark (CD-ROM).

Hardin, B. O. and Drnevich, V. P. (1972), "Shear Modulus and Damping in Soils: Design Equations and Curves," *Journal of Soil Mechanics and Foundations Division*, ASCE, Vol. 98, No. 7, pp. 667-692.

Hardin, B.O. and Richart, F.E., Jr. (1963). "Elastic Wave Velocities in Granular Soils," *Journal of the Soil Mechanics and Foundations Division*, Proceedings of the ASCE, Vol. 89, No. SM 1, pp. 33 – 65.

Harichandran, R. S., G. Y. Baladi, and M. Yeh, (1989). "Development of a Computer Program for Design of Pavement Systems Consisting of Bound and Unbound Materials," Department of Civil and Environmental Engineering, Michigan State University, Lansing, Michigan.

Hatipoglu, B., Edil, T., and Benson, C. (2008). Evaluation of base prepared from road surface gravel stabilized with fly ash, *GeoCongress 2008 ASCE Geotechnical Special Publication,* 177, New Orleans, LA, pp. 288-295.

Huang, Y. (1993). *Pavement analysis and design*, 1st Ed., Prentice-Hall, Inc., Englewood Cliffs, New Jersey.

Janz, M. and Johansson, S.-E. (2002). "The Function of Different Binding Agents in Deep Stabilization," Report 9. Swedish Deep Stabilization Research Centre, Linkoping, Sweden.

Kersten, M.S. and Skok, E.L. (1968). *Application of AASHO Road Test Results to Design of Flexible Pavements in Minnesota*, MHD Investigation No. 183, Interim Report, University of Minnesota, MN.

Kim, D. S., and Stokoe II, K. H. (1992), "Characterization of Resilient Modulus of Compacted Subgrade Soils Using Resonant Column and Torsional Shear Tests," Transportation Research Record, 1369, Transportation Research Board, National Research Council, Washington, DC, pp. 83-91.

Kokusho, T. (1980). "Cyclic Triaxial Test of Dynamic Soil Properties for Wide Strain Range," *Soils and Foundations*, Vol. 20, No. 2, pp. 45-60.

Kopf, F., and Adam, D. (2004). "Load plate test with the light falling weight device," *Proc., 16th European Young Geotechnical Engineers* Conference – EYGEC, Vienna.

Lenngren, C. (1992). "Discussion: Effects of buffers on falling weight deflectometer loadings and deflections, By Lukanen, E.O.," *Transportation Research Record* No. 1355, Transportation Research Board, Washington, D. C., 51.

Li, L., Benson, C. H., Edil, T. B., Hatipoglu, B. (2008). "Sustainable Construction Case History: Fly Ash Stabilization of Recycled Asphalt Pavement Material," *Geotechnical and Geological Engineering*, Vol. 26, No. 2, pp. 177-188.

Lukanen, E.O. (1980). *Application of AASHO Road Test Results to Design of Flexible Pavements in Minnesota,* Investigation No. 183, Report No. FHWA-MN-80-09, Minnesota Department of Transportation, MN.

MnDOT (2005). *Standard Specifications for Construction*, Minnesota Department of Transportation, St. Paul, MN.

Nazzal, M. D, Abu-Faraskh, M., Alshibli, K., and Mohammad, L. (2004). "Evaluating the potential use of a portable LFWD for characterizing pavement layers and subgrades," *Proc., Geo-Trans 2004 – Geotechnical Engineering for Transportation Projects*, Vol. 1, Geotechnical Special Publication No. 126, , Los Angeles, Ca.

Nazzal, M. D, Abu-Faraskh, M., Alshibli, K., and L. Mohammad. (2007). "Evaluating light falling-weight deflectometer device for in-situ measurement of elastic modulus of pavement layers," *Proc., 86th Annual Transportation Research Board Meeting*, Washington D.C., Paper No. 07-0035.

NCHRP (2004). *Laboratory Determination of Resilient Modulus for Flexible Pavement Design*, *National Cooperative Highway Research Program Research Results Digest*, 285, pp 1-48.

Rada, G. and M. W. Witczak, 1981. "A Compressive Evaluation of Laboratory Resilient Moduli Results for Granular Materials," *Transportation Research Record No. 810*, Transportation Research Board, Washington D.C.

Richart, F.E., Jr., Hall, J.R., and Woods, R.D. (*1970). Vibrations of Soils and Foundations,* Prentice Hall, Inc., Eaglewood Cliffs, NJ.

Rosa, M. (2006). "Effect of Freeze and Thaw Cycling on Soils Stabilized using Fly Ash," *MS Thesis*, University of Wisconsin-Madison, Madison, WI.

Santamarina, J.C., Klein, K.A., and Fam, M.A. (2001). *Soils and Waves*. John Wiley & Sons Ltd., West Sussex, England, 488 pp.

Sawangsuriya, A., and Edil, T. B. (2005). "Evaluating stiffness and strength of pavement materials." *Geotechnical Engineering*, 158(4), 217-230.

Sawangsuriya, A., Edil, T. B., Bosscher, P. J. (2005). "Relationship between Soil Stiffness Gauge Modulus and Other Test Moduli for Granular Soils." *Transportation Research Record*, 1849, Transportation Research Board, National Research Council, Washington, DC, pp. 3-10.

Schuettpelz, C. (2008). "Evaluation of The Influence of Geogrid Reinforcement on Stiffness in Compacted Base Course Material," *MS Thesis*, University of Wisconsin-Madison, Madison, WI.

Seed, H. B. and Idriss, I.M. (1970), "Soil Moduli and Damping Factors for Dynamic Response Analyses," Report No. EERC 70-10, University of California, Earthquake Engineering Research Center, Berkeley, CA.

Skok, E. L., Timm, D. H., Brown, M. L., Clyne, T. R., Johnson, E. (2003). "Best Practices for the Design and Construction of Low Volume Roads Revised," Report No. MN/RC – 2002-17REV.

Tanyu, B.F. (2003). "Working Platforms for Flexible Pavements Using Industrial By-Products." *PhD. Thesis*, University of Wisconsin – Madison, WI.

Tanyu, B. F., Kim, W. H., Edil, T. B., and Benson, C. H. (2003), "Comparison of Laboratory Resilient Modulus with Back-Calculated Elastic Moduli from Large-Scale Model Experiments and FWD Tests on Granular Materials," Resilient Modulus Testing for Pavement Components, *ASTM STP 1437, Paper ID 10911*, G. N. Durham, A. W. Marr, and W. L. De Groff, Eds., ASTM International, West Conshohocken, PA.

Tastan, E. (2005). "Stabilization of Organic Soil using Fly Ash," *MS Thesis*, University of Wisconsin-Madison, Madison, WI.

Terzaghi, K., and Peck, R. B. (1967). *Soil Mechanics in Engineering Practice*, 2nd Ed., John Wiley & Sons, Inc., New York.

Wen, H., Tharaniyil, M., Ramme, B. and Krebs, U. (2004). "Field performance evaluation of class C fly ash in full-depth reclamation: case history study," *Journal of the Transportation Research Board,* 1869, pp. 41-46.

White D., Thompson, M., and Vennapusa P. (2007), "Field Validation of Intelligent Compaction Monitoring Technology for Unbound Materials," Report No. MN/RC-2007-10, Center for Transportation Research and Education, Iowa State University, Ames, IA.

Zorn, G. (2003). Operating manual: *Light drop-weight tester ZFG2000*, Zorn Stendal, Germany.

TABLES

Table 2.14. Index properties for Class 5 base, RPM, and RSG.

Sample	D_{50} (mm)	C_u	C_c	G_s	w_{opt} (%)	$\gamma_{d\,max}$ (kN/m^3)	Asphalt Content (%)	LL (%)	PL (%)	Gravel Content (%)	Sand Content (%)	Fine Content (%)	USCS Symbol	AASHTO Symbol
Class 5 base	2.25	33.3	0.7	2.72	5.0	20.9	-	NP	NP	36.6	59.3	4.1	SP	A-1-a
RPM	3.89	89.5	2.5	2.64	7.5	21.2	4.6	NP	NP	46.0	43.0	10.6	GW-GM	A-1-a
RSG	0.80	40.0	1.0	2.73	7.5	22.6	-	21	14	28.6	59.0	12.4	SC-SM	A-2-4

D_{50} = median particle size, Cu = coefficient of uniformity, Cc = coefficient of curvature, Gs = specific gravity, w_{opt} = optimum water content, $\gamma_{d\,max}$ = maximum dry density, LL = liquid limit, PL = plastic limit, NP = nonplastic.

Note: Particle size analysis conducted following ASTM D 422, Gs determined by ASTM D 854, $\gamma_{d\,max}$ and w_{opt} determined by ASTM D 698, USCS classification determined by ASTM D 2487, AASHTO classification determined by ASTM D 3282, asphalt content determined by ASTM D 6307, and Atterberg limits determined by ASTM D 4318.

Table 15.2. Columbia fly ash physical properties and chemical composition (from Tastan 2005).

Parameter	Columbia	Typical Class C
SiO_2 , %	31.1	40
Al_2O_3 , %	18.3	17
Fe_2O_3 , %	6.1	6
$SiO_2 + Al_2O_3 + Fe_2O_3$, %	55.5	63
CaO , %	23.3	24
MgO , %	3.7	2
SO_3 , %	-	3
CaO/SiO_2	0.8	-
$CaO/(SiO_2+Al_2O_3)$	0.4	-
Loss on Ignition, %	0.7	6
Fineness, amount retained on #325 sieve, %	12	-

Table 2.16. Maximum dry unit weights and optimum CBRs for Class 5 base, RPM, and RSG with and without fly ash.

Material	Fly Ash Content (%)	Optimum Water Content* (%)	Maximum Dry Unit Weight (kN/m^3)	CBR (%)
Class 5 base	0	5.0	20.9	10
RPM	0	7.5	21.2	22
	10	8.5	20.4	67
	15	9.5	20.1	134
RSG	0	7.5	22.6	21
	10	6.6	22.0	84

* Optimum water content for dry unit weights.

Table 3.1. Variables used for LWD Measurements.

Base Material	Input Variable			
	Drop Height (mm)	r (mm)	ν	f
Class 5	500	100	0.35	2
RPM			0.35	2
RSG			0.35	$\pi/2$
Base + Fly Ash			0.20	2

Table 4.1. Measured Deflections at the end of 10,000 Cycles of Loading from LSME

Base Material	Layer Thickness (mm)	Base Elastic (mm)	Base Plastic (mm)	Subgrade Elastic (mm)	Subgrade Plastic (mm)	Total Deflection(mm)
Class 5 Gravel	200	0.065	0.630	0.154	0.217	1.066
	300	0.059	0.761	0.150	0.130	1.100
RPM	200	0.052	0.963	0.157	0.171	1.343
	300	0.073	1.060	0.139	0.069	1.311
RSG	200	0.165	1.981	0.160	0.213	2.519
	300	0.118	1.656	0.140	0.120	2.034
RPM + Fly Ash	300	0.024	0.034	0.058	0.000	0.116
RSG + Fly Ash	300	0.022	0.000	0.061	0.013	0.096

*Materials with fly ash reported at 28 days of curing

Table 4.2. Summary Resilient Modulus (SRM) and power model fitting parameters k_1 and k_2 (Eq. 3.2) for base materials with and without fly ash.

Material	Test method	Thickness (mm)	Fly Ash Content (%)	Curing Time (d)	Measured Parameters		
					k_1	k_2	SRM (MPa)
Class 5 base	Lab*	300	0	-	13.6	0.534	236
	LSME	200		-	19.7	0.53	284
		300		-	29.5	0.53	426
RPM	Lab*	300	0	-	49.2	0.344	309
	LSME	200		-	50	0.34	307
		300		-	82	0.34	505
	Lab*	300	10	7	1753	0	1753
		300		28	2702	0	2702
	LSME	300		7	483	0	483
		300		28	845	0	845
RSG	Lab	300	0	-	21.6	0.44	226
	LSME	200		-	11	0.44	115
		300		-	20.6	0.44	216
	Lab	300	10	28	5150	0	5150
	LSME	300		7	673	0	673
		300		28	918	0	918

Note: Summary Resilient Modulus is calculated at a bulk stress of 208 kPa.
* Reported by Camargo (2008)

Table 4.3. Granular Equivalent (GE) Factors adopted from Skok et. al (2003).

Material	Type of material	GE Factor
Hot Mix Asphalt	Spec. 2360/2350	2.25
Road-mix Surface (base)	Spec 2321	1.50
Bituminous-Treated Base (rich/lean)	Spec 2204	1.50/1.25
Aggregate Base	Spec. 3138(Class 5 & 6)	1.00
Aggregate Base	Spec. 3138(Class 3,4 & 7)	0.75
Select Granular	Spec 3149.2C	0.50

FIGURES
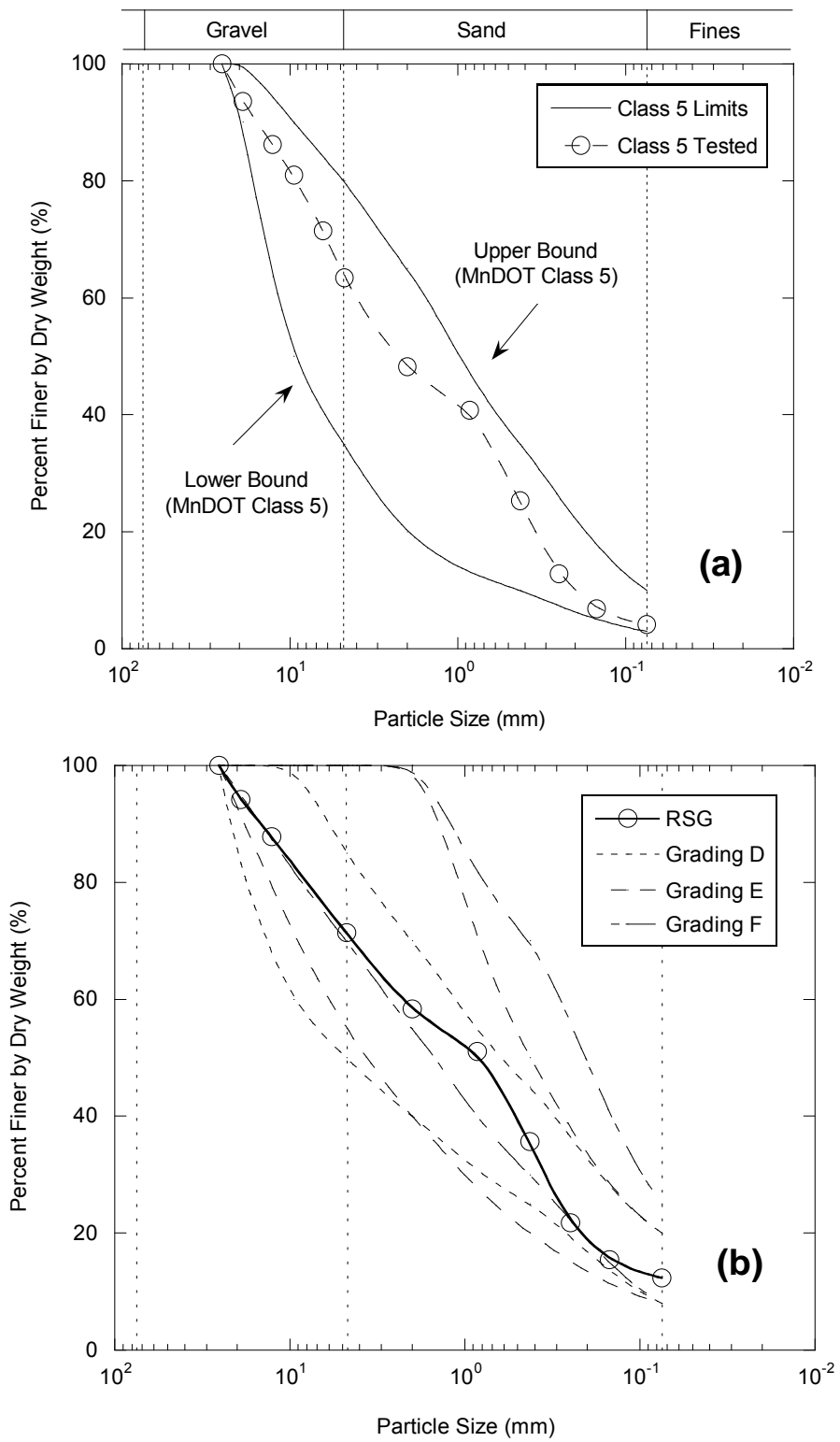
Fig. 2.18. Particle size distribution for Class 5 base used in this study with MnDOT Class 5 specifications (a) and RSG with AASHTO surface course specifications (b).
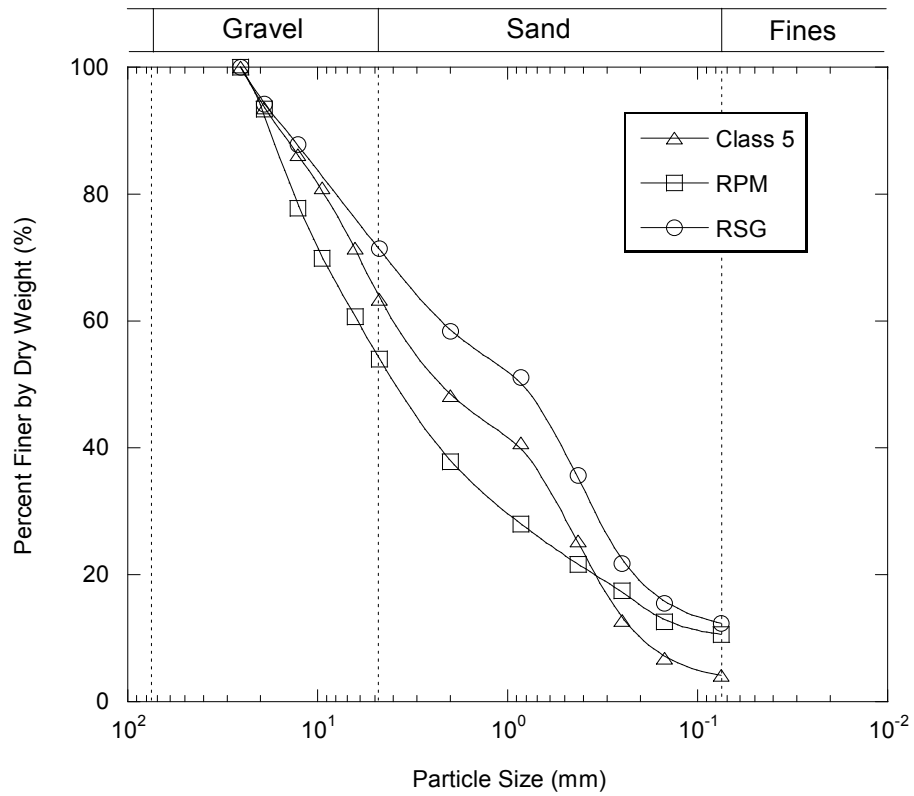
Fig. 19.2. Particle size distributions for Class 5 base, RPM, and RSG.
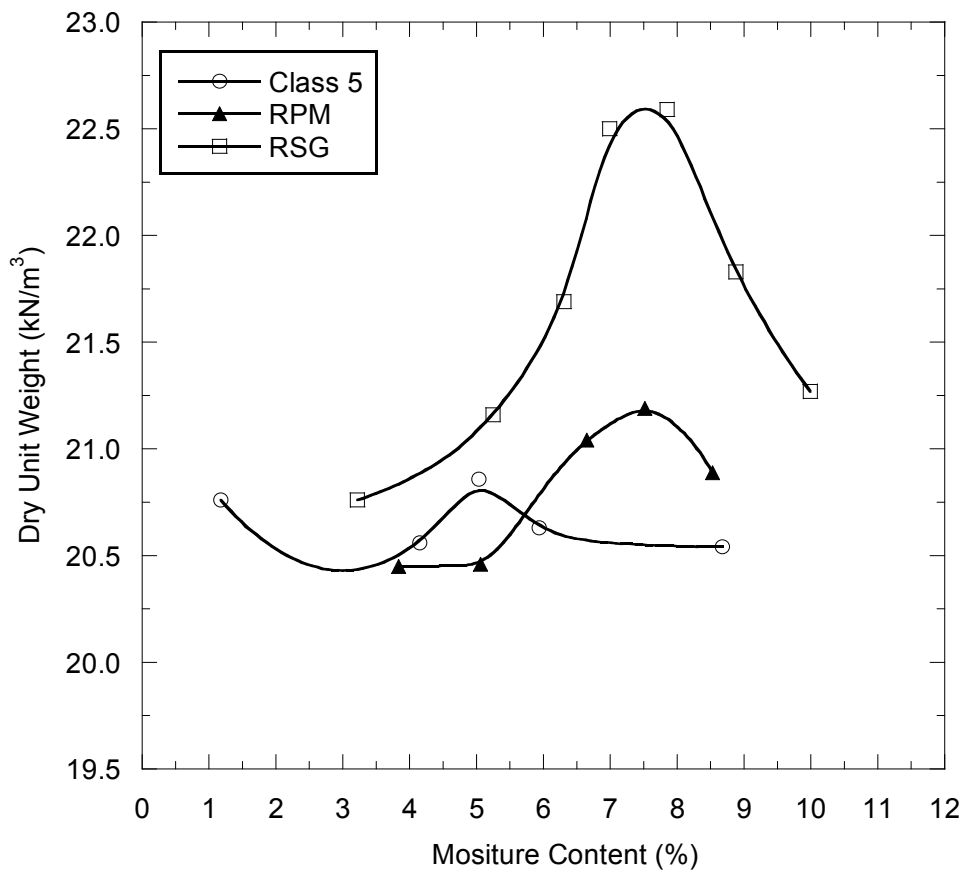
Fig. 2.20. Compaction curves for Class 5 base, RPM, and RSG for standard compactive effort.

Cyclic Load

Circular
Steel Plate
(d = 0.25 m)

Ground Surface

Base (Test Materials)

0.20 - 0.30 m

Reinforced
Concrete
Pit Walls

Sand Layer

2.50 m

3.00 m
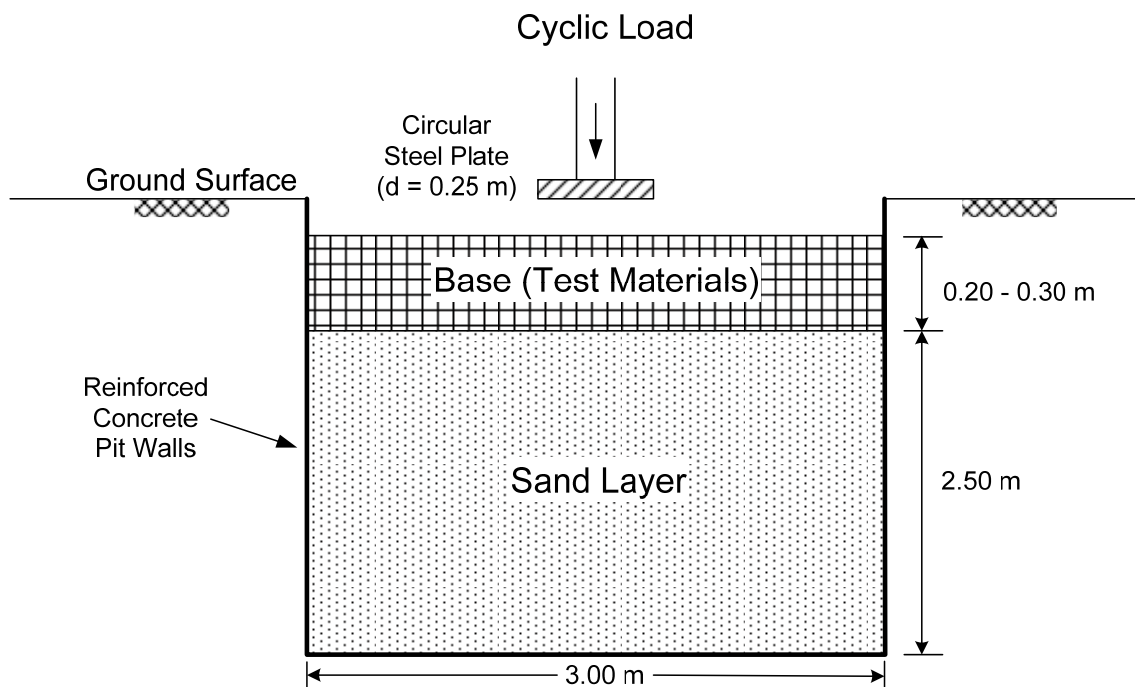
Fig. 3.1. Schematic cross section of Large-Scale Model Experiment (adopted from Tanyu et. al 2003).
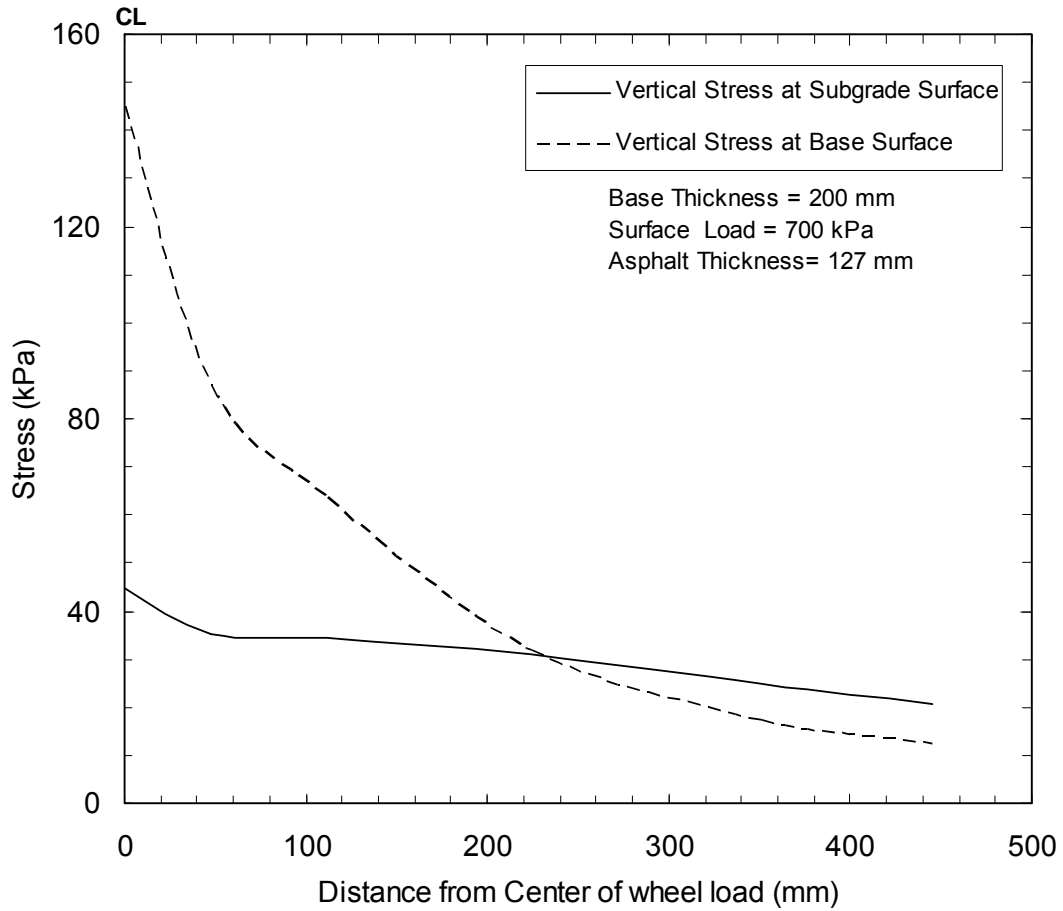
Fig. 3.2. Stress predicted by MICH-PAVE at the surface of a base course and subgrade layer at varying distances from the center of loading.

Fig. 3.3. SSG Displaying an Elastic Modulus Measurement of Class 5 Gravel.

Fig. 3.4. Measurement of Elastic Modulus with a Keros 100 LWD.
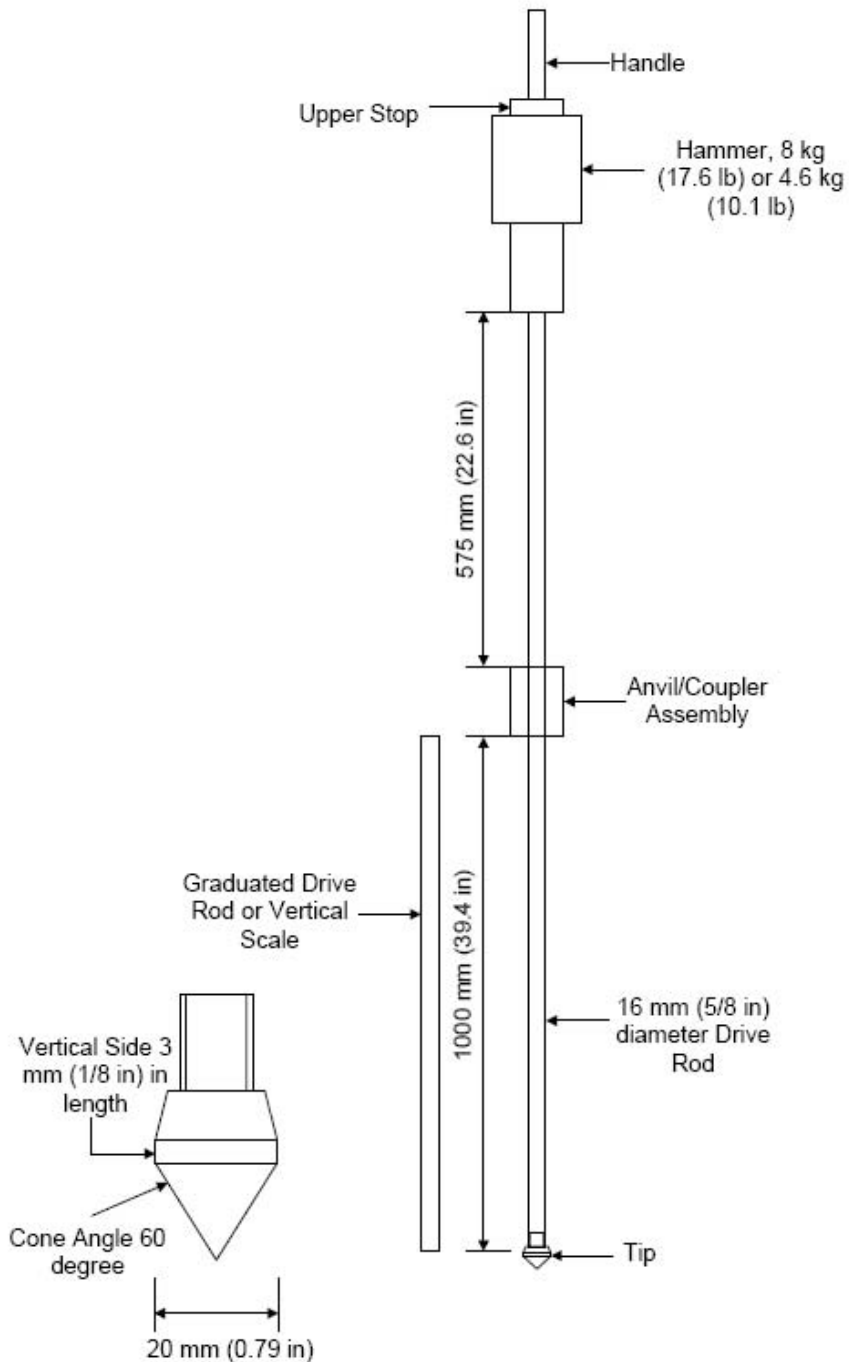
Fig. 3.5. Dynamic Cone Penetrometer (DCP)
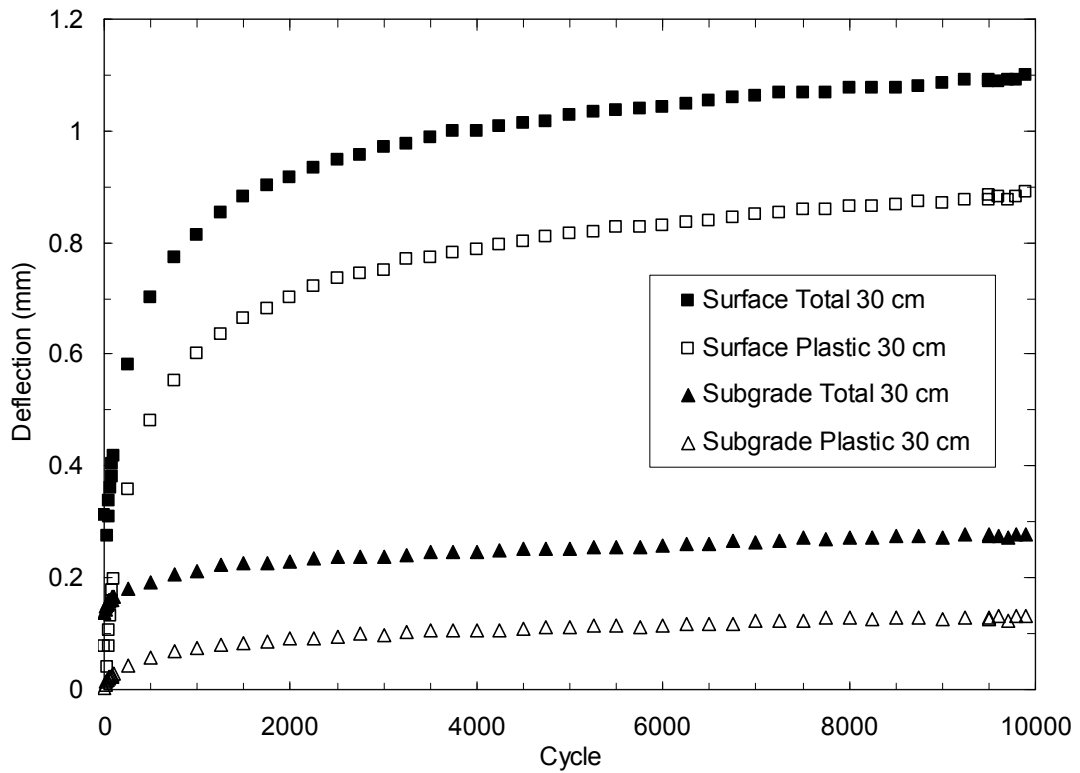
Fig. 4.1. **Total Deflection and Plastic Deformation at the Surface of the Base and Subgrade vs. Number of Load Cycles for Class 5 gravel.**
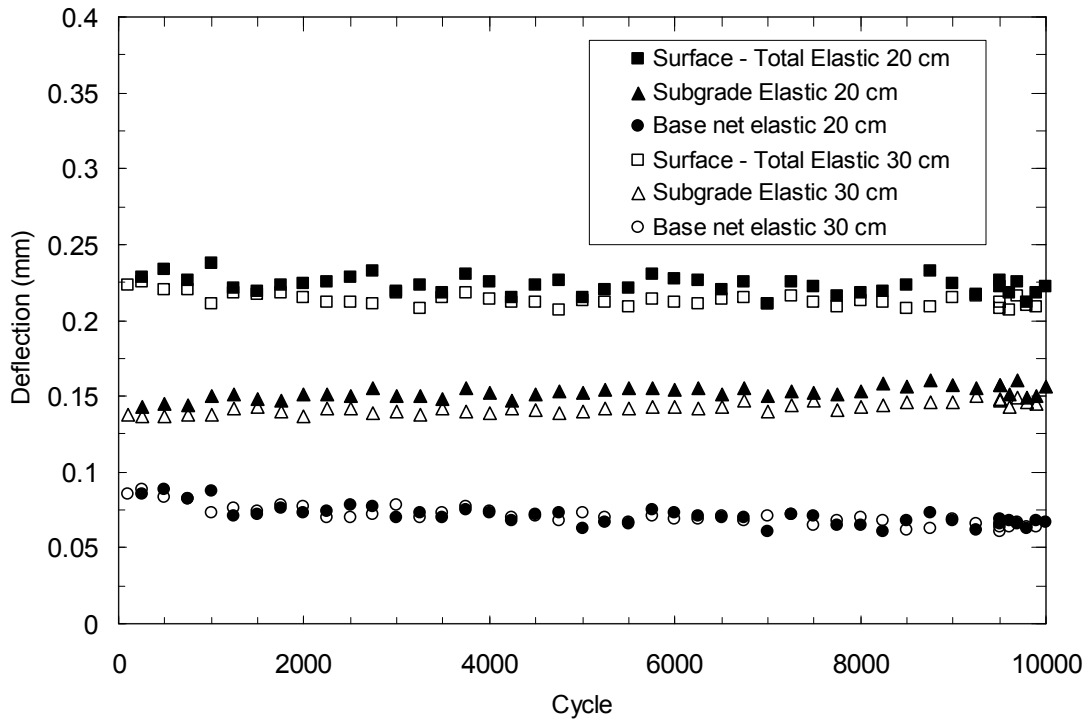
Fig. 4.2. Surface, Subgrade and Net Base Elastic Deflections for 200 and 300 mm thick layers of Class 5 gravel.
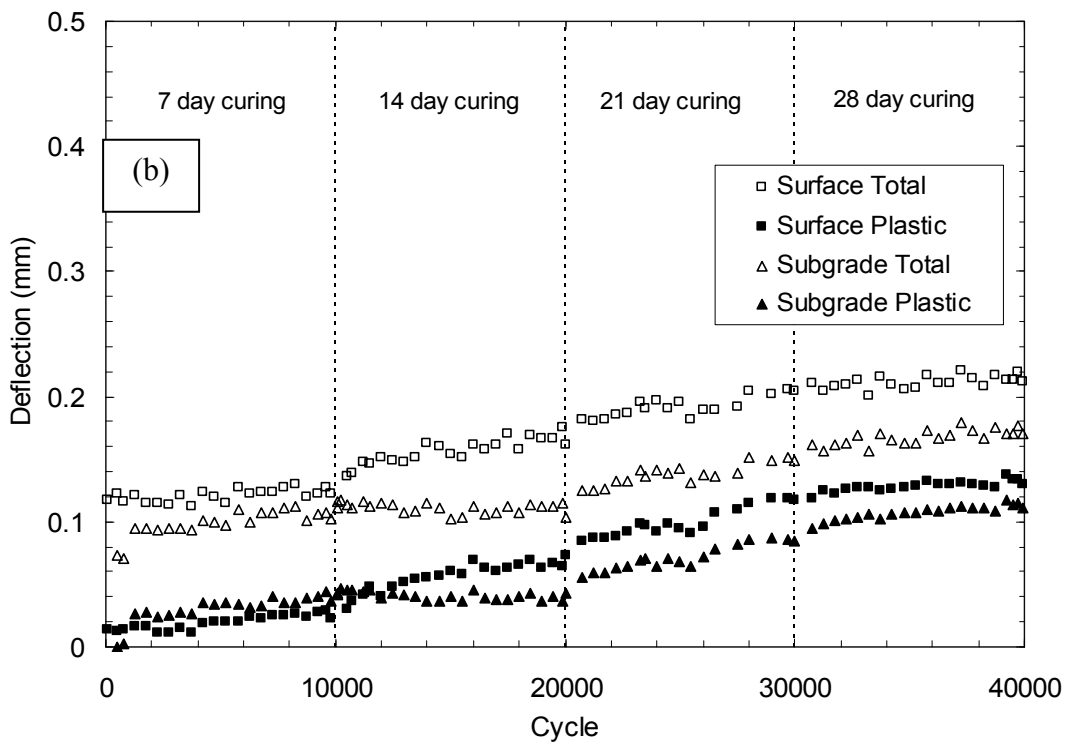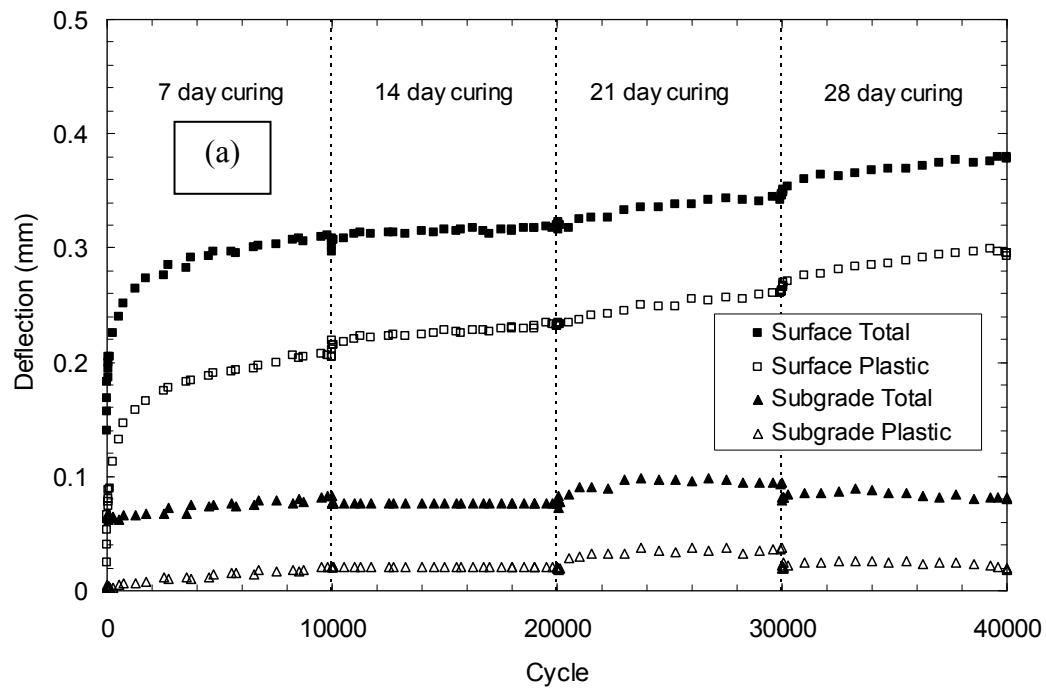
Fig. 4.3. Total Deflection and Plastic Deformation vs. Number of Load Cycles for (a) RPM and (b) RSG blended with fly ash.
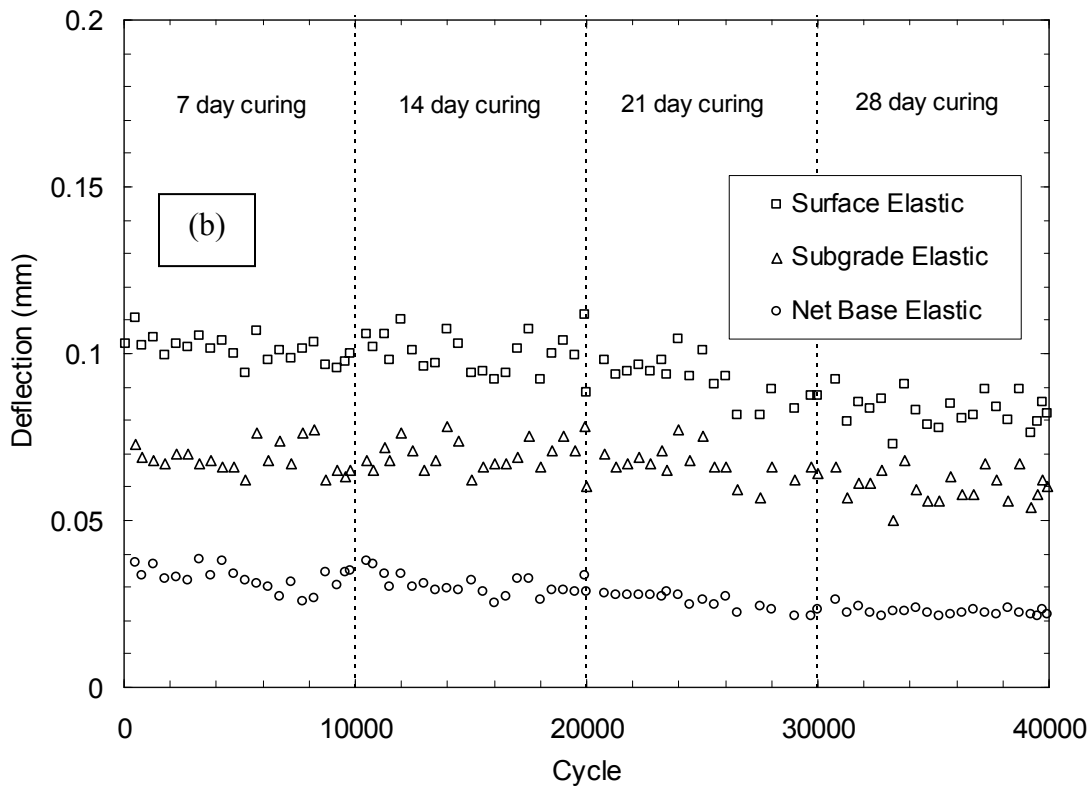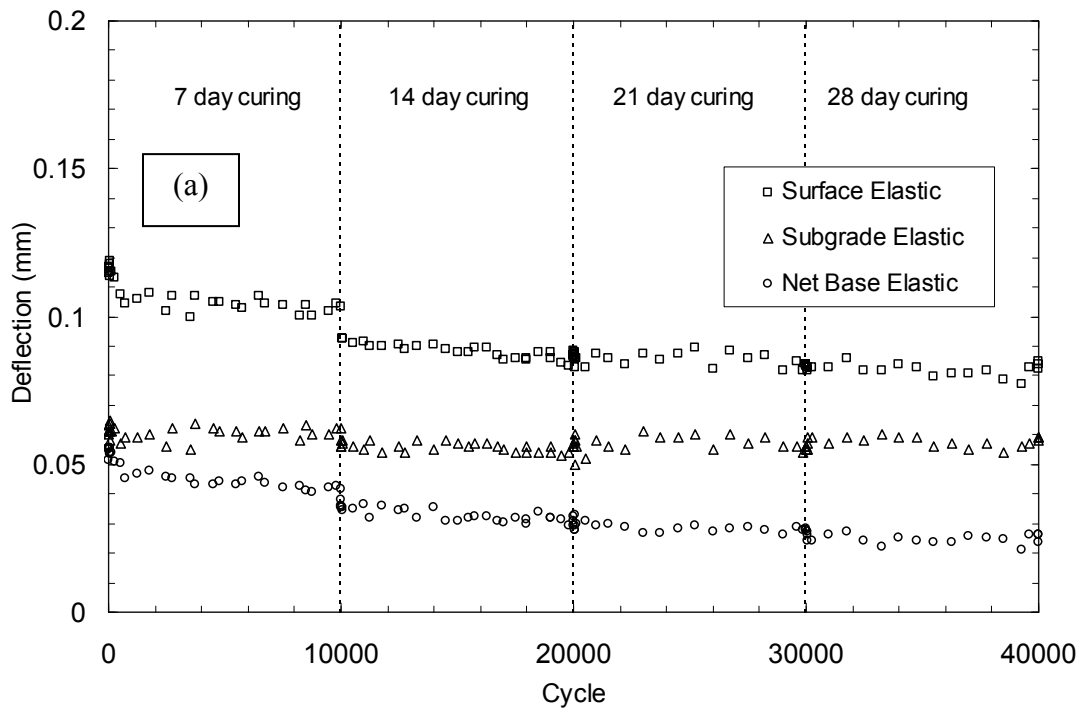
Fig. 4.4. Elastic Deflections vs. Number of Load Cycles for (a) RPM and (b) RSG blended with fly ash.
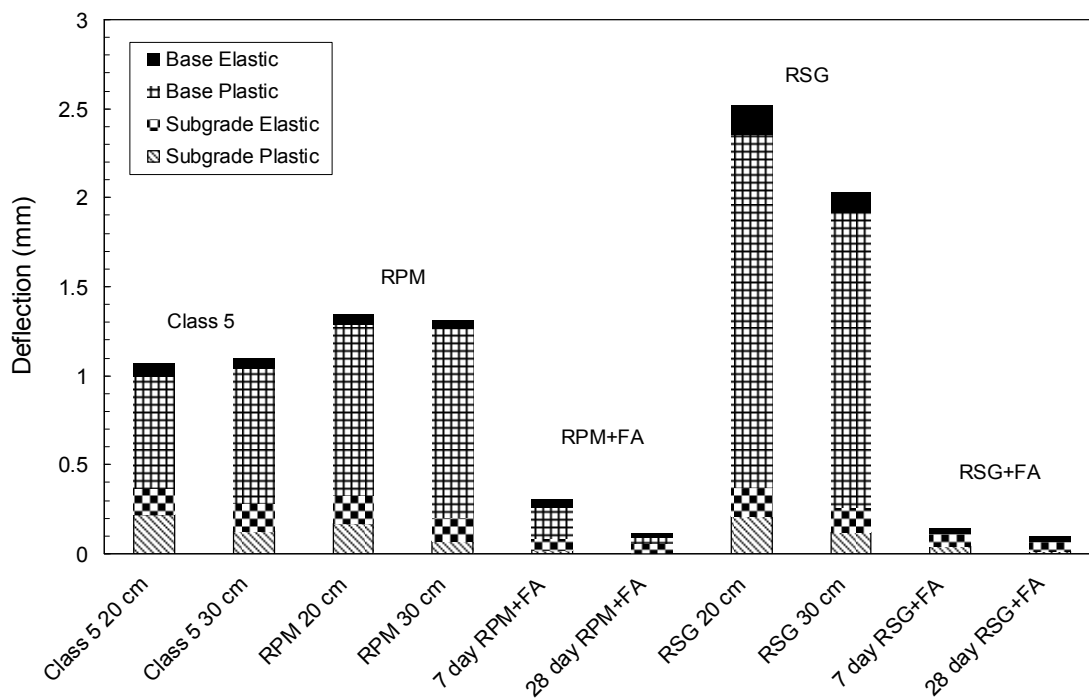
Fig. 4.5. Comparison of elastic deflection and plastic deformation measured in LSME.
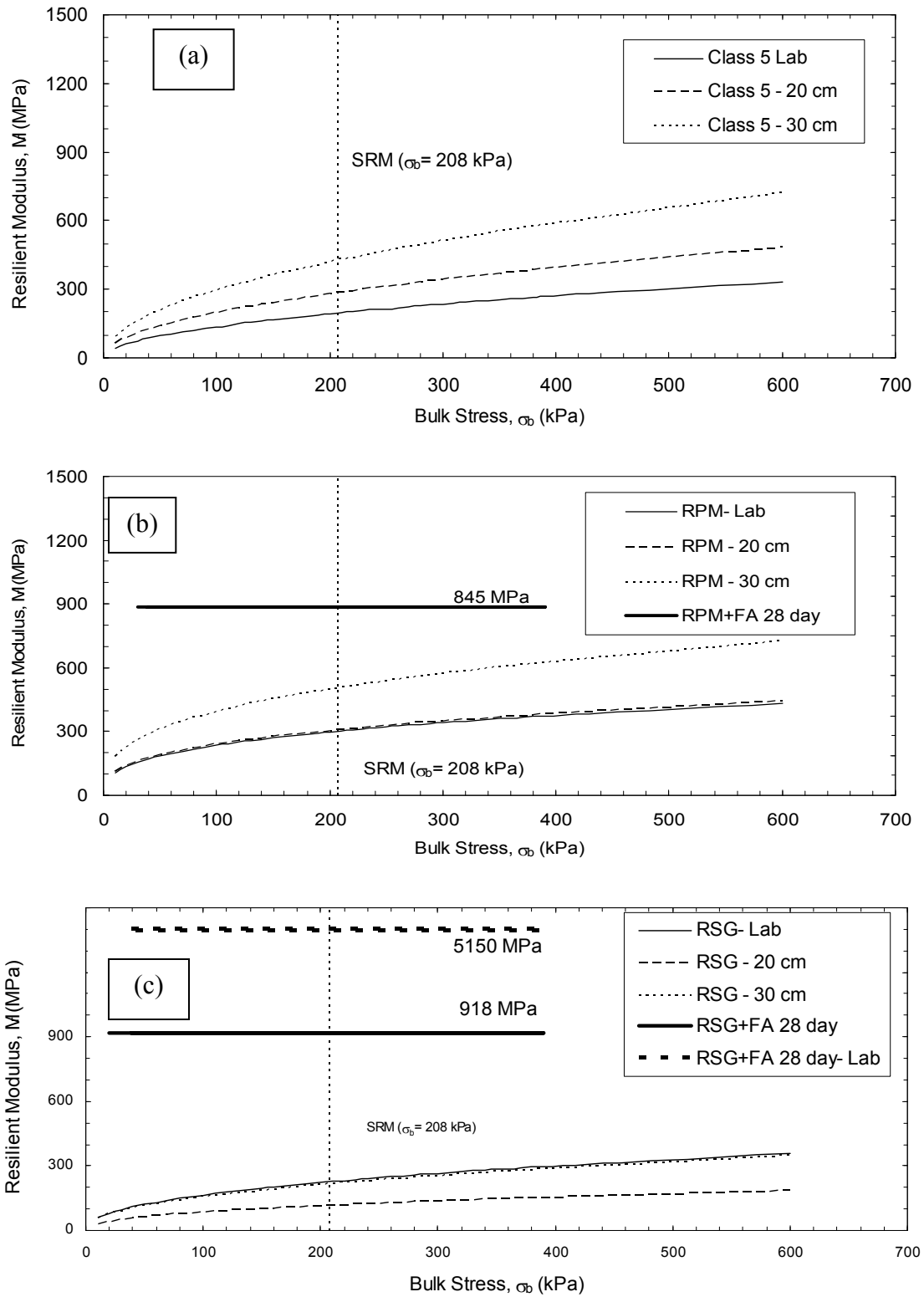
Fig. 4.6. Resilient Modulus vs. Bulk Stress Determined from LSME and Laboratory Tests for (a) Class 5, (b) RPM, and (c) RSG.
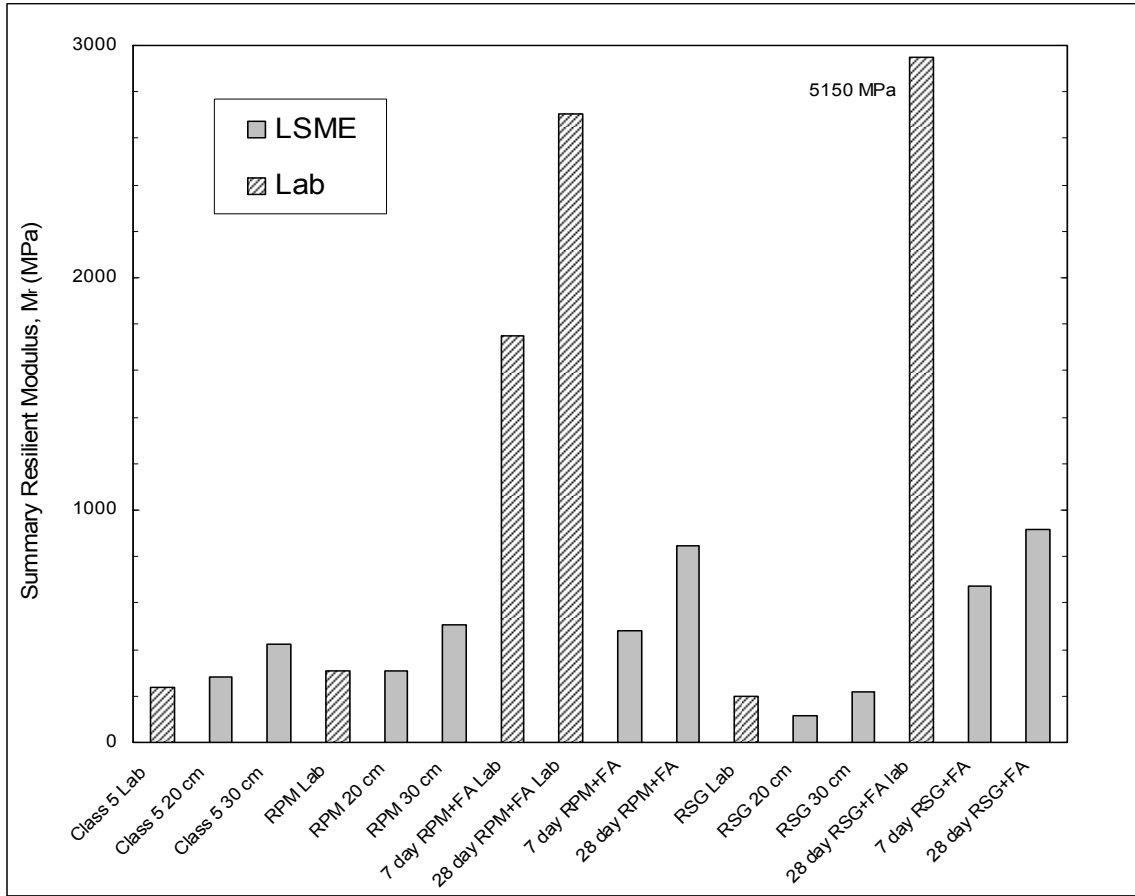
Fig. 4.7. Summary Resilient Modulus of Laboratory and LSME tests at Bulk Stress of 208kPa.
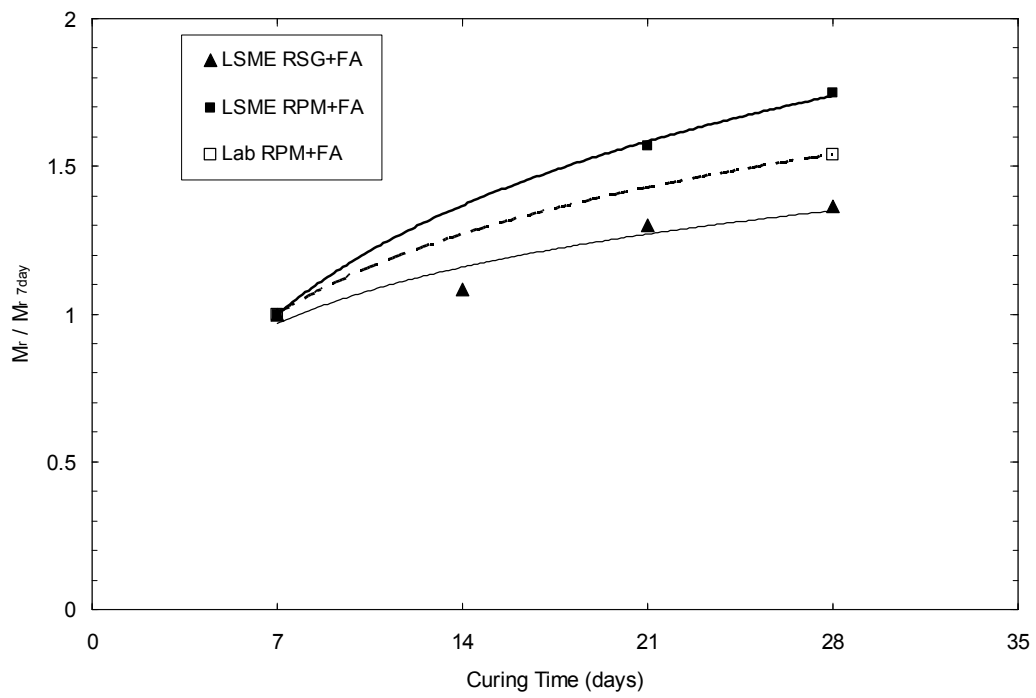
Fig. 4.8. Rate of increase in resilient modulus with curing time.
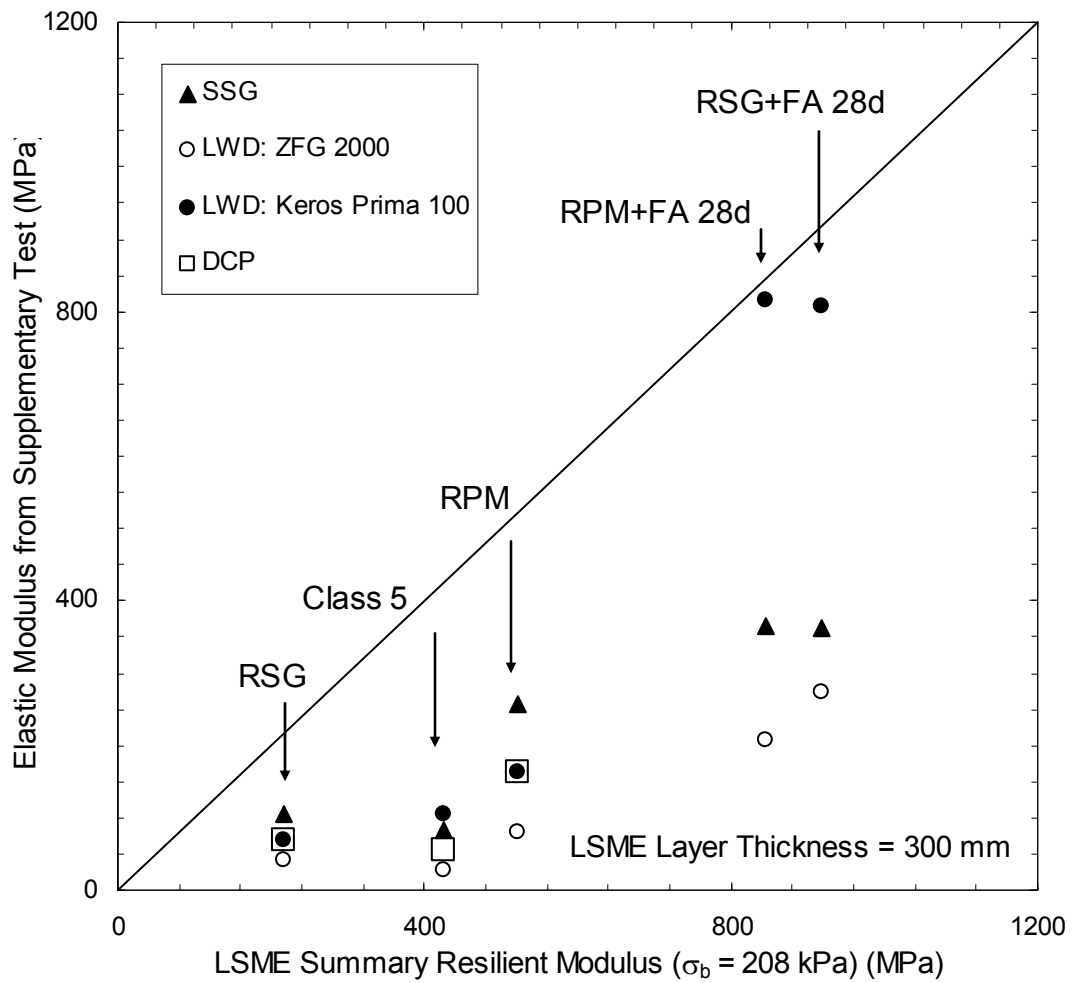
Fig. 4.9. Comparison of LSME Summary Resilient Modulus with the elastic modulus determined from supplementary tests.
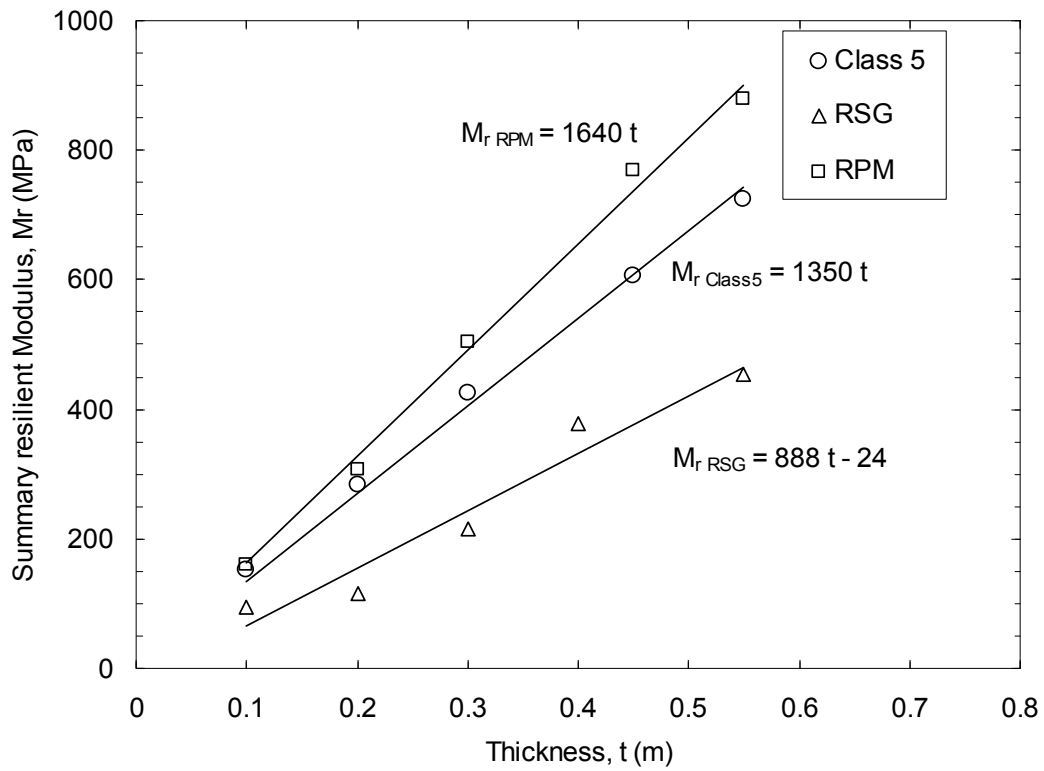
Fig. 4.10. SRM vs. Base Layer Thickness.
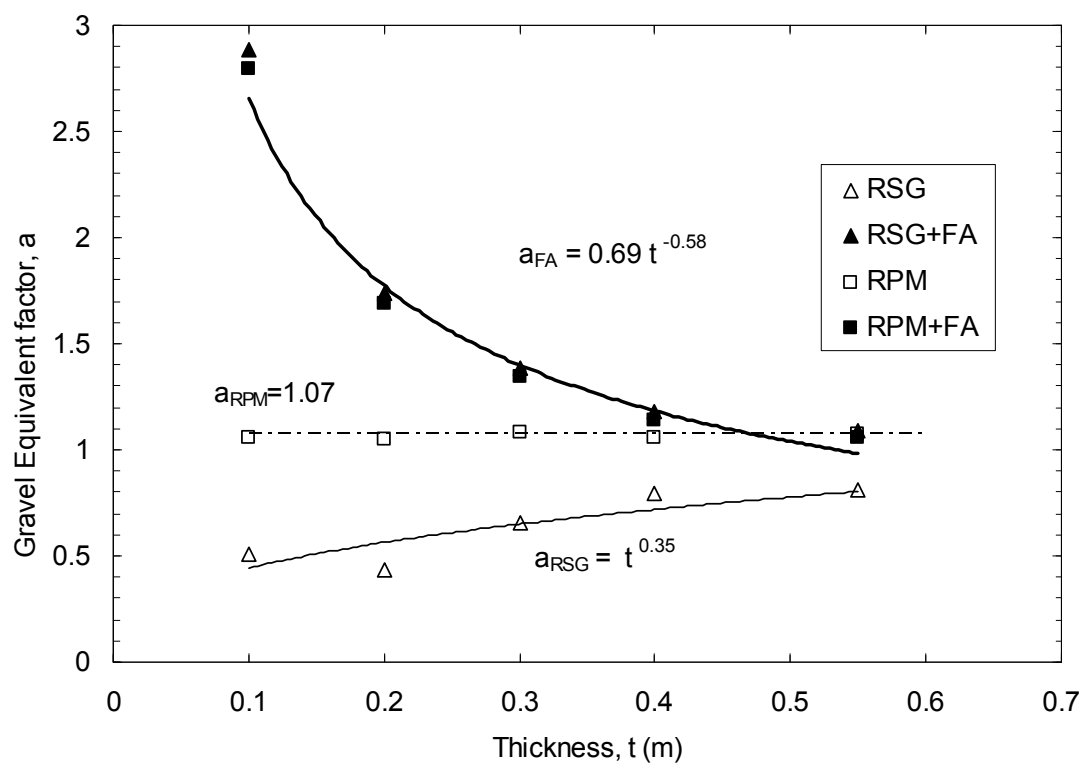
Fig. 4.11. GE Factor vs. Base Layer Thickness.
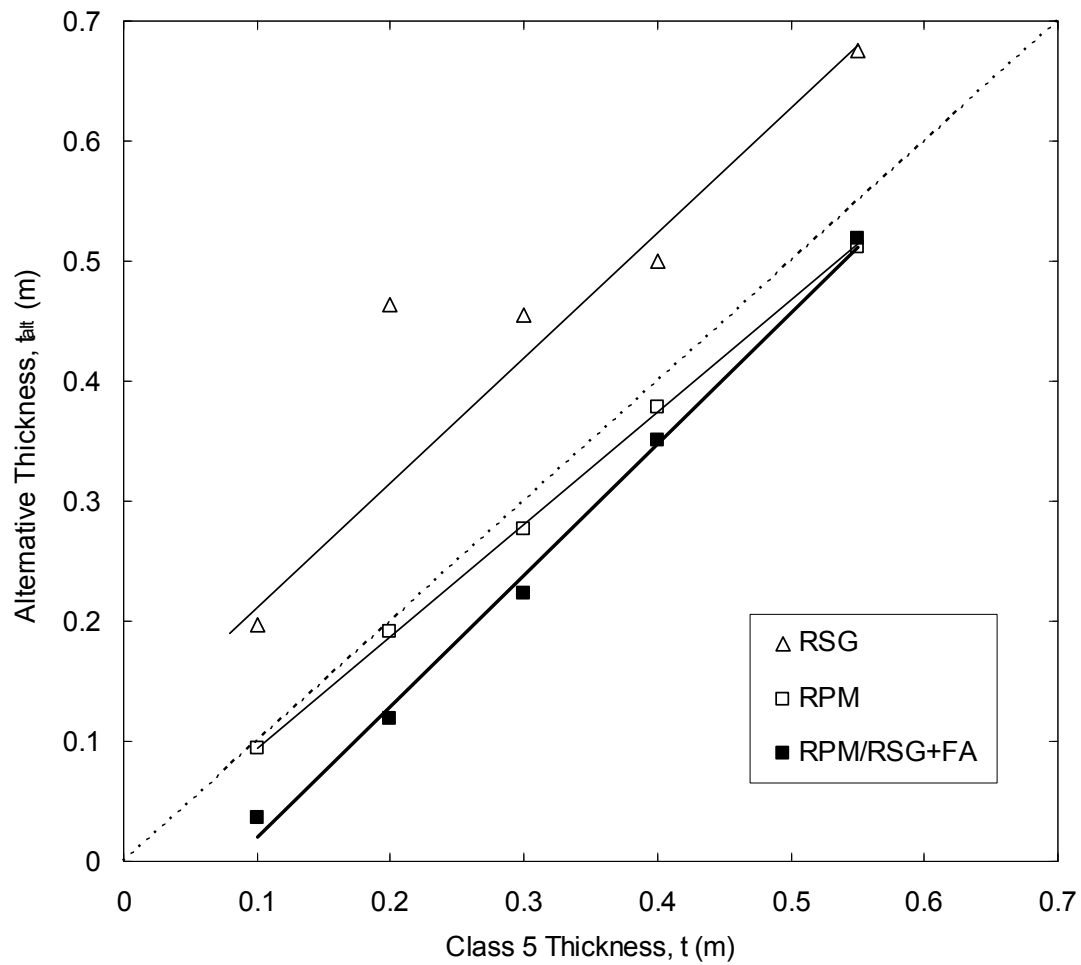
Fig. 4.12. Alternative Material Thickness as a function of Class 5 thickness.

ATTACHMENT A: STRAIN DEPENDENCY OF MODULUS

A.1 INTRODUCTION

The base course elastic modulus measured in the LSME is sensitive to the thickness of the layer being evaluated (i.e. thicker layers have a higher elastic modulus at a given bulk stress). The sensitivity of modulus to layer thickness reflects the varying levels of strain in the layers having different thicknesses, which is known to affect the elastic modulus of granular materials (Seed and Idriss, 1970, Hardin and Drnevich 1972, Edil and Luh 1978). Several studies have investigated the effect of strain level on modulus of layered pavement systems. Kim and Stokoe (1992) and Tanyu et al. (2003) demonstrated the effect of strain level in evaluating the resilient modulus of subgrade and various working platforms. Sawangsuriya et al. (2005) used the strain dependency of elastic modulus to predict the strain level of modulus in the soil stiffness gauge (SSG) for medium sand and crushed rock. Schuettpelz (2008) described the stress and strain dependency of modulus by finding a correlation between low strain elastic modulus (from seismic tests) and laboratory resilient modulus.

The strain-stress dependency of elastic modulus can be described with a backbone curve (Seed and Idriss, 1970, Hardin and Drnevich 1972). The backbone curve describes the ratio of shear modulus (or elastic modulus) at a given shear strain to the low strain shear modulus (or elastic modulus) as a function of shear strain. Different test equipment and methods result in various stress and strain levels, so both strain dependency and stress levels are taken into account in comparing the modulus provided from different test methods and materials.

Kokusho (1980) examined some of the properties affecting modulus including confining stress. Modulus increases with confining pressure because the soil deforms less with the increased confinement of particles. A higher modulus is expected with a higher confining pressure while the strain level remains constant.

To consider the effect of confining pressure on the modulus, low strain modulus was measured at different bulk stresses by means of seismic tests. The predicted modulus of the material from MICH-PAVE was normalized with the low strain modulus for a specific bulk stress.

A.2 MEASUREMENT OF LOW STRAIN MODULUS

A.2.1 Micro-Electro-Mechanical Systems (MEMS) Accelerometers

Small MEMS accelerometers were used to measure low strain modulus (maximum modulus) of different materials in the LSME. The MEMS accelerometers, developed by Analog Devices, are 4 mm x 4 mm x 1.5 mm in size and are sensitive to both static (e.g., gravity) and dynamic (e.g., vibration) accelerations.

The accelerometers used for all tests in this research are Analog Devices ADXL 203CE dual axis MEMS having a sensitivity of 1000 mV/g up to 1.5 g. The corresponding 18 mm by 18 mm printed circuit boards (PCB) manufactured by Sparkfun Electronics are shown in Fig. A.1. The accelerometers measure particle accelerations caused by a propagating elastic wave as it travels vertically through soil, and also measure the horizontal and vertical components of the acceleration caused by the gravitational field. Each printed circuit board contains 0.1 μF filtering capacitors and a 1 MΩ resistor required for operation.

Four to six accelerometers (depending on the layer thickness) were used to measure change of velocity using the elastic wave arrival in the LSME. The use of small MEMS accelerometers spaced a few centimeter apart allows the detection of small changes in velocity similar to the way that geophones can detect these changes on the order of meters and kilometers in field scale seismic studies (Schuettpelz, 2008). Although MEMS accelerometers can be used on a scale of centimeters, great care must be taken to ensure precise measurement of the distance between accelerometers. A small change in the separation distance between accelerometers can produce a large change in the calculated velocity leading to unreliable results.

Prior to placing each accelerometer in the soil layer, they were first coated with a durable, water tight epoxy seal (Fig. A.2.). The seal not only ensures that water or dust will not shortcut the electronic components of the system, but also mechanically protects the fragile accelerometer, PCB, and wires. When several accelerometers are situated a known distance apart (50 mm in this study), the velocity of a propagating elastic wave can be calculated by choosing the arrival time of the elastic waves (V_s or V_p) in the soil. The elastic wave propagation of RSG is shown in Fig. A.3. The first arrival time was determined manually by extending the most linear portion of the wave form to the x-axis. Although the accelerometers are equipped to measure two components of vertical and horizontal acceleration, only the vertical component is necessary to compute the elastic wave velocity.

A.2.2. Elastic Wave Velocity Measurement with MEMS Accelerometers

MEMS accelerometers were used to measure the dynamic response of the accelerometer to the propagation of an elastic wave generated by hitting the loading plate with a hammer. As the elastic wave progresses into the soil the acceleration changes and the arrival of the elastic wave can be captured with each accelerometer. The velocity of an elastic wave between accelerometers can be calculated knowing the arrival time (indicated by the acceleration) of the wave at each accelerometer and the distance between accelerometers.

The wave equation shows that particle displacement is related to both the stiffness and density of a particulate medium. The velocity of wave propagation increases with applied load and an increase in soil stiffness. P-wave velocity (V_p) in particulate media is dependent on the elastic modulus (E), Poisson ratio (ν) and density (ρ) (Santamarina et al. 2001; Graff 1975; Richart et al. 1970):

$$V_p = \sqrt{\frac{E(1-\nu)}{\rho(1+\nu)(1-2\nu)}} \tag{A.1}$$

Elastic modulus can be calculated with V_p measured in seismic tests, and ρ and ν of the material:

$$E = \frac{V_p^2 \rho(1+\nu)(1-2\nu)}{(1-\nu)} \tag{A.2}$$

where ν was considered to be 0.35 for the material without fly ash and 0.20 for RPM and RSG mixed with fly ash. The low strain elastic modulus for the material being evaluated is shown in

Fig. A.4. The smallest low strain modulus (E_s) is that of Class 5 gravel while RPM has the greatest E_s among the material without fly ash. E_s of RPM has a good agreement with the results of LSME and laboratory (NCHRP 1-28) resilient modulus tests. The higher E_s of RSG compared with Class 5 is likely due to the effect of P-wave velocity within the pore water of RSG which was compacted at a higher optimum water content than Class 5. The stress dependency of material without fly ash can be described with Hertz contact theory (1971) where the relationship between force and displacement in particulate media is non-linear. As grain boundary contact areas continue to flatten with more applied force, the amount of deformation in the form of displacement over the soil column decreases. A decrease in deformation as force increases results in an increased stiffness of soil.

Materials blended with fly ash showed a constant modulus in the applied range of stress. The stress independency of modulus for these materials is due to the cementation of fly ash binding the soil particles together. RPM blended with fly ash has the higher E_s.

A.3. CURVE OF STRESS- STRAIN DEPENDENCY OF MODULUS (BACKBONE)

MICH-PAVE was used to back calculate the LSME test results to predict the resilient modulus at various stress and strain levels within the pavement layers using the relationship described by Eqn. 3.2. Shear strain was calculated using the back calculated vertical strain (Kim and Stokoe, 1992, Tanyu, 2003):

$$\gamma = \varepsilon \, (1+\nu) \tag{A.3}$$

where γ is the shear strain, ε is the vertical strain and ν is Poisson ratio.

The backbone curve was developed using the above shear strain and normalized resilient modulus at different bulk stresses. The normalized resilient modulus was determined using Eqn. A.4:

$$\text{Normalized resilient modulus} = \frac{M_r}{E_s} \tag{A.4}$$

where M_r is the predicted resilient modulus from MICH-PAVE model for a particular bulk stress, and E_s is the low strain elastic modulus determined from seismic tests for the same bulk stress. The resulting backbone curve, or change of normalized modulus as a function of shear strain, is shown in Fig. A.5. The results of LSME backcalculation and laboratory tests (NCHRP 1-28) are summarized in Table A.1. Care should be taken when using the results of seismic tests to normalize the resilient modulus. Scatter of the data, specifically at low bulk stresses, can be misleading when evaluating the proper low strain elastic modulus used to normalize the resilient modulus.

The results of back calculated LSME tests for different thicknesses and laboratory resilient modulus tests (NCHRP 1-28) are placed together on the backbone curves shown in Fig. A.5. The backbone shape describes the stress-strain behavior of the base material being evaluated and is unique for each material. The LSME produces smaller strain levels than the laboratory resilient modulus test (NCHRP 1-28A). Therefore the strain level in the base course of a full-scale pavement system may be smaller than that produced in the laboratory resilient

modulus and therefore a higher modulus would be expected. The change of strain level in thicker material was evaluated by the means of backbone curves, and a smaller strain level was observed in a thicker base course layer due to the larger stress distribution within the layer.

No stress dependency was observed for the materials mixed with fly ash as shown in Fig. A.4 and confirmed by the results of laboratory resilient modulus tests where k_2 in Eqn. 3.2 was calculated to be 0 for the cemented materials. To verify the effect of strain and stress level on the modulus of the materials blended with fly ash in the LSME, several tests were performed with different load levels corresponding to different strain levels. The results showed no stress and strain dependency of modulus for the materials cemented with fly ash in a range of applied stress and strain considered to be typical of the load from vehicle tires transferred to the base course in a pavement system (Fig. A.6).

Although backbone curves were used to compare the results of LSME tests and laboratory tests associated with strain level, they also were used to extrapolate the change of modulus with thicknesses not evaluated in this study.

A.4. PREDICTING BASE LAYER RESILIENT MODULUS FOR VARIOUS THICKNESSES OF BASE COURSE MATERIAL

LSME tests were conducted on RPM, RSG and Class 5 gravel in thicknesses of 200 and 300 mm, and RPM and RSG blended with fly ash at a thickness of 300 mm. The LSME test results for RPM, RSG and Class 5 are shown in Fig. A.7 with base layer thickness on the horizontal axis, and the summary resilient modulus (SRM) at a bulk stress of 208 kPa graphed on the vertical axis. The goal is to predict the M_r as a function of base layer thickness of material for calculation of the granular equivalent (GE) factor.

Since performing LSME tests is time consuming and labor intensive, additional methods are required to predict the SRM of different materials over a range of thicknesses. Effects of strain and stress levels should be taken into account in predicting the base M_r for thicknesses not tested in the LSME. Resilient modulus increases with increasing layer thickness due to changes of strain and stress levels within the soil layer. As material thickness increases, deflections decrease because of a lower strain level at a constant load, resulting in the higher M_r of soil.

The method used to predict M_r from the thickness of the base layer is demonstrated for RPM and can be used for Class 5 and RSG as well. MICH-PAVE was used to model the nonlinear elastic behavior of the layered pavement system with the stress-dependent modulus function (Eqn. 3.2). The assumption was made that k_2 would not vary with thickness of a base material. A two-layer system was modeled with a base course over a subgrade material. The subgrade was considered to be linearly elastic with a modulus of 70 MPa determined from the average back calculated moduli from the LSME tests. The applied load was same used for LSME tests.

The first trial consisted of a 450 mm thick layer of RPM. MICH-PAVE predicted the stress and strain based on an assumed k_1. To verify the assumed k_1, shear strain and normalized modulus were calculated to be used in conjunction with the backbone curve.

The stress and strain predicted from MICH-PAVE associated with the assumed k_1 could then be compared to the backbone curve as shown in Fig. A.8. The SRM was also calculated as 570 MPa, corresponding to a bulk stress of 208 kPa. The predicted data did not fit properly on the RPM backbone curve for the assumed k_1 in the first trial so additional attempts were made to

find a better fit to the backbone curve for the 450 mm thick layer of RPM. Additional trials were conducted by changing k_1, shown in Fig. A.8. The SRM corresponding to the best backbone fit of 450 mm thick RPM was 768 MPa.

The above method can be used to predict the proper modulus of the material for several thicknesses, shown in Fig A.9 for RPM. Predicted moduli (SRM) for a range of thicknesses of RPM are shown in Fig. A.10, along with the back calculated M_r for thicknesses tested in the LSME. The variation of modulus as a function of thickness is expected to level off for thicknesses greater than 550 mm while the normalized modulus enters to the nonlinear section of the backbone curve.

The same methodology can be used for other materials tested in the LSME.   Fig. A.10 shows the change of SRM with thickness for RSG and Class 5 as well as RPM which was used to predict the GE factors of RPM and RSG.

Table A.2. Summary resilient modulus and low strain elastic modulus used to develop the backbone curve

Material	test	Bulk stress (σ_b)	Low strain modulus E_s	SRM[1] (Mr)	Normalized modulus Mr / E_s	Shear strain (γ)
Class 5	Lab (NCHRP 1-28)	100-800	600-800	130-460	0.16-0.25	$5\text{-}10 \times 10^{-4}$
	LSME 200 mm	81-207	500-800	180-280	0.37	4.5×10^{-4}
	LSME 300 mm	45-175	320-750	195-400	0.58	2.5×10^{-4}
RPM	Lab (NCHRP 1-28)	100-500	1000-1400	150-400	0.21-0.30	$1.5\text{-}4 \times 10^{-4}$
	LSME 200 mm	70-220	900-1300	200-300	0.24	3×10^{-4}
	LSME 300 mm	40-180	700-1450	280-500	0.38	2×10^{-4}
RSG	Lab (NCHRP 1-28)	100-600	500-1000	130-500	0.28-0.35	$3\text{-}7 \times 10^{-4}$
	LSME 200 mm	90-250	540-980	80-130	0.15	10^{-3}
	LSME 300 mm	70-220	400-800	130-230	0.29	5×10^{-4}
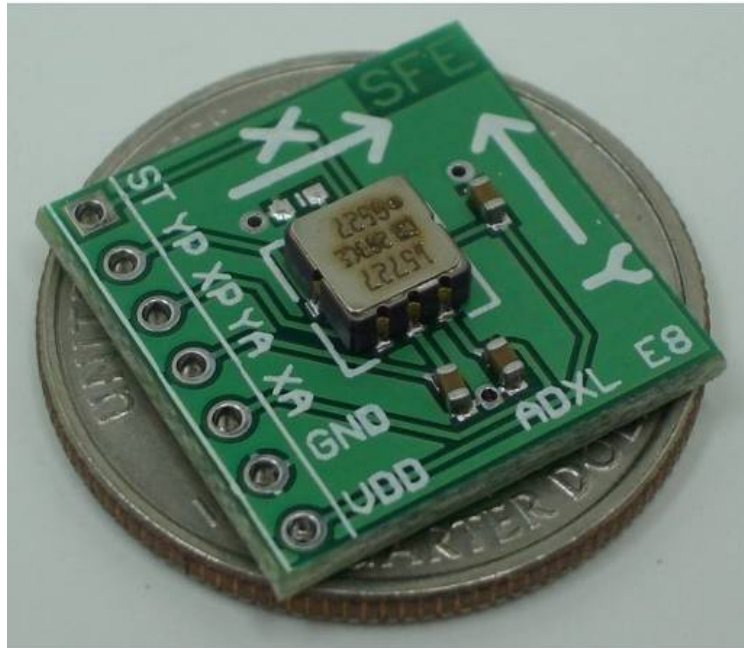
Fig. A.2. Analog Devices ADXL 203CE accelerometer and corresponding printed circuit board (PCB, Sparkfun Electronics), (adopted from Schuettpelz, 2008).
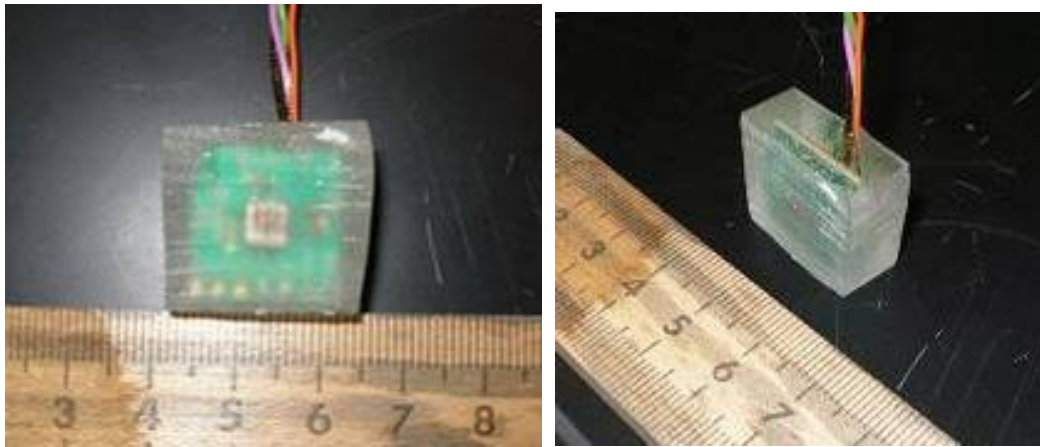
Fig. A.2. Smoothcast 327 coating applied to MEM accelerometer and PCB (ruler gradations are in cm), (adopted from Schuettpelz, 2008).
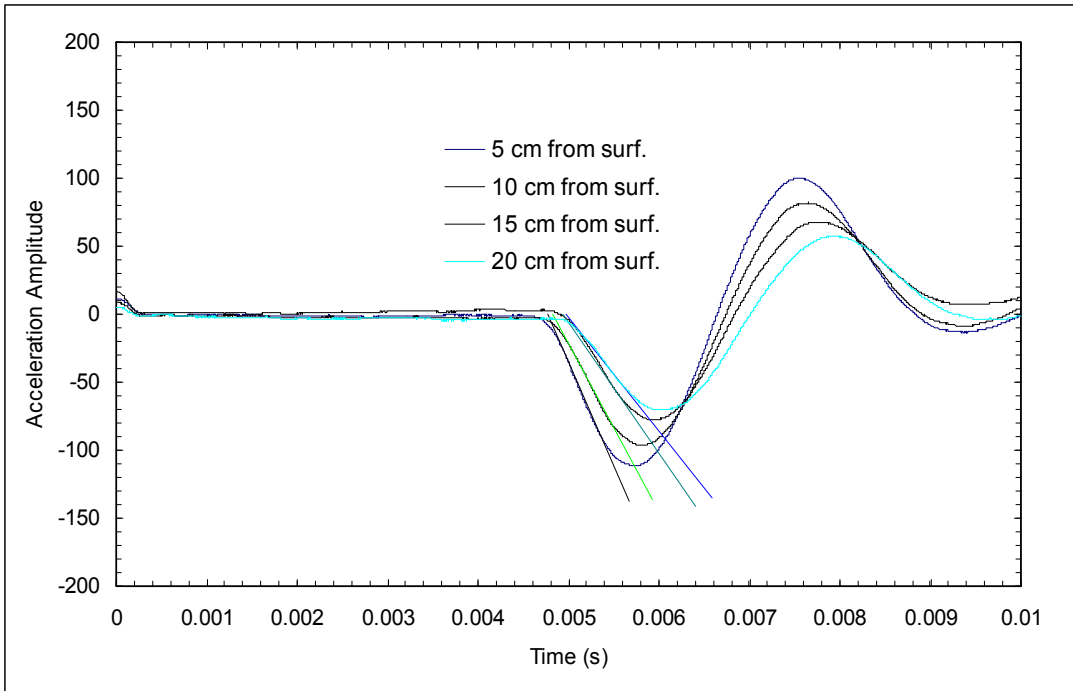
Fig. A.3. Elastic wave propagation and choosing the first arrival time for RSG.
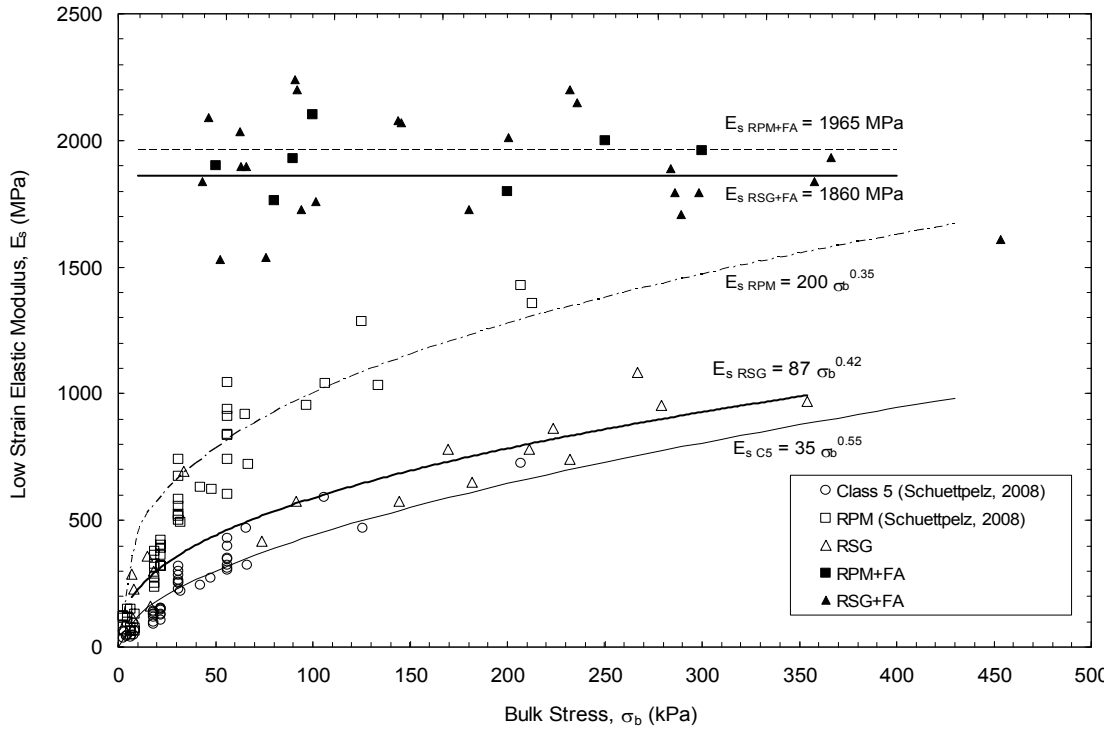
Fig. A.4. Low strain elastic modulus as a function of bulk stress.
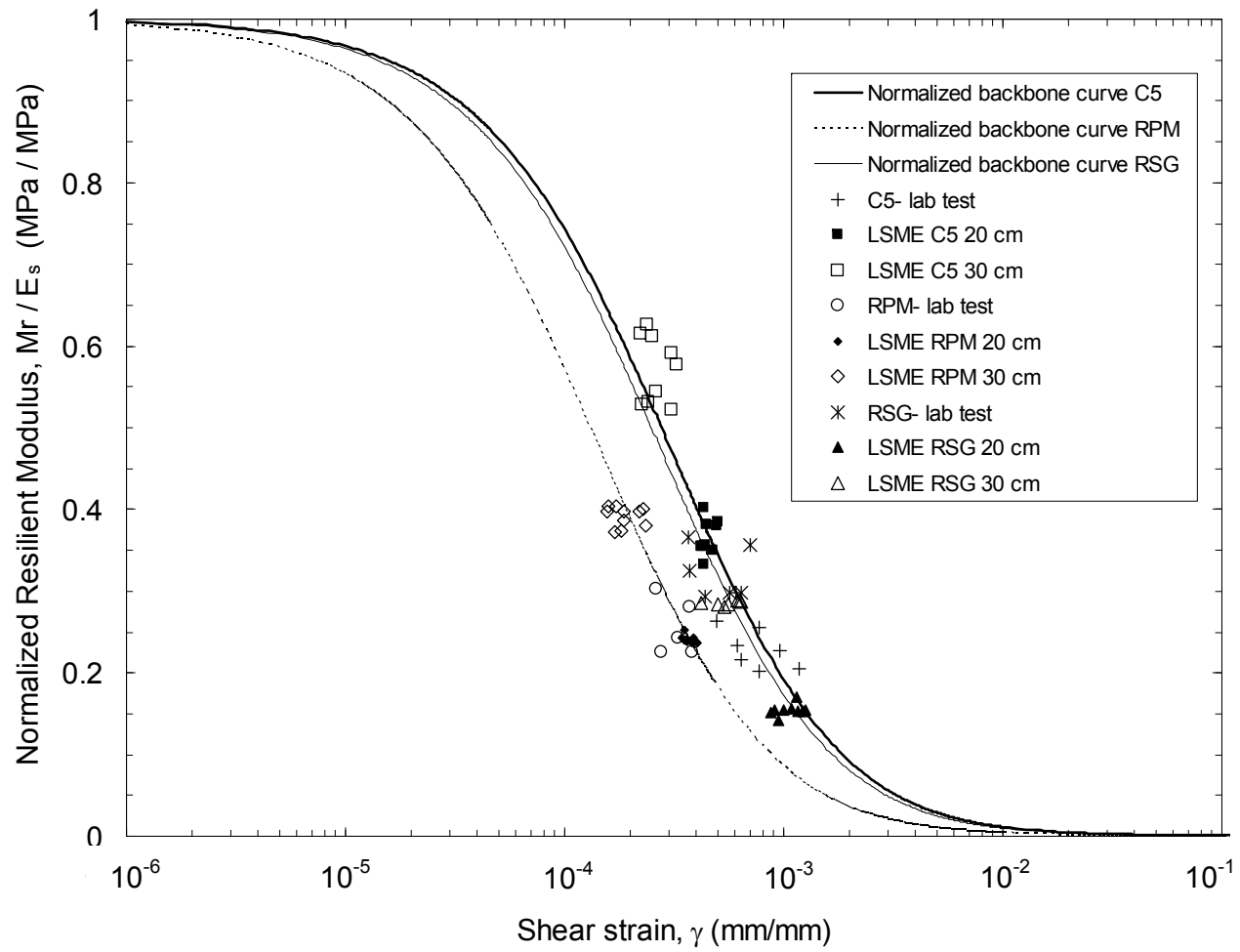
Fig. A.5. LSME and laboratory data placed on Backbone curve.
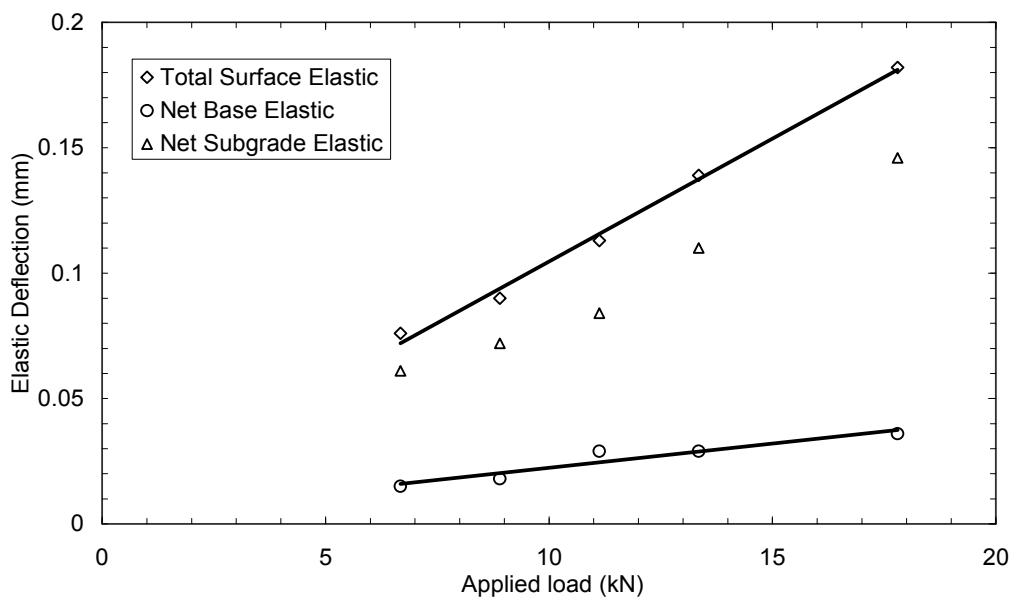
Fig. A.6. Evaluating the stress and strain dependency on modulus of RSG blended with fly ash in LSME.
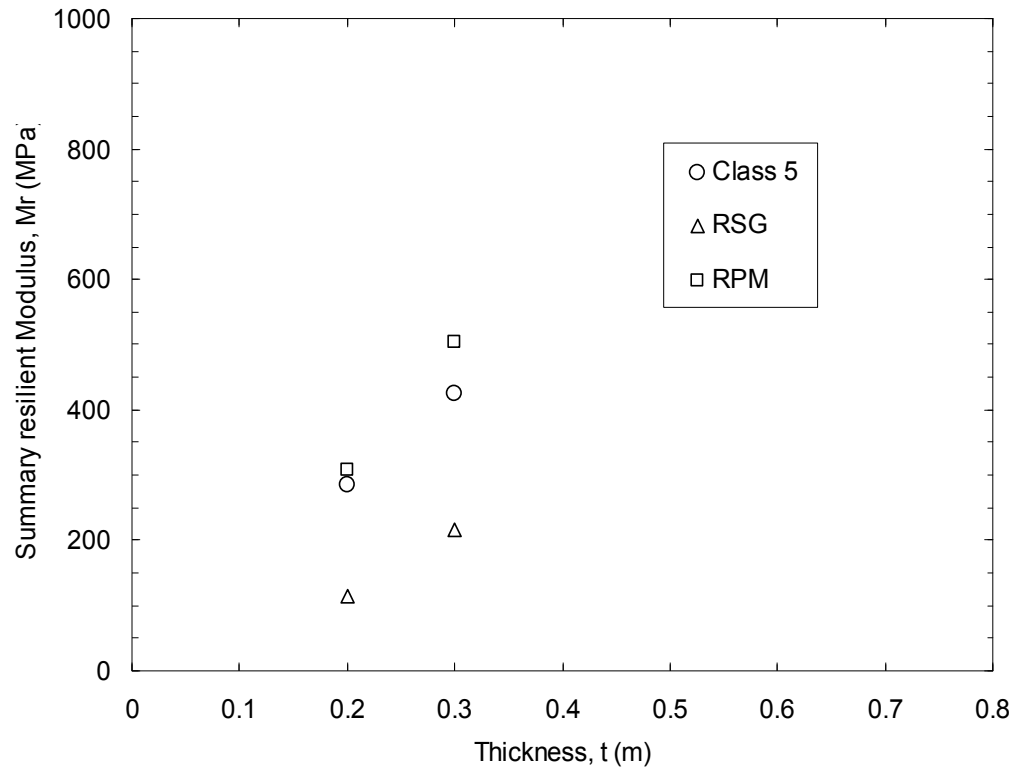
Fig. A.7. Summary resilient modulus as a function of base course thickness in LSME.
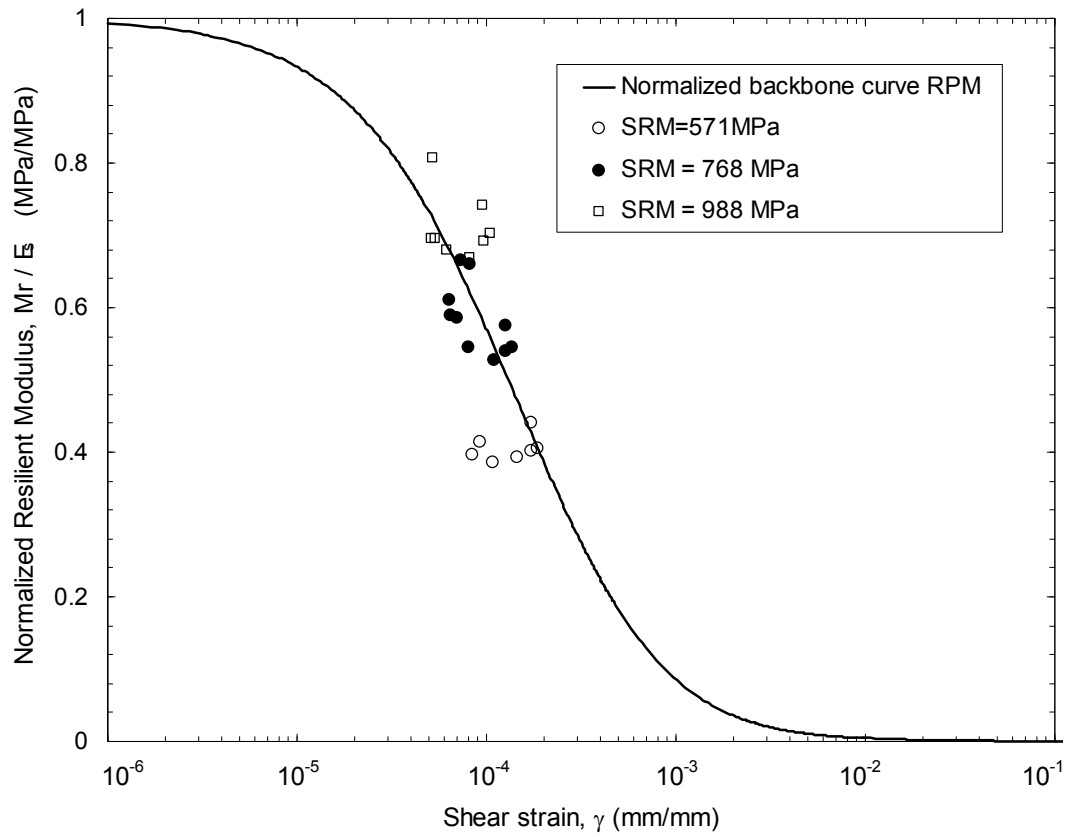
Fig. A.8. Various trials conducted to predict the summary resilient modulus (SRM) for 450 mm thick RPM.
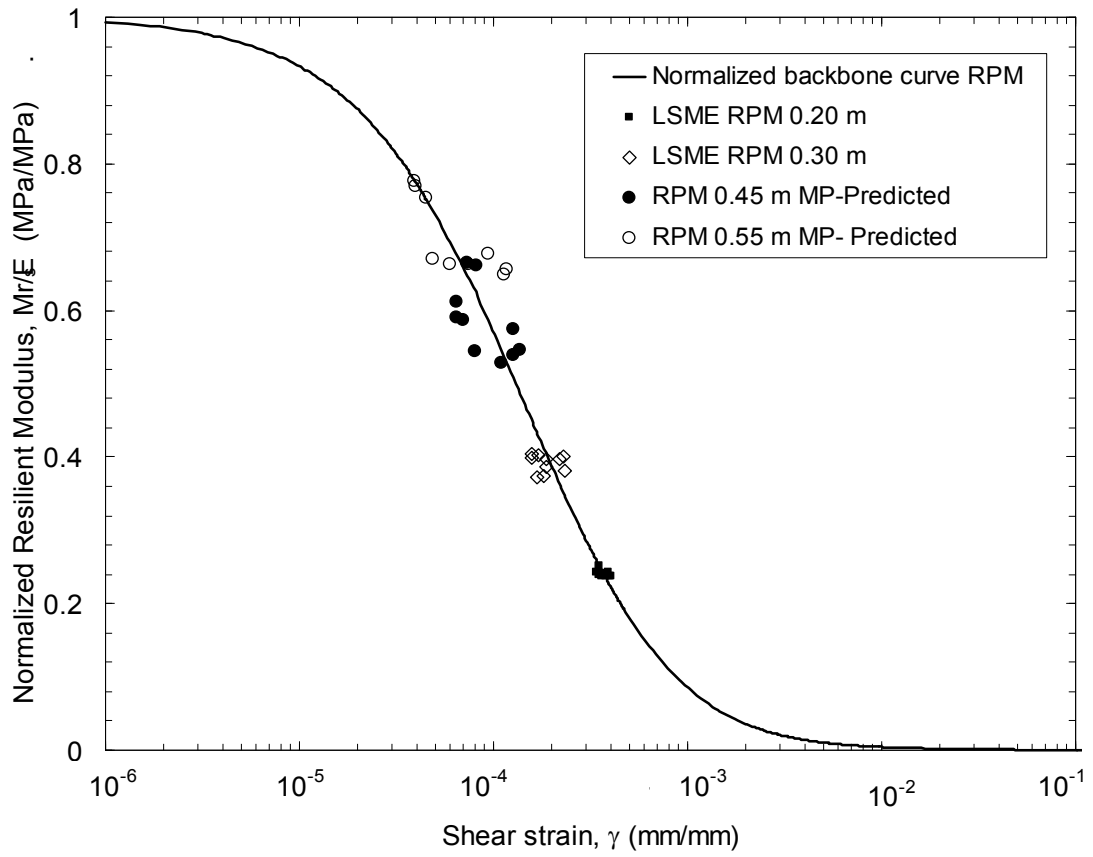
Fig. A.9. Prediction of summary resilient modulus for multiple layer thicknesses of RPM.
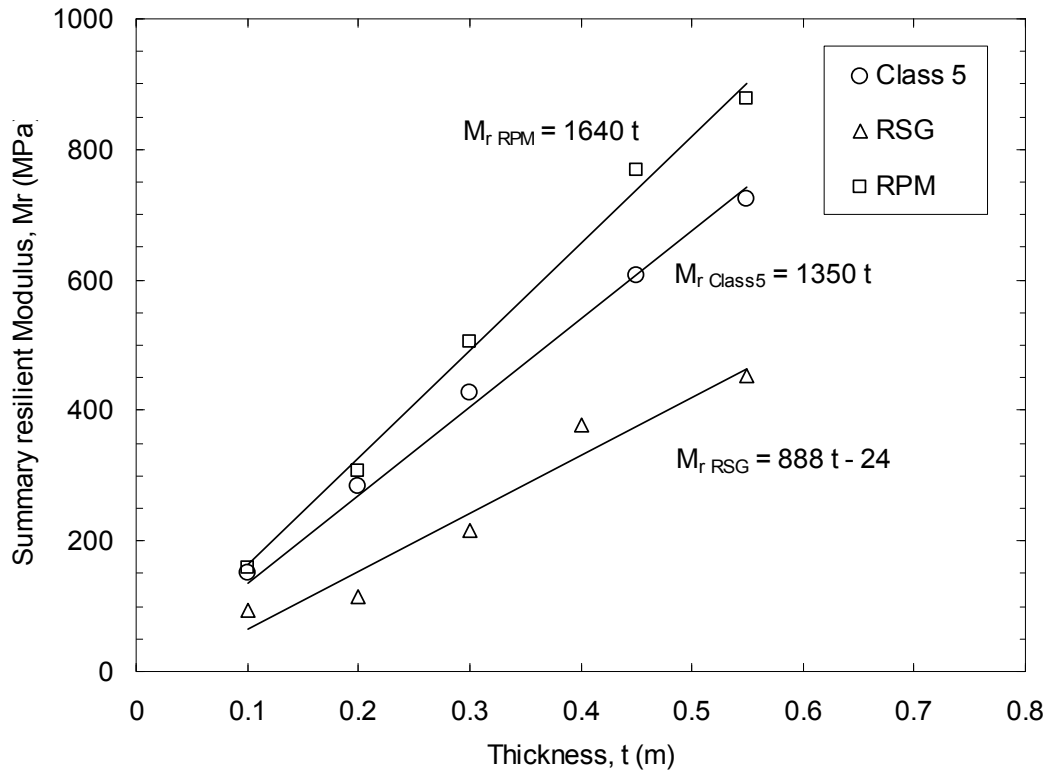
Fig. A.10. SRM as a function of thickness.

ATTACHMENT B: BASE COURSE TESTING PROTOCOL

B.1 INTRODUCTION

Light weight deflectometers (LWDs) are used to determine the soil stiffness as a convenient method in road construction. The basis of this device is to measure the deflection due to the drop of a weight on the ground. The data are used to determine the modulus of soil being tested. Currently several different LWD devices are commercially available from at least four manufacturers (Zorn, Pavement Consultants, Dynatest, Al-engineering). To use LWDs successfully, the conditions under which these devices measure deflection and elastic modulus should be known. A study conducted by White et al. (2007) compared the measured LWD elastic modulus (E_{LWD}) from different types of LWDs. E_{LWD} is calculated using elastic half space theory where all underlying soil layers are considered to consist of one uniform elastic layer. LWD measurements including applied load and deflection are used to calculate E_{LWD} which is equivalent to the modulus of the combined pavement layers.

Although the operation of various LWDs are similar, they vary in how they measure deflection and plate contact stress associated with different plate sizes, buffers, and sensor characteristics which result in varying modulus. White et al. (2007) described correlations between E_{LWD}, DCP and laboratory resilient modulus tests (AASHTO T 307). He also listed the various effective parameters on the LWD measurements such as plate size, loading time, location of transducer sensors, buffer and spring characteristics.

In this study, two types of LWD were used to determine elastic modulus of the base course material: a Keros 100 (Dynatest, Denmark) and a ZFG 2000 (Zorn, Germany). E_{LWD} was compared with the modulus calculated from large scale model experiments (LSME), and a method was developed to take the differences in stress level into account as well as the effect of the subgrade between the two methods.

B.2 METHODS

B.2.1. LWDs

The Keros 100 contains a 10-kg weight that is dropped to produce a dynamic load on a plate. A load sensor measures the load pulse, and a geophone at the center of the plate measures the corresponding soil deflection. The ZFG 2000 consists of a 10-kg weight and a plate stress is assumed based on a pre-defined calibration for a falling weight. The plate deflection is measured using an accelerometer. For both devices, the modulus for a specific drop height (DH) for either device can be calculated as:

$$E = \frac{f(1-v^2)\sigma r}{d}$$
(B.1)

where σ is the peak stress applied at the surface, r is the radius of the loading plate, f is a factor that depends on the stress distribution under the loading plate, v is the Poisson ratio, and d is the deflection corresponding to the peak stress (White et. al 2007). The variables used for each material tested are described in Table 3.1, where f values were adopted from Terzaghi and Peck (1967). The Keros 100 allows the input of a particular f and v for a given material while

measuring σ and d for calculating E. However, the ZFG 2000 uses fixed constants for f, ν and σ, so the internally calculated E reported by the ZFG 2000 was not used; instead, E was calculated with Eqn. B.1 using the measured d and the assumed values of ν and f for the material being tested.

LWD tests were performed by preloading with three load pulses or seating blows, and then measuring the average deflection for an additional three load pulses. The ZFG 2000 assumes a constant applied load based on calibration tests performed on a concrete surface, while the Keros 100 measures the actual applied load during the test using a set load cell. Theoretically, the applied force on a surface cannot be constant, but is dependent on the material stiffness. Since LWD tests are commonly conducted on compacted layers of soil which are relatively stiff, any error associated with the assumption of a constant applied force in performing calculations may not be practically significant.

The constant force of the ZFG 2000 can be estimated for a certain drop height using equation B.2:

$$F = \sqrt{2 \times m \times g \times h \times k} \tag{B.2}$$

where F is the applied force, m is the mass of a falling weight, g is the gravitational acceleration, h is the drop height, and k is a spring constant (362396.2 N/m). According to this formula, the drop height to achieve an applied force of 7.07 kN is 703 mm (White et al 2007). However, based on the manufacturer's calibration tests on a concrete pad, an applied force of 7.07 kN was experimentally found to be 720 mm. The difference between the theoretical and experimental determined drop height is apparently attributed to non-linearity in the spring buffers during dynamic loading. A relationship between drop height and the estimated applied force for a 10 kg drop weight using equation B.2 with comparison to calibrated applied forces (provided by manufacturer) is shown in Figure B.1.

Davich (2005) reported laboratory test measurements performed to investigate error introduced from using an assumed applied load and concluded that the assumption of constant force can lead to an over-estimation of modulus of only 4% to 8%, based on testing soft to very stiff materials.

These tests should be performed by placing the plate on a flat surface in a way that full contact between the plate and the surface is achieved. The manufacturer suggests using a thin layer of sand at locations where a flat contact surface cannot be obtained.

B.2.2 Factors Influencing E$_{lwd}$

Factors that influence E$_{LWD}$ are detailed by White et al (2007) and include plate size, plate rigidity, plate contact stress, type and location of deflection transducer, measured load, loading rate and buffer stiffness. The effect of stress level (applied load) and underlying soil layers should also be considered when the proper modulus is to be estimated for a base course layer.

Fleming et al. (2002) provided a discussion on the influence of the type and location of the deflection measuring sensor (i.e. on the plate versus on the ground). The Zorn device, for example, has an accelerometer built into the plate so that the deflection of the plate is calculated by integrating twice. The Keros 100 has a geophone placed in direct contact with the ground

surface through a hole in the center of the plate (measuring deflections of the ground). The different locations of the deflection transducers may be the cause of the different measurements. Van Gurp et al. (2000) investigated this issue and concluded that measurement on the ground was more comparable to the laboratory triaxial measurements at in-situ stress levels. The velocity measurements on the bearing plate were observed to produce larger deflections relative to measurements on the ground. Therefore, devices, which use transducers to measure deflections in the plate, are expected to measure larger deflections as evidenced by many field studies (Weingart 1993, ZTVA –StB 1997, Shahid et al. 1997, Fleming et al. 1998, Fleming 1998 and 2001).

Other studies indicate that the rate of loading can affect E_{LWD}. The loading rate can be controlled by varying the spring stiffness of the buffers placed between the drop weight and contact plate. Fleming (2000) reports that a comparatively lower stiffness buffer provides more efficient load transfer and better simulates static plate loading conditions. Lenngren (1992) reports that with using a stiffer buffer, the load pulse time history is shortened and the resulting E_{FWD} is increased by 10 to 20% on some asphalt concrete pavements while other locations showed little or no difference. According to Adam et al (2002), the applied load pulse can vary by about 30% with a change in rubber buffer temperature from 0 to 30°C, while it remains more constant for a steel spring buffer, which is used by the ZFG 2000 (White et al, 2007).

B.3. DISCUSSION

B.3.1 Comparison of LWD and LSME Modulus

The modulus from the two LWDs compared to the back calculated modulus form the LSME tests is illustrated in Fig. B.2. In almost all cases, the LWD modulus is lower than the calculated LSME modulus. However, the modulus of material blended with fly ash by the Keros 100 is close to the LSME modulus, possibly because of the negligible effect of the imposed small strain on the subgrade by the base course. Therefore no correction would probably be required to the Keros 100 modulus for materials blended with fly ash.

A procedure was developed to compare the LWD and LSME modulus more accurately by making certain corrections to account for the effect of the existing subgrade and the stress and strain level associated with the applied load and plate size. In this study, first, the Keros 100 modulus was corrected to the LSME modulus. Then the ZFG 2000 was correlated with the Keros 100 allowing the same correction to be made to compare with the LSME.

In this study, LWDs with plate size of 200 mm were used and the load applied to the surface resulting from the dropping weight was observed to vary from 5.7 to 5.9 kN (average applied stress equal to 185 kPa) due to the spring characteristics of the buffer. The LSME test utilized a 250 mm diameter plate applying a stress level up to 140 kPa. As discussed in Chapter 3, the load applied to the base course in the LSME was adjusted to account for a truck load on an asphalt concrete surface, Therefore Keros measurements were corrected to the LSME stress level. Also, the maximum load of the loading pulse was treated as a static load in evaluating the effect of stress level and subgrade on the base course modulus even though the duration of the loading pulse was observed in a range of 20 to 30 milliseconds, which would impact the measured LWD modulus and LWD deflections as well (Section B.2.2).

MICH-PAVE was used to compare the LSME and Keros 100 modulus and take into account the effect of subgrade and the stress level. The mechanical parameters of the subgrade

and base course thicknesses such as modulus and Poisson's ratio used in the LSME tests were input into MICHPAVE, along with the average applied load and plate size of the LWD-KEROS. The stress dependent modulus of the different base course materials calculated from the LSME tests along with thicknesses were applied to the LWD analysis to compare the measured deflections in the LSME with the deflections of the Keros 100. The net base elastic deflection from the Keros 100 test ($\delta_{NB\text{-}LWD\text{-}K}$) was found by subtracting the elastic deflection at the subgrade surface from the total elastic deflection on base course surface. The net base elastic deflection under the applied load is an indicator of the base course performance and is presented in Fig. B.3. $\delta_{NB\text{-}LWD\text{-}K}$ was found to be 18% of the measured deflection at the surface.

$\delta_{NB\text{-}LWD\text{-}K}$ was plotted against the measured net base elastic deflection from the LSME (δ_{NB}) in Fig. B.4. $\delta_{NB\text{-}LWD\text{-}K}$ is shown to be similar to δ_{NB} as all points lie close to the 1:1 line, suggesting that the LSME and Keros 100 test results are comparable considering the effect of subgrade, stress level, and plate size. Although load duration was not considered directly in this study, its effect was already taken into account by comparing the LSME and Keros 100 deflections.

The corrected Keros 100 base course modulus can be calculated by first determining the net base elastic deflection from LWD Keros deflection (figure B.3) and then using Fig. B.5 which shows the back calculated LSME modulus as a function of net base elastic deflection (δ_{NB}). Eqn. B.3 can be used to calculate the modulus:

$$M_r = 22\delta_{NB}^{0.96} \tag{B.3}$$

where δ_{NB} (mm) is the net base elastic deflection (or corrected Keros 100 deflection to net base elastic, $\delta_{NB\text{-}LWD\text{-}K}$), and M_r (MPa) is the back calculated resilient modulus of the LSME.

The Keros 100 modulus of material blended with fly ash is almost the same as the LSME modulus resulting from the negligible effect of subgrade and stress independency of the material in the range of applied stresses in a pavement structure. Therefore it is suggested to use the directly calculated modulus from the Keros 100 for materials blended with fly ash.

This comparison method was developed for the Keros 100, but an extra step is required for correcting the ZFG 2000 due to the differences in transducer sensor types causing variation of the measured modulus. To make the correction simpler, a correlation between the measured Keros 100 and ZFG 2000 deflections was determined so that the same relationships used in comparing the Keros 100 and LSME modulus could be used for comparing the ZFG 2000 and LSME modulus with corrected deflections.

B.3.2 Correlation between ZFG 2000 and KEROS 100 deflections

White et al (2007) proposed the following equation to correlate between the deflections of the ZFG 2000 and Keros 100:

$$\delta_{LWD\text{-}K} = 0.57\ \delta_{LWD\text{-}Z} \quad (\delta_{LWD\text{-}Z} = 1.75\ \delta_{LWD\text{-}K}) \tag{B.4}$$

where $\delta_{LWD\text{-}K}$ is the measured deflection from the Keros 100 and $\delta_{LWD\text{-}Z}$ is the measured deflection from the ZFG 2000. The data collected in this study also followed this relationship as shown in Fig. B.6.

Using Eqn. B.4, the measured ZFG 2000 deflection is converted to a Keros 100 deflection, and the methodology discussed in Section B.3.1 is applied. Since the measured Keros 100 modulus is comparable with the LSME modulus for material blended with fly ash (E_{LWD-K} = E_{LSME}) the correlation between ZFG 2000 and KEROS 100 is all that is required to correct the ZFG 2000 modulus to the LSME as shown in Fig. B.7. The proposed equation for correction of ZFG 2000 modulus for the material blended with fly ash is given as:

$$E_{LWD-Z}= 0.42\ E_{LWD-K}\ \text{-}67 \tag{B.5}$$

where E_{LWD-Z} and E_{LWD-K} (MPa) are the measured moduli from Zorn and Keros devices, respectively. By rearranging Eqn. B.5 and making E_{LWD-K} equal to E_{LSME}, the corrected ZFG 2000 modulus comparable to the LSME modulus can be given as:

$$E_{LWD-Z\ cor}= 2.4\ E_{LWD-Z} + 159 \tag{B.6}$$

The corrected moduli of both LWD models are shown in Fig. B.8 as compared to the LSME modulus.

Care should be taken while using the proposed method in this report, because all corrections were made assuming the subgrade modulus was equal to 70 MPa as determined from the LSME back calculations. This method can be applied to similar subgrade conditions as in this study.

B.3.3 Effect of subgrade modulus

The corrected LWD modulus can be used only with the same subgrade conditions as used in the LSME tests. To account for different subgrade moduli, the following method was proposed.

The granular equivalency was considered as a proper tool to evaluate the structural sufficiency of a pavement system. As various pavement systems subjected to the same deflection under the same stress level are considered equivalent, the LWD measurements were used to provide the equivalency of different pavement systems. The main step to use LWD in evaluating the equivalency of pavement systems is to provide a correlation between the LWD deflections and the granular equivalency of a pavement system.

In this study, granular equivalency of different base courses (Class 5, RPM, RSG and material with fly ash) was calculated based on the LSME tests as discussed in Chapter 4. The change of granular equivalent factor as a function of measured Keros 100 deflection for the set of materials being evaluated is shown in Fig. B.8. The GE factor decreased linearly with increase in the LWD deflection. However materials with the same LWD Keros deflection were found to have the same granular equivalency, i.e. Class 5 and RPM. Moreover, Class 5 with different thicknesses had the same granular equivalent factor while the LWD measurements were different. It shows the importance of layer thickness in the equivalency of the pavement systems, i.e. the thicker base course of the same material causes a stiffer support in pavement system due to the lower strain under the applied load. The effect of thickness is taken into account by means of granular equivalency; GE (mm) is calculated as:

$$GE = a_{base}\ D_{base} \tag{B.6}$$

where a_{base} is the granular equivalent factor of base course and D_{base} is the base course thickness. The granular equivalency as a function of LWD Keros deflection was illustrated in Fig. B.9. The linear relationship between granular equivalency and Keros 100 deflection was found while the granular equivalency decreased as the measure LWD Keros deflection increased. All materials blended with fly ash showed the higher GE and lower LWD deflection due to the high stiffness of these materials. Moreover, a thicker base course is required for the relatively looser material like RSG to meet the required granular equivalency of the pavement system.

Typically the required granular equivalency of a pavement system is provided due to the stiffness of subgrade material (MN Design and Construction of low volume load, 2002 and Investigation 183 (Application of AASHO Road Test Results to Design of Flexible Pavements in Minnesota)). In this study, the required granular equivalency was accounted for the effect of subgrade, and GE (Fig. B.9) was normalized using the required GE.

Fig. B.11 shows the relationship between static plate modulus of subgrade (roadbed) and R-value from stabilometer test. The R-value is used to calculate required granular equivalency as shown in Fig. B.12. To convert the calculated modulus by LWD-Keros to the static plate modulus (E_{PLT}) three corrections were made.

1. The correlation between Keros and ZFG LWDs as (White, 2007):

$$E_{LWD-K} = 1.75 \, E_{LWD-Z} \qquad (B.7)$$

2. Since the LWD with 200 mm plate was used in this study, some theoretical equations and experimental investigations (after White, 2007) proposed a 200 mm plate modulus can be approximately 1.3 to 1.5 times higher than that of a 300 mm plate:

$$E_{LWD-200} = 1.3\text{-}1.5 \, E_{LWD-\,300} \qquad (B.8)$$

3. Hildebrand (2003) presented a comparison study between static plate load test, and the portable LWD (Zorn) on a granular base layer construction project. Results showed that there is a "good" correlation between static plate load test and E_{LWD-Z3}. Relationship between static plate load and modulus of LWD-ZORN is as follows:

$$E_{PLT} = 2.41 \, E_{LWD-Z300} \qquad (B.\,9)$$

Combining Eqn. B.7 and B.9 results in the following equation:

$$E_{PLT} = E_{LWD-K} \qquad (B.10)$$

where, E_{PLT} is the modulus of the static plate load test.

In this study, the R-value of the subgrade was introduced to be 40 using Eqn. B.10, Fig. B.11, and subgrade modulus equal to 70 MPa as measured from LSME results. R-Value was used to predict the required granular equivalency (GE) of the pavement system. GE was selected to be 686 mm (27 in) and the granular equivalency (GE) was normalized using the required GE, $GE_{required}$ as shown in Fig. B.13. The linear relationship was introduced to the normalized granular equivalency (GE) and LWD Keros deflections. This chart was generalized for varying

18 kip ESALs from 10^5 to 2×10^6 as illustrated in Fig. B.14. This chart can be used to inspect the quality of road construction compared with the design target. Also, the same charts can be provided for LWD Zorn following the same method.
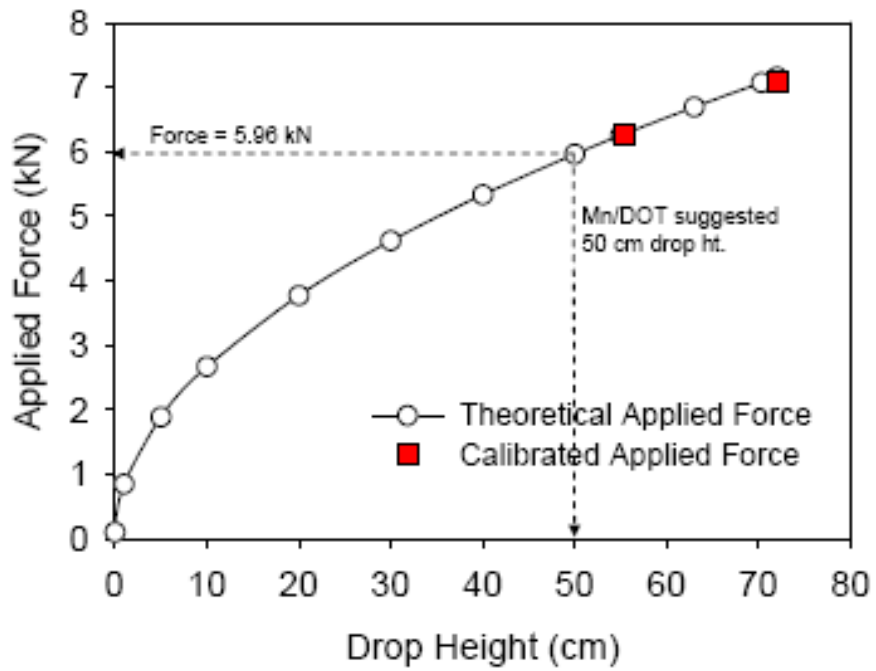
Fig. B.1. Calibration curve of LWD- Zorn
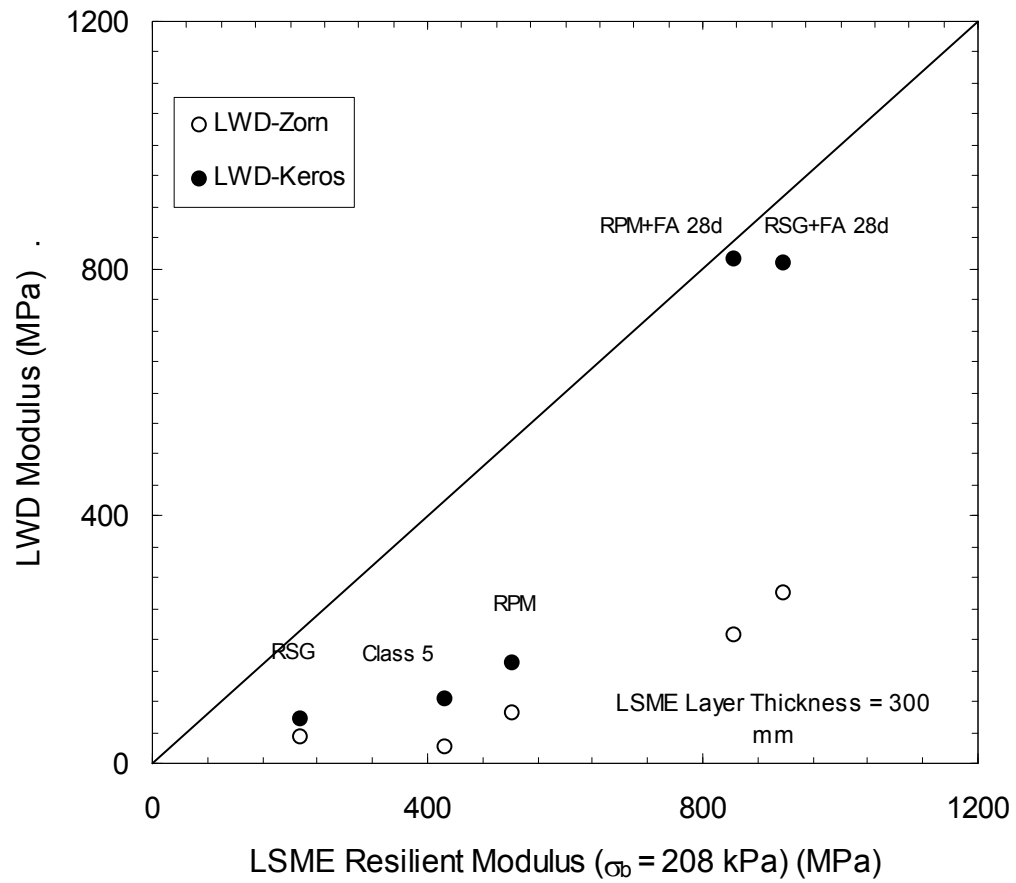
Fig. B.2. Comparison between the LWD modulus and LSME resilient modulus.
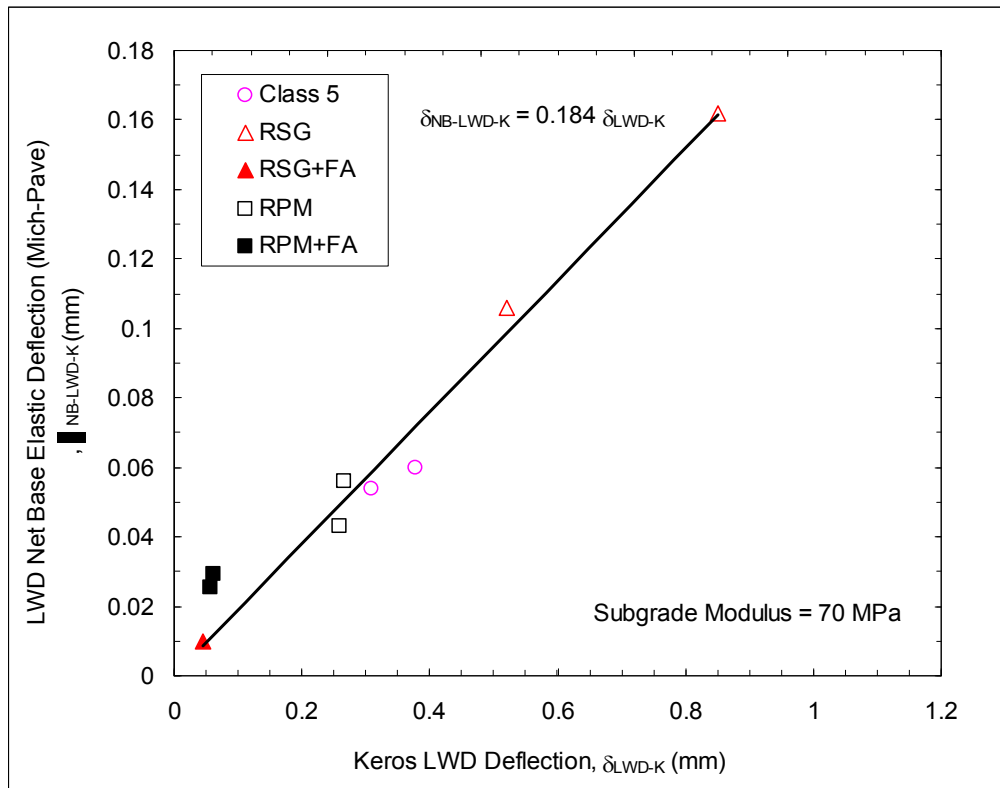
Fig. B.3. LWD net base elastic deflection as a function of measured KEROS 100 deflection for subgrade modulus of 70 MPa.
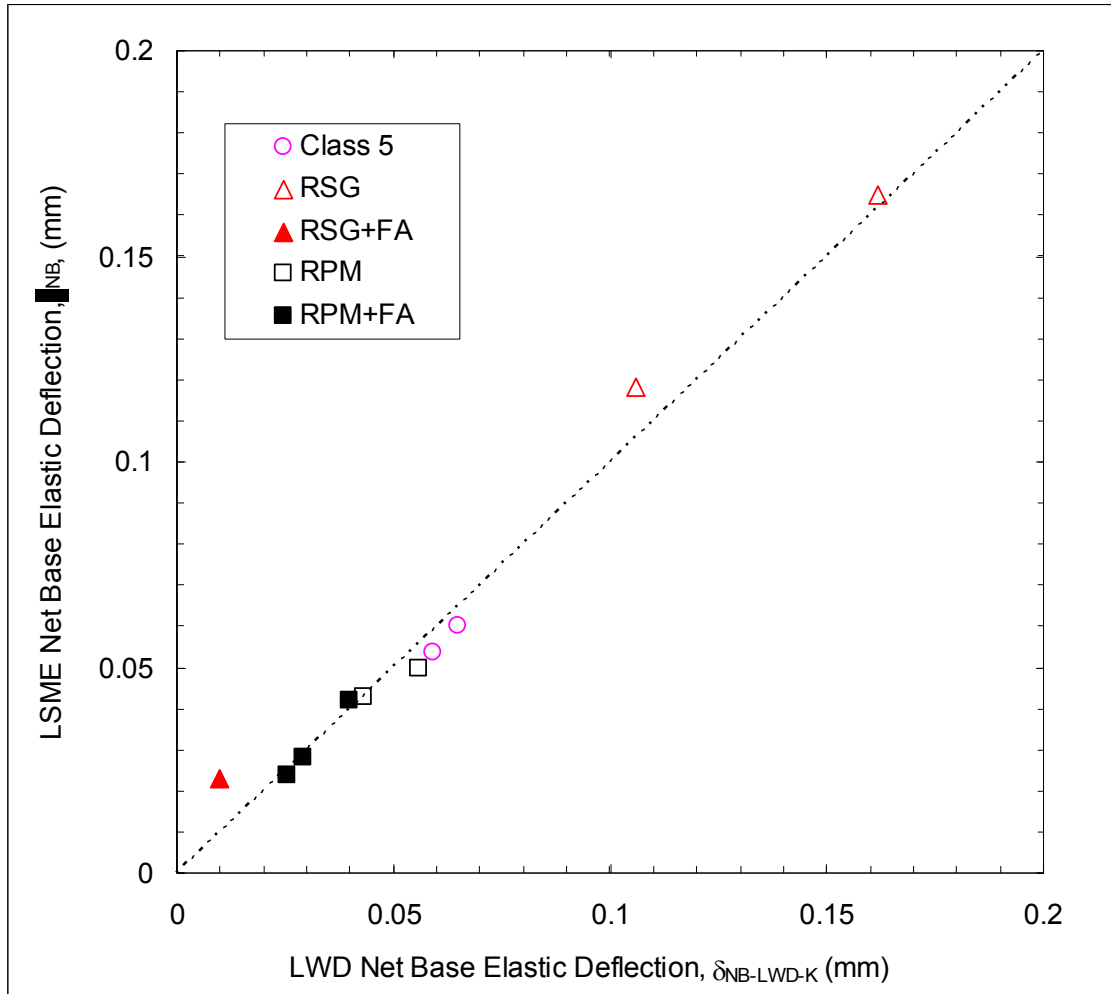
Fig. B.4. LWD net base elastic deflection against measured one in LSME test.
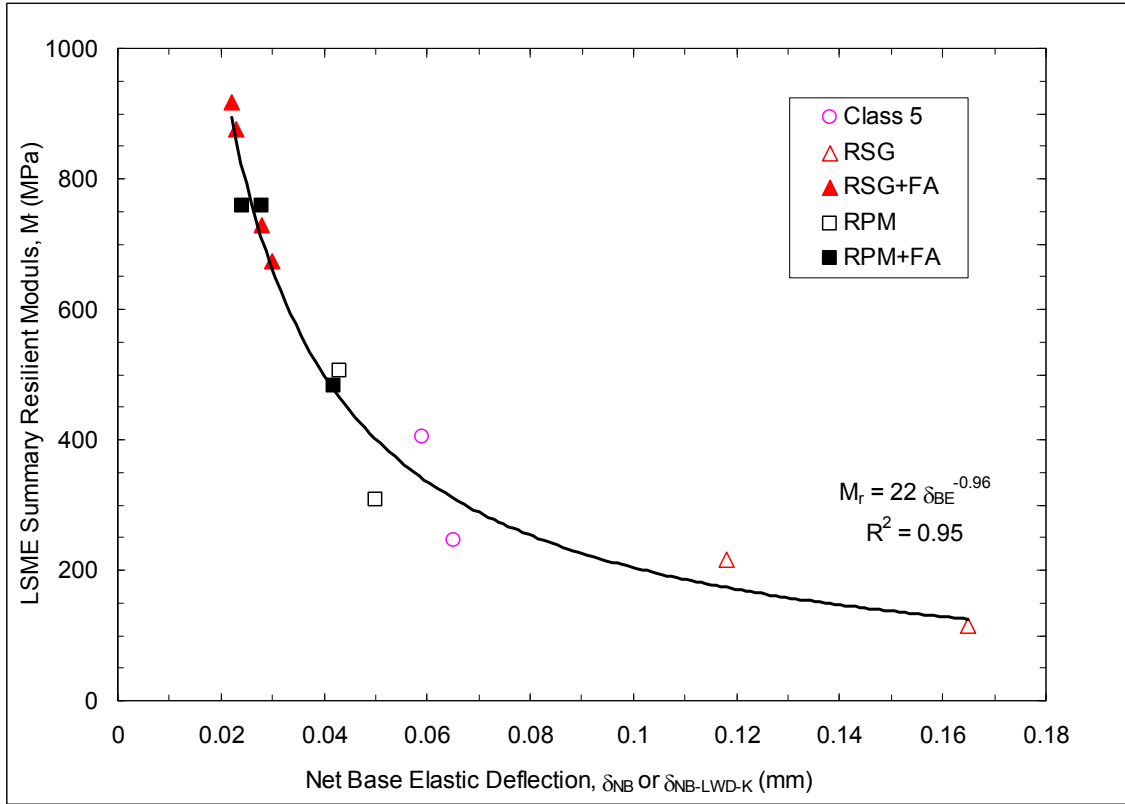
Fig. B.5. LSME modulus as a function of net base elastic deflection.
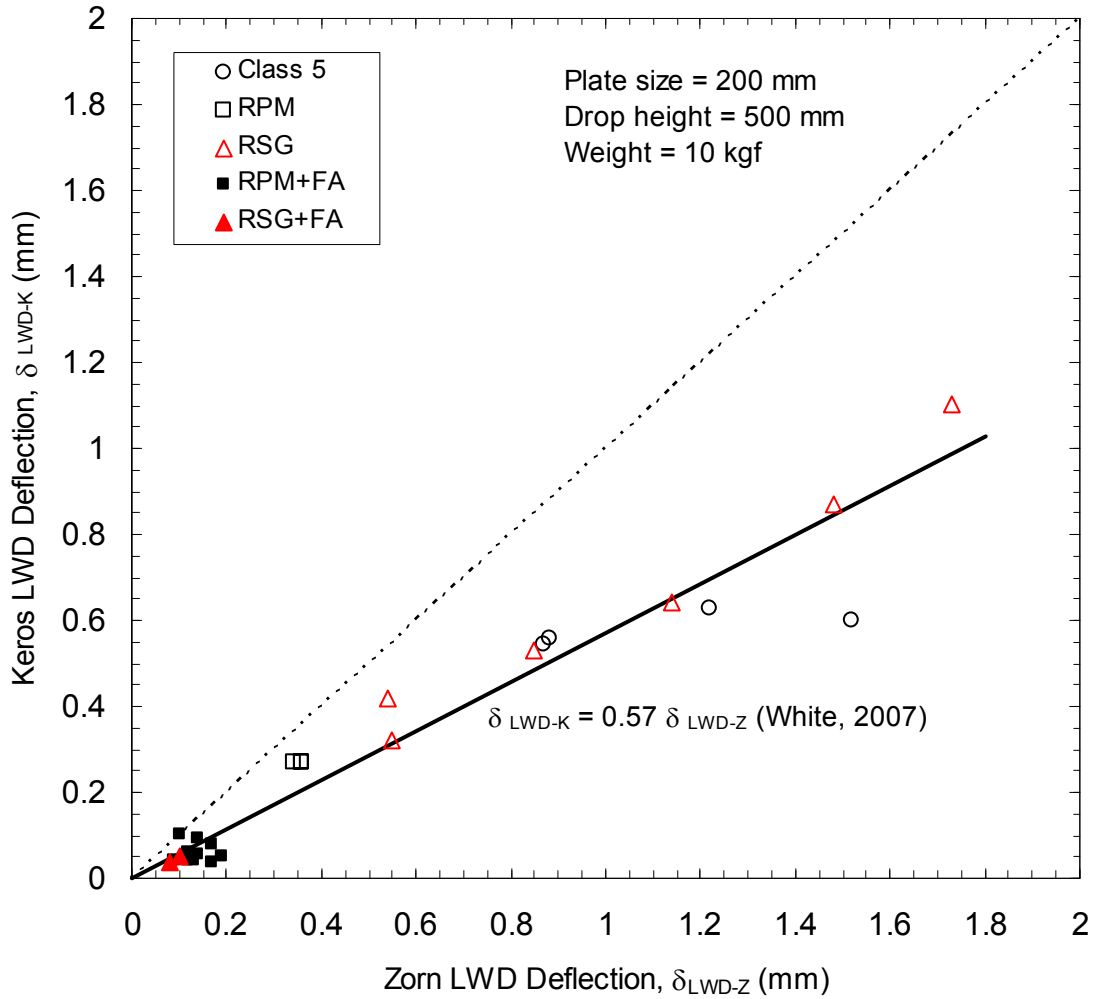
Fig. B.6. Keros 100 deflection as a function of the Zorn ZFG 2000 LWD deflection.
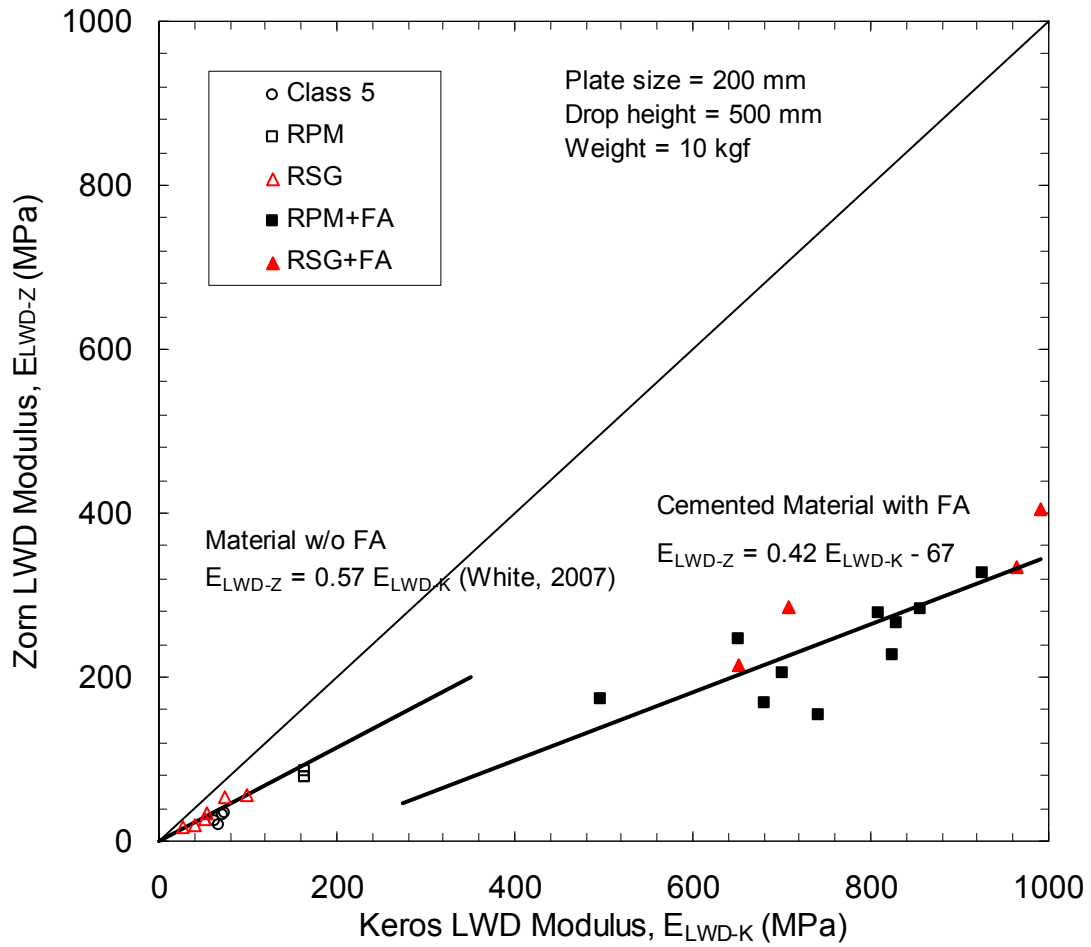
Fig. B.7. Correlation between elastic modulus of ZFG 2000 and Keros 100.
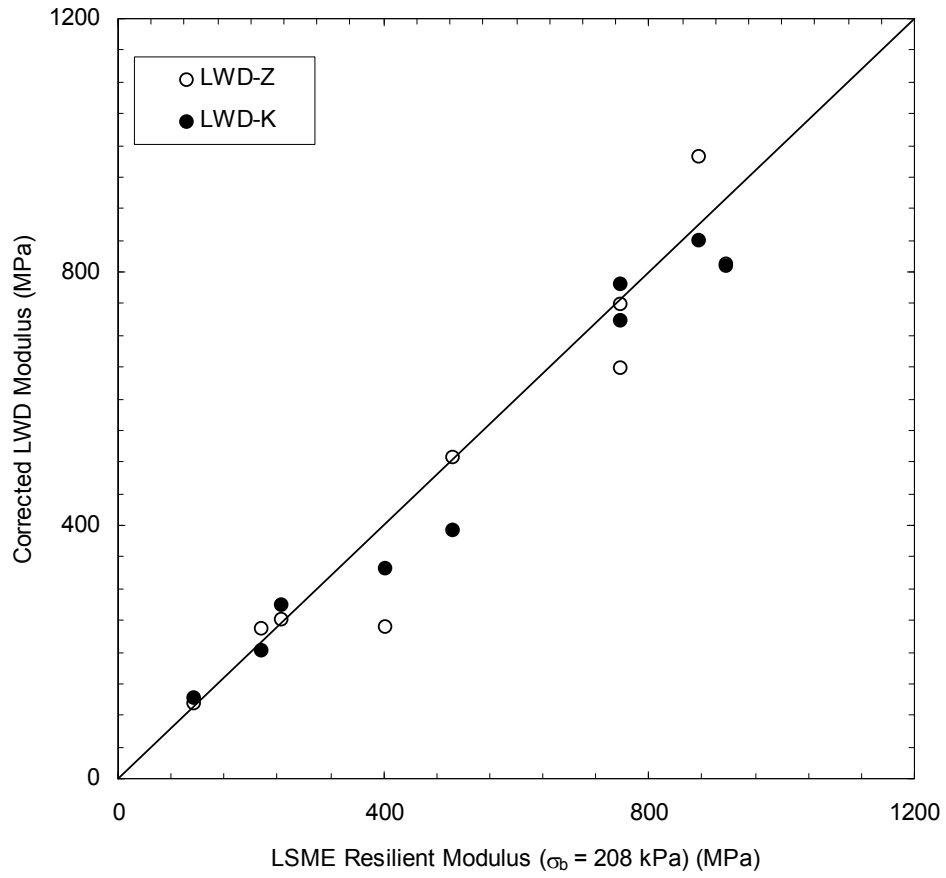
Fig. B.8. Corrected LWD modulus due to subgrade effect, stress level and loading plate compared with LSME modulus.
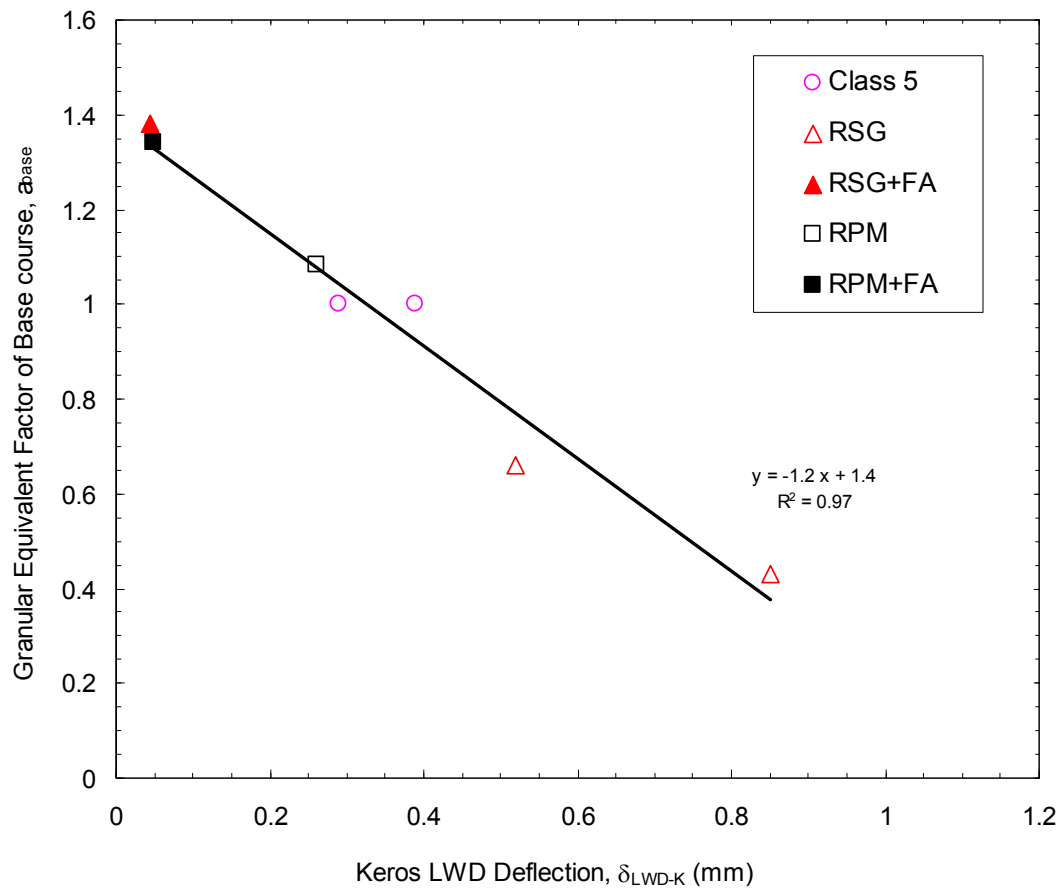
Fig. B.9. Granular equivalent factor as a function of measured Keros LWD deflection.
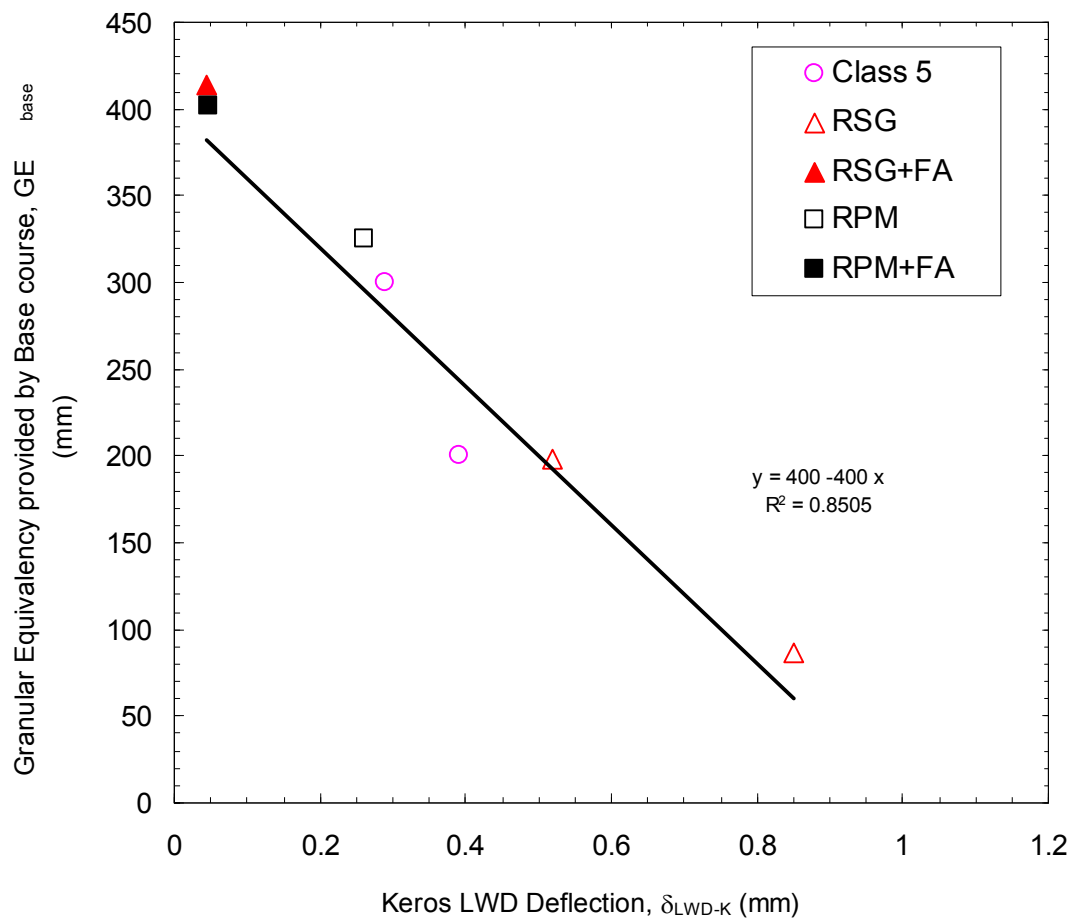
Fig. B.10. Granular equivalency in mm as a function of Keros LWD deflection.
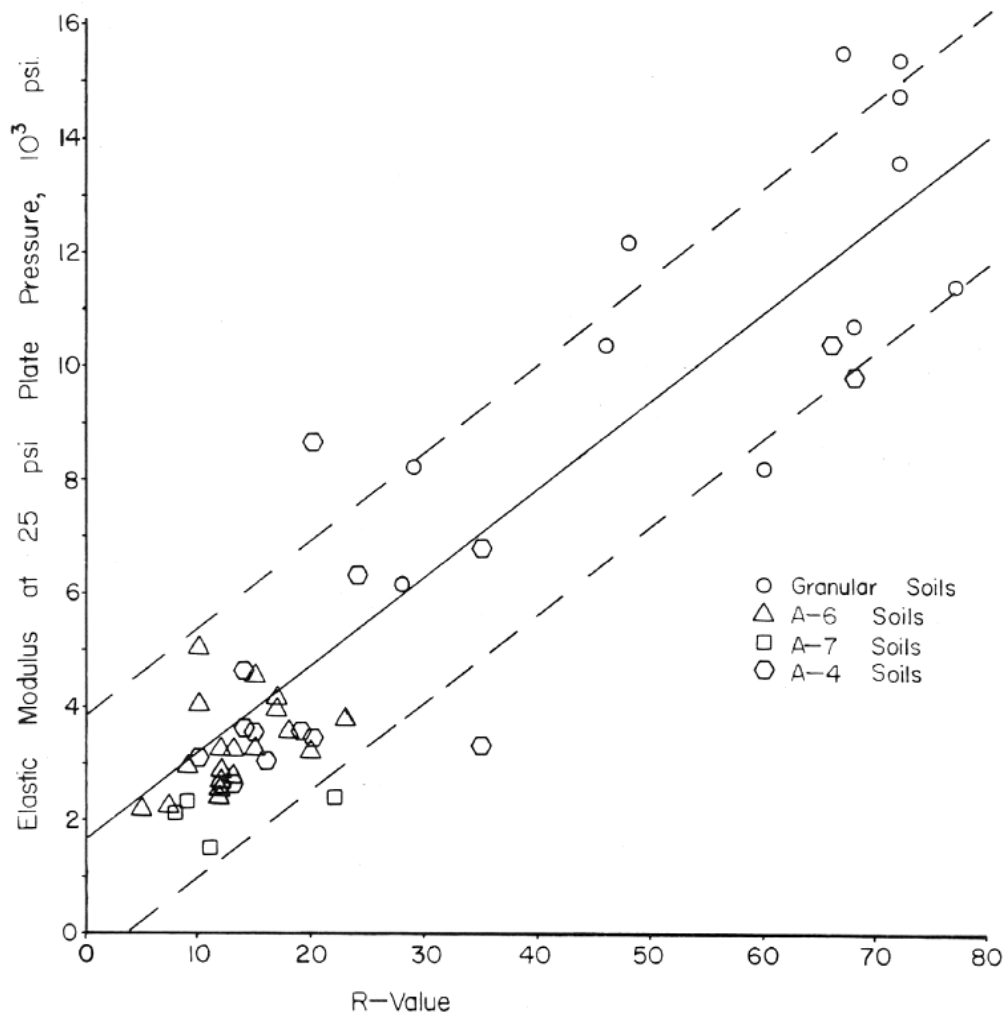
Fig. B.11. Relationship between R-value and static loading plate modulus (from Kersten et al, 1968 and Lukanen, 1980).
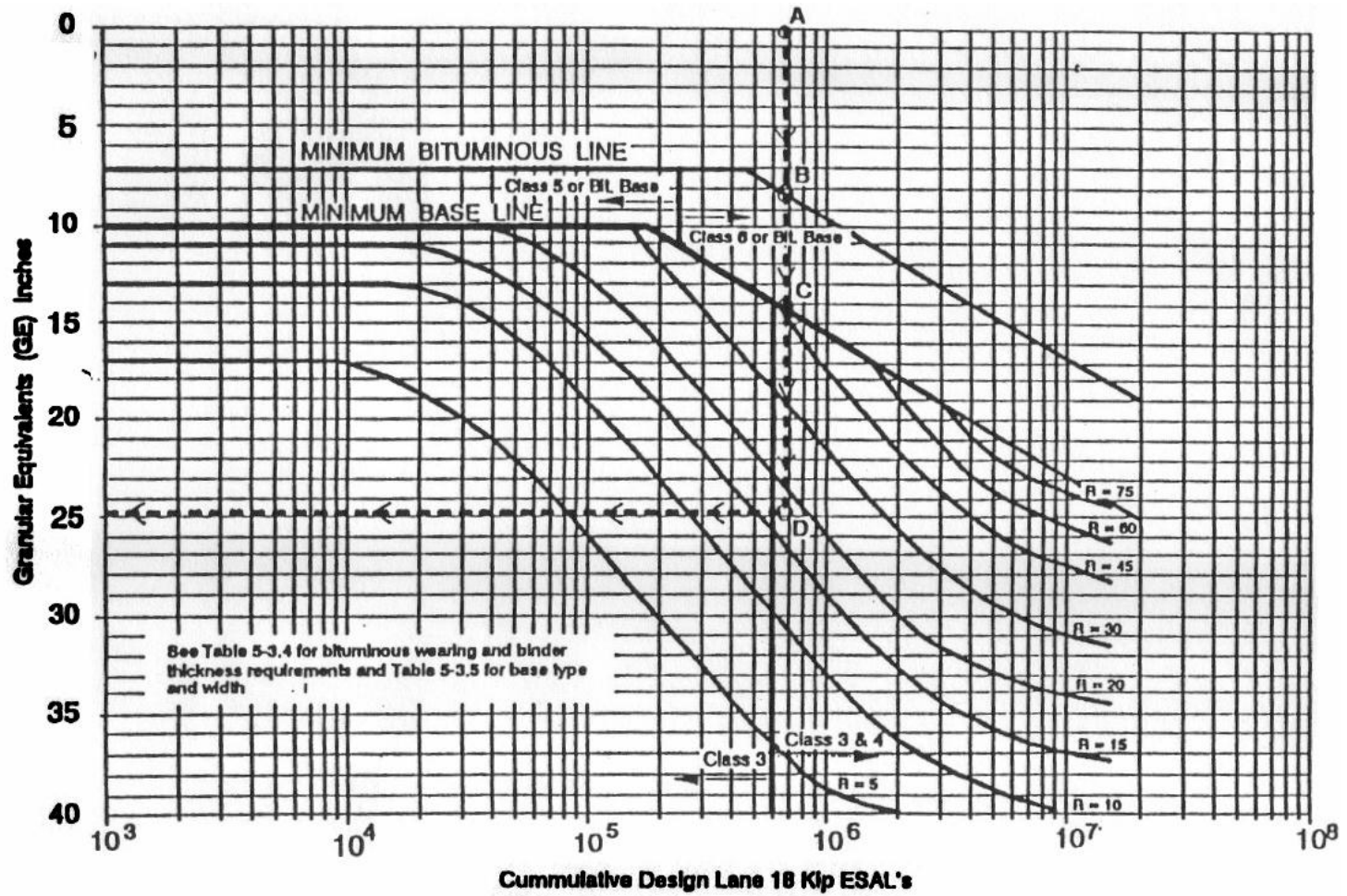
Fig. B.12. Required granular equivalency as a function of R-value (from Skok et al, 2003).
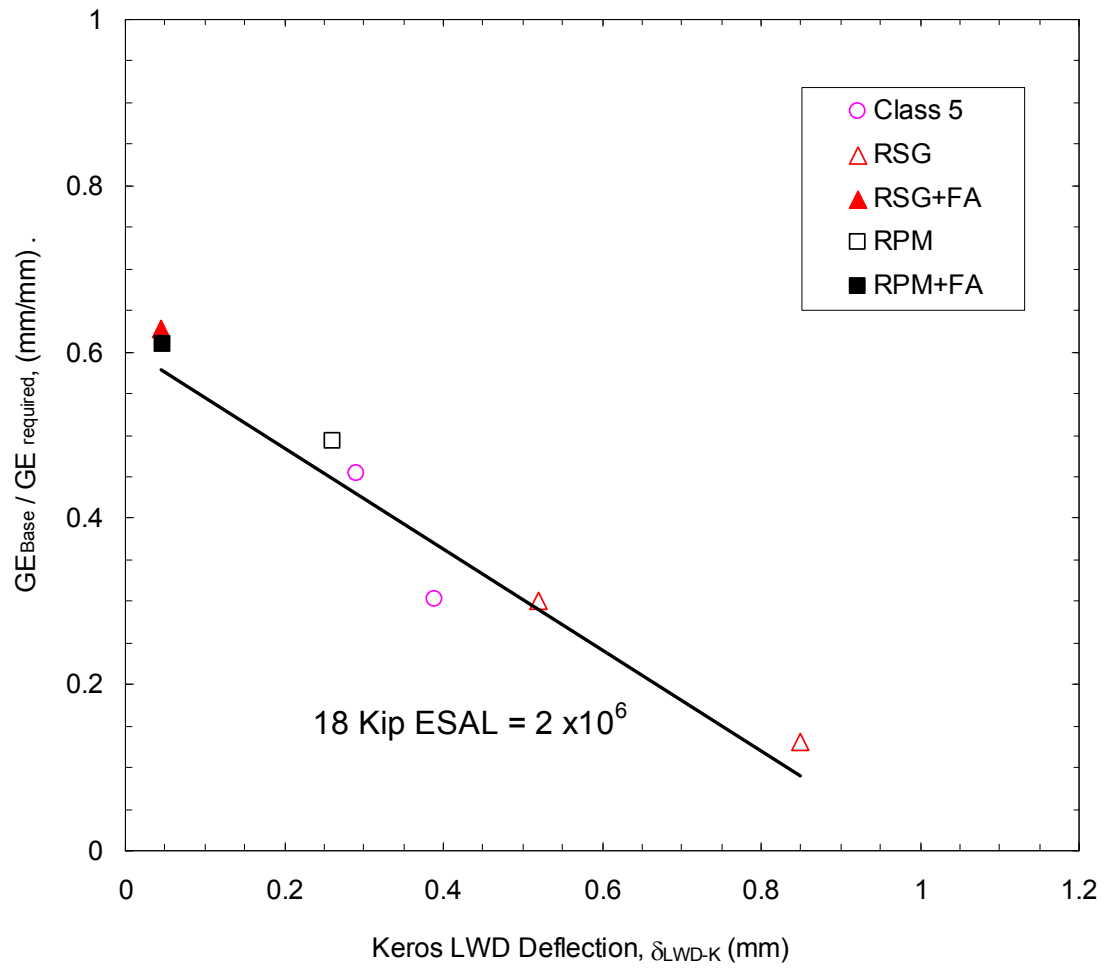
Fig. B.13. Normalized granular equivalency as a function of Keros LWD deflection.
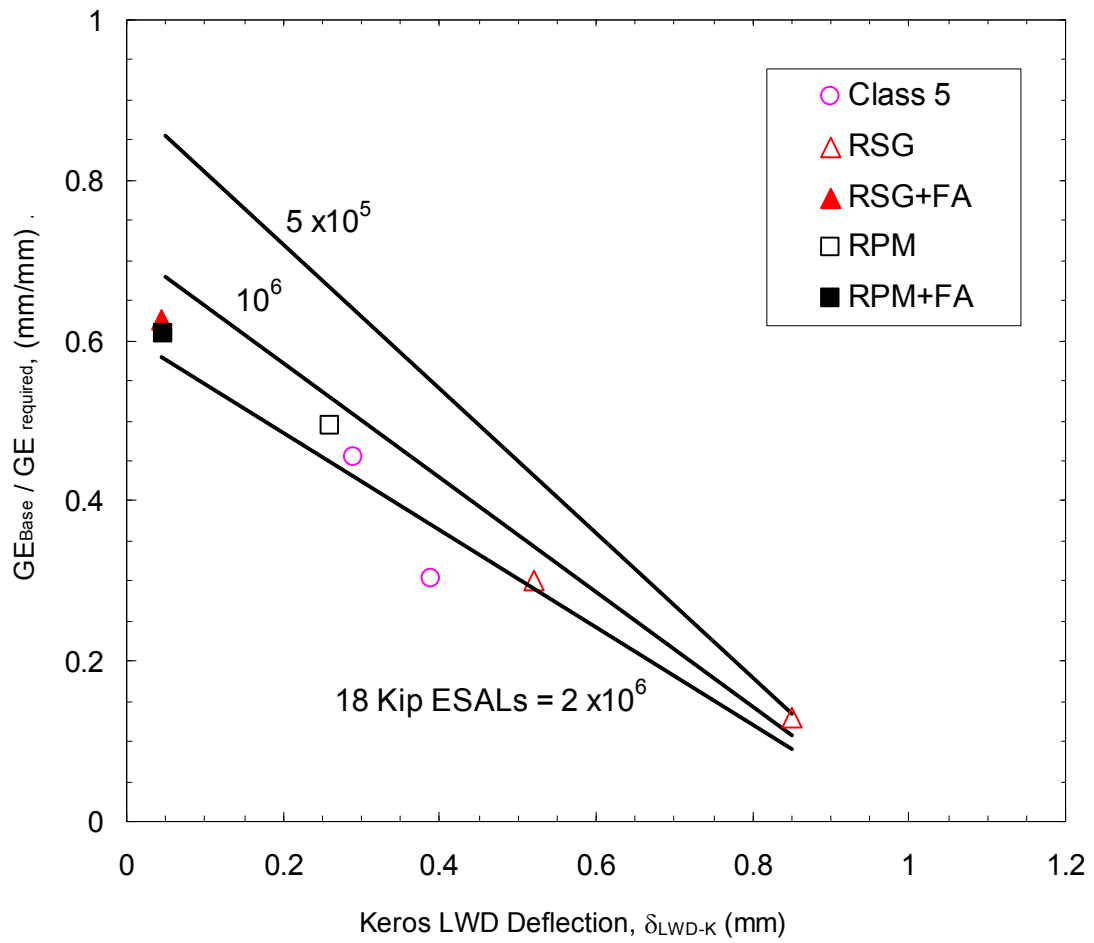
Fig. B.14. Normalized granular equivalency as a function of Keros LWD deflection with varying 18 kip ESAL.

APPENDIX D

REPORT FOR TASK 4

MECHANICAL MONITORING OF FIELD DEMONSTRATION SITES

USE OF FLY ASH FOR RECONSTRUCTION OF BITUMINOUS ROADS: MONITORING A FLY-ASH STABILIZED PAVEMENT MATERIAL IN WASECA, MINNESOTA

REPORT FOR TASK 4

Mechanical Monitoring of Field Demonstration Sites

Prepared by:

Lin Li
Tuncer B. Edil
Craig H. Benson
Bulent Hatipoglu
Paul Bloom

Department of Civil and Environmental Engineering
University of Wisconsin-Madison
Madison, WI 53706

and

Department of Soil, Water, and Climate
University of Minnesota
St. Paul MN

December 2008

TABLE OF CONTENTS

LIST OF FIGURES

1. INTRODUCTION

Two road paving projects using fly ash soil stabilization were subjected to continued environmental and mechanical monitoring. These demonstration projects were part of previous Mn/DOT funded studies (Li et al. 2006 and Hatipoglu et al. 2006) Self-cementing Class C fly ash from a coal-fired electric power plant was used to stabilize the recycled pavement material (RPM) during the rehabilitation of a 0.5-km section of flexible pavement along 7th Avenue and 7th Street in Waseca, MN (Li et al. 2006). RPM was prepared by pulverizing the existing asphalt pavement and underlying materials to a depth of 300 mm below ground surface using a CMI RS-650-2 road reclaimer. The uppermost 75 mm of the RPM was removed and then Class C fly ash (10% by dry weight) was spread uniformly on the surface using truck-mounted lay-down equipment similar to that described in Edil et al. (2002). The fly ash was mixed with the RPM to a depth of 150 mm using the road reclaimer, with water being added during mixing using a water truck. This mixture, which contained 10% fly ash by dry weight, was compacted within 1-2 h by a tamping foot compactor followed by a vibratory steel drum compactor. The fly ash stabilized RPM (SRPM) was cured for 7 d and then overlain with 75 mm of HMA. Field monitoring of the site was continued under this new present LRRB project after the completion of the original project and submission of the initial report in 2006. Environmental data and field performance data collected through 2008 have been analyzed and are presented in this report.

At another project fly ash was used to stabilize an existing gravel road to form a base (Hatipoglu et al. 2006) for HMA pavement. This project was conducted during reconstruction of a 3.5-km section of County Road 53 in Chisago County, MN that was being converted from a gravel road to a paved road. Fly ash from Riverside Unit 7 (Class C) and Riverside Unit 8 (off-specification) in Minneapolis, MN was used for stabilization. The fly ash was mixed with a CMI RS-650-2 road reclaimer into the existing road surface gravel (RSG) to a depth of 250 mm, with water being added during mixing using a water truck. This mixture, which contained 10% fly ash by dry weight, was compacted within 1-2 hr by a tamping foot compactor followed by a vibratory steel drum compactor.

The stabilized road surface gravel (S-RSG) was overlain with 51 mm nonwearing course and 38 mm wearing course (total 89 mm) of HMA within 3 to 7 d after compaction. Field monitoring of the site was continued under the present LRRB project after completion of the original project in 2006. Environmental data and field performance data collected through 2008 have been analyzed and are presented in this report. Environmental monitoring was conducted through April 2008, at which time the monitoring station was disassembled per agreement with the landowner adjacent to CR 53.

2. ENVIRONMENTAL DATA

2.1 METEOROLOGICAL AND SUBSURFACE CONDITIONS

2.1.1 WASECA

The field instrumentation system installed at Waseca is shown in Fig. 1. Air temperature and subsurface temperature of the SRPM and subgrade between October 2004 and August 2008 are shown in Fig. 2. Data are not shown for a portion of 2006 due to an instrument malfunction. The air temperature ranged from -29.5 ^{o}C and 38.6 ^{o}C during the monitoring period, with sub-freezing temperatures occurring between November and April each year. Temperature of the SRPM ranged between -15 ^{o}C and 39 ^{o}C. This layer was frozen for about 3-4 months each winter. The subfreezing temperatures penetrated after major cold air temperature spells in December and February. Temperature of the subgrade ranged between -5 ^{o}C and 33 ^{o}C and varied seasonally with the air temperature. The magnitude and frequency of variation diminishes with depth, which reflects the thermal damping provided by the pavement materials. Overall, the main layer that experienced freezing was the SRPM although some penetration occurred below this layer. Thus, the main frost effects on the pavement would be expected to emanate from this layer.

The volumetric water contents of SRPM and subgrade between October 2004 and August 2008 are shown in Fig.3. The volumetric water contents drop when the soil temperature begins to fall below 0 ^{o}C (volumetric water contents are not reported in these figures for periods when freezing was established). These apparent drops in water content reflect freezing of the pore water. The water content measured by WCRs is determined by measuring the velocity of an electromagnetic wave propagated along the probe. The velocity of the wave varies with the apparent dielectric constant of the soil, which is dominated by the dielectric constant of the water phase. When the pore water freezes, the dielectric constant of the water phase drops significantly and this appears as a drop in water content in WCR data (Benson and Bosscher 1999).

Higher volumetric water contents were recorded in the fine-textured subgrade (maximum of about 44%) than the SRPM (maximum of 32%), which reflects the greater affinity of fine-textured soils to retain water. No spikes are present in the water content records, which reflects the ability of the HMA to impede infiltration during precipitation and snow melt events and to limit evaporation during drier periods. The annual variation in water content in the subgrade is between 12 and 44%, and the annual variation in water content in SRPM is between 10 and 34%. Higher water contents are recorded in the summer months, when greater precipitation occurs.

The precipitation record for the site was obtained from the NOAA weather station in Waseca, MN. The cumulative precipitation is shown in Fig. 4a for the period from October 2004 to June 2008. The seasonal variation in percolation is also reflected in the percolation collected in the lysimeter, as shown in Fig. 4b.

2.1.2 Chisago CR 53

The field instrumentation system installed at CR 53 is shown in Fig. 5. Air temperature and relative humidity between November 2005 and April 2008 are shown in Fig. 6. The air temperature ranged from -29.5 ^{o}C and 35 ^{o}C during the monitoring period, with sub-freezing temperatures occurring between November and April. The relative humidity ranged between

13.6% and 100% during the monitoring period. Precipitation at the site was obtained from the NOAA weather station in Cambridge, MN. Cumulative precipitation for the monitoring period is shown in Fig. 7.

Subsurface temperatures and volumetric water contents at various depths in the pavement are shown in Figs. 8 - 12. (Locations of the sensors that were used to collect the data are shown in Fig. 5.). Subsurface temperatures varied seasonally with the air temperature. The magnitude and frequency of variation diminished with depth, which reflects the thermal damping provided by the pavement materials. Temperature of the SRSG (Sensors 3 and 4) ranged between -10 $^{\circ}$C and 40 $^{\circ}$C (Figs. 8 and 9) and temperature of the RSG ranged between -10 $^{\circ}$C and 48 $^{\circ}$C (Figs. 10 and 12). Both the SRSG and RSG layers experienced subfreezing temperatures for 3-4 months each winter.

Subfreezing temperatures penetrated the S-RSG and RSG after periods of sustained cold air temperature in December and February. Temperature of the subgrade ranged between -8 $^{\circ}$C and 3 7°C (Figs. 8 and 9), and dropped below the freezing point for 1-2 months each winter.

Volumetric water contents are shown in Figs. 8 and 9 for the S-RSG layer, in Fig. 10 for the RSG layer, and Fig. 11 for the subgrade. The volumetric water contents drop dramatically when the soil temperature falls below 0 $^{\circ}$C (volumetric water contents are not reported in these figures for periods when freezing was established). These apparent drops in water content reflect freezing of the pore water.

Higher volumetric water contents were recorded in the fine-textured subgrade (maximum = 51%) than the coarse-grained RSG (maximum = 31%), which reflects the greater affinity of fine-textured soils to retain water. The volumetric water content of SRSG, however, was as much as 52%, which reflect the presence of fly ash. No spikes are present in the water content records, which reflect the ability of the HMA to impede infiltration during precipitation and snow melt events and to limit evaporation during drier periods. Higher water contents were recorded in the spring and early summer, when snowmelt and thawing occur and greater precipitation generally occurs.

The seasonal variation in water content is also reflected in the drainage collected in the lysimeter, as shown in Fig. 13 when a significant rise is recorded in April 2006. Due to the malfunction of the lysimeter, there is no drainage collection after June 2006.

3. FIELD MECHANICAL DATA

3.1 WASECA

Maximum deflections from the FWD tests for the 40-kN drop are shown in Fig. 15(a) for November 2004 and August 2005. FWD tests were conducted in November 2004 and August 2005 to define the as-built condition and the condition after one year of winter weather. In November 2004, the air and ground temperatures were decreasing although there was no frost penetration. In August 2005, ground temperatures and the volumetric water contents in SRPM and subgrade were significantly higher compared to November 2004 (see Figs. 2 and 3). Maximum deflection, which is measured at the center of the loading plate, is a gross indicator of pavement response to dynamic load. In situ stiffness measured with the SSG is shown Fig. 15b for the RPM and SRPM after 7 d of curing.

Similar deflections were measured during both surveys, suggesting that the SRPM had maintained its integrity even after exposure to freezing and thawing. The deflection at Stations 4-10 is slightly higher in 2005 than 2004. However, this difference is not caused by a decrease in modulus of the SRPM, as shown subsequently. A more likely cause is the higher temperature of the HMA in August relative to November. There is a marked increase in deflections in August 2005. The SRPM stiffness as measured by SSG shows some variation but does not indicate any weakness around Station 4.

Elastic moduli of the SRPM that were obtained by inversion of the FWD data are shown in Fig. 15a. For the inversion, a three-layer profile was assumed that consisted of asphalt (75-mm thick), SRPM (150-mm thick), and an infinitely thick subgrade. Modulus of the asphalt was allowed to vary between 345 and 11,750 MPa and the Poisson's ratio was set as 0.4. The SRPM was assumed to have a Poisson's ratio of 0.35 and the modulus was allowed to vary between 70-9400 MPa. The subgrade was assumed to have a Poisson's ratio of 0.35.

The modulus of the SRPM varies between 57 and 1248 MPa (mean = 262 MPa) in November 2004 and between 79 and 1379 MPa (mean = 252 MPa) in August 2005. Most of the SRPM moduli are less than 200 MPa. The most significant exception is the very high modulus at Station 3 and 8. This modulus is believed to be an anomaly caused by the coarse gravel subgrade near Station 3 and 8, which was not included in the inversion. The moduli obtained in November 2006 have a mean of 234 MPa, indicating stable conditions.

Moduli obtained from the FWD inversion are compared with those obtained from the resilient modulus tests on field-mix specimens and the moduli computed from the stiffness measured with the SSG in Fig. 15b. Elastic modulus (E) was computed from the SSG stiffness (K_{SSG}) using (Sawangsuriya et al., 2003):

$$E = \frac{K_{SSG}(1-\upsilon^2)}{1.77\,R} \tag{1}$$

where R is the outside radius of the SSG foot (0.057 m) and υ is Poisson's ratio (assumed to be 0.35). Moduli obtained from the resilient modulus test on field-mix samples are markedly lower than those obtained from the FWD. SSG gives 50% higher moduli than the moduli obtained from the resilient modulus test. November 2007 FWD data appear anomalously high compared to other moduli data here and elsewhere. However, the additional moduli data obtained on August 2005 and November 2006 from the FWD are consistent.

3.2 CHISAGO CR 53

Maximum deflections from the FWD tests for the 40-kN drop are shown in Fig. 16 (a) for November 2005, May 2006, October 2006, and November 2007. Maximum deflection, which is measured at the center of the loading plate, is a gross indicator of pavement response to dynamic load. Stiffness of the subgrade and S-RSG, measured with a soil stiffness gauge (SSG) after construction, is shown in Fig. 16 (b) for comparative purposes.

During the surveys conducted in November 2005, 2006, and 2007, the air and ground temperatures were decreasing, although there was no frost penetration. In May 2006, ground temperatures and the volumetric water contents both in RSG and S-RSG layers were significantly higher compared to November 2005, 2006 and 2007 (see Figs. 8, 9, and 10) and thawing was complete. The volumetric water content of the subgrade layer was comparable during all four FWD testing dates (see Fig. 11). The deflections in May 2006 are markedly higher than those measured during the October-November surveys, with particularly large deflections recorded at Stations 60+00 to 80+00. This increase in deflection reflects thaw softening of the subgrade, as described in Jong et al. (1998). The variation observed in the maximum deflections from the FWD mimic the variation in subgrade stiffness recorded with the SSG. The surveys from October 2006 and November 2007 indicate that the pavement is much stiffer in the fall, that the stiffness diminished only slightly since construction, and that the pavement stiffness during the fall period has remained stable.

Elastic moduli of the S-RSG that were obtained by inversion of the FWD data from are shown in Fig. 17 (a). For the inversion, a three-layer profile was assumed that consisted of asphalt (89 mm), S-RSG (250 mm), and an infinitely thick subgrade.

Modulus of the asphalt was allowed to vary between 345 and 11,750 MPa and the Poisson's ratio was set as 0.4. The S-RSG was assumed to have a Poisson's ratio of 0.35 and the modulus was allowed to vary between 70-9400 MPa. The subgrade was assumed to have a Poisson's ratio of 0.35. The inverted moduli from the FWD are shown along with moduli computed from the SSG stiffness in Fig. 17 (b). The method in Sawangsuriya et al. (2003) was used to convert the SSG stiffness to a modulus. Modulus of the S-RSG varied between 513 and 1098 MPa (mean = 741 MPa) in November 2005 and between 74 and 199 MPa (mean = 156 MPa) in May 2006. Most of the S-RSG moduli are 600-700 MPa in November 2005. In May 2006, S-RSG moduli are 100 to 200 MPa at most stations, with the exception of the very low modulus at Station 70+00. The moduli obtained in October 2006 and November 2007 have means of 350 and 378 MPa, indicating a stable condition in the RSG.

4. CONCLUSIONS

This report has described monitoring data from a city street and a county road where cementitious fly ash (10% by weight) was used in sub base stabilization during re-construction of a city street and paving of a gravel road. Mechanical and environmental monitoring were collected and evaluated.

For the Waseca city street moduli obtained from the FWD inversion were compared with those obtained from resilient modulus tests on field-mix specimens and moduli computed from stiffness measurements made with a SSG. Moduli obtained from the resilient modulus tests on field-mix samples were markedly lower than those obtained in the field in November 2004, 2005, 2006, and 2007. Data from the FWD surveys indicated that the field moduli remained stable over 4 yr, despite several seasons of freezing and thawing.

For CR 53 gravel road paving project the FWD surveys conducted in October 2006 and November 2007 indicate that the modulus of the RSG decreased slightly since construction, but is remaining stable at about 350 MPa. Modulus of the S-RSG was markedly lower in May 2006 compared to the moduli obtained from surveys conducted in October and November. However, this drop in modulus reflects the seasonal effect of thaw softening rather than a systematic drop in modulus of the S-RSG.

REFERENCES

Benson, C.H. and Bosscher, P.J., 1999. Time-domain reflectometry in geotechnics: a review. In: W. Marr and C. Fairhurst (Editors), Nondestructive and Automated Testing for Soil and Rock Properties, ASTM STP 1350. ASTM International, West Conshohocken, PA, pp. 113-136.

Edil, T.B. et al., 2002. Field evaluation of construction alternatives for roadways over soft subgrade. *Transportation Research Record*, No. 1786: National Research Council, Washington DC, pp. 36-48.

Hatipoglu, B., Edil, T.B., and Benson, C.H. 2006. "Fly Ash Stabilization of Gravel Road as Base for Pavement at Chisago County Road 53, Minnesota", Geo Engineering Report No. 06-19, Department of Civil and Environmental Engineering, University of Wisconsin-Madison.

Jong, D., Bosscher, P., and Benson, C. 1998. Field Assessment of Changes in Pavement Moduli Caused by Freezing and Thawing, J. *Transportation Research Board*, 1615, 41-50.

Li, L., Benson, C.H., Edil, T.B. and Hatipoglu, B. 2006. "Fly Ash Stabilization of Recycled Asphalt Pavement Material in Waseca, Minnesota." Geo Engineering Report N0. 06-18, Department of Civil and Environmental Engineering, University of Wisconsin-Madison.

Sawangsuriya, A., Edil, T.B. and Bosscher, P.J. 2003"Relationship Between Soil Stiffness Gauge Modulus and Other Test Moduli for Granular Soils," *Transportation Research Record*, No. 1849, Paper No. 03-4089, National Research Council, Washington INTRODUCTION D. C., 2003, pp. 3-10

FIGURES

Pavement

Mixing of recycled asphalt pavement material with fly ash

150 mm

Subgrade

Datalogger (CR10)

Air Temperature & Relative Humidity Probe

Snowfall Adaptor & Rain Gauge

Solar Panel (12V DC)

(a)
(b)

battery

telephone

● Thermocouple (109 Temp Probe)

□ Water Content Reflectometer (CS616)
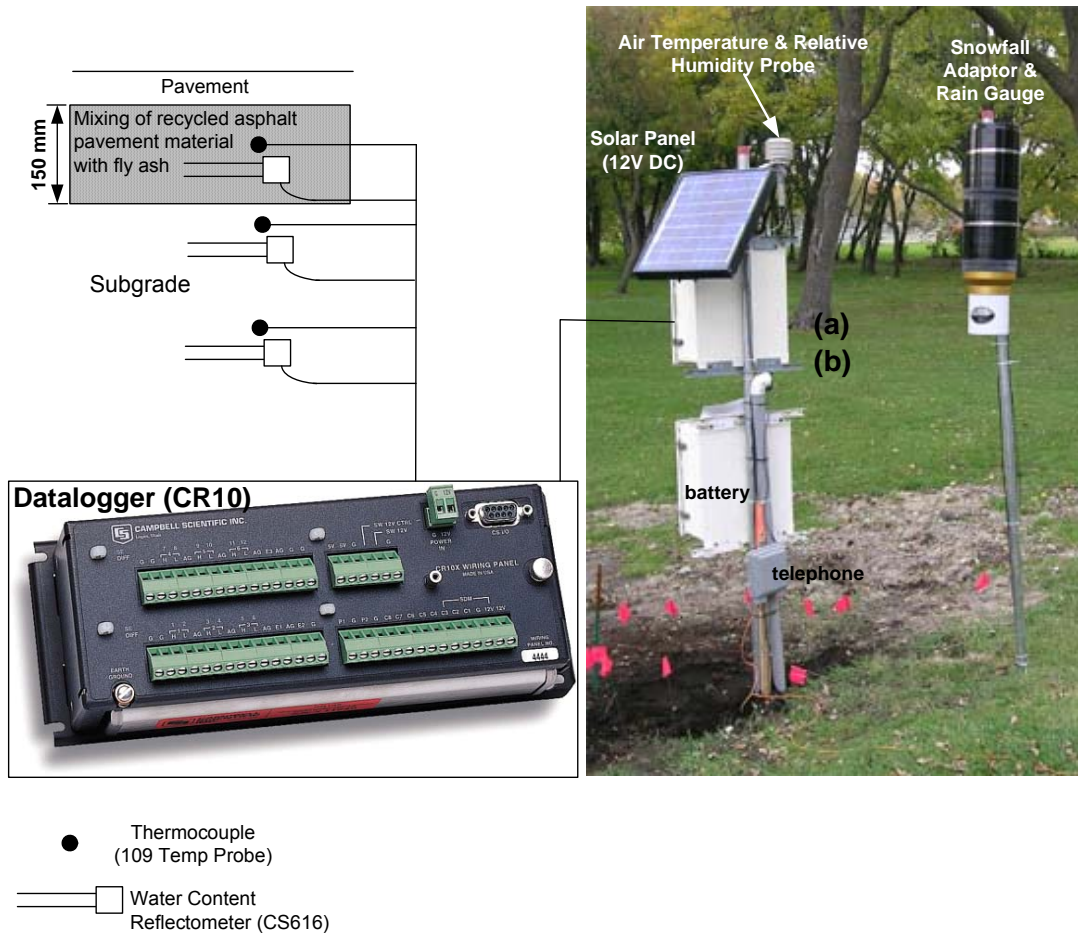
Fig. 1. Waseca: layout and photograph of field monitoring instrumentation system.
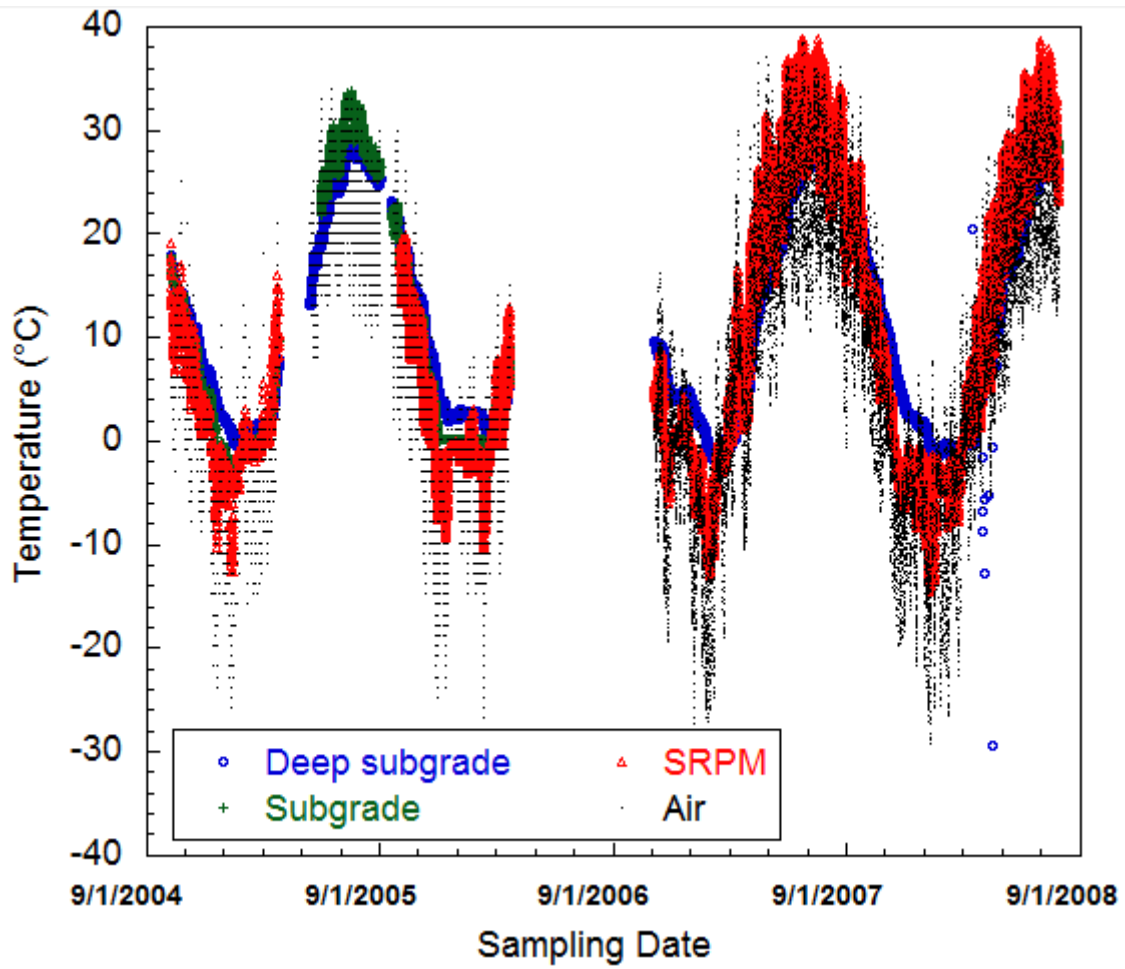
Fig. 2. Waseca air and subsurface temperatures of the SRPM and subgrade. Soil temperature measured at three depths: 150 mm bgs (mid-depth in SRPM), 425 mm bgs (subgrade) , and 675 mm bgs (deep subgrade).
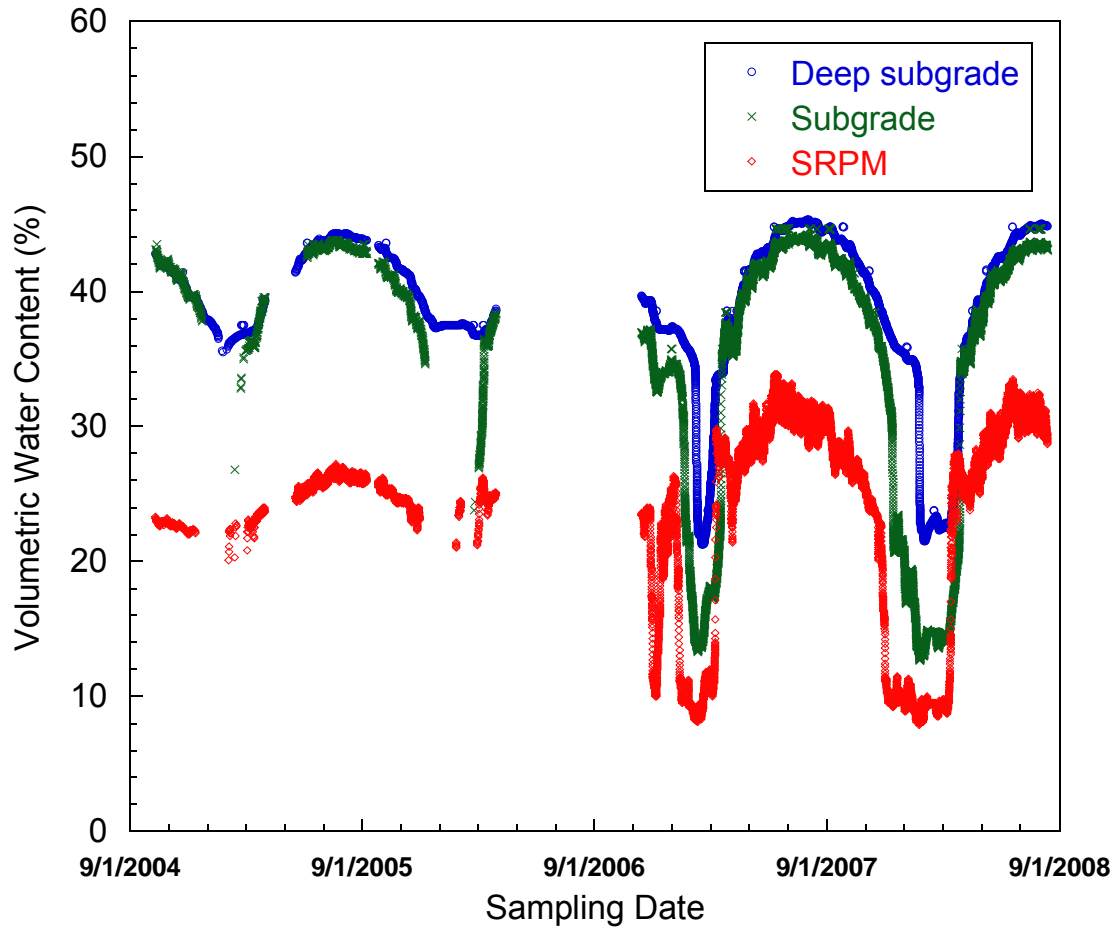
Fig. 3. Waseca volumetric water content of the SRPM and subgrade. Water content measured at three depths: 150 mm bgs (mid-depth in SRPM), 425 mm bgs (subgrade), and 675 mm bgs (deep subgrade).
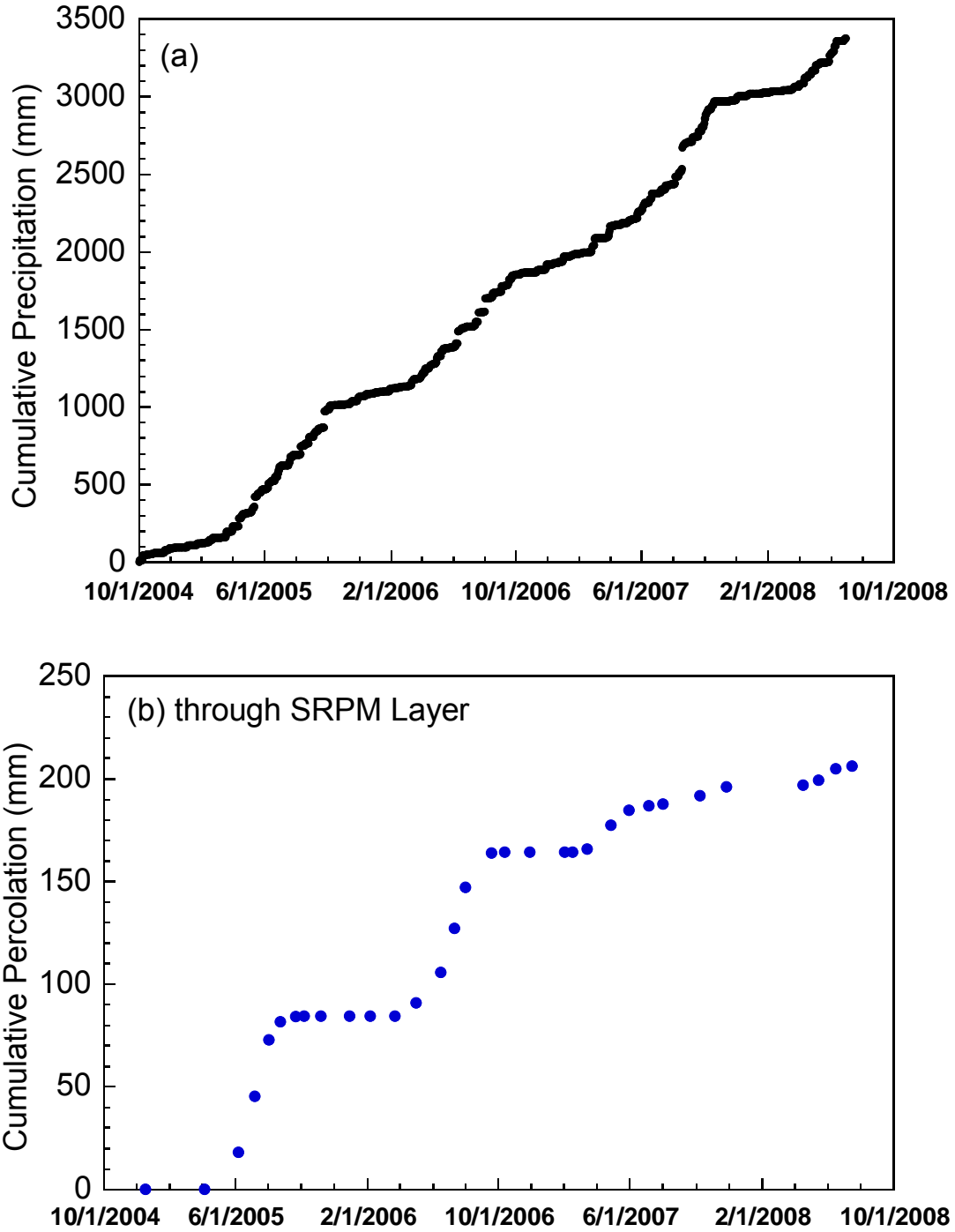
Fig. 4. Cumulative precipitation at Waseca, MN (a), and cumulative percolation through the SRPM layer (b) as measured by the volume of leachate collected. Base of lysimeter is located at the bottom of the SRPM layer.

Sensor ID	Depth of sensor from ACP surface (mm)
S1	700.0
S2	445.0
S3	216.0
S4	241.0
S5	420.0
S6	685.0
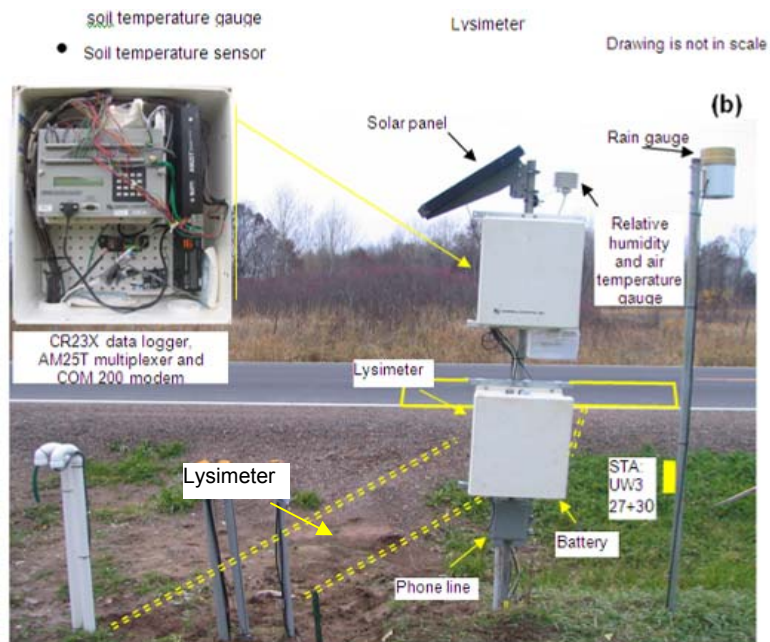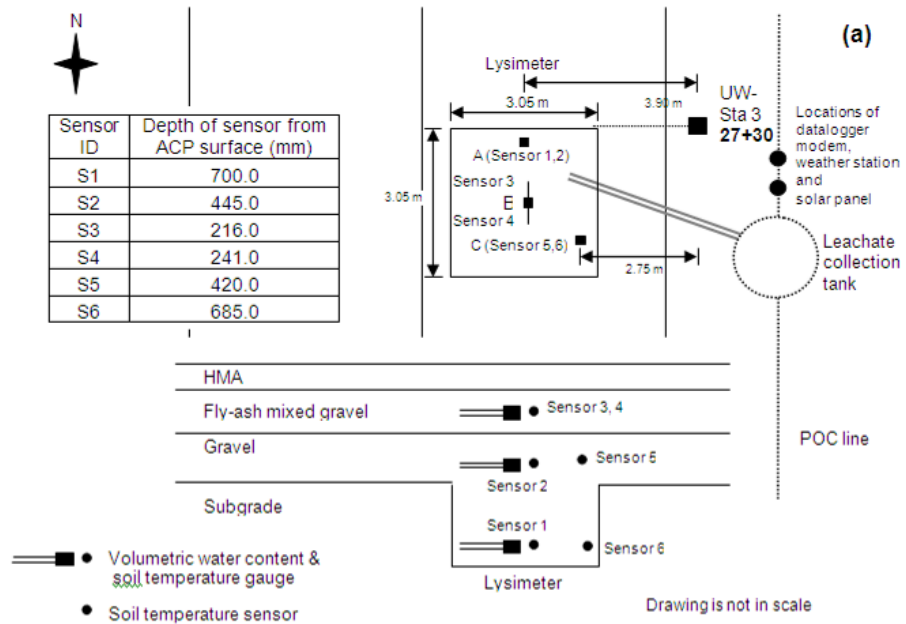
Fig. 5. CR 53 layout (a) and photograph of field monitoring instrumentation system (b).
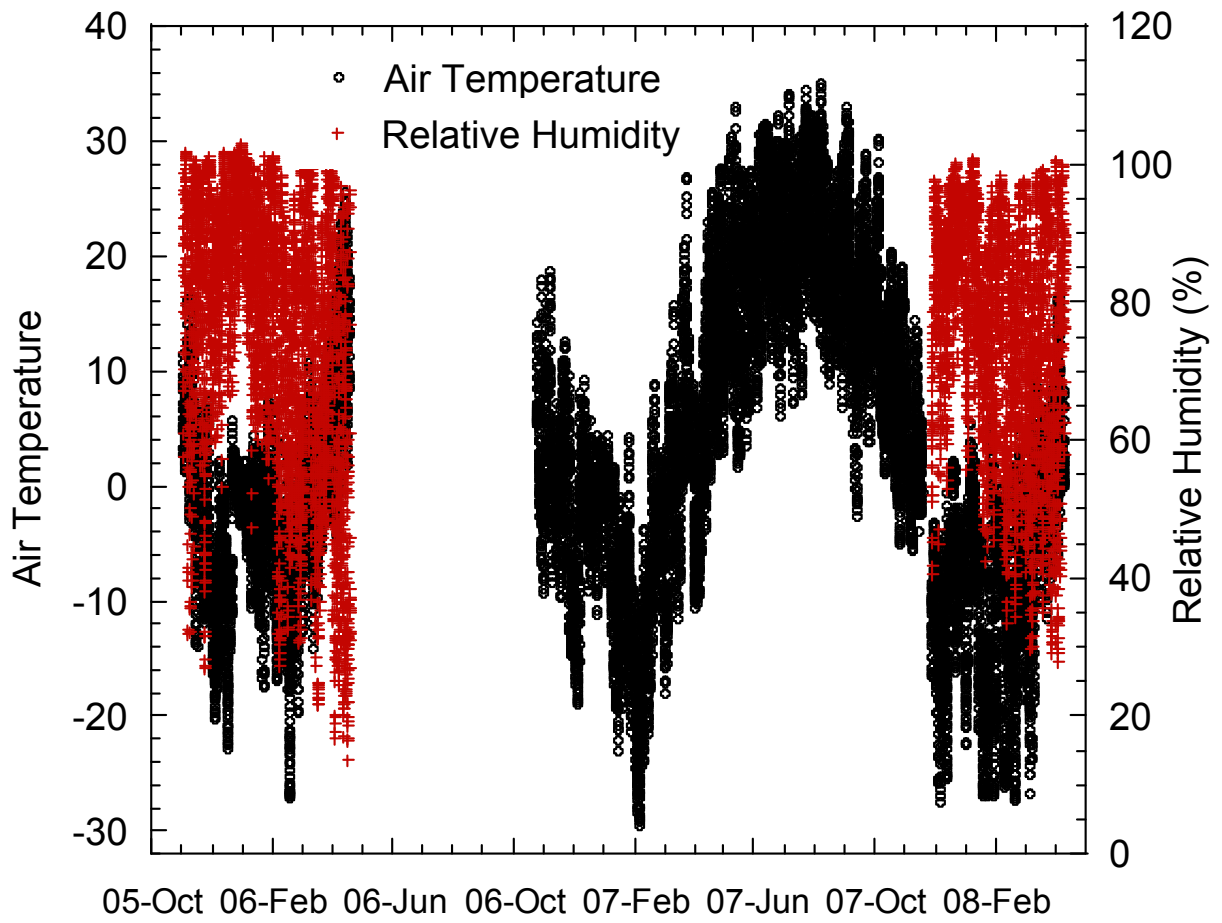
Fig. 6. Air temperature and relative humidity at CR 53.
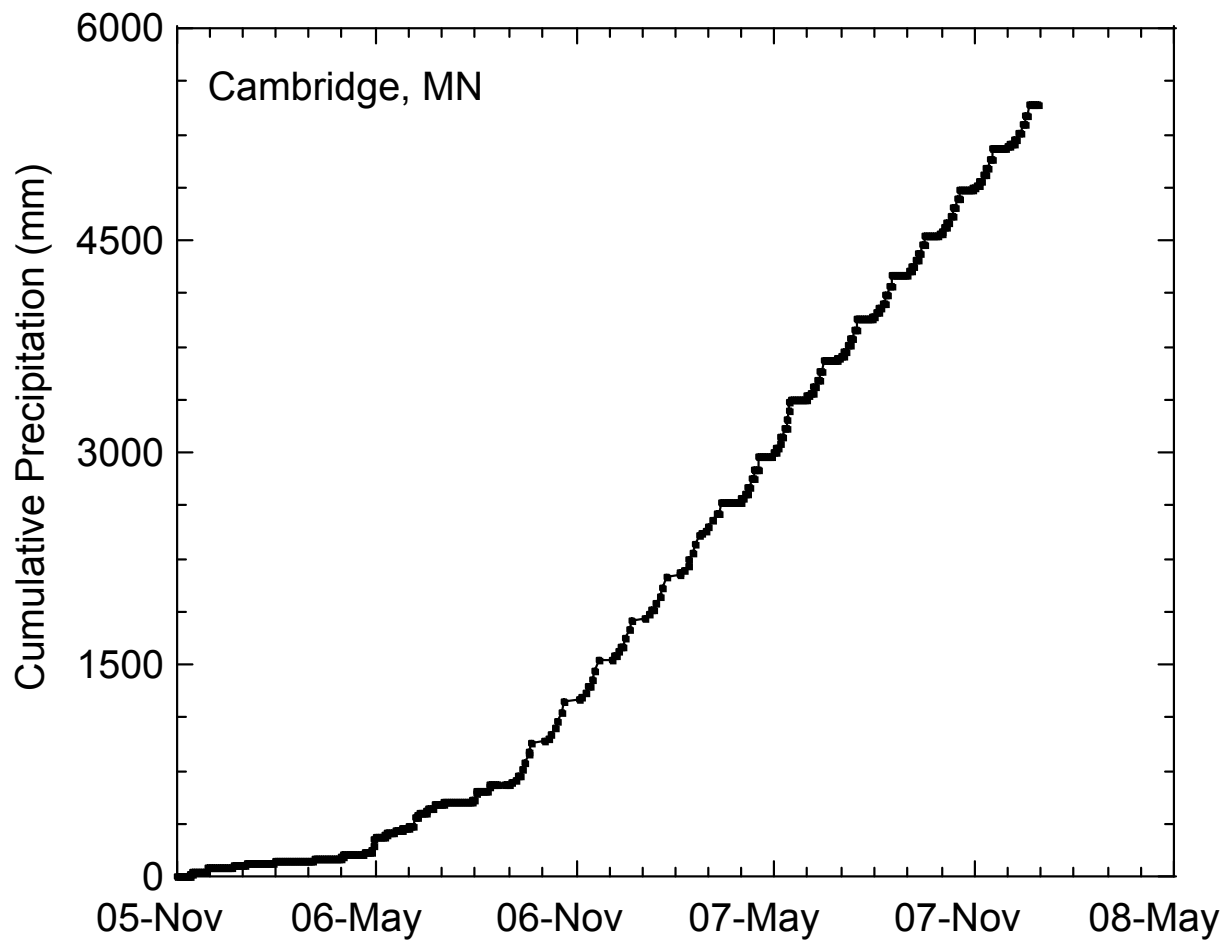
Fig. 7. Cumulative precipitation recorded by NOAA at Cambridge, MN.
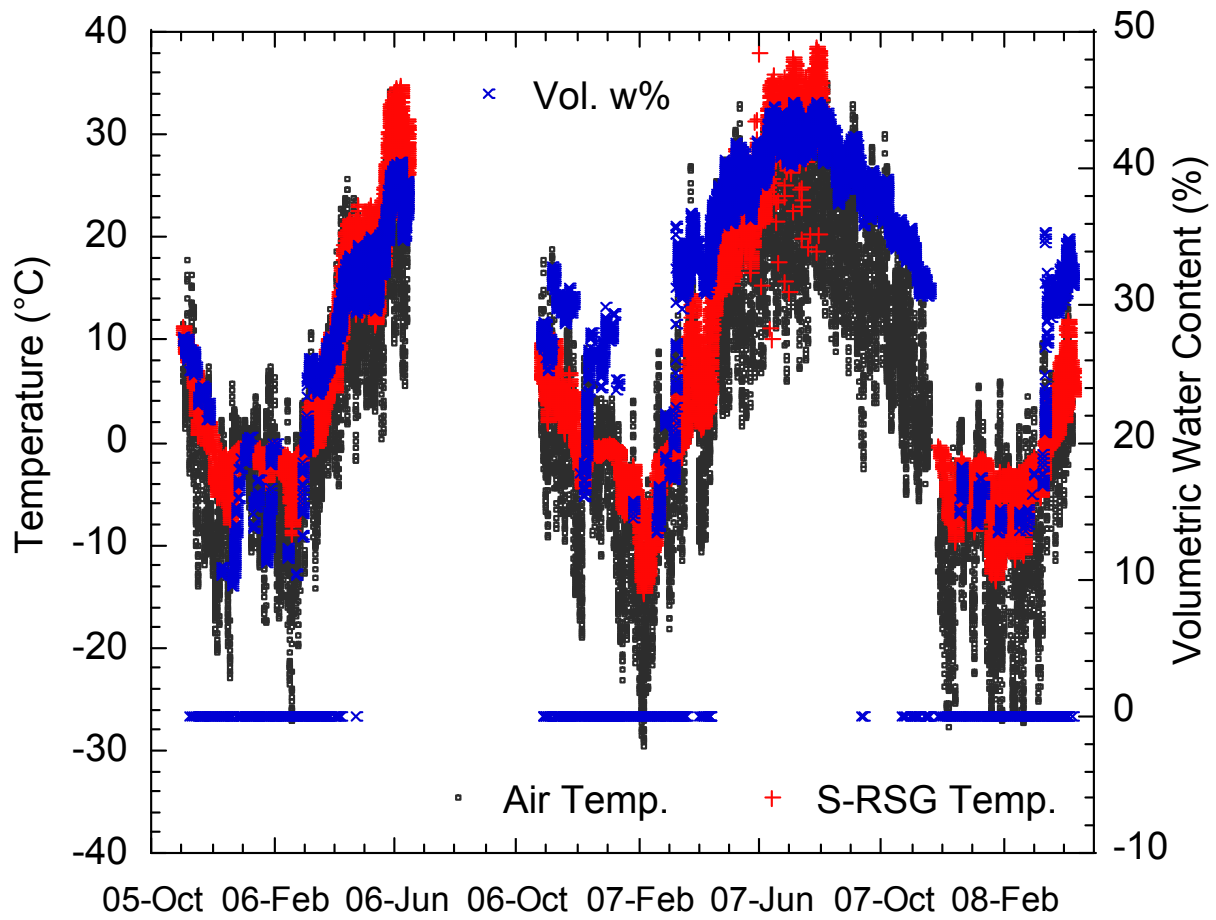
Fig. 8. CR 53 soil temperature and volumetric water content measurements in the S-RSG at 216 mm depth from the HMA pavement surface.
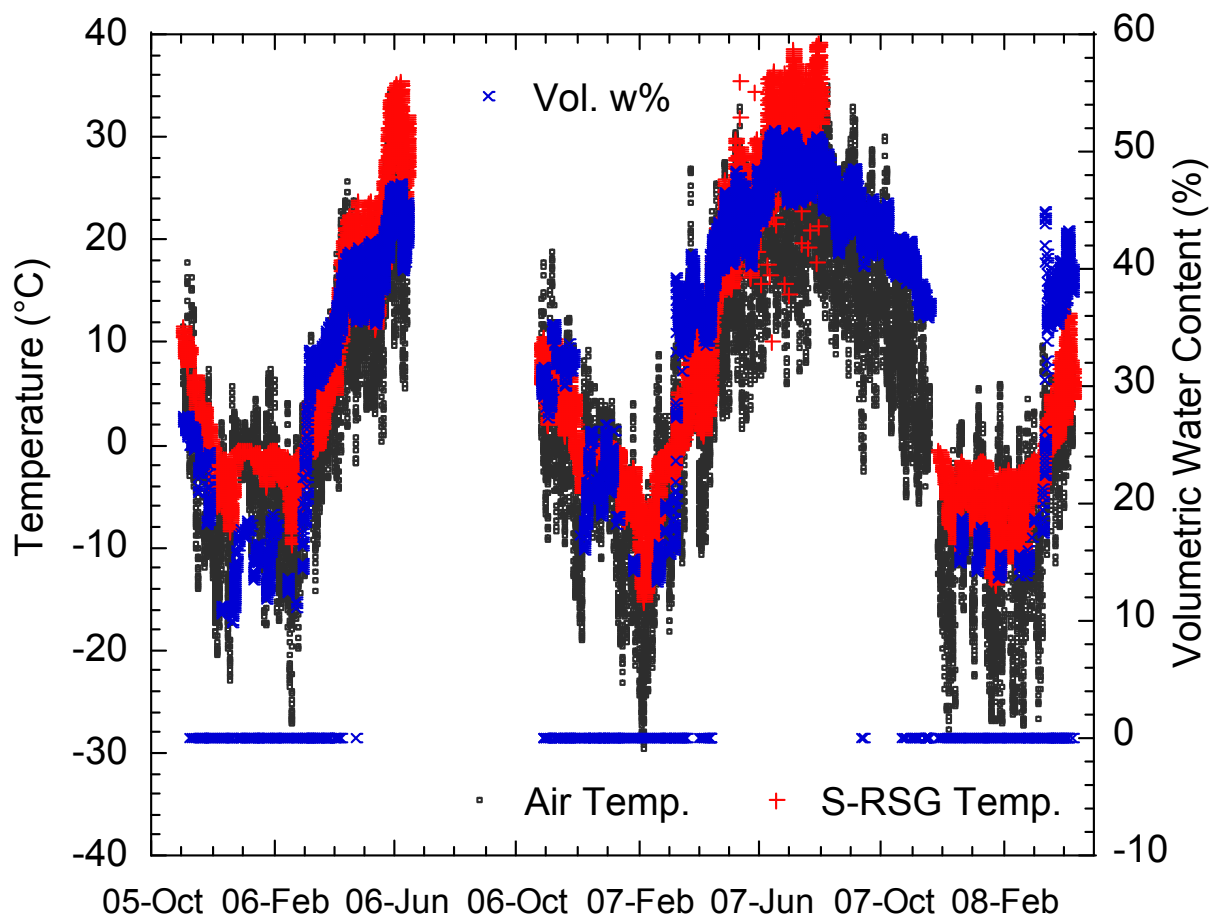
Fig. 9. CR 53 soil temperature and volumetric water content measurements in S-RSG at 241 mm depth from the HMA pavement surface.
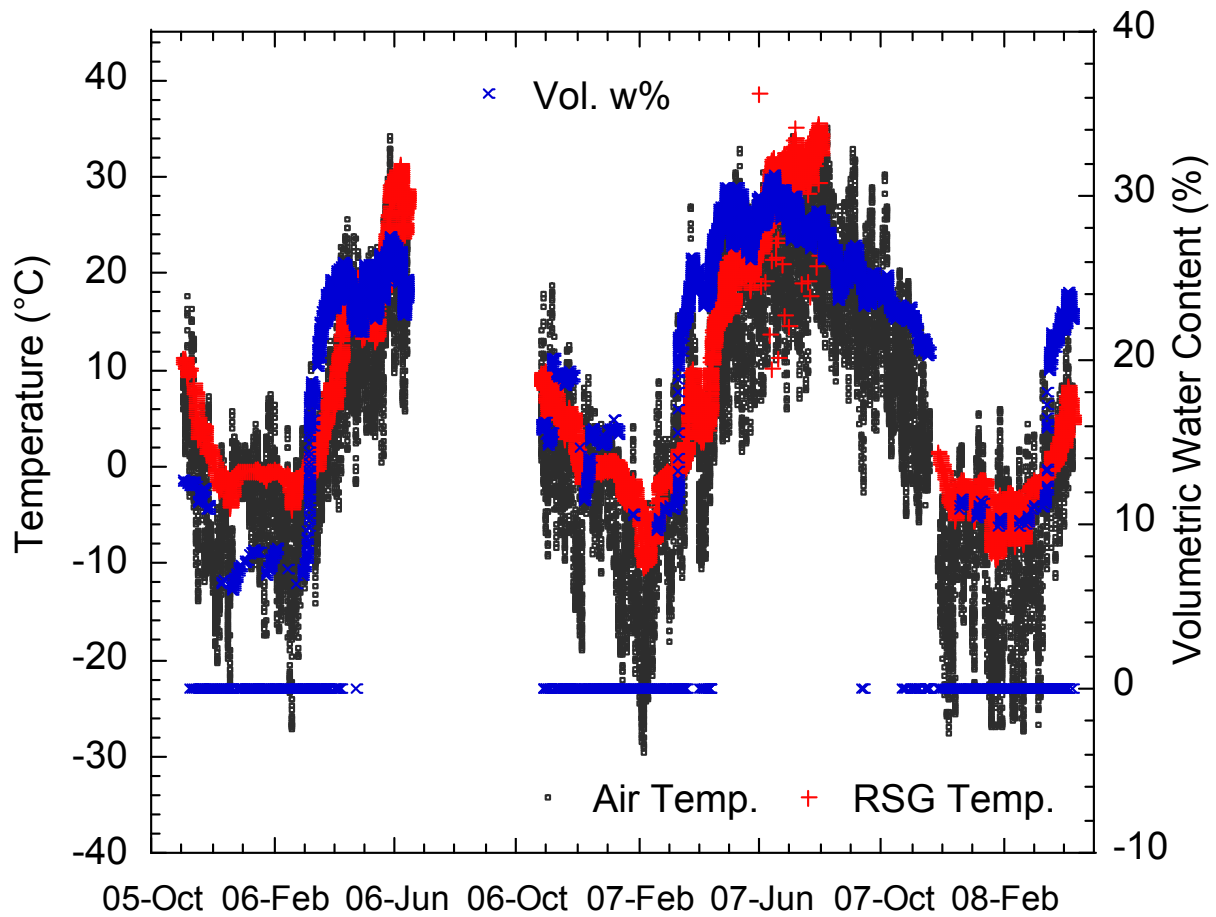
Fig. 10. CR 53 soil temperature and volumetric water content measurements in RSG at 445 mm depth from the HMA pavement surface.
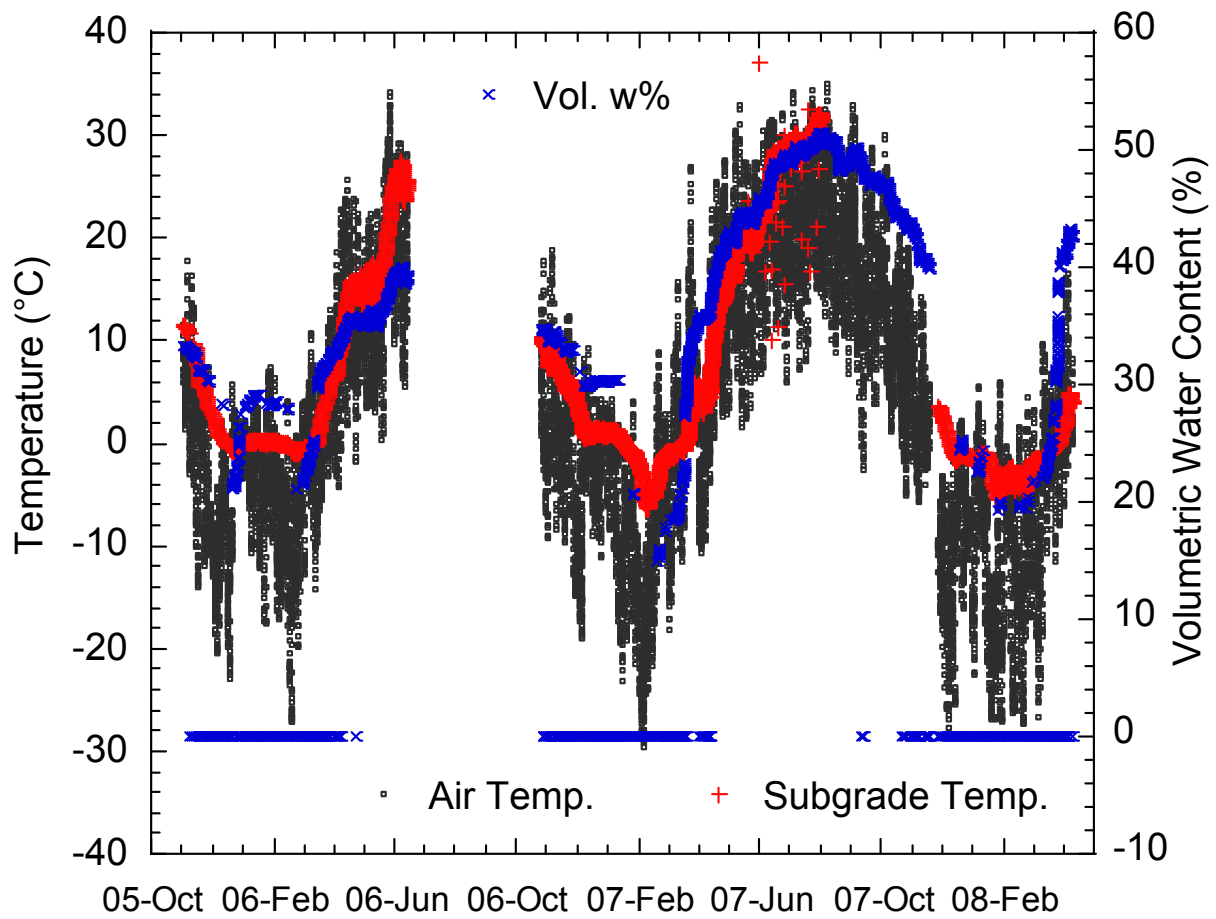
Fig. 11. CR 53 soil temperature and volumetric water content measurements in subgrade at 700 mm depth from the HMA pavement surface.
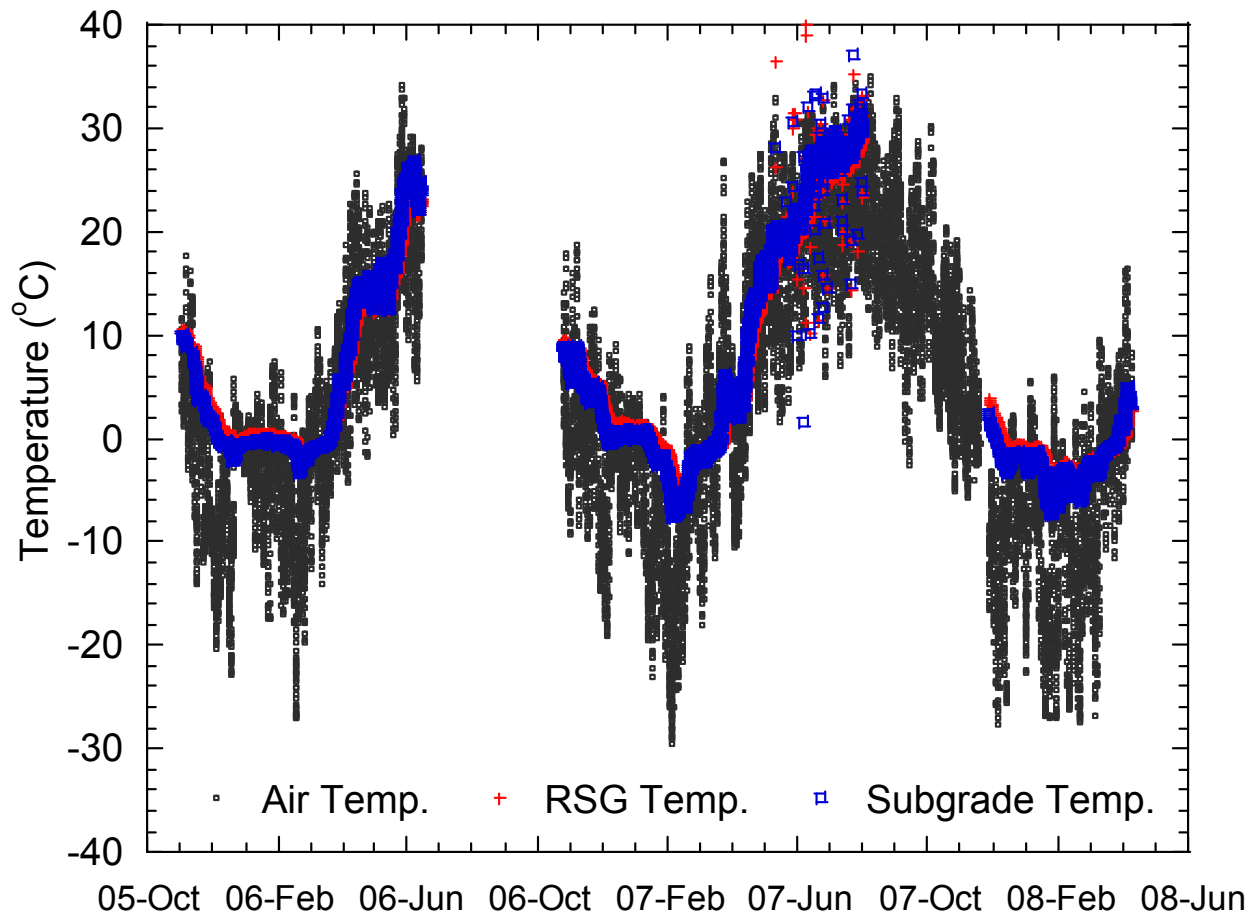
Fig. 12. CR 53 soil temperature measurements in RSG at 420 mm depth and in subgrade at 685 mm depth from the HMA pavement surface.
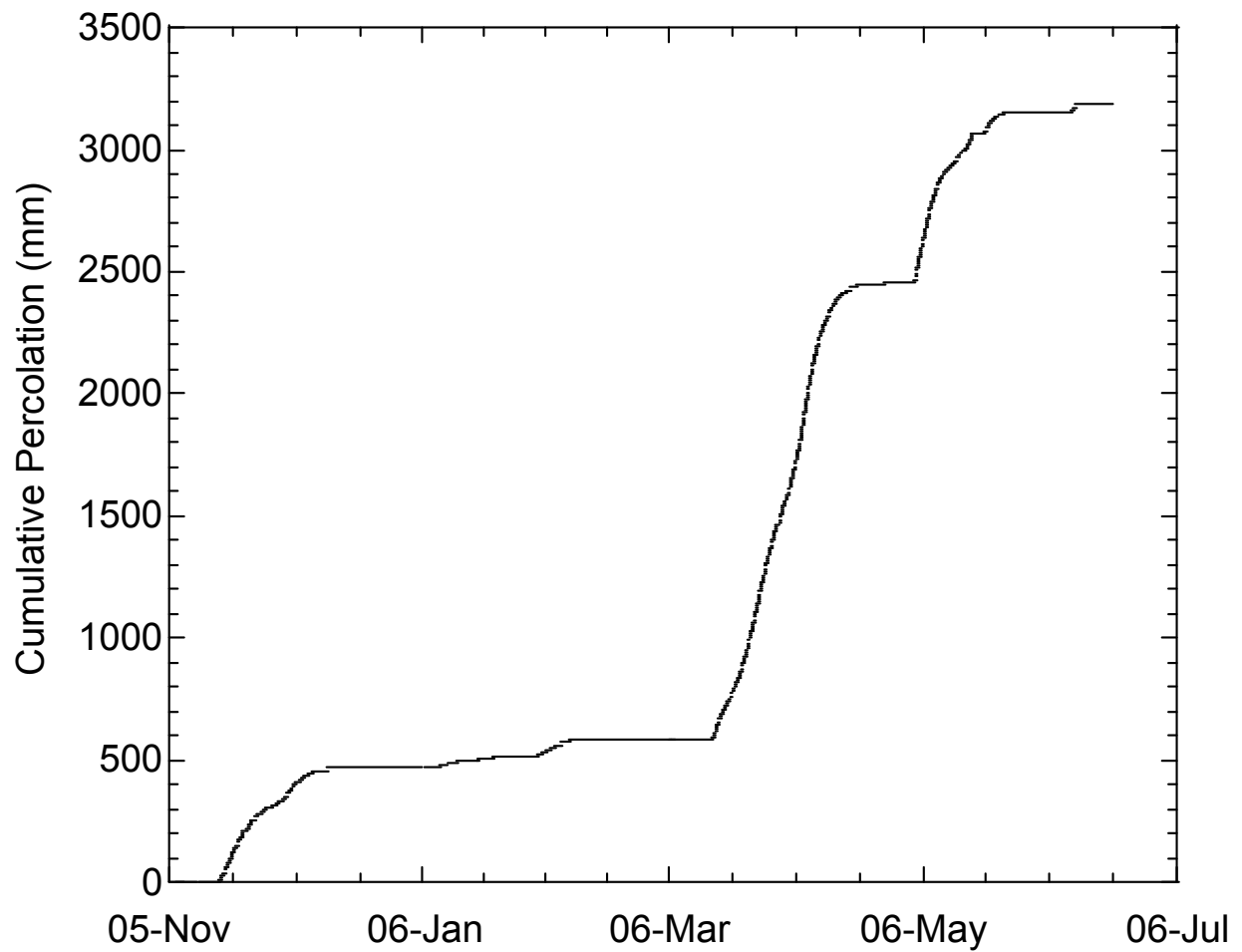
Fig. 13. Cumulative percolation collected by the lysimeter.
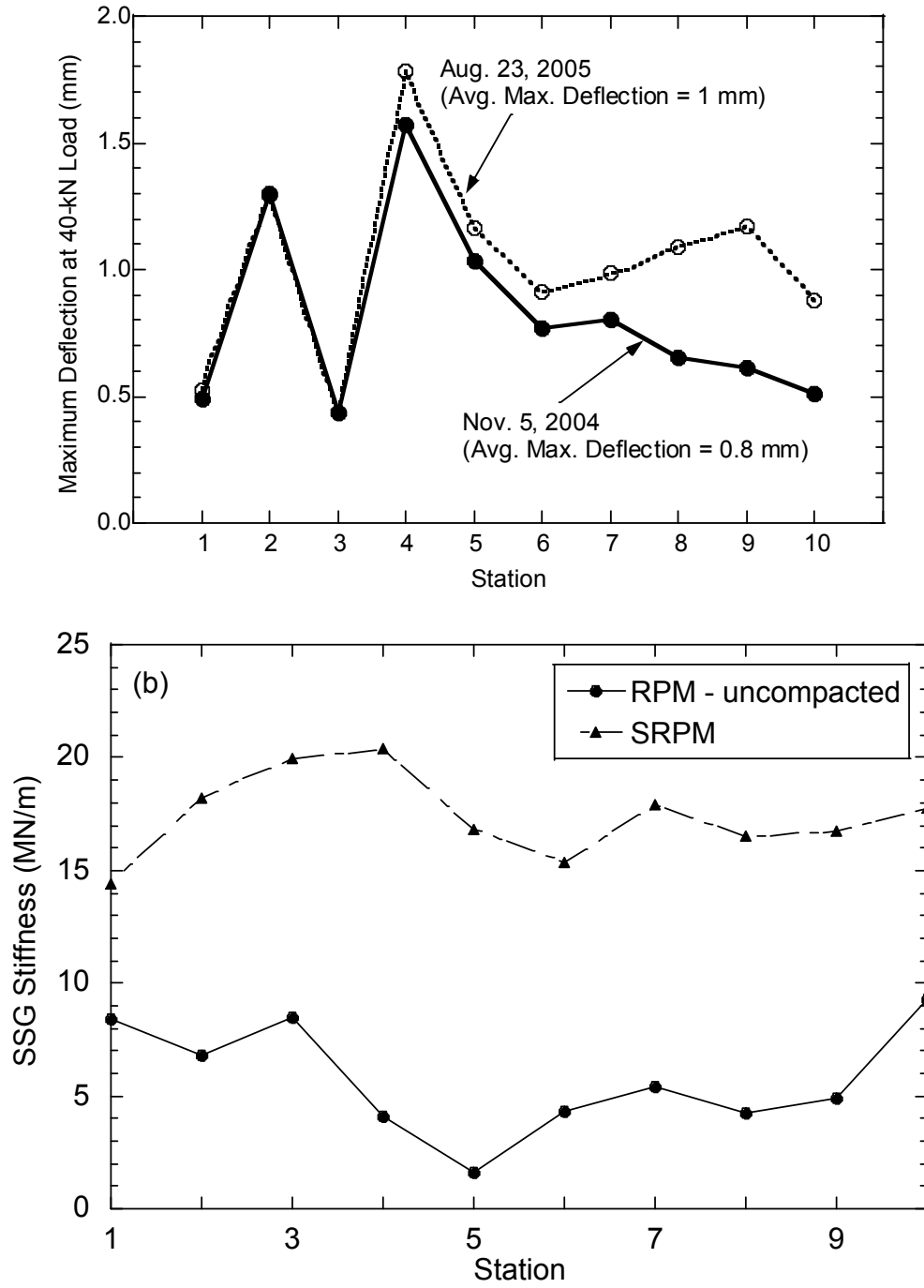
Fig. 14. Waseca maximum deflection – deflections from the center sensor at 40 kN load (a) and soil stiffness gauge stiffness of uncompacted RPM and SRPM after compaction and after 7 d of curing (b).
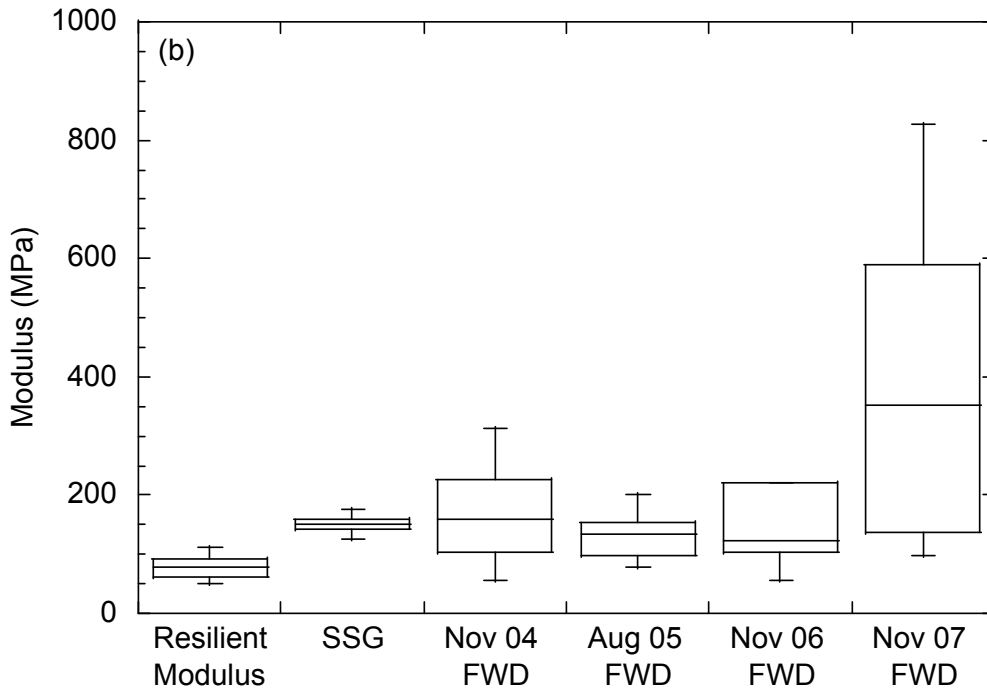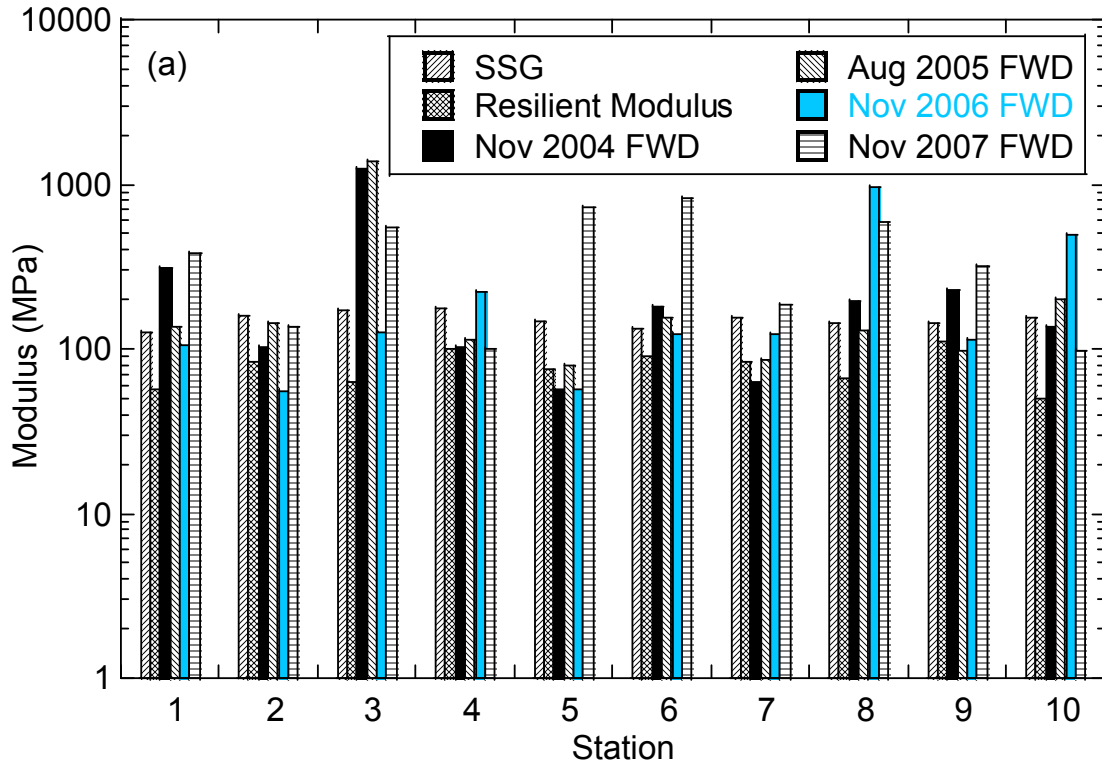
Fig. 15. Waseca modulus of SRPM obtained by inverting FWD data, from SSG measurements, and from resilient modulus tests conducted in the laboratory: (a) modulus along the alignment and (b) box plots of each set of modulus measurements.
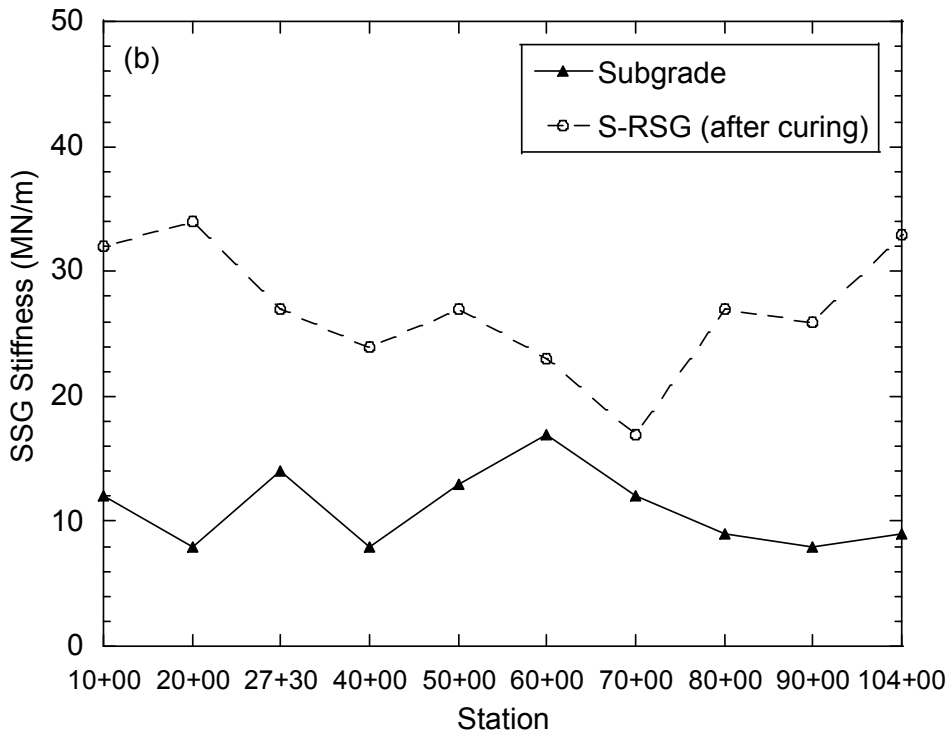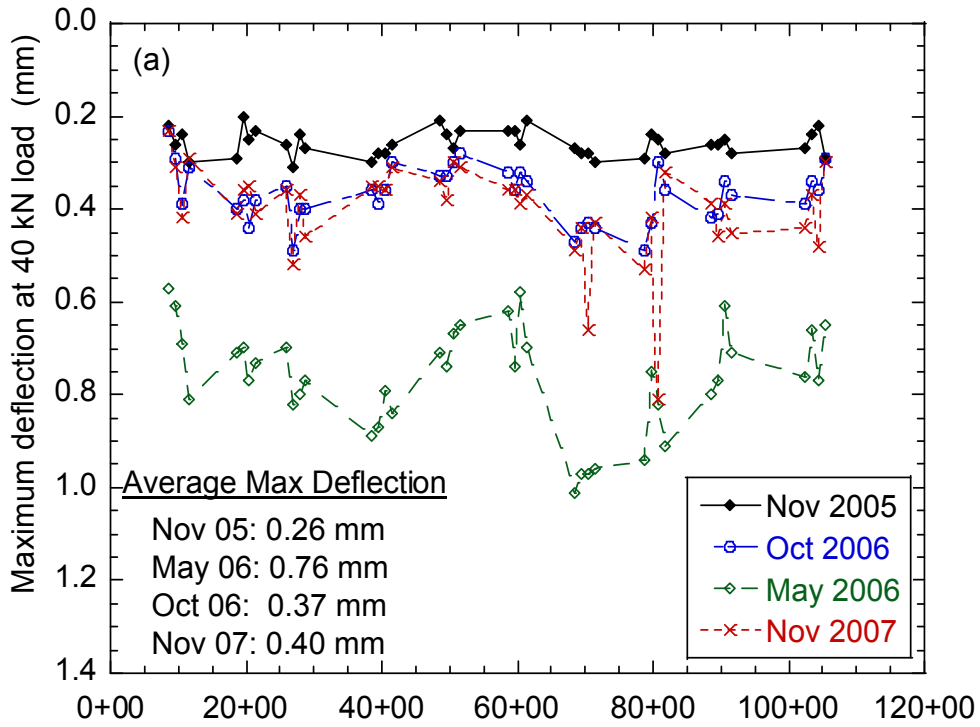
Fig. 16. CR 53 maximum FWD deflections at 40 kN load (a) and soil stiffness gauge stiffness of subgrade, S-RSG after compaction and after 7 d of curing (b).
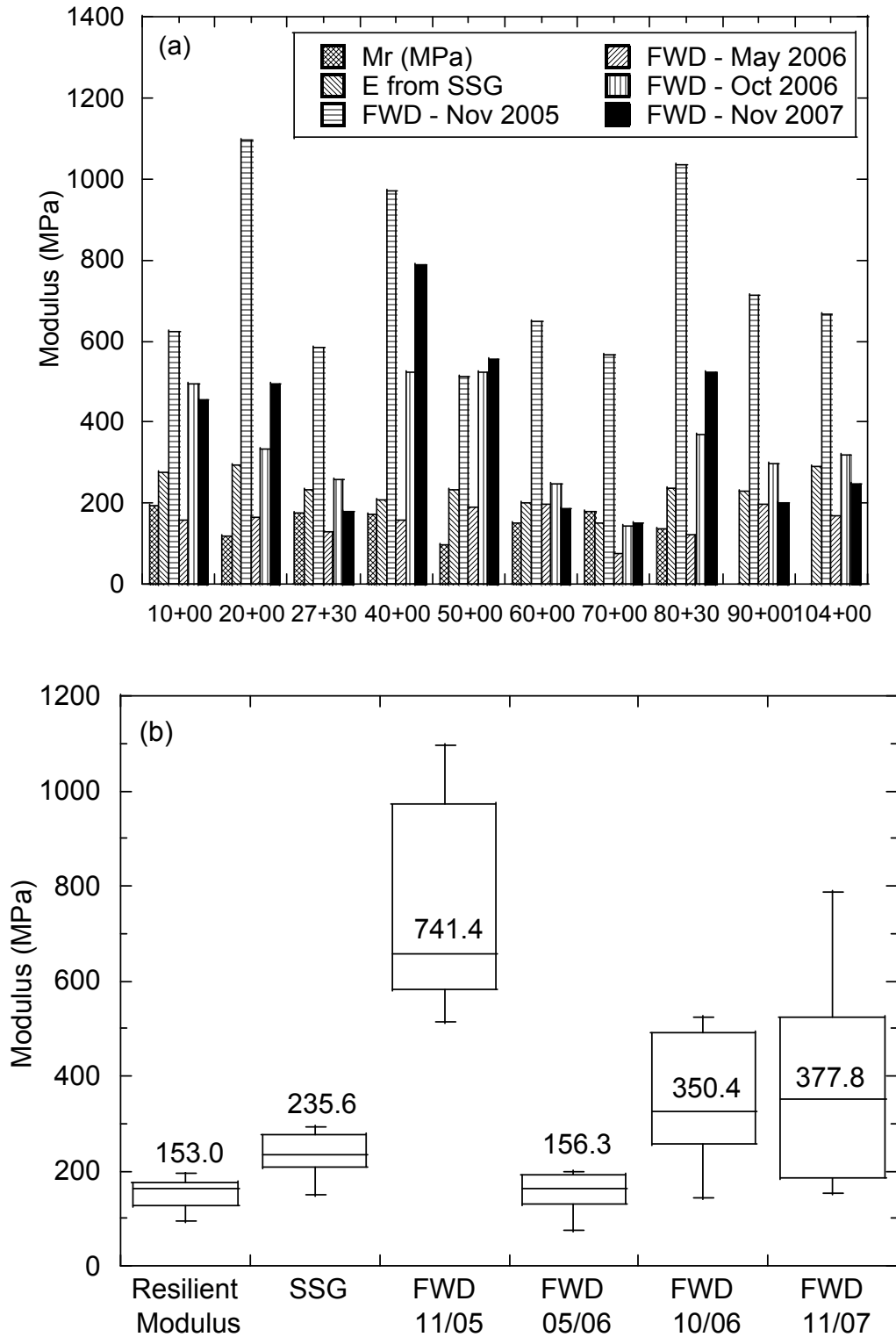
Fig. 17. CR 53 elastic modulus from laboratory resilient modulus, SSG and FWD tests for S-RSG at each station (a) and statistical evaluation of results (b).

APPENDIX E

REPORT FOR TASK 5

LYSIMETER LEACHATE MONITORING OF FIELD DEMONSTRATION SITES AND LEACHATE MODELING USING SESOIL

USE OF FLY ASH FOR RECONSTRUCTION
OF BITUMINOUS ROADS

REPORT FOR TASK 5

LYSIMETER LEACHATE MONITORING OF FIELD DEMONSTRATION
SITES AND LEACHATE MODELING USING SESOIL

Prepared by:

Paul Bloom
Shahida Quazi
Department of Soil, Water, and Climate
University of Minnesota
St. Paul, MN 55108

Craig H. Benson
Tuncer B. Edil
Department of Civil and Environmental Engineering
University of Wisconsin-Madison
Madison, WI 53706

January 2009

TABLE OF CONTENTS

LIST OF TABLES AND FIGURES

1. INTRODUCTION

Two road paving projects using fly ash soil stabilization were subjected to continued environmental and mechanical monitoring. These demonstration projects were part of previous Mn/DOT funded studies (Li et al. 2006 and Hatipoglu et al. 2006) Self-cementing Class C fly ash from a coal-fired electric power plant was used to stabilize the recycled pavement material (RPM) during the rehabilitation of a 0.5-km section of flexible pavement along 7th Avenue and 7th Street in Waseca, MN (Li et al. 2006). At another project fly ash was used to stabilize an existing gravel road to form a base (Hatipoglu et al., 2006) for HMA pavement. This project was conducted during reconstruction of a 3.5-km section of County Road 53 (CR 53) in Chisago County, MN that was being converted from a gravel road to a paved road. Fly ash from Riverside Unit 7 (Class C) and Riverside Unit 8 (off-specification) in Minneapolis, MN was used for stabilization. More details about these projects were presented in the report for Task 4.

Field monitoring of the two sites was continued under this new LRRB project after the completion of the original project and submission of the initial report in 2006. Monitoring of the pavement began in September 2004 and continued through the summer of 2005 and then resumed in the spring of 2006, continuing through October of 2008. Leachate draining from the pavement was monitored using a pan 4 m wide, 4 m long, lysimeter installed at each site below the stabilized subgrade material.

Leachate data of the elements of concern in the fly ash collected through 2008 are presented in this report. In addition the results of modeling of transport of elements of concern out of the fly ash stabilized RPM and into shallow ground water using the Seasonal Soil Compartment (SESOIL) model are presented in this report.

2. ENVIRONMENTAL DATA

2.1 METEOROLOGICAL AND SUBSURFACE CONDITIONS

2.1.1 Waseca

The field instrumentation system installed at Waseca is shown in the report for TASK 4. Briefly the air temperature ranged from -29.5 $^{\circ}$C to 38.6 $^{\circ}$C during the monitoring period, with sub-freezing temperatures occurring between November and April each year. Temperature of the stabilized RPM (SRPM) ranged between -15 $^{\circ}$C and 39 $^{\circ}$C. This layer was frozen for about 3-4 months each winter. Higher volumetric water contents were recorded in the fine-textured subgrade (maximum of about 44%) than the SRPM (maximum of 32%), which reflects the greater affinity of fine-textured soils to retain water. No spikes are present in the water content records, which reflect the ability of the HMA to impede infiltration during precipitation and snow melt events and to limit evaporation during drier periods. The annual variation in water content in the subgrade is between 12 and 44%, and the annual variation in water content in SRPM is between 10 and 34%. Higher water contents are recorded in the summer months, when greater precipitation occurs.

The precipitation record for the site was obtained from the NOAA weather station in the University of Minnesota Research and Outreach Center near Waseca, MN. The precipitations events and volumetric drainage are shown in Fig. 2 for the period from October 2004 to August of 2008. The seasonal variation in percolation is also reflected in the percolation collected in the lysimeter, as shown in Fig 2, however, the annual drainage water volume decreased with time from 2005 to 2008.

3. TRACE ELEMENTS IN LYSIMETER DRAINAGE

Approximately 3300 L of leachate corresponding to 206 mm of total percolation was collected during the monitoring period from September 2004 to August 2008. This corresponds to 4.3 pore volumes of flow (PVF) through the SRPM by the end of July 2008. During this period, pH of the drainage was near neutral (6.4 – 7.5) and the redox condition was modestly oxidizing (Eh = 48-283 mV).

Concentrations of trace elements were determined in the lysimeter drainage water for July – September 2005 and then from March 2007 – August 2007. The samples collected in 2005, filtered through 0.045 μm membranes, and were analyzed with Inductively Coupled Plasma – Mass Spectrometry (ICP-MS) (U of WI) and in 2007 and 2008 the samples were analyzed with Inductively Coupled Plasma Optical Emission Spectrometry (ICP-OES) (U of WI and U of MN). ICP-MS is more sensitive for some elements than is ICP-OES. We detected the lower concentrations of some elements in 2005 than in the other 2 years; e.g. molybdenum (Fig. 3). In Fig. 3 values less than the instrumental detection limit are shown as zeros. For five elements, concentrations exceeded USEPA MCLs and/or HRLs established by the Minnesota Dept. of Public Health (MNDPH) at least one time: arsenic (As), antimony (Sb), and thallium (Tl). There is no MCL or HRL for lead (Pb) but there is an "action level" of 0.015 mg/L, which was exceeded. There are no primary MCL or HRL values for Mn but the USEPA lists secondary limit of 50 μg/L, a value that was exceed. Also Fe exceeded the 300 μg/L secondary standard, but only in 2005. In the other two years Fe was not detected.

Concentrations Sr, Ba, B, and Mn elements with K_d <50 and concentrations well above the instrumental detection of the ICP instruments (elements with good precision); showed pronounced seasonal differences (Fig 2A and 2B). These elements have higher concentrations when there is more water flow. Unlike Sr, Ba and B, manganese is sensitive to redox potential, with reduction of insoluble Mn(IV) oxide to soluble Mn^{2+} at low redox. Low redox potentials can occur in soils when the pores fill with water and air is prevented from entry into the soil. Measured Eh values below 250 mv indicates that the moisture in the subgrade zone is often sufficient to result in the reduction of Mn oxides to soluble Mn^{2+} (McBride, 1994) This potential is not low enough to reduce Fe(III) oxides and hydroxides to soluble Fe^{2+}. However, some Fe was found in the drainage water in 2005.

For the other elements there was little apparent pattern to the concentrations with time (Fig. 3C, 3D, 3E and 3H). Beryllium (Be), Se, Cd, Co, Mo and Ni were not detected in any of the samples collected and were below the detection limits reported in Table 1. Silver (Ag) was detected once with a value of 0.003 μg/L and for As, very low concentrations were reported from the ICP-MS in 2005 (1 to 2 μg/L). No As was detected with ICP-OES in 200 7 and 2008 except for one value of 48 μg/L (Fig 3 H). This concentration is close enough to the detection limit of 30 μg/L to be considered a random error but we used this number to represent a worst-case situation (Table 1).

4. MODELING OF LEACHATE CONCENTRATIONS

We used the Seasonal Soil Compartment Model (SESOIL) to predict soils leachate concentrations based on the total concentration of elements of concern that are in the ash stabilized RPM. The SESOIL model uses the soil adsorption constants (K_d) at pH 7, assuming linear partition between adsorbed component and solution. The K_d values were taken from a USEPA soil screening guidance document (USEPA, 1996) that presented a review of the literature with selected pH dependent K_d values. The SESOIL model was used by the Minnesota Pollution Control Agency (MPCA) in development of the Soil Leaching Value (SLV) limits that are used to set upper limits in polluted soils that are protective of groundwater (MPCA, 1998). The MPCA SLV worksheets were used in the development of the Screening Tool for Using Waste Materials in Paving Projects (STUWMPP), developed in a previous LRRB project, for use as part of due diligence when planning a project with fly ash subgrade stabilization (Friend, et al., 2008). In the determination of SLV limits the MPCA calculated reduction of leachate concentrations in the unsaturated zone using SESOIL to determine the concentrations of leachate delivered to the groundwater (MPCA, 1998).

4.1 LYSIMETER LEACHATE

In the modeling of leachate from the lysimeter under the 7th street in Waseca we assumed 75 mm of pavement over 150 mm of RPM treated with 10 % fly ash (Figure 1). We estimated the concentrations for the elements of concern using the data for Xcel Energy Riverside 6 fly ash and soil data for the Waseca area that are in the STUWMPP database (Friend et al., 2004 and Grosenheider et al., 2006). The hydraulic properties of the pavement and fly ash stabilized subgrade were those used in the WiscLEACH modeling in the Task 6 report. The monthly rainfall values were based on the monthly mean values reported for the weather station on the University of Minnesota Southern Research and Outreach Center near Waseca. We matched the measured annual leaching of 50 cm/y by reducing the monthly rainfall by a factor of 10 and setting the evapotranspiration to zero. The 15 cm of ash treated soil was divided into ten equal segments all with the same initial concentration. In SESOIL the chemical species being modeled is initially located at the center of each segment, which results in a delay in the initial leaching due to retardation over the last 0.75 cm of the column of fly ash treated RPM (e.g. Fig. 4)

4.2 LEACHING TO GROUNDWATER

We used SESOIL to predict the leachate concentrations in leachate that is delivered to an aquifer at 2 m depth. In this calculation we used the soil hydraulic properties in the Task 6 report and the same Kd values as in the modeling of lysimeter leaching.

5. RESULTS OF MODEL CALCULATIONS

5.1 LYSIMETER LEACHATE

The time course for the calculated lysimeter leaching of the most mobile element, Se is shown in Fig. 4 and the more strongly retarded B in Fig. 5. The plots show that the SESOIL model predicts small seasonal differences in leachate concentrations. The gap from time zero to the time when SESOIL yields a leachate concentration is an artifact of the model calculation. Selenate is the most mobile of the species studied, with a Kd of 4.3, which yields a retardation coefficient of 22. This indicates that the Se mobility is 22 times slower than the water moving through the soil column and that the leaching last 0.75 cm from the middle of the bottom segment of the SRPM. The least mobile species is, Pb^{2+}, which has a retardation coefficient of 18,000.

Model runs of 25 years were sufficient to capture the maximum leachate concentrations for all Be, Pb and V. Runs of at least 270 y for Be, 570 y for Pb and 170 y for V were needed for these elements to appear in the leachate. The general shape of concentration *vs.* time plots is all the same with highest concentrations in the first leachate. However, this does not account for the possibility of occluded or coprecipitated elements leaching out of solid matrices which likely explains the lower initial concentrations in the lysimeter leachate for some elements shown in Fig. 3. Leaching from particles could, at least in part, account for the high concentrations that follow time periods with little leaching (e.g. Fig. 3B). Diffusion out of the matrix will occur even when there is no leaching.

The maximum predicted concentrations and the maximum measured lysimeter leachate concentrations are shown with the MCL and HRL values in Table 1. In general, the model overestimates mobility and the maximum model calculated concentrations in the leachate are higher than the measured values. Exceptions are mercury (Hg), for which the predicted and measured values are essentially identical, and Sb and Pb, for which the model values were lower than that of the measured values. Experimental Kd values are generally determined under laboratory conditions with soluble salts added to soil to form surface sorbed ions. However, in the fly ash treated RPM (and soils) some elements are tied up by coprecipitation in solid phases, or inclusion in solid particles. Possible solid phases include $CaCO_3$, gypsum and iron oxyhydroxides (Bloom and Gollany et al., 2001). The very low predicted concentration for Pb suggests that the very high Kd value used for this element may be unrealistically high. Also, for some elements the model assumed the most mobile of several possible species for an element. For example, we assumed that all of the Cr is chromate anion, a mobile form, rather than as the 3+ cation, which is quite immobile, and for Se we assumed selenate anions, rather than the selenite anions, a less mobile form.

5.2 CALCULATED DELIVERY OF LEACHATE TO A 2 METER WATER TABLE

Because SESOIL is limited to model runs of 999 years, only the most mobile elements (K_d <25), attained maximum concentrations during our model runs. The maximum calculated values for Sb, B, Mo, Se and Cr and time to maximum concentration are given in Table 2. The calculated time for Se to reach the groundwater at 2 m is over 150 years, while the time required

for B to reach the groundwater is 950 years (Fig. 4B and 5B and Table 2). The chromatographic effect during leaching spreads these Se leaching over 150 years and reduces the maximum concentration by a factor of 8 compared to the predicted maximum leachate concentration. The maximum leachate concentrations for all of the elements reported in Table 2 were reduced by a factor of 8 compared to the calculated lysimeter leachate concentrations.

The model concentrations in Table 2 for Ag and B are less than the MCL but almost twice the MCL value for Se and is almost 4 times the MCL value for Cr. There are no specified limits for Mo. However, this analysis does not account for the fact that the modeling of leachate from the SPRM greatly over predicted the concentrations of these elements in leachate (Table 1). Also, these concentrations do not consider dilution after the leachate mixes with the flowing groundwater. The dilution depends on the area affected by the elevated concentrations of elements of concern, the rate of groundwater flow, the depth of mixing in the groundwater and the angle of intersection of groundwater flow with the centerline of the road. These factors can be used to calculate a Dilution Attenuation Factor (DAF), a divisor applied to leachate concentrations. When the factors influencing the DAF are not well known MPCA uses a default value of 10 (MPCA, 1998).

Applying a dilution factor of 8 to all the model lysimeter concentrations in Table 1 for leaching to a 2 m depth results in concentrations that are less than or equal to the MCL/HRL limits, except for the previously mentioned Cr, Se, As, Ba, Tl, and Mn. Applying a DAF to these numbers brings all the values below the MCL except Mn. Applying a dilution factor of 8 to the all of the measured lysimeter leachate results in concentrations that are all below the regulatory limits except Mn and Th. In the case of both Mn and Tl, a divisor of 8 results in concentrations within of factor of 3.5 of the MCL limits.

5.2.1 Parametric Analysis of Model Results

We conducted a parametric analysis of model for leaching to groundwater using the Se as an example. The predicted solution concentrations varied directly with the total concentration in the SRPM and the thickness of the SRPM but were little affected by the annual drainage volume. The divisor factor that results from leaching through subsoils varied directly with the thickness of the subsoil layer between the SRPM and the ground water.

6. CONCLUSIONS

Three years of leachate monitoring from the lysimeter under the SRPM at Waseca showed that generally the measured values were below the MCL and HRL risk-based human health limits for groundwater. However, some concentrations in excess of the limits were measured for As, Sb, Pb, and Tl. In addition, Mn exceeded the secondary "nuisance" MCL secondary limit.

The SESOIL model which uses the total concentrations of the elements in the SRPM, over-predicts concentrations in the lysimeter leachate at Waseca, except for Pb and Sb. For many of the more highly mobile elements the model greatly over predicts the measured leachate. This is due to the fact that the model assumes that all of the elements are present only as the most mobile ionic form and the model does not consider tie-up within mineral structures in the mixture of ash and RPM.

REFERENCES

Benson, C.H. and Bosscher, P.J., 1999. Time-domain reflectometry in geotechnics: a review. In: W. Marr and C. Fairhurst (Editors), Nondestructive and Automated Testing for Soil and Rock Properties, ASTM STP 1350. ASTM International, West Conshohocken, PA, pp. 113-136.

Bloom, Paul R., and Gollany, Hero 2001. Water quality in runoff from fly ash-stabilized pads pp. 2-1 to 2-26 *In.* Environmental Evaluation for of the use of Ash in Soils Stabilization Applications EPRI, Palo Alto CA, and U.S. Department of Energy, Pittsburg, PA: 2001:1005213.

Edil, T.B. et al., 2002. Field evaluation of construction alternatives for roadways over soft subgrade. Transportation Research Record, No. 1786: National Research Council, Washington DC, pp. 36-48.

Friend, M.S., P.R. Bloom, T.R. Halbach, K. E. Grosenheider, M.R. Johnson (2004). Screening Tool for Using Waste Materials in Paving Projects (STUWMPP), Minnesota Local Road Research Board. http://www.cts.umn.edu/Publications/ResearchReports/reportdetail.html?id=989

Kim E. Grosenheider, Paul Bloom, Thomas R. Halbach, Matt Simick July 2006 Chemical Inventory and Database Development for Recycled Material Substitutes. Mn/DOT 2006-28.

Li, L., Benson, C.H., Edil, T.B. and Hatipoglu, B. 2006. "Fly Ash Stabilization of Recycled Asphalt Pavement Material in Waseca, Minnesota." Geo Engineering Report N0. 06-18, Department of Civil and Environmental Engineering, University of Wisconsin-Madison.

MPCA 1998 Draft guidelines risk based guidance for the soil leaching pathway user's guide, http://www.pca.state.mn.us/cleanup/pubs/user0598.pdf

McBride M.B. 1994. Environmental chemistry of soils. Oxford University Press, New York.

Sawangsuriya, A., Edil, T.B. and Bosscher, P.J. 2003"Relationship Between Soil Stiffness Gauge Modulus and Other Test Moduli for Granular Soils," *Transportation Research Record,* No. 1849, Paper No. 03-4089, National Research Council, Washington D. C., 2003, pp. 3-10.

U.S. Environmental Protection Agency. 1996a. Soil Screening Guidance: Technical Background Document,USEPA Office of Solid Waste and Emergency Response, EPA/540/R-95/128.

TABLES

Table 17. Measured and modeled maximum lysimeter leachate concentrations compared to groundwater health based limits.

Element	Kd LKg^{-1})	Maximum Model Leachate Concentration (mgL^{-1})	Lysimeter Leachate Data (mgL^{-1})	MCL*/HRL** (mgL^{-1})
Antimony (Sb)	45	0.006	0.022	0.006
Arsenic (As)	29	0.22	0.076	0.01
Barium (Ba)	42	25	0.176	2
Beryllium (Be)[¥]	1700	0.00008	<0.001	0.004
Boron (B)	24	4.13	0.16	0.6
Cadmium (Cd)	110	0.005	<0.003	0.005
Chromium (Cr) (VI)	18	3.08	0.005	0.1
Cobalt (Co)	100	0.188	<0.004	-
Copper (Cu)	40	1.15	0.014	1.3
Lead (Pb)[@]	3500	0.005	0.125	0.015
Manganese (Mn)	65	10.5	2.83	0.1
Mercury (Hg)	82	0.00005	0.00006	0.002
Molybdenum (Mo)	20	0.16	<0.004	-
Nickel (Ni)	88	0.565	0.013	0.1
Selenium (Se)	4.3	0.692	<0.03	0.05
Silver (Ag)	13	0.173	0.0003	0.03
Strontium (Sr)	48	10.37	0.47	-
Thallium (Tl)	71	0.011	0.056	0.002
Tin (Sn)	74	0.024	0.011	4
Vanadium (V)	1000	0.088	0.002	0.05
Zinc (Zn)	75	1.26	0.028	2

NB: *MCL: Maximum Contaminant Level

    **HRL: Health Risk Limit (Minnesota Department of Health)

   [¥]Berylium: Maximum leachate concentration was detected after 265 years

   [@]Lead: Maximum leachate concentration was detected after 567 years

Table 2. Calculated maximum leachate concentration of elements at 2 m depth

Element	Leachate	
	Maximum Concentration (mg/L)	Years
Silver (Ag)	0.023	490
Boron (B)	0.50	950
Molybdenum (Mo)	0.022	750
Selenium (Se)	0.092	160
Chromium (Cr) (VI)	0.37	670

FIGURES

(a)

10 m

7th street

Lysimeter

7th Avenue

5th street

8th street

10 m

(b)

75 mm HMA

150 mm Fly Ash Stabilized RPM

Subgrade
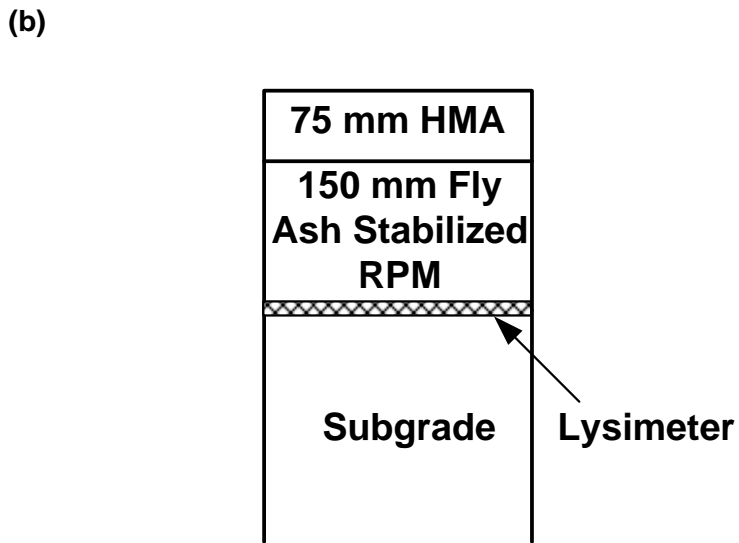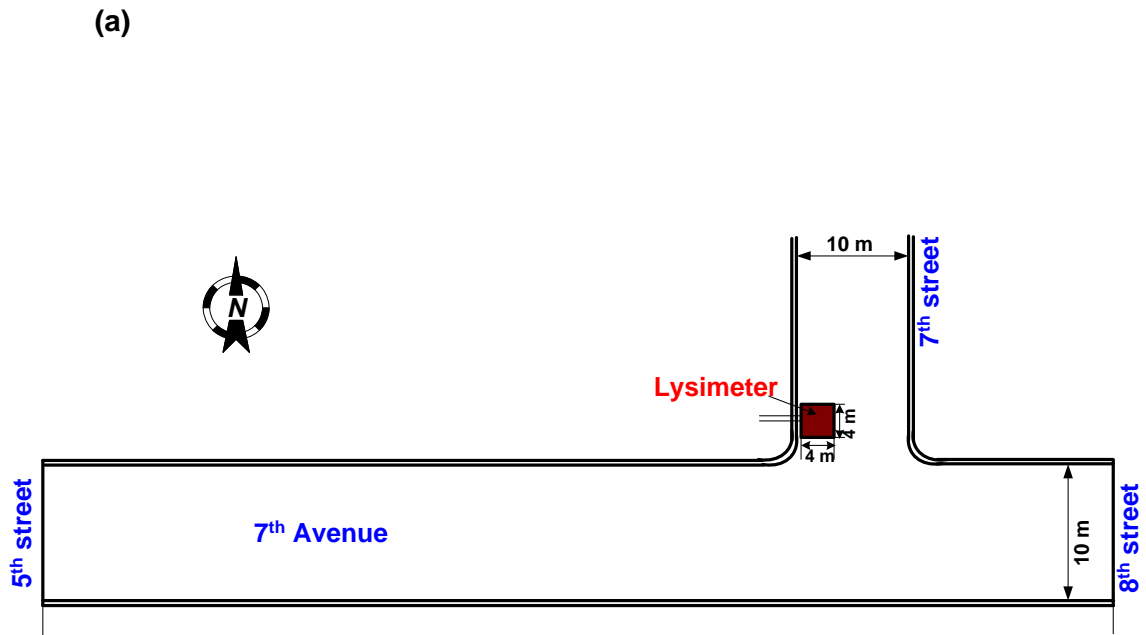
Lysimeter

Figure 10. Fly ash stabilized RPM test sections at Waseca site: (a) layout of lysimeter (b) profiles of pavement structures at the lysimeter.
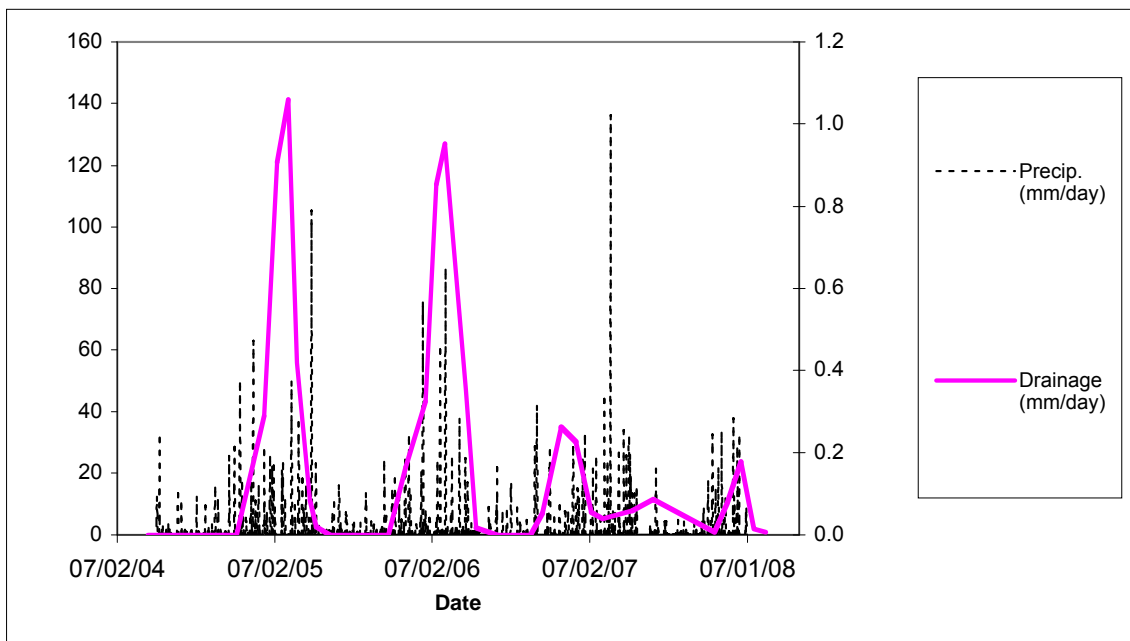
Figure 2. Precipitation and drainage water flow rates.
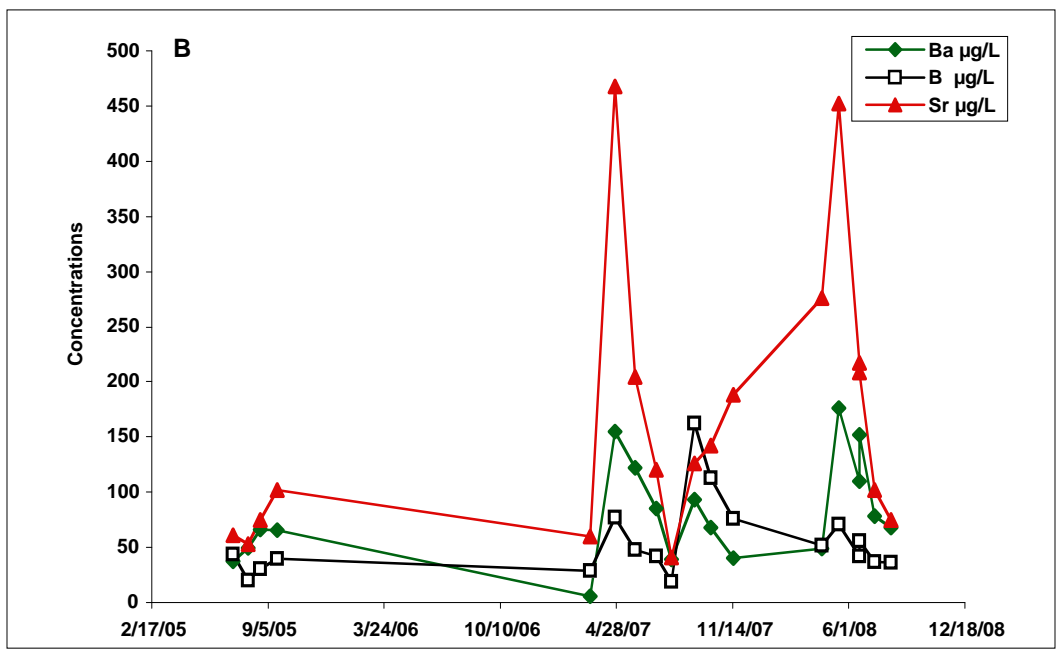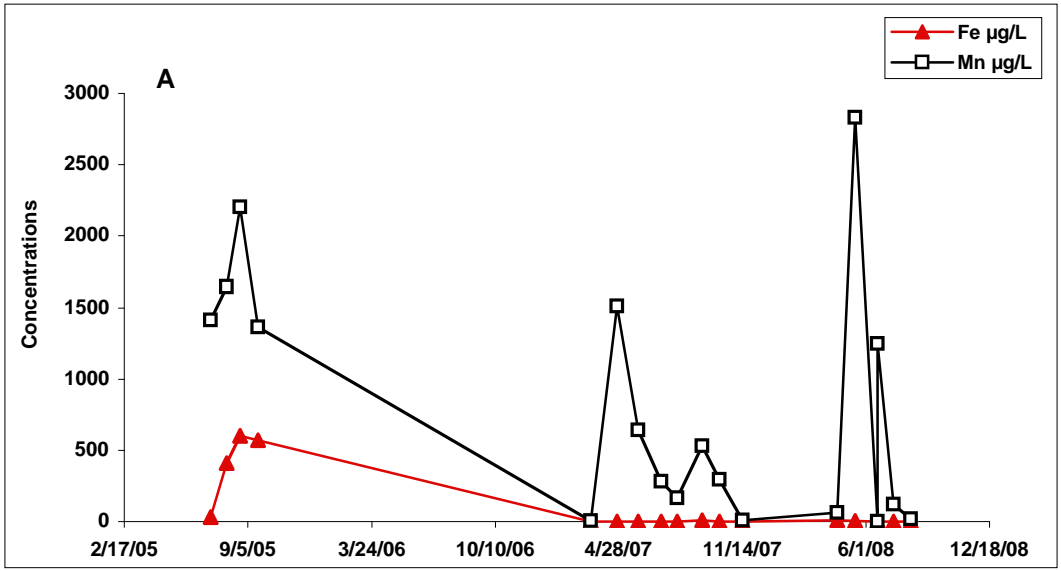
Figure 311 A and B. Concentrations (µg/L) of trace elements in leachate collected in lysimeter at Waseca.
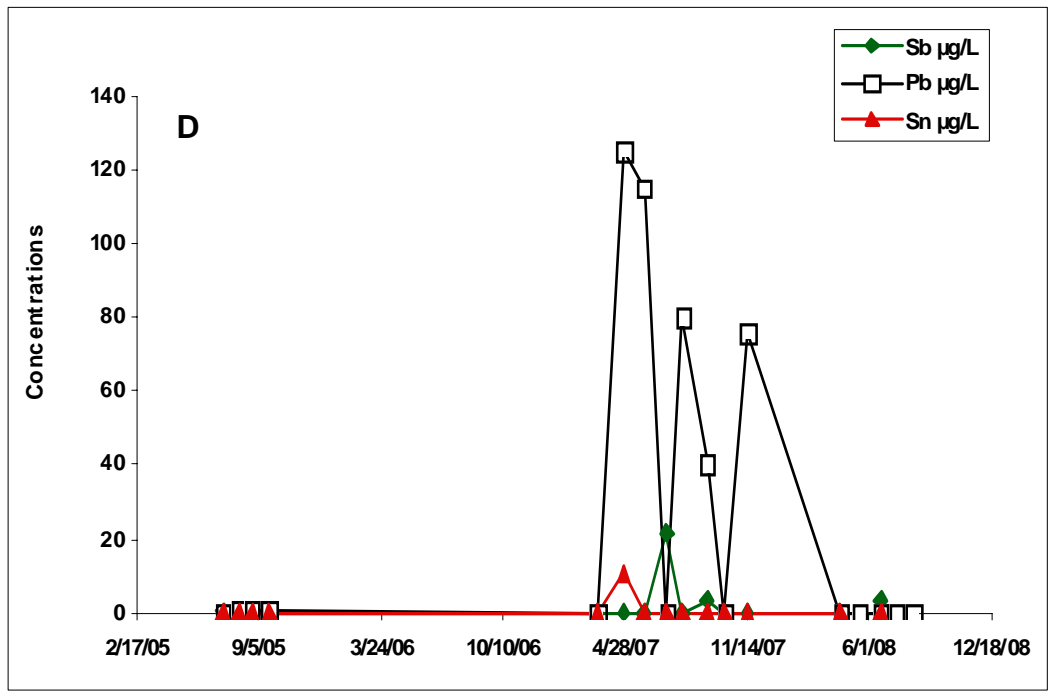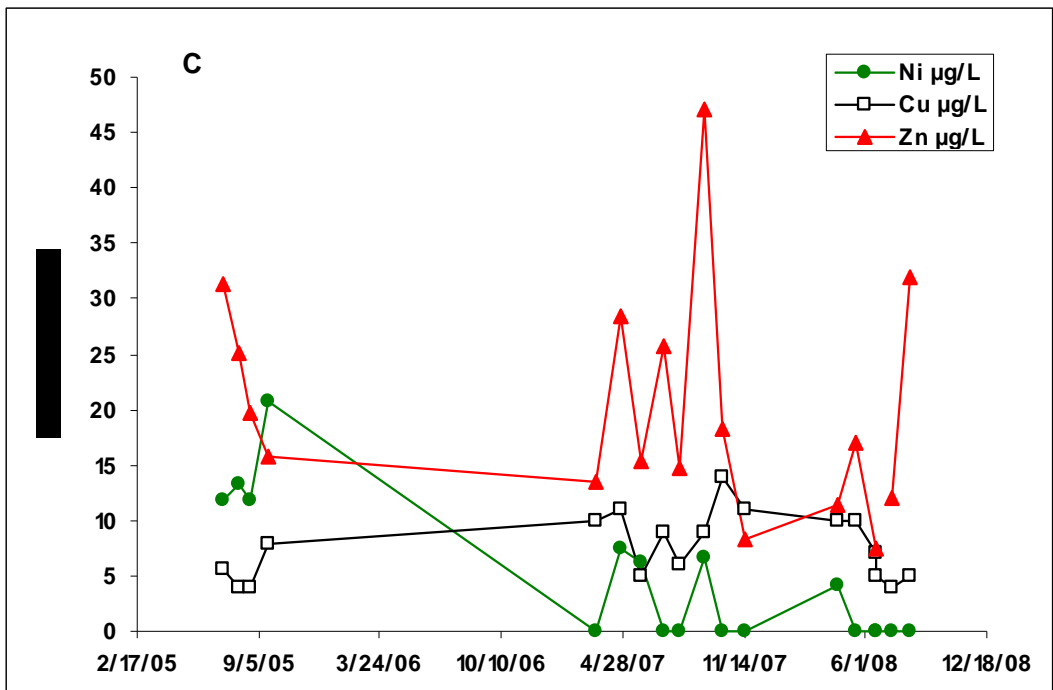
Figure 3 C and D. Concentrations (µg/L) of trace elements in leachate collected in lysimeter at Waseca.
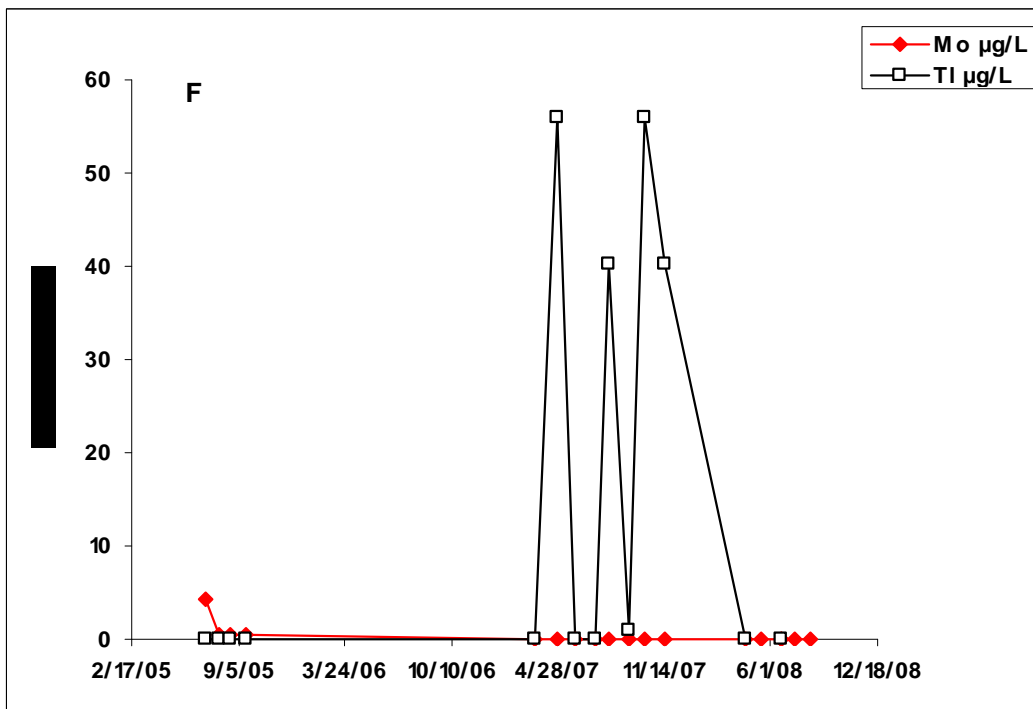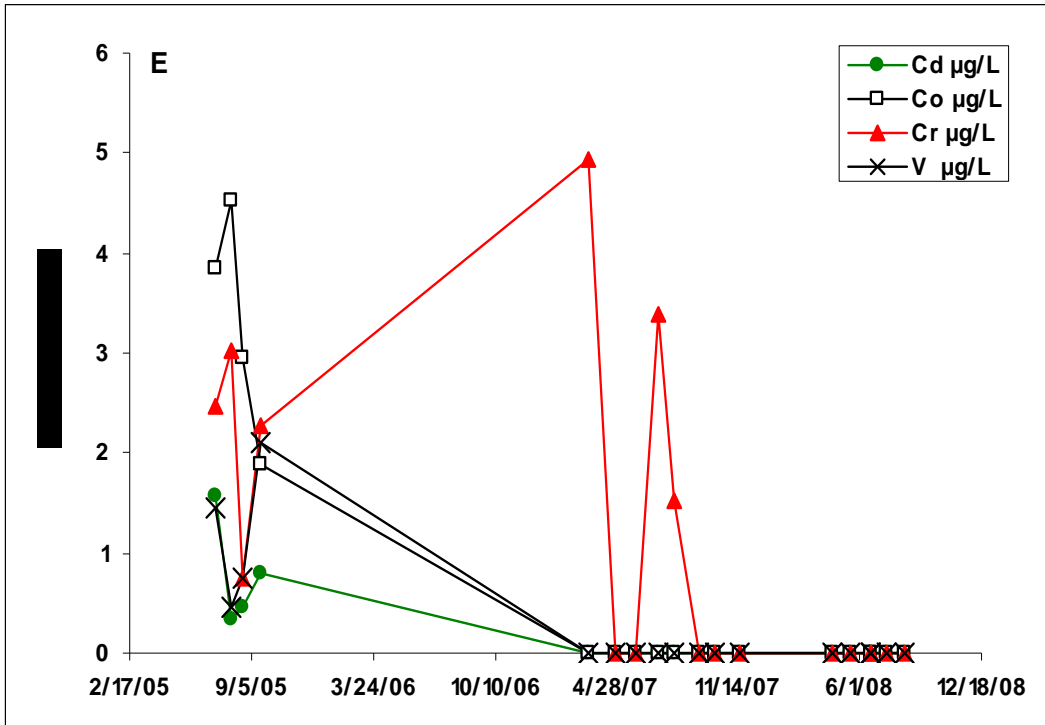
Figure 3 E and F. Concentrations (µg/L) of trace elements in leachate collected in lysimeter at Waseca.
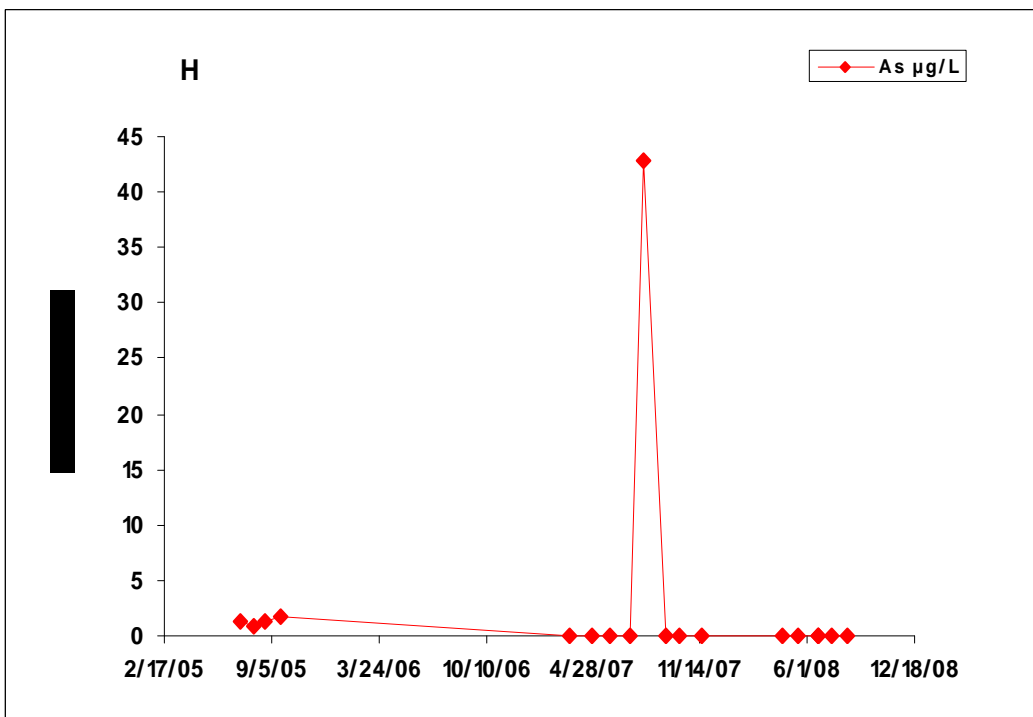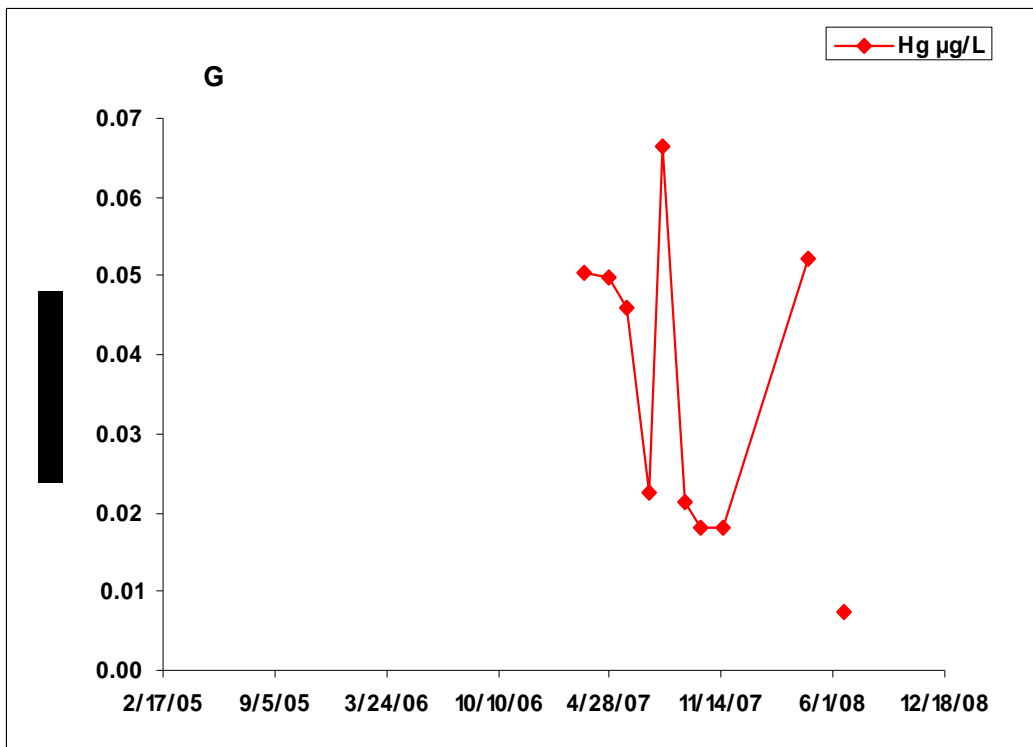
Figure 3 G and H. Concentrations (µg/L) of trace elements in leachate collected in lysimeter at Waseca.
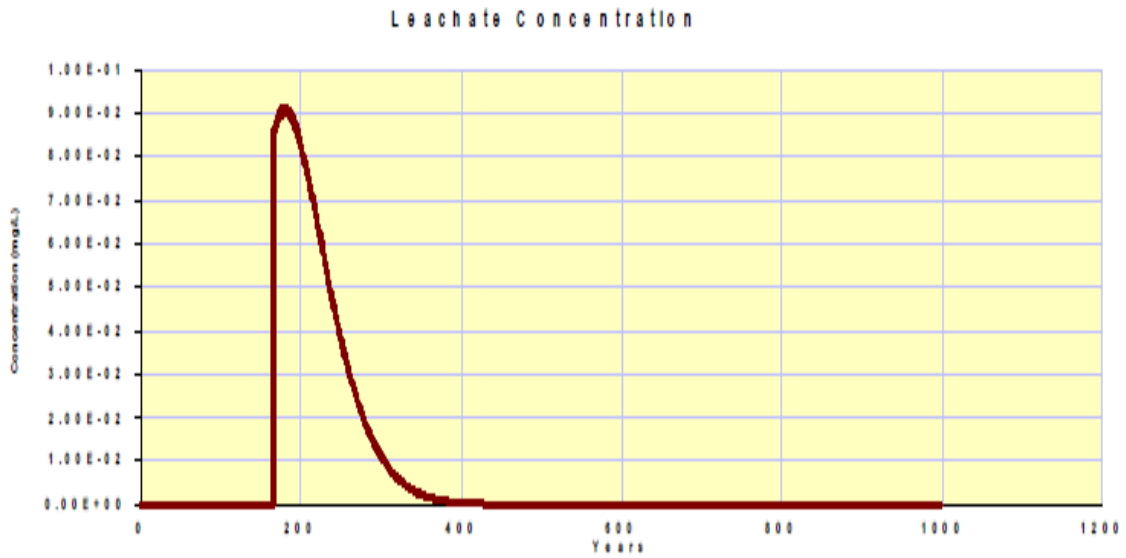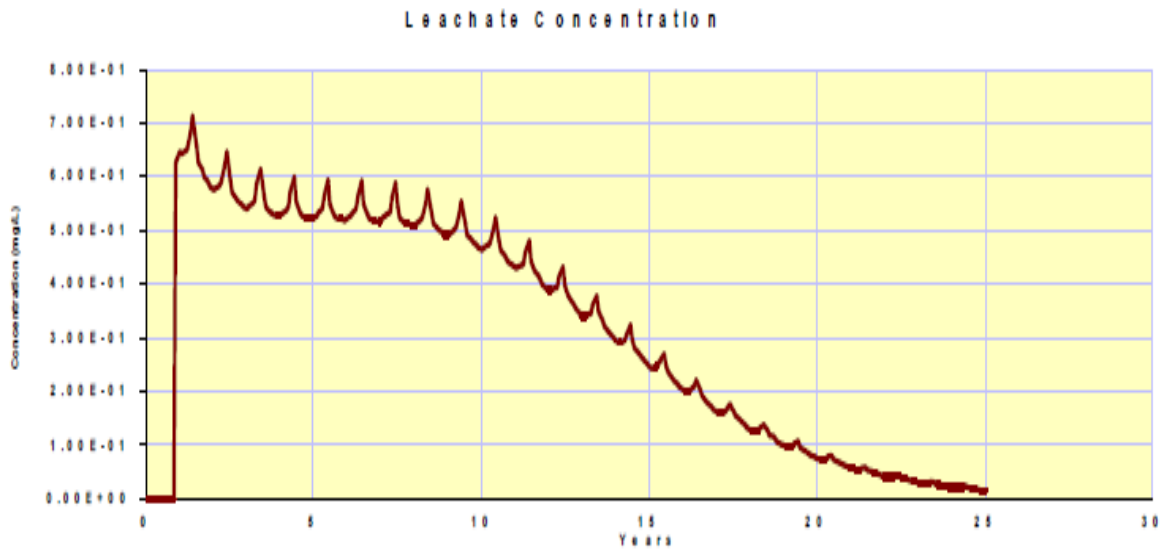
Figure 12 (a) Calculated lysimeter leachate concentration of selenium (Se) with respect to time, and (b) leachate concentration of selenium (Se) with respect to time (maximum time-999 years) at a 2 m depth.
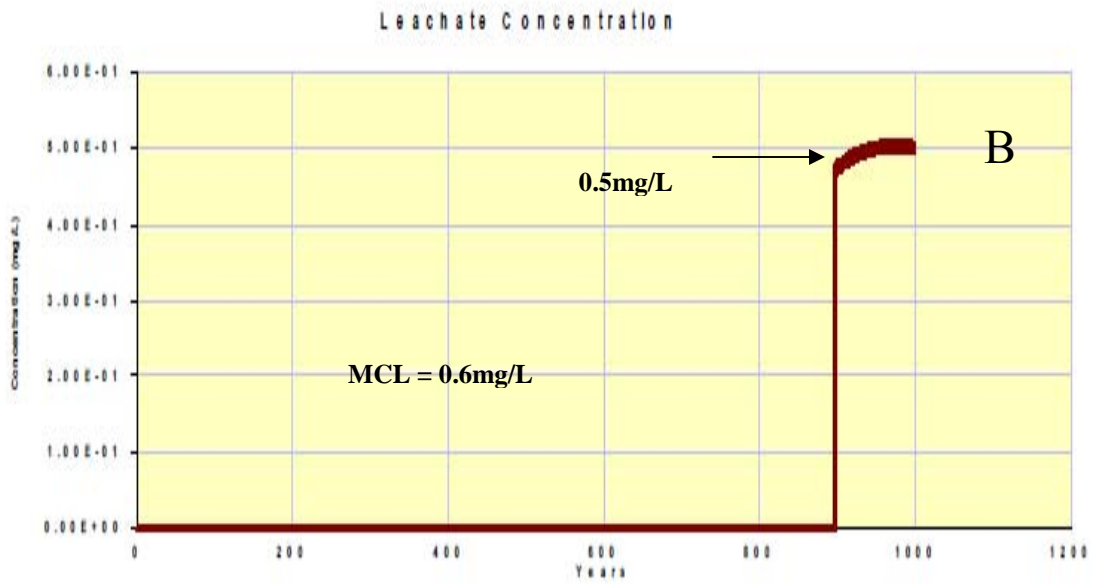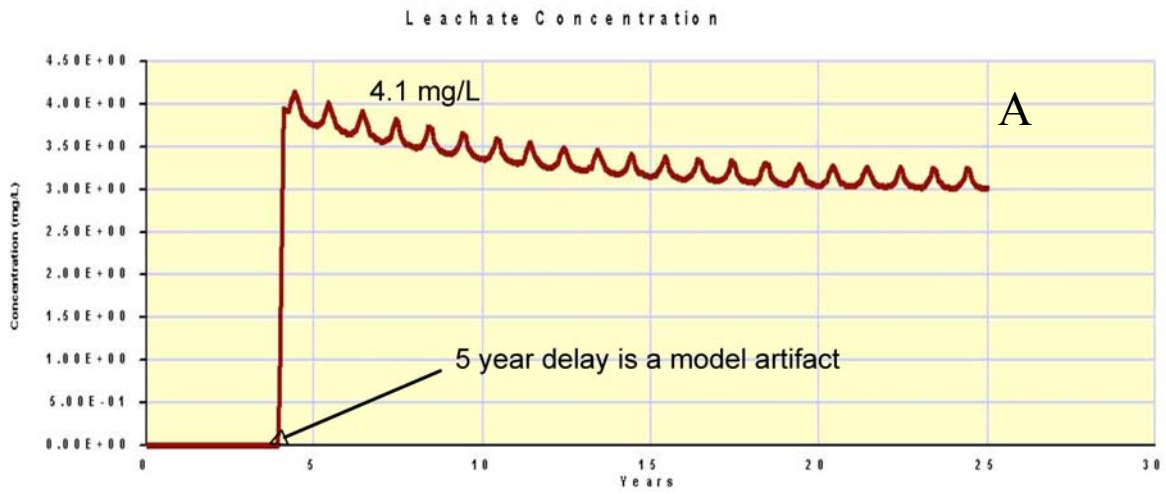
Figure 13. Calculated lysimeter leachate concentration of Boron (B) with respect to time (A) and leachate concentration of Boron (B) with respect to time (maximum time-999 years) at a 2 m depth.

APPENDIX F

REPORT FOR TASK 6

ASSESSING GROUNDWATER IMPACTS FROM A FLY-ASH STABILIZED PAVEMENT MATERIAL USED FOR RECONSTRUCTION OF A BITUMINOUS ROAD: WASECA, MINNESOTA

USE OF FLY ASH FOR RECONSTRUCTION
OF BITUMINOUS ROADS

REPORT FOR TASK 6

ASSESSING GROUNDWATER IMPACTS FROM A FLY-ASH
STABILIZED PAVEMENT MATERIAL USED FOR RECONSTRUCTION
OF A BITUMINOUS ROAD: WASECA, MINNESOTA

Prepared by:

Lin Li
Craig H. Benson
Tuncer B. Edil
Department of Civil and Environmental Engineering
University of Wisconsin-Madison
Madison, WI 53706

February 2009

This report represents the result of research conducted by the authors and does not necessarily represent the views or policies of the Minnesota Local Road Research Board or the Minnesota Department of Transportation

TABLE OF CONTENTS

LIST OF TABLES

LIST OF FIGURES

1. INTRODUCTION

Class C fly ash from a coal-fired electric power plant was used to stabilize a recycled pavement material (RPM) during rehabilitation of a 0.5-km section of flexible pavement along 7th Avenue and 7th Street in Waseca, MN (Li et al. 2006a). The RPM was prepared by pulverizing the existing asphalt pavement and underlying materials to a depth of 300 mm below ground surface using a CMI RS-650-2 road reclaimer. The uppermost 75 mm of the RPM was removed and then Class C fly ash (10% by dry weight) was spread uniformly on the surface using truck-mounted lay-down equipment similar to that described in Edil et al. (2002). The fly ash was mixed with the RPM to a depth of 150 mm using the road reclaimer, with water being added during mixing using a water truck. The mixture was compacted within 1-2 h of blending, was cured for 7 d, and finally overlain with 75 mm of hot-mix asphalt (HMA).

One concern with using fly ash to stabilize pavement materials is the potential for ground water impacts caused by leaching of trace elements contained in the fly ash (Li et al. 2006b). To evaluate this issue at the Waseca site, a lysimeter was installed beneath the pavement to monitor the volume of leachate transmitted by the pavement and concentrations of trace elements in the leachate. The lysimeter was used to collect leaching data from 2004 to 2008. Data from the lysimeter describe conditions at the bottom of the pavement profile. To make inferences regarding how leaching may impact ground water, however, predictions need to be made with a model that accounts for leaching from the pavement along with flow and transport in the vadose zone and ground water.

In this study, the model WiscLEACH was used to evaluate how leaching of trace elements might impact ground water over time at the Waseca site. The model was first calibrated and validated using data from a column leach test (CLT) conducted in the laboratory and the leaching data collected using the lysimeter. Predictions of trace element concentrations in ground water at the Waseca site were then made for a 100-yr service period. The model was also used parametrically to identify variables having the great impact on trace element concentrations in ground water in response to leaching from an overlying pavement containing a layer stabilized with fly ash.

2. WiscLEACH MODEL

The conceptual model consists of a fly-ash stabilized recycled pavement material layer (SRPM) in a typical roadway structure as shown in Fig. 1. As water percolates down through the profile, trace elements leach from the SRPM and then migrate downward through the subgrade soils until they reach the groundwater. Flow in the SRPM and subgrade is assumed to occur only in the vertical direction and transport is assumed to follow the advection-dispersion-reaction equation with instantaneous and reversible sorption and a linear isotherm. Bin-Shafique et al. (2006) show that this assumption is valid for stabilized inorganic soils and typical subgrades.

Trace elements that reach the groundwater are transported horizontally and vertically, although the flow of groundwater is assumed to occur predominantly in the horizontal direction. Transport in groundwater is also assumed to follow the ADRE with instantaneous and reversible sorption and a linear isotherm. In both layers, chemical and biological reactions that may consume or transform trace elements are assumed to be absent. The SRPM and all soils in the profile are assumed to be homogenous and isotropic.

2.1. VADOSE ZONE

The ADRE for one-dimensional steady-state vertical flow with two-dimensional dispersion and linear reversible sorption is (Bear 1979):

$$R\frac{\partial C}{\partial t} = D_x \frac{\partial^2 C}{\partial x^2} + D_z \frac{\partial^2 C}{\partial z^2} - v_z \frac{\partial C}{\partial z} \tag{1}$$

where C is the solute concentration, t is time, x is lateral distance from the centerline of pavement, z is depth below surface of pavement, v_z is the seepage velocity in vertical direction, D_x and D_z are the hydrodynamic dispersion coefficients in the x and z directions, and R is the retardation factor. Flow in the vadose zone is assumed to occur under a unit hydraulic gradient and is controlled by the least conductive layer in the profile. Thus, the seepage velocity in Eq. 1 equals $min(q/n_i, K_{si}/n_i)$, where q is the precipitation rate and K_{si} and n_i are the hydraulic conductivity and effective porosity of each of the layers in the profile (pavement, SRPM, and subgrade). The hydrodynamic dispersion coefficients are computed assuming $D = \alpha v + \tau D_o$, where α is the dispersivity, τ is the tortuosity, and D_o is the molecular diffusion coefficient.

Leij et al. (1991) provide an analytical solution to Eq. 1 that can be used for any empirically defined leaching pattern. For this case, the initial and boundary conditions are assumed as follows:

$$C(x, z, t = 0) = 0.0 \tag{2a}$$

$$\left(v_z C - D_z \frac{\partial C}{\partial z}\right)\Big|_{z=z_B} = \begin{cases} v_z f(t) & \text{at } -L < x < L \\ 0.0 & \text{otherwise} \end{cases} \tag{2b}$$

$$\frac{\partial C}{\partial x}(\pm\infty, z, t) = 0 \tag{2c}$$

$$\frac{\partial C}{\partial z}(x, \infty, t) = 0 \tag{2d}$$

where f(t) is the trace element concentration as a function of time at the bottom of the SRPM, z_B is the depth at the bottom of the SRPM, $L = W_p/2$, and W_p is width of the pavement. Eq. 2a implies that no trace elements initially exist in the subgrade and Eq. 2b indicates that the flux of trace elements into the subgrade from the overlying SRPM is the product of the concentration and the seepage velocity. The function f(t) is defined empirically as a collection of points describing the leaching pattern, with linear interpolation between the points. Eqs. 2c and 2d indicate that transport by dispersion and diffusion is negligible at distances far from the surface of the pavement and the centerline of the profile. The solution to Eqs. 1 and 4 for $z > z_B$ is (Leij et al. 1991):

$$C(x,z,t) = \frac{1}{4}\int_0^t f(t-\tau)\frac{v_z}{R}\left[\sqrt{\frac{R}{\pi D_z \tau}}\exp\left(-\frac{(R(z-z_B)-v_z\tau)^2}{4RD_z\tau}\right) - \frac{v_z}{2D_z}\exp\left(\frac{v_z(z-z_B)}{D_z}\right)\right.$$
$$\left. \text{erfc}\left(\frac{R(z-z_B)+v_z\tau}{\sqrt{4RD_z\tau}}\right)\right]\left[\text{erfc}\left(\frac{x-L}{\sqrt{4D_x\tau/R}}\right) - \text{erfc}\left(\frac{x+L}{\sqrt{4D_x\tau/R}}\right)\right]d\tau \tag{3}$$

Eq. 3 is applied from the top of subgrade to the GWT (Fig. 1).

2.2.   GROUNDWATER

When groundwater flow occurs predominantly in the horizontal direction, transport in groundwater can be described with the following form of the ADRE (Leij et al. 2000):

$$R_w \frac{\partial C}{\partial t} = D_{xw}\frac{\partial^2 C}{\partial x^2} - v_h\frac{\partial C}{\partial x} + D_{zw}\frac{\partial^2 C}{\partial z^2} - v_z\frac{\partial C}{\partial z} \tag{4}$$

where C is solute concentration, t is time, v_h is the seepage velocity in the horizontal direction, v_z is the seepage velocity in the vertical direction, D_{xw} and D_{zw} are the hydrodynamic dispersion coefficients in the x and z directions, and R_w is the retardation factor in groundwater. An implicit assumption when using Eq. 4 is that the cross-dispersion terms are negligible, which is reasonable for predominantly horizontal flow in a uniform and isotropic medium.

Leij et al. (2000) provide an analytical solution to Eq. 4 for the following initial and boundary conditions:

$$C(x,z,t=0) = 0 \tag{5a}$$

$$\left(v_z C - D_{zw}\frac{\partial C}{\partial z}\right)\Bigg|_{z=z_{GWT}} = \begin{cases} v_z g(x, z_{GWT}, t) & x_1 < x < x_2 \\ 0 & \text{otherwise} \end{cases} \tag{5b}$$

$$\frac{\partial C}{\partial x}(\pm\infty, z, t) = 0 \tag{5c}$$

$$\frac{\partial C}{\partial z}(x, \infty, t) = 0 \tag{5d}$$

where z_{GW} is the depth of the groundwater table, $g(t)$ is the trace elements concentration at the groundwater table from the vadose zone, and x_1 and x_2 define the lateral extent over which $g(t)$ applies. Eq. 5a implies that the groundwater is initially free of trace elements and Eq. 5b indicates that the flux of trace elements entering the groundwater equals the advective of flux of trace elements in the vadose zone at the groundwater table. Eqs. 5c and 5d indicate that the diffusive and dispersive fluxes in groundwater are negligible for distances very far from the centerline of the pavement and the groundwater.

The analytical solution to Eqs. 4 and 5 for $z > z_{GW}$ is (Leij et al. 2000):

$$\begin{aligned} C(x,z,t) = \int_0^t \frac{v_z g(t-\tau)}{2R_w}&\left[\operatorname{erfc}\left(\frac{R_w(x-x_2)-v_h\tau}{\sqrt{4R_w D_{xw}\tau}}\right) - \operatorname{erfc}\left(\frac{R_w(x-x_1)-v_h\tau}{\sqrt{4R_w D_{xw}\tau}}\right)\right] \\ &\left[\sqrt{\frac{R_w}{\pi D_{zw}\tau}}\exp\left(-\frac{(R_w(z-z_{GWT})-v_z\tau)^2}{4R_w D_{zw}\tau}\right) - \right. \\ &\left. \frac{v_z}{2D_{zw}}\exp\left(\frac{v_z(z-z_{GWT})}{D_{zw}}\right)\operatorname{erfc}\left(\frac{R_w(z-z_{GWT})+v_z\tau}{\sqrt{4R_w D_{zw}\tau}}\right)\right]d\tau \end{aligned} \tag{6}$$

Eq. 6 accounts for solute transport from a line source at the groundwater table between x_1 and x_2. This feature was used to account for the horizontally varying concentration in the vadose zone that occurs in response to the different seepage velocities inside and outside the pavement and the effects of horizontal dispersion near the edges of the domain defined by $x = \pm L$ (Fig. 1). Eq. 6 is applied for a series of contiguous line sources extending along the groundwater table, with the combined effect obtained by superposition.

Eqs. 3 and 6 are programmed in WiscLEACH and are used to predict trace element concentrations in the vadose zone and groundwater table as a function of space and time. Gaussian quadrature is used to numerically integrating Eqs. 3 and 6. The Windows interface for WiscLEACH makes entering the input and display of the output simple and straightforward. Additional details on the model can be found in Li et al. (2006b).

3. COLUMN TEST DATA

A column leach test (CLT) was conducted on a specimen of SRPM collected during construction of the Waseca site. The specimen was compacted in the field in a standard Proctor compaction mold (height = 116 mm, diameter = 102 mm) to the same dry unit weight as the in situ SRPM. After compaction, the specimen was sealed in plastic and cured for 7-d prior in a 100% humidity environment.

A CLT was conducted on the cured specimen following the procedure described in ASTM D 4874, except a flexible-wall permeameter was used instead of a rigid-wall permeameter. Flow was oriented upward and was driven by a peristaltic pump set to provide a Darcy velocity of 2 mm/d. The effective confining pressure was set at 15 kPa to simulate the in situ condition. A 0.1 M LiBr solution was used as the permeant liquid to simulate percolate in regions where salt is used to manage ice and snow (Bin-Shafique et al. 2006). Effluent from the column was collected in sealed Teflon bags to prevent interaction with the atmosphere. Leachate was removed from the bags periodically ($\approx$ 30 to 60 mL of flow accumulation), the volume of the leachate was measured, the pH was recorded, and a sample was prepared for chemical analysis by filtering with a 0.45 μm filter and preservation with nitric acid to pH < 2.

All effluent samples were analyzed by inductively coupled plasma-mass spectrometry (ICP-MS) following the procedure described in USEPA Method 200.8. Analysis was conducted for the following elements (detection limits in μg/L in parentheses): Ag (0.02), As (0.1), B (0.2), Ba (0.02), Be (0.02), Ca (5), Cd (0.08), Co (0.01), Cr (0.04), Cu (0.07), Hg (0.2), Mo (0.08), Mn (0.03), Ni (0.05), Pb (0.01), Sb (0.02), Se (2.0), Sn (0.04), Sr (0.01), Tl (0.006), V (0.06), and Zn (0.2).

Effluent from the CLT had pH between 7.3 and 7.8, which is consistent with the pH of leachate collected in the lysimeter. Concentrations of trace elements in the effluent from the CLT on the SRPM are shown in Fig. 2. Elements having peak concentrations less than 1 μg/L and elements not typically associated with health risks (Ca and Mn) are not shown in Fig. 2. Elements having peak concentrations exceeding 100 μg/L are shown in Fig. 2a, whereas those with peak concentrations less than 100 μg/L are shown in Fig. 2b. Most of the elements have concentrations below USEPA MCLs and Minnesota HRLs. The exceptions are for B (peak = 2196 μg/L, no MCL, HRL = 600 μg/L,), Pb (peak = 19 μg/L, MCL = 15 μg/L, HRL = 15 μg/L), Se (peak = 60 μg/L, MCL = 50 μg/L, HRL = 30 μg/L), and Sr (peak = 4023 μg/L, no MCL, HRL = 4000 μg/L). The peak Mn concentration (468 μg/L, not shown in Fig. 2) was also above the current Minnesota HRL for Mn, but is less than the proposed HRL.

The elution behavior observed in the CLT effluent follows two patterns: (i) lagged response, where the concentration initially increases and then falls, and (ii) persistent leaching, where the concentration initially increases and then remains relatively constant. Similar patterns have been reported by other investigators (Edil et al. 1992, Creek and Shackelford 1992, Palmer et al. 2000, Sauer et al. 2005). Most of the elements with peak concentrations exceeding 100 μg/L (Fig. 2a) exhibit the persistent leaching pattern (B, Ba, Sr, and Mo), whereas those exhibiting lagged response typically have peak concentrations less than 100 μg/L (Fig. 2b) (Co, Cr, Pb, and Se). The exceptions are Cu and Zn, which have peak concentrations exceeding 100 μg/L and exhibited a lagged response, and As and V, which have peak concentrations less than 100 μg/L and exhibit the persistent leaching pattern.

4. COMPARISON WITH FIELD LEACHING DATA AT WASECA

4.1. LEACHING DATA AT WASECA

The pavement profile at Waseca is shown in Fig. 3a. The pavement is 10.4 m wide and has curb and gutter (no shoulder). A detailed description of the pavement can be found in Li et al. (2008b). Monitoring of the pavement began in September 2004 and continued until July 2008. Leachate draining from the pavement was monitored using a pan lysimeter installed near the intersection of 7th Street and 7th Avenue (Fig. 3b). The lysimeter is 4 m wide, 4 m long, and 200 mm deep and is lined with 1.5-mm-thick linear low density polyethylene geomembrane. The base of the lysimeter was overlain by a geocomposite drainage layer (geonet sandwiched between two non-woven geotextiles). SRPM was placed in the lysimeter and compacted using the same method employed when compacting SRPM in other portions of the construction project (Li et al. 2008b).

Water that collects in the drainage layer was directed to a sump plumbed to a 120-L polyethylene collection tank buried adjacent to the roadway. The collection tank was insulated with extruded polystyrene to prevent freezing. Leachate that accumulates in the collection tank was removed periodically with a pump. The volume of leachate removed was recorded with a flow meter and samples were collected to determine concentrations of Ag, As, B, Ba, Be, Ca, Cd, Co, Cr, Cu, Hg, Mo, Mn, Ni, Pb, Sb, Se, Sn, Sr, Tl, V, and Zn. The field and laboratory data that were collected are compiled in Li et al. (2008a, b) along with a description of the analytical methods.

Field leachate concentrations of five trace elements (As, Se, Pb, TI, and Sb) exceeded USEPA MCLs at least one time (Fig. 4a). Concentrations of these five trace elements exhibited a portion of the "delayed-response" pattern; they increased over the first 2 to 4 pore volumes of flow (PVF), and then remained relatively constant or dropped during the last year of monitoring ($\approx$ 4.0 -4.3 PVF). Diminishing concentrations probably would have been observed had the lysimeter been monitored for a longer period of time. Corresponding effluent concentrations for these five trace elements from the CLT are shown in Fig. 4b.

Approximately 3200 L of leachate corresponding to 206 mm of total drainage occurred during the monitoring period (Fig. 5a). The distribution of volumetric leachate flux is shown in Fig. 5b. The 50th percentile volumetric leachate flux ($q_{50\%}$) is 0.055 mm/d and the 90th percentile ($q_{90\%}$) is 0.85 mm/d.

4.2. MODEL CALIBRATION

Selenium data from the lysimeter and the CLT were used for model calibration. Hydraulic properties and transport parameters used for simulations of the Waseca site are in Table 1. Saturated hydraulic conductivity of the SRPM was measured in a flexible-wall permeameter following the methods in ASTM D 5084 (Li et al. 2006a). Saturated hydraulic conductivity of the silty clay subgrade at Waseca was assumed to be similar to the hydraulic conductivity of the silty clay subgrade described in by Bin-Shafique et al. (2002). Effective porosity and dispersivity of the HMA, the SRPM, and the subgrade were obtained from CLT tracer data described in Bin-Shafique et al. (2002). Elution of Se from the SRPM layer was

defined using Se data from the CLT via the user-defined leaching pattern in WiscLEACH (Table 2, Fig. 6a). Retardation factors for Se in the SRPM and the subgrade were obtained from Bin-Shafique et al. (2002). The molecular diffusion coefficient for Se was obtained from Lerman (1979).

WiscLEACH was calibrated by conducting simulations where the seepage velocity was varied until the Se concentrations predicted by WiscLEACH at the bottom of the pavement were comparable to Se concentrations measured in the lysimeter leachate. The seepage velocity was systematically varied between the 50th and 90th percent leachate flux measured in the lysimeter (Fig. 5b). Good agreement was obtained using a seepage velocity corresponding to a leachate flux of 0.27 mm/d ($\approx 75^{th}$ percentile volumetric leachate flux in the lysimeter), as shown in Fig. 6b. The predicted concentrations in Fig. 6b correspond to the bottom of the layer of SRPM (z_B) (Figs. 1, 3a), where the lysimeter was located.

Potential impacts to ground water due to leaching of Se were evaluated by using the calibrated model to predict concentrations at a point of compliance (POC) 1.5 m from the edge of the pavement. This POC corresponds to the approximate location of a sidewalk on a residential street with a curb, which defines the right of way for the street. Predictions were made for a 100-yr period, which required that leaching data from the CLT be extrapolated beyond the range of the last measurement. The extrapolation consisted of assuming that the concentration decreased linearly to zero between the last data point and 80 PVF (Fig. 7a).

Predicted maximum concentrations at the POC as a function of depth in groundwater are shown in Fig. 7b over the 100 yr simulation period. The points in Fig. 7b correspond to peak concentrations and occur at different times. Thus, Fig. 7b is a profile of *maximum* concentration over a 100-yr period rather than a more conventional profile of concentration with depth at a given time. Times corresponding to the peak concentrations are also shown in Fig. 7b. For example, at 4 m below the pavement surface, the maximum concentration is 13.0 μg/l and occurs at 34 years

The profile in Fig 7b also illustrates that dilution and attenuation occur between the SRPM and the POC. The peak Se concentration in the SRPM is 60 μg/L, which is above the USEPA MCL (50 μg/L). However, the peak concentration at the POC is only 13 μg/l, which is nearly five times lower than the peak concentration in the SRPM. Thus, data from leaching tests such as the CLT or a batch water leach test do not necessarily reflect conditions in ground water that are relevant for assessing environmental impacts. Other factors, such as dilution and attenuation, need to be considered.

4.3.   VALIDATION AND REFINEMENT

WiscLEACH was used to predict concentrations of As and Sb in the lysimeter using the seepage velocity identified by calibration with the Se data. Predictions were not made for TI or Pb because the field data for these elements were suspect. Field concentrations of Tl were two orders of magnitude lower than Tl concentrations from the CLT, which suggested that the Tl concentrations were anomalous or a source other than SRPM was responsible for the Tl observed in the field. The field data for Pb were considered suspect because sequential measurements made between 1.5 and 2.8 yrs after monitoring began included very high concentrations (> 30 μg/L) and concentrations below the detection limit.

Predictions for Sb and As were made using the same input parameters employed for the Se simulations, except effluent concentrations for Sb and As from the CLT were input using the user-defined option for leaching patterns. The retardation factor was also adjusted until the predicted and measured concentrations were in reasonable agreement.

Measured and predicted concentrations of Sb and As are shown in Fig. 8. The predicted Sb concentrations are in general agreement with the measured Sb concentrations (Fig. 8a). Good agreement also exists early in the record for As (< 0.5 yr, Fig. 8b) Only one data point later in the record is above the detection limit (at ≈2 yr), and the As concentration associated with this point is 4 times higher than the predicted concentration. However, this data point is surrounded by 8 other data points where the concentration is below the detection limit. Thus, the high As concentration around 2 yr may be anomalous.

Potential impacts to ground water due to leaching of Sb and As were estimated using the same approach that was employed for Se. Maximum concentrations as a function of depth over a 100-yr service life are shown in Fig. 9a for As and Fig. 9b for Sb. For As, concentrations at the POC are below MCLs at all depths. For Sb, concentrations remain below the MCL for depths < 3.5 m, and are slightly above the MCL at 4 m.

5. PARAMETRIC STUDIES

As the findings in Sec. 4 show, concentrations of trace elements at the POC are lower than the peak concentration from a CLT due to dilution and attenuation. To evaluate how dilution and attenuation are affected by design variables (e.g., breadth of the pavement, SRPM thicknesses, depth to groundwater, hydraulic properties of the layers, transport properties, etc.), parametric simulations were conducted with WiscLEACH where independent variables were varied one at a time in a systematic manner. All other variables were held constant using the same input data employed for the Waseca site (Tables 1 – 3). Se was used as the trace element of interest because the peak Se concentration from the CLT exceeded the MCL.

5.1.   GEOMETRIC AND TRANSPORT VARIABLES

The key geometric and transport variables are the depth to the groundwater, the SRPM layer thickness, the pavement width, and the peak concentration from the SRPM (Li et al. 2006b). Predictions obtained by systematically varying these parameters are shown in Figs. 10 and 11. These findings indicate the following:

• Increasing the depth to groundwater results in lower concentrations at the POC (Fig. 10a) due to greater dispersion and attenuation in the vadose and saturated zones.

• Increasing the thickness of the SRPM layer causes an increase an increase in concentration at the POC because the total mass available for leaching increases as the thickness of the SRPM layer is increased (Fig. 10b).

• Increasing pavement width causes higher concentrations at the POC because the fly ash source is distributed over a broader area, which increases the mass transmitted to ground water and decreases dispersion (Fig. 11a).

• Increasing the peak concentration eluted from the SRPM later (C_{in}) causes an increase in peak concentrations at the POC, as expected (Fig. 11b).

Based on these analyses, concentrations at a POC should be lower when ground water is deeper, a thinner SRPM layer is employed, the pavement width is narrower, or the peak concentration eluted from the byproducts layer is lower.

5.2.   HYDRAULIC VARIABLES

Hydraulic variables include the hydraulic conductivity and porosity of the pavement, SRPM, subgrade, and aquifer material; the regional hydraulic gradient in groundwater; and the precipitation rate. The seepage velocity in the vadose zone is controlled systematically by the precipitation rate and hydraulic conductivity and porosity of the pavement, SRPM, and the subgrade (Li et al. 2006b). Thus, the effect of these variables was assessed by varying the seepage velocity.   Similarly, the seepage velocity in the saturated zone is controlled systematically by the hydraulic conductivity, porosity, and hydraulic gradient in the saturated zone. Thus, the effect of these variables was assessed by varying the seepage velocity in the saturated zone.

The effect of varying the seepage velocity in the vadose and saturated zones is illustrated in Fig. 12, which shows concentrations at the POC as a function of depth for various seepage velocities in the vadose zone or groundwater. The peak concentration at the POC decreases as the seepage velocity in the vadose zone decreases (Fig. 12a) or as the seepage velocity in groundwater increases (Fig. 12b). These seepage velocities have an opposite effect. Increasing the seepage velocity in the vadose zone increases the amount of mass transmitted to ground water, whereas increasing the seepage velocity in the saturated zone results in more dilution (Li et al. 2006b). These findings indicate that lower concentrations in ground water can be expected at sites where the pavement profile contains a less conductive layer (e.g., HMA with low air voids content, PCC pavement, or finer-grained subgrade) or the flow rate in underlying ground water is higher.

6. SUMMARY AND PRACTICAL IMPLICATIONS

This report has described a study conducted using the computer model WiscLEACH, field data from a local road in Waseca, MN that was reconstructed using base course comprised of reclaimed pavement material stabilized with cementitous fly ash (SRPM), and data from column leaching tests conducted in the laboratory on samples of SRPM collected during construction at the Waseca site. Concentrations of Se in leachate collected beneath the road with a pan lysimeter were used to calibrate WiscLEACH for conditions at Waseca. The calibrated model was then used to predict concentrations of other trace elements with modest adjustments to the retardation factor being made for the other elements. Parametric simulations were also conducted to evaluate how site variables affect trace element concentrations in ground water at sites employing SRPM.

Good agreement was obtained between predicted and measured concentrations after modest calibration by adjusting the seepage velocity in the vadose zone within the range measured on site. This suggests that reliable predictions can be made with WiscLEACH when column leach test data and realistic hydrological parameters for the pavement layers, subgrade, and the aquifer are used as input. Simulations for the Waseca site also showed trace element concentrations generally remained below MCLs at the edge of the right of way for at least 100 yr even for those elements where the peak concentration eluted from the SRPM exceeded the MCL.

Parametric simulations conducted with the model showed that several site specific factors can reduce trace element concentrations in ground water caused by leaching from SRPM. These include greater depth to ground water, presence of a less permeable layer within the pavement profile, use of a thinner layer of SRPM, and application to narrower roadways. Lower concentrations in ground water also occur when ground water flows more rapidly.

REFERENCES

Bear J. 1979. *Hydraulics of Groundwater*. McGraw-Hill Inc., New York.

Bin-Shafique, S., Benson, C.H., and Edil, T.B. 2002. "Leaching of heavy metals from fly ash stabilized soils used in highway pavements." Geo Engineering Report No. 02-14, Department of Civil and Environmental Engineering, University of Wisconsin-Madison.

Bin-Shafique, S., Benson, C.H., Edil, T.B. and Hwang, K. 2006. "Leachate concentrations from water leach and column leach tests on fly-ash stabilized soils." *Environmental Engineering Science*, 23 (1): 53-67.

Creek D.N. and Shackelford C.D. 1992. "Permeability and leaching characteristics of fly ash liner materials." *Transportation Research Record*, 1345: 74-83.

Edil, T.B., Sandstrom, L. K., and Berthouex, P. M. 1992. "Interaction of inorganic leachate with compacted pozzolanic fly ash," *Journal of Geotechnical Engineering*, American Society of Civil Engineers, Vol. 118, No. 9, 1992, pp. 1410-1430.

Edil, T.B., Benson, C. H., Bin-Shafique, M. S., Tanyu, B. F., Kim, W. H. and Senol, A. 2002. "Field evaluation of construction alternatives for roadways over soft subgrade." *Transportation Research Record*, No. 1786: National Research Council, Washington DC, pp. 36-48.

Leij, F.J., Skaggs, T.H. and van Genuchten, M.T., 1991. "Analytical solutions for solute transport in three-dimensional semi-infinite porous media." *Water Resources Research*, 27(10): 2719-2733.

Leij, F.J., Priesack, E. and Schaap, M.G., 2000. "Solute transport modeled with Green's functions with application to persistent solute sources." *Journal of Contaminant Hydrology*, 41(1-2): 155-173.

Lerman, A. 1979. *Geochemical Processes in Water and Sediment Environments*. John Wiley and Sons, New York.

Li, L., Benson, C.H., Edil, T.B. and Hatipoglu, B. 2006a. "Fly Ash Stabilization of Recycled Asphalt Pavement Material in Waseca, Minnesota." Geo Engineering Report No. 06-18, Department of Civil and Environmental Engineering, University of Wisconsin-Madison.

Li, L., Benson, C.H., Edil, T.B. and Hatipoglu, B. 2006b. "Estimating Groundwater Impact from Coal Combustion Products in Highways." *Waste and Resource Management*, 159: 151-163.

Li, L., Edil, T.B., Benson, C.H. and Hatipoglu, B. 2008a. "Use of Fly Ash for Reconstruction of Bituminous Roads: Monitoring of a Fly Ash Stabilized Pavement Material in Waseca,

Minnesota." Geo Engineering Report No. 08-30, Department of Civil and Environmental Engineering, University of Wisconsin-Madison.

Li, L., Benson, C.H., Edil, T.B. and Hatipoglu, B. 2008b. "Sustainable Construction Case History: Fly Ash Stabilization of Recycled Asphalt Pavement Material." *Geotechnical and Geological Engineering*, 26: 177-187.

Palmer, B. G., Edil, T. B. and Benson, C. H. 2000. "Liners for Waste Containment Constructed with Class F and C Fly Ashes," *Journal of Hazardous Materials*, 2000, Vol. 18, Nos. 2-3, pp. 133-161.

Sauer J.J., Benson C.H. and Edil T.B. 2005. "Leaching of Heavy Metals from Organic Soils Stabilized with High Carbon Fly Ash." Geo Engineering Report No. 05-01, Departmental of Civil and Environmental Engineering, University of Wisconsin-Madison.

TABLES

Table 18. Hydraulic properties and transport parameters for pavement layers and aquifer input to WiscLEACH[1].

	Pavement	Fly ash stabilized RPM	Subgrade	Aquifer
Layer characteristics	75 mm hot-mixed asphalt[2]	150 mm SRPM[2]	Silty clay[2]	Silty soil[2,3]
Width: m	10.4[4]	10.4[4]	As wide as model domain[5]	As wide as model domain[5]
Saturated hydraulic conductivity K_s: cm/s	5.8×10^{-5}	$3 \times 10^{-5, 6}$	$3.2 \times 10^{-7, 7}$	$1.2 \times 10^{-4, 7}$
Effective porosity[7] n	0.33	0.33	0.33	0.35
Hydraulic gradient[7]	1.0	1.0	1.0	0.001
Longitudinal dispersivity[7]: m	0.004	0.004	0.004	1.0
Transverse dispersivity[7]: m	0.002	0.002	0.002	0.003

[1]At Waseca site. Point of compliance (POC) is 1.5 m from the pavement edge (typical right-of-way for city street).
[2]Li et al. (2006a)
[3]Ground water is at least 2 m below ground surface based on field observations during lysimeter construction
[4]Two-lane city street with curb
[5]Model domain is 40 m wide and 12 m deep
[6]Li et al. (2006b), measured in flexible-wall permeameter
[7]Bin-Shafique et al. (2002)

Table 19. Effluent concentrations from CLT on SRPM used as input to the WiscLEACH.

Pore Volumes of Flow (PVF)	Selenium (Se)	Arsenic (As)	Antimony (Sb)
0.525	3.12	1.4	0.3
0.791	53.5	7.2	3.1
0.940	53.2	-	6.0
1.129	59.8	7.1	-
1.323	47.5	-	-
1.520	37.5	5.2	8.3
1.767	29.2	-	-
1.991	27.1	4.6	9.1
3.197	15.7	3.1	10.6
5.593	19.0	6.1	14.0
6.547	13.4	3.9	11.2

Table 20. Maximum dry unit weights and optimum CBRs for Class 5 base, RPM, and RSG with and without fly ash.

	Selenium (Se)	Arsenic (As)	Antimony (Sb)
USEPA MCL[1], µg/L	30.0	10.0	6.0
Retardation factor R^2	3.5^2	3.0^3	1.8^3
Molecular diffusion coefficient[4], cm^2/s	1.3×10^{-6}	3.0×10^{-7}	2.4×10^{-6}

[1]Li et al. (2008a)
[2]Bin-Shafique et al. (2002)
[3]Best fit of WiscLEACH prediction with the measured effluent concentration from field lysimeter at Waseca site
[4]Lerman (1979)

FIGURES
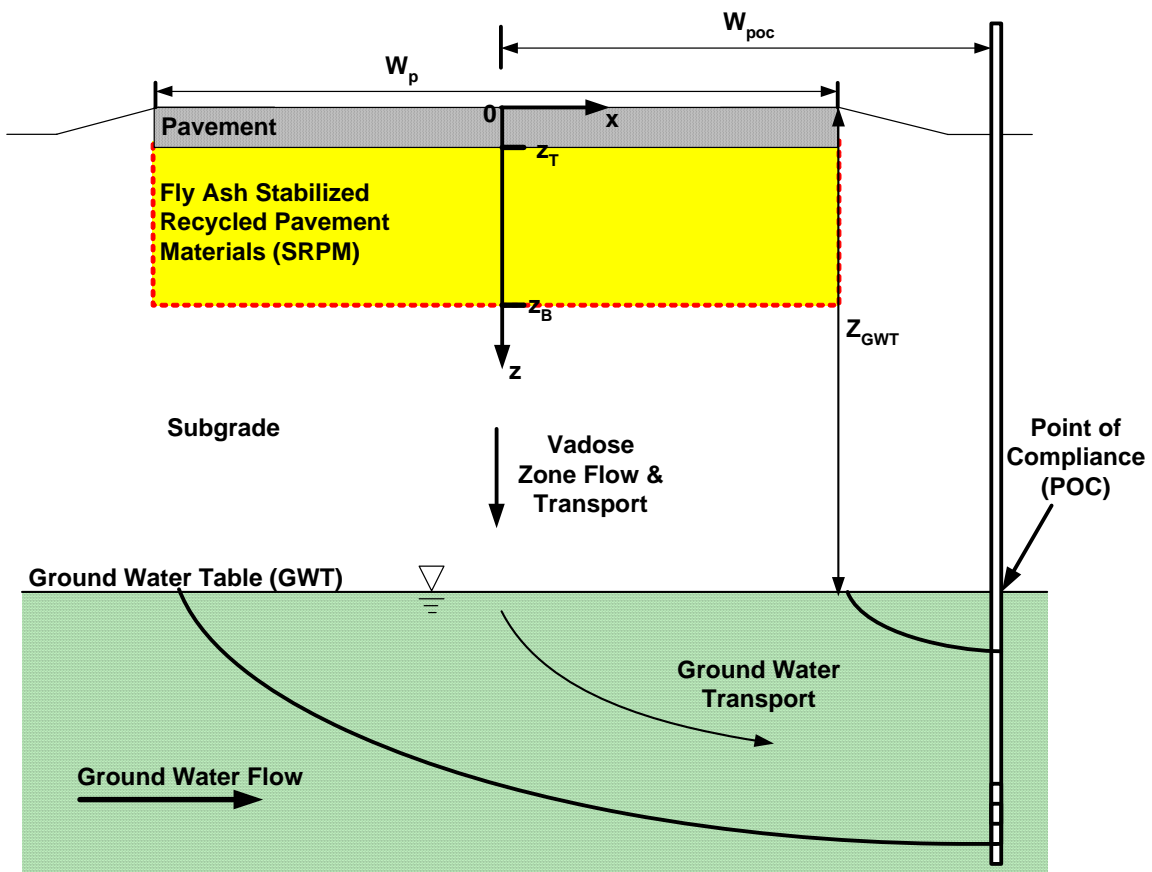
Figure 14. Conceptual model in WiscLEACH for predicting impacts to the vadose zone and groundwater caused by leaching from a pavement structure with a SRPM layer.
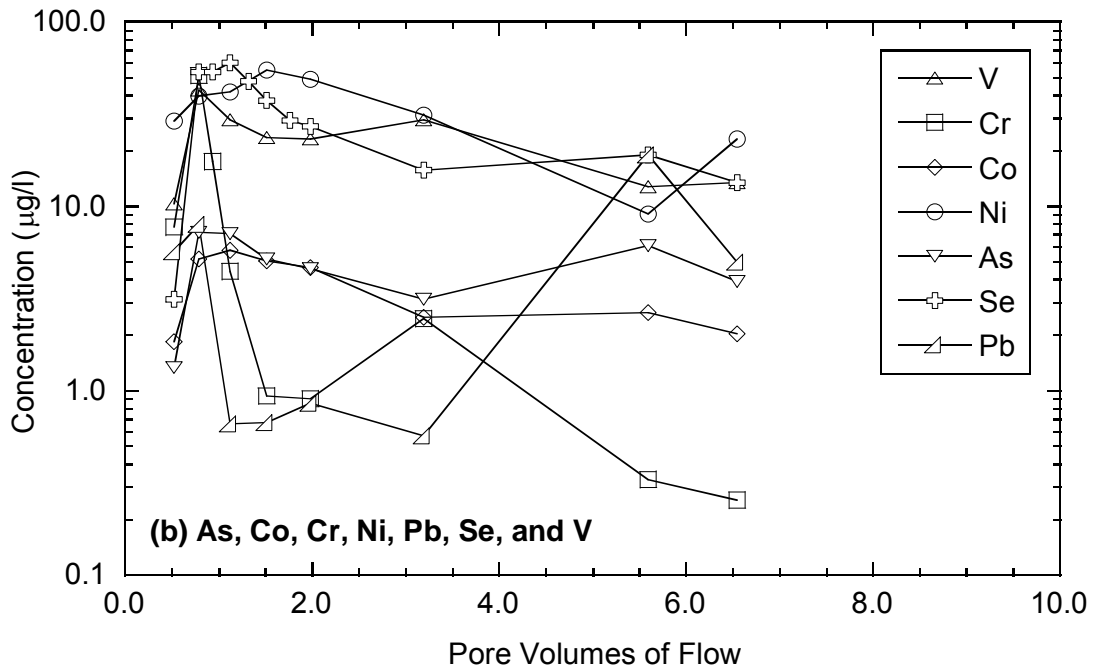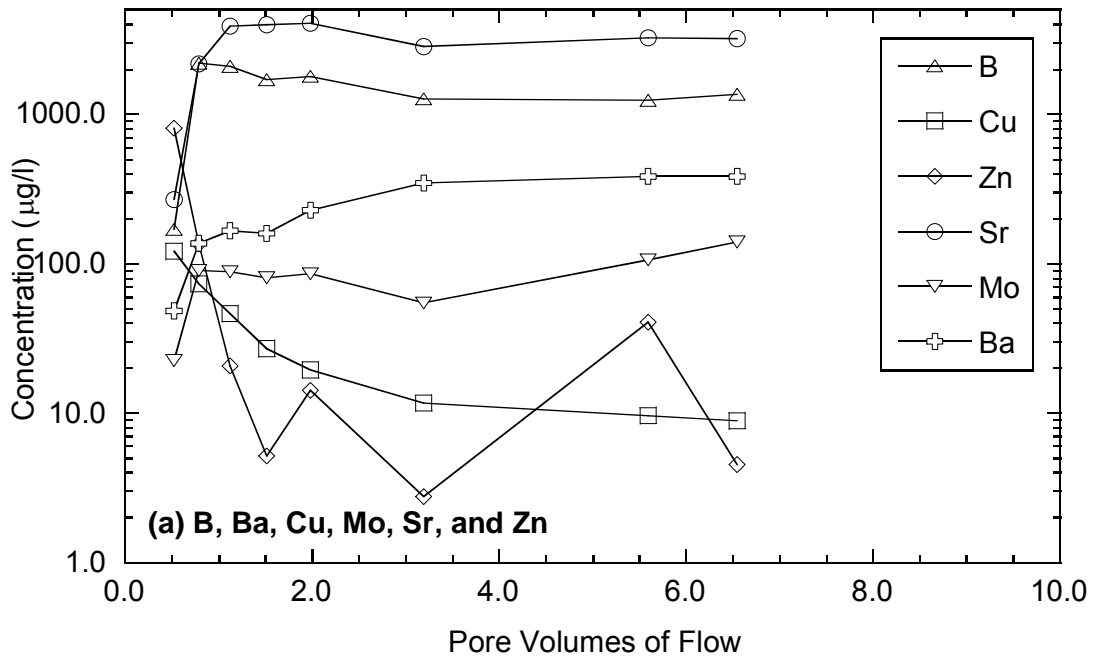
Figure 15. Concentrations of trace elements in effluent from CLT on SRPM: (a) elements with peak concentrations exceeding 100 μg/L and (b) elements with peak concentrations less than 100 μg/L.

(a)

75 mm HMA

150 mm Fly
Ash Stabilized
RPM

Subgrade | Lysimeter

(b)

N

10 m

7th street

Lysimeter

5th street

7th Avenue

4 m

10 m

8th street
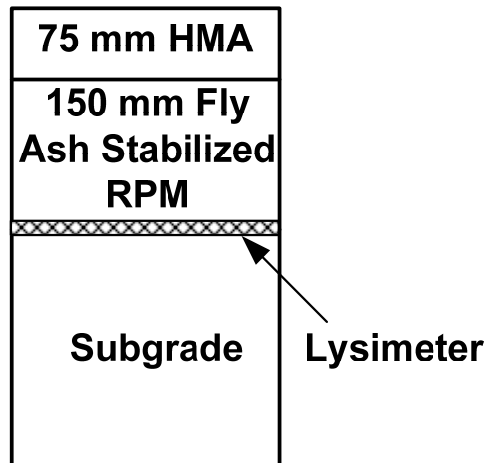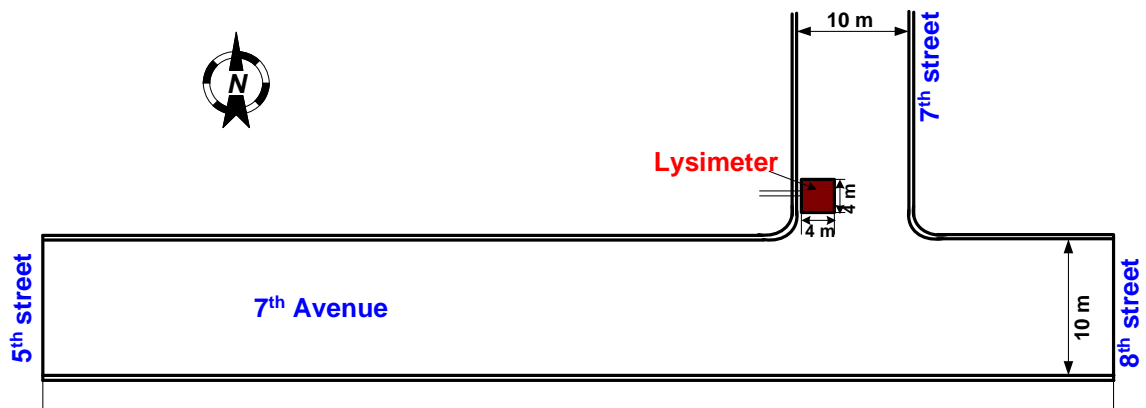
Figure 16. Reconstructed road at Waseca site: (a) profile of the pavement structure at the lysimeter and (b) location of the lysimeter.
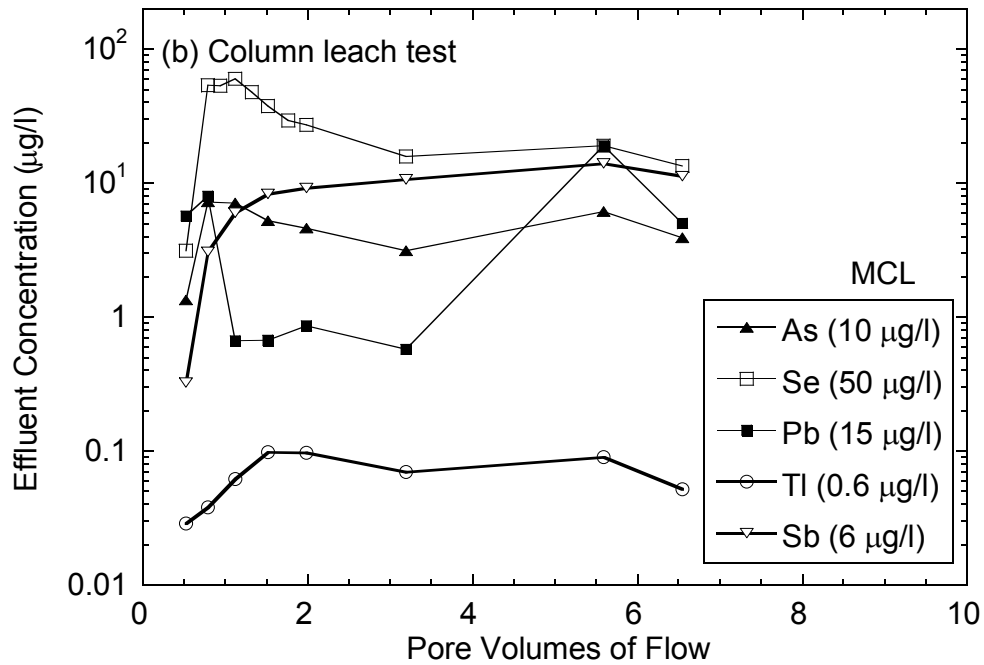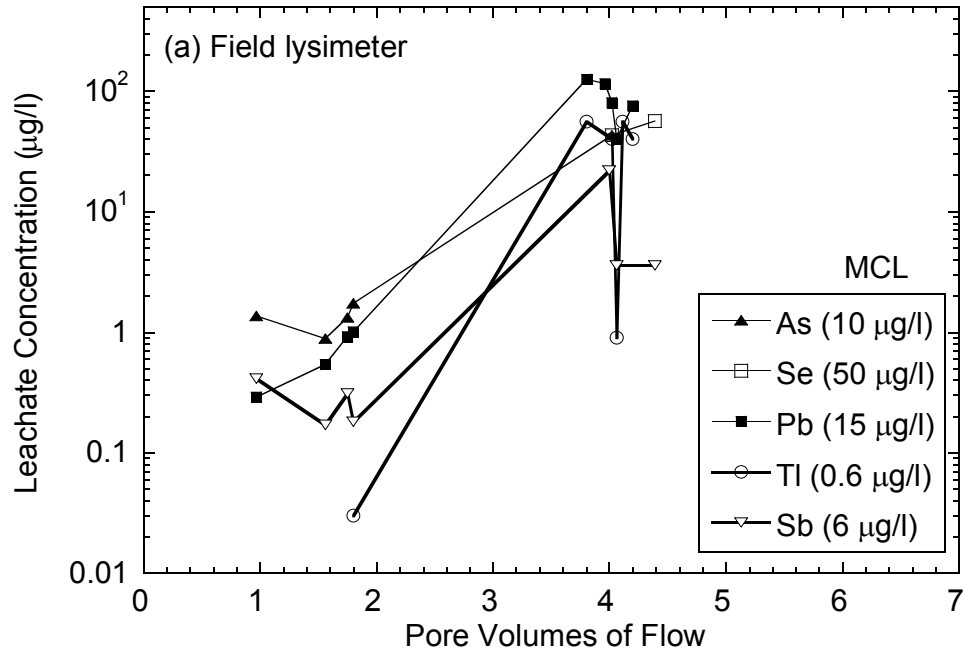
Figure 17. Concentrations of trace elements (a) in leachate collected in lysimeter exceeding USEPA MCLs and (b) in effluent from column leaching test on SRPM.
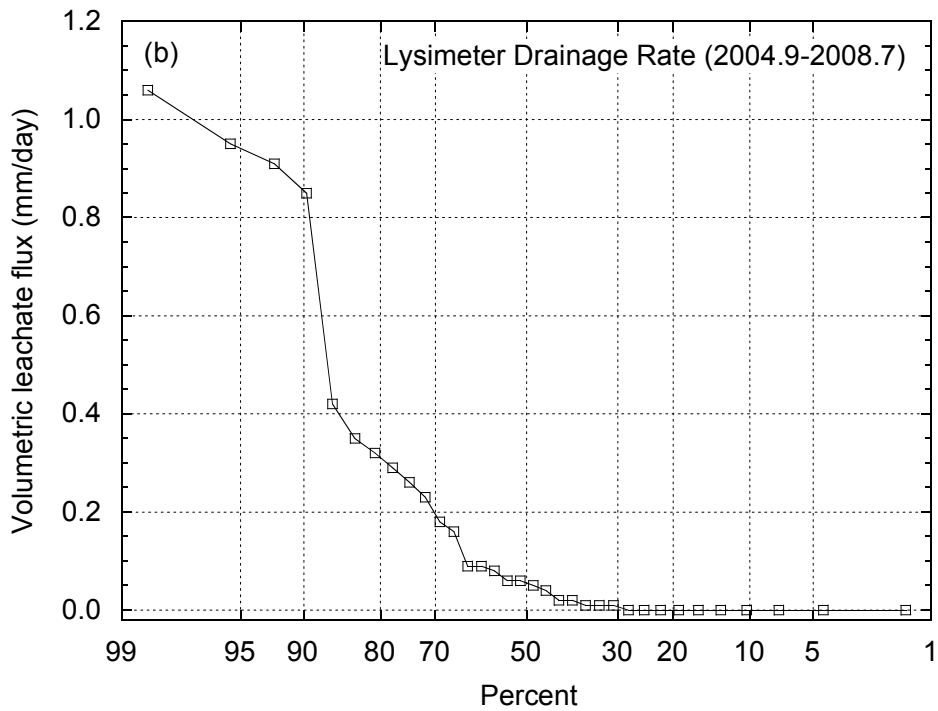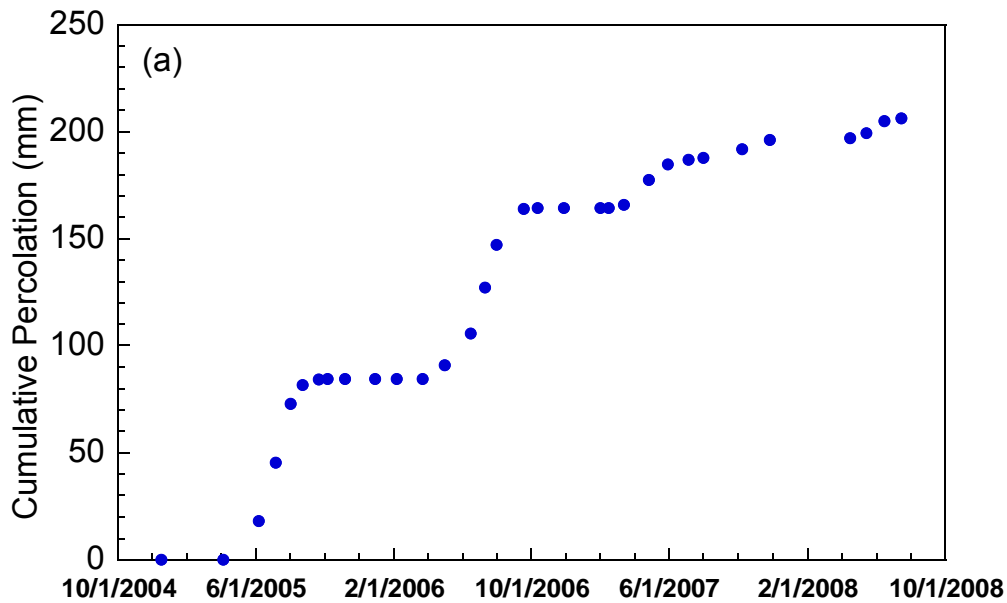
Figure 18. Cumulative percolation (a) and volumetric leachate flux (b) from the lysimeter between September 2004 to July 2008. Base of lysimeter is located at the bottom of the SRPM layer.
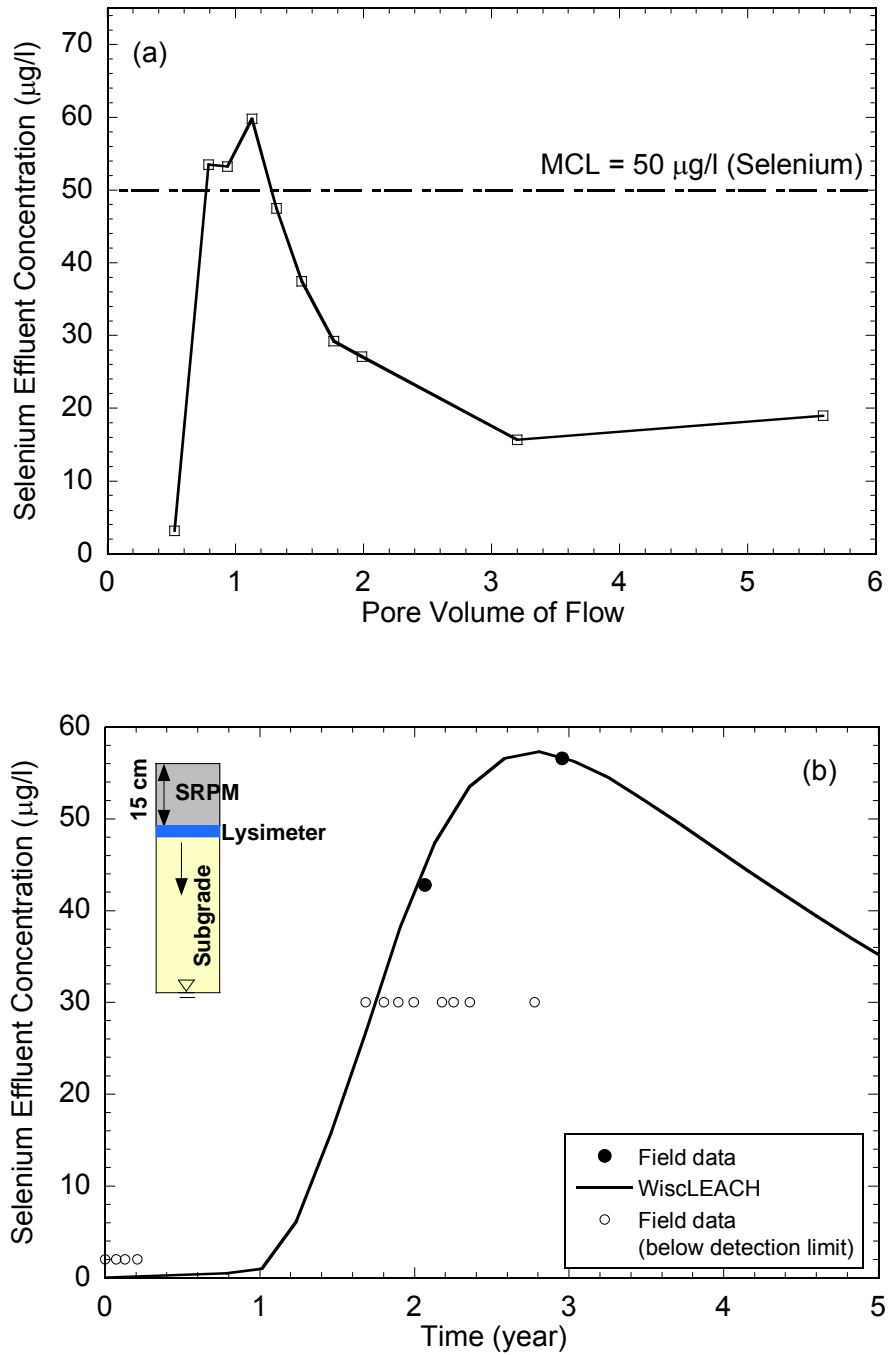
Figure 19. Selenium concentrations in leachate from CLT on SRPM (a) and measured and predicted selenium concentration in lysimeter at the Waseca site (b). Simulation was conducted using 75th percentile volumetric leachate flux measured in the lysimeter (0.1 m/yr).
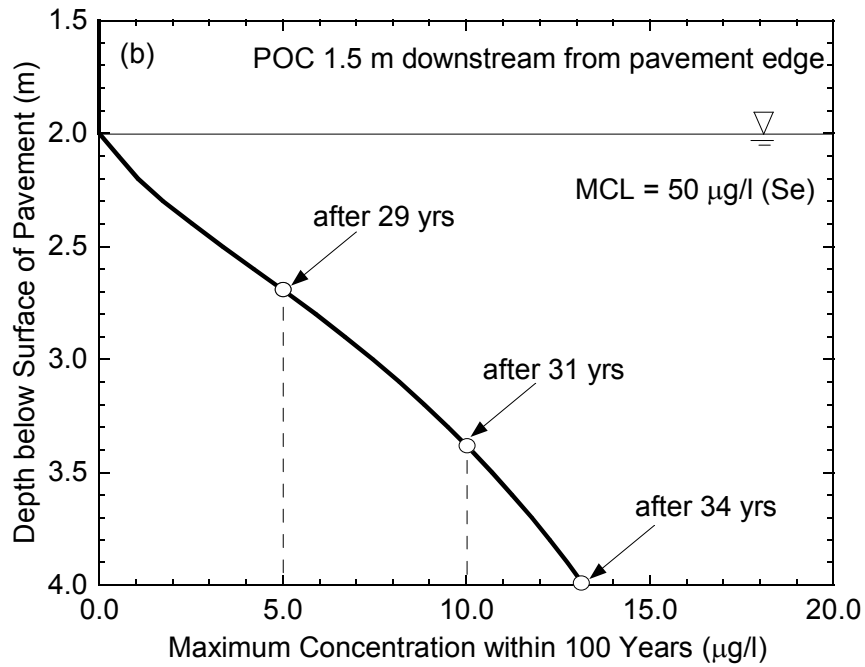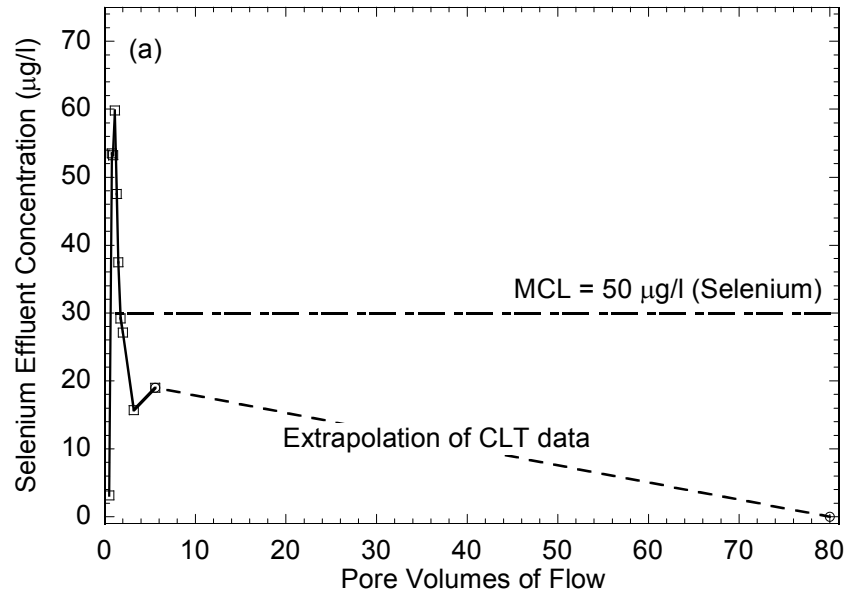
Figure 20. Selenium concentrations in leachate from CLT extrapolated for 100 yr (a) and predicted maximum concentrations at POC over 100-yr period at the Waseca site (b). POC is 1.5 m down gradient from pavement edge. Simulation was conducted using 75th percentile volumetric leachate flux measured in the lysimeter (0.1 m/yr).
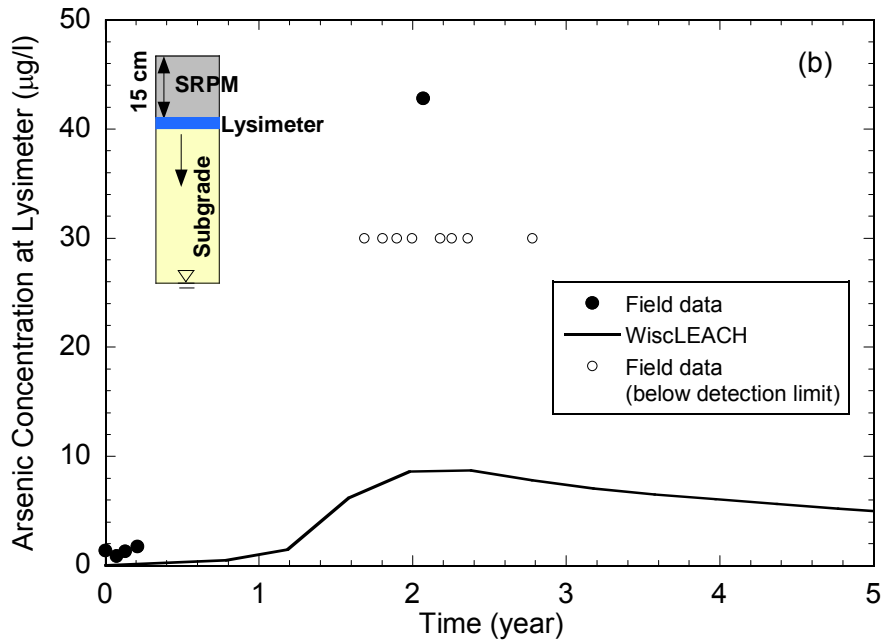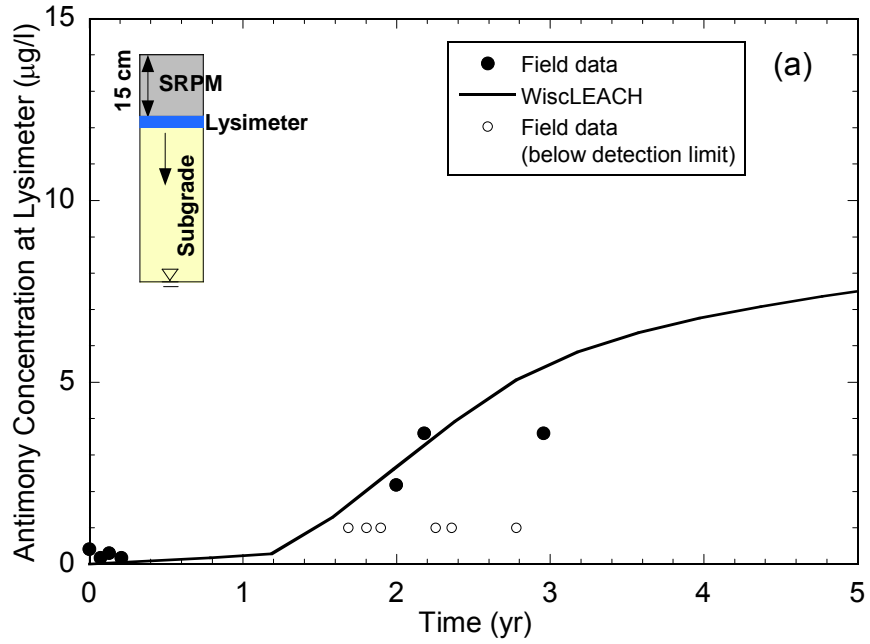
Figure 21. Predicted antimony (Sb) (a) and arsenic (As) (b) concentrations in leachate in lysimeter at the Waseca site (b). Detection limit is higher for data between 1 and 3 yr due to change in analytical methods.
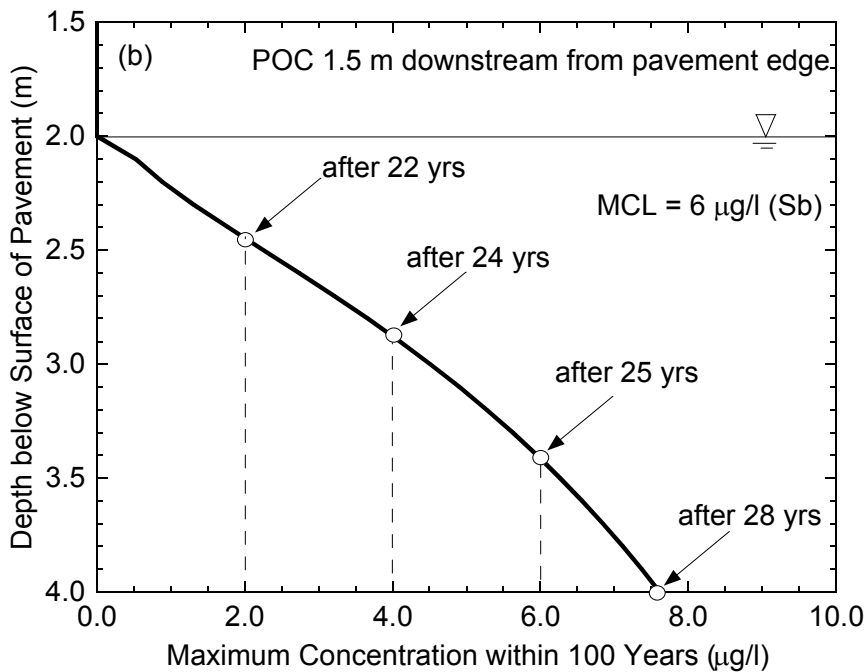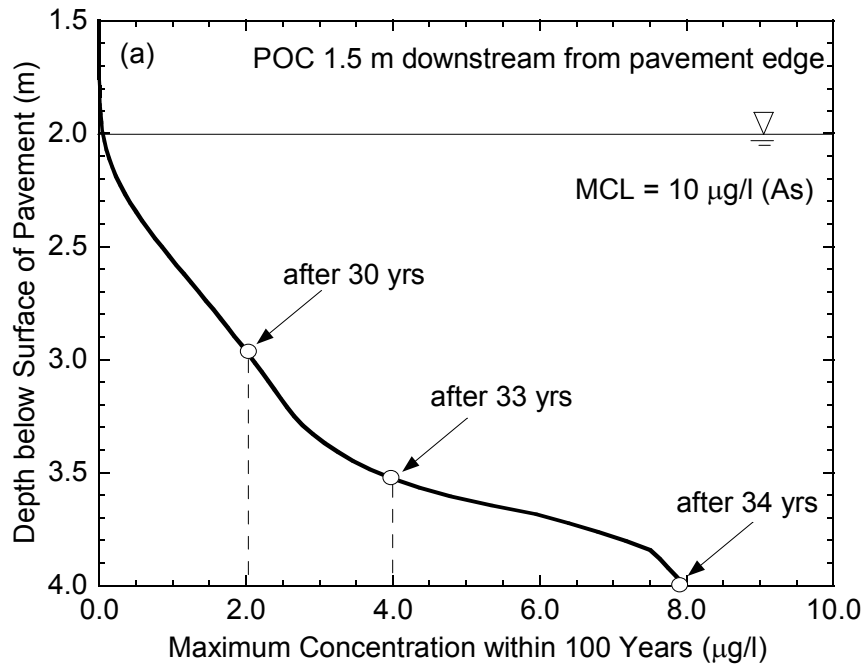
Figure 22. Maximum concentrations at POC for arsenic (a) and antimony (b) over a 100-yr period in the Waseca site. POC is 1.5 m down gradient from pavement edge. Simulation was conducted using measured volumetric leachate flux from lysimeter (0.1 m/yr).
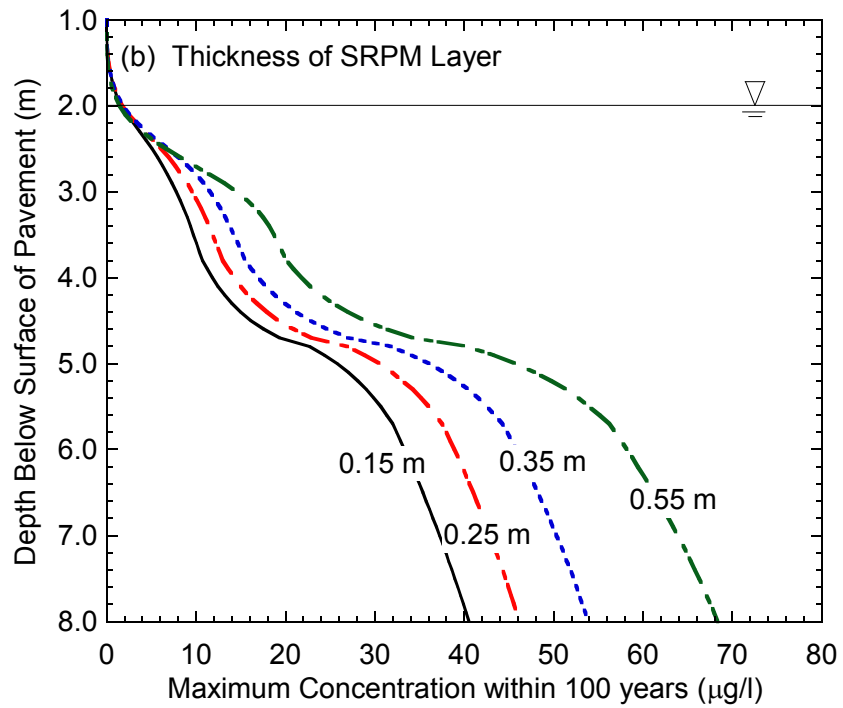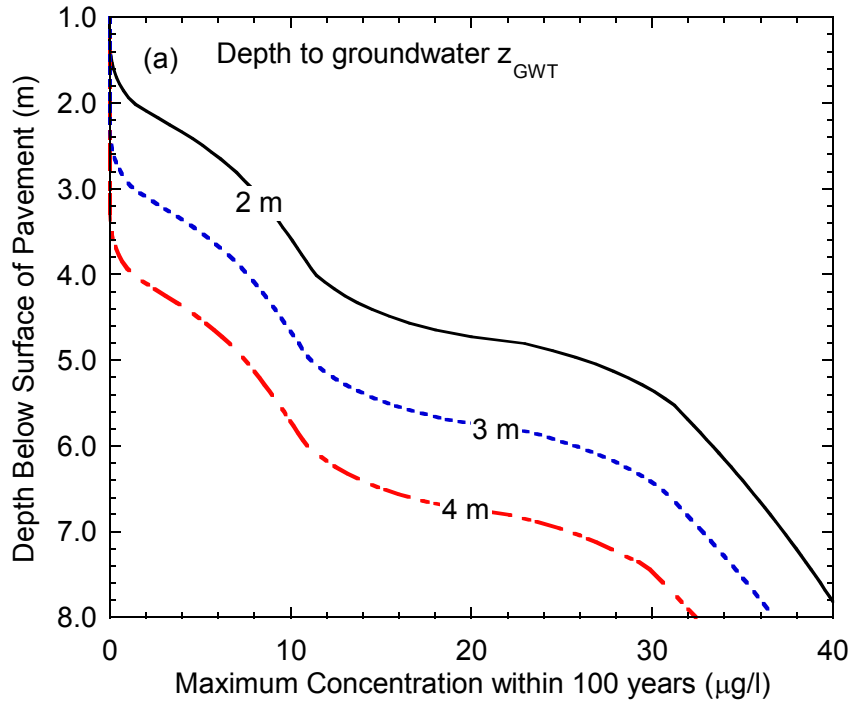
Figure 23. Predicted maximum selenium concentrations at POC over 100-yr period as a function of depth to groundwater (a) and thickness of SRPM layer (b). POC is 1.5 m down gradient from pavement centerline. Simulation was conducted using measured volumetric leachate flux from lysimeter (0.1 m/yr).
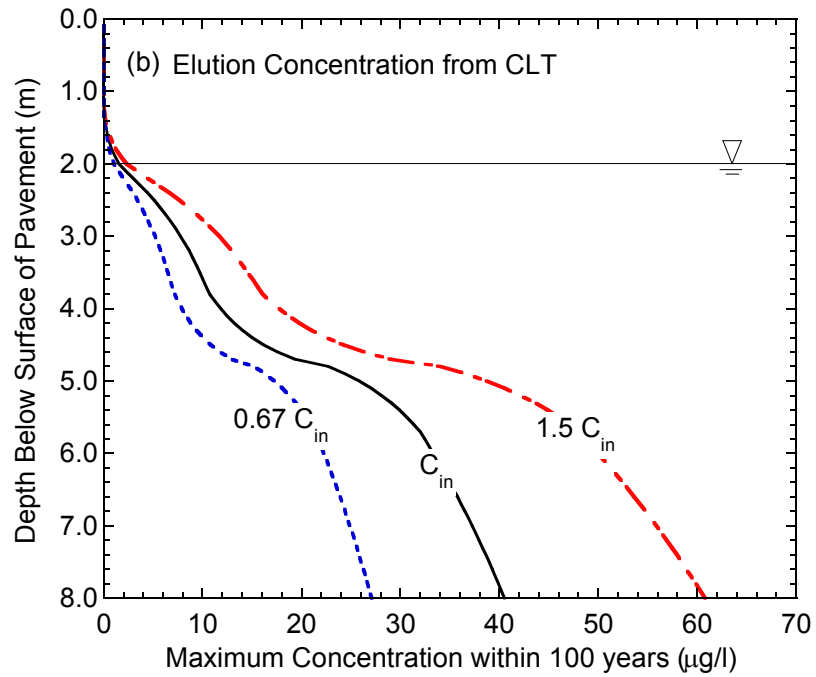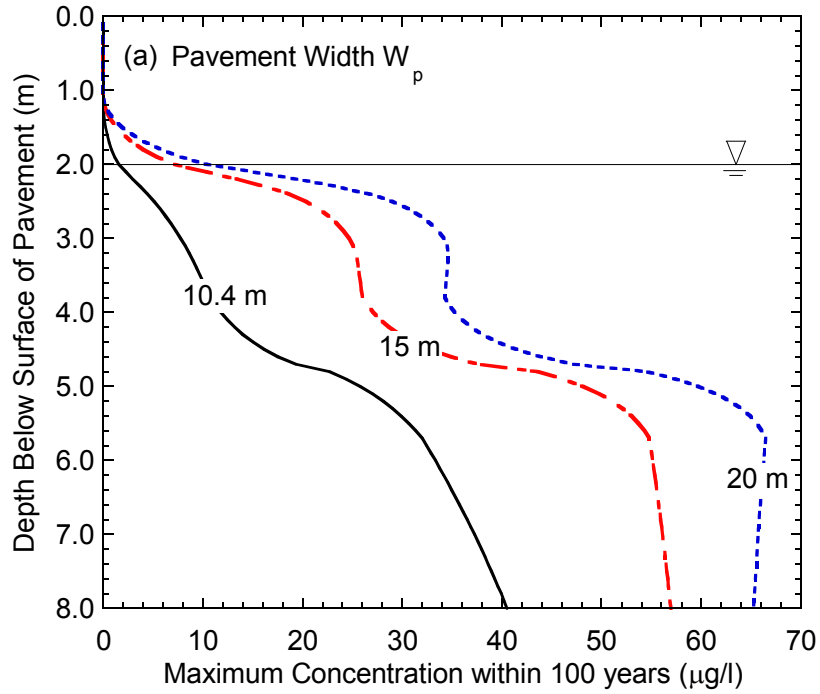
Figure 24. Predicted maximum selenium concentrations at POC over 100-yr period as a function of pavement (a) width and maximum elution concentration C_{in} from CLT (b). POC is 1.5 m down gradient from pavement centerline. Simulation conducted using measured volumetric leachate flux from lysimeter (0.1 m/yr)
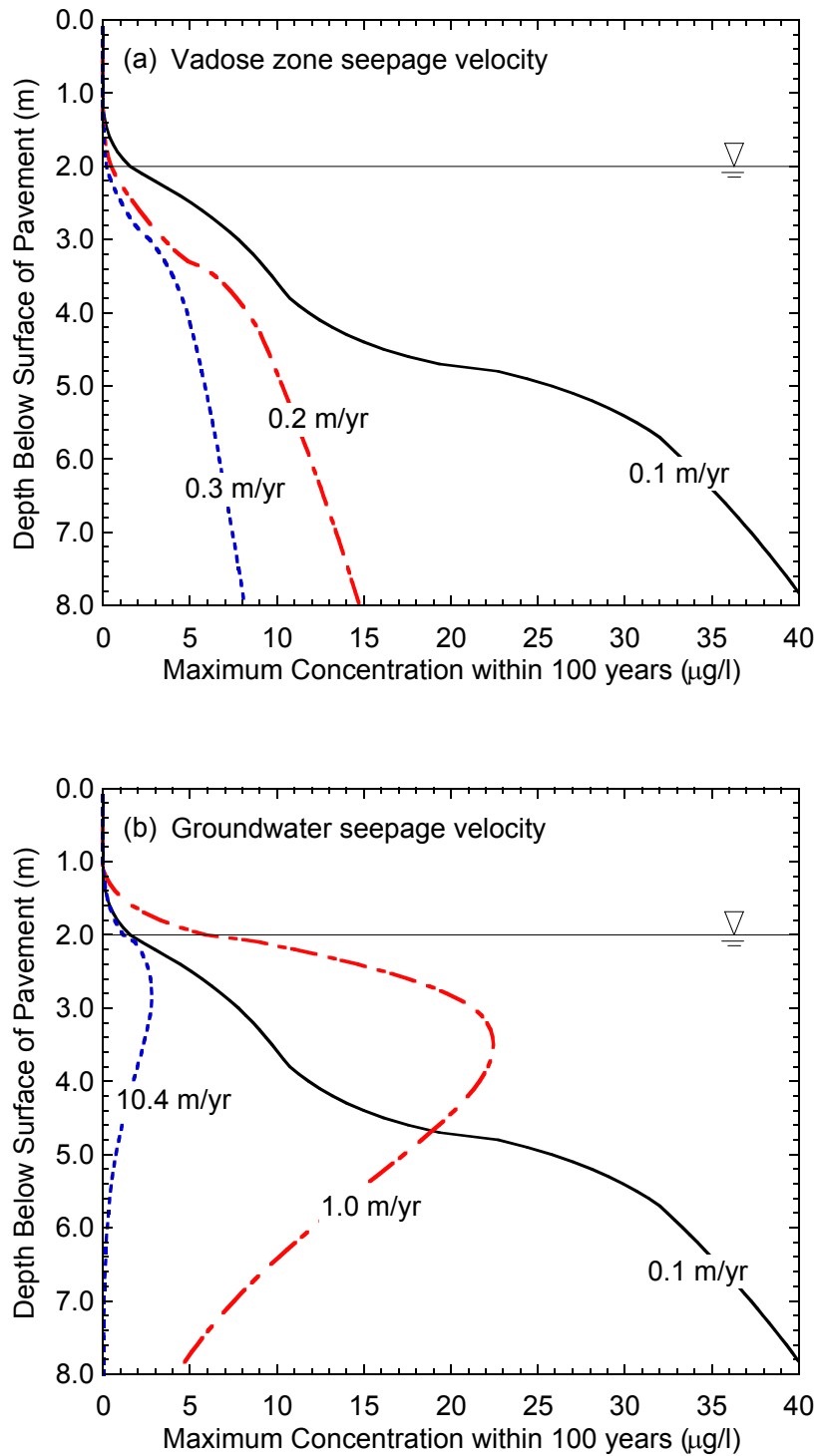
Figure 25. Predicted maximum selenium concentrations at POC over 100-yr period as a function of seepage velocity in the vadose zone (a) and groundwater (b). Simulation was conducted using measured volumetric leachate flux from lysimeter (0.1 m/yr).POC is 1.5 m down gradient from pavement edge.